Layered Atom Arrangements in Complex Materials

Los Alamos
NATIONAL LABORATORY
— EST.1943 —

The World's Greatest Science Protecting America

Layered Atom Arrangements in

Complex Materials

Kurt E. Sickafus

Robin W. Grimes*

Siobhan M. Corish

Antony R. Cleave*

Ming Tang

Chris R. Stanek

Blas P. Uberuaga

James A. Valdez

*Department of Materials, Imperial College of Science, Technology and Medicine,
Prince Consort Road, London SW7 2BP, UK

Los Alamos
NATIONAL LABORATORY
— EST. 1943 —

The World's Greatest Science Protecting America

Contents

List of Tables

List of Figures

Layered Atom Arrangements in Complex Materials

Kurt E. Sickafus,[1] Robin W. Grimes,[2] Siobhan M. Corish,[1] Antony R. Cleave,[2]

Chris R. Stanek,[1] Blas P. Uberuaga,[1] and James A. Valdez[1]

[1]Materials Science and Technology Division, Los Alamos National Laboratory,

Los Alamos, NM 87545, USA

[2]Department of Materials, Imperial College of Science, Technology and Medicine,

Prince Consort Road, London SW7 2BP, UK

ABSTRACT

In this report, we develop an atom layer stacking model to describe systematically the crystal structures of complex materials. To illustrate the concepts, we consider a sequence of oxide compounds in which the metal cations progress in oxidation state from monovalent (M^{1+}) to tetravalent (M^{4+}). We use concepts relating to geometric subdivisions of a triangular atom net to describe the layered atom patterns in these compounds (concepts originally proposed by Shuichi Iida[§]). We demonstrate that as a function of increasing oxidation state (from M^{1+} to M^{4+}), the layer stacking motifs used to generate each successive structure (specifically, motifs along a $\overline{3}$ symmetry axis), progress through the following sequence: MMO, MO, $M_{\frac{r}{s}}O$, $MO_{\frac{r}{s}}O_{\frac{u}{v}}$, MOO (where M and O represent fully dense triangular atom nets and $\frac{r}{s}$ and $\frac{u}{v}$ are fractions used to describe partially filled triangular atom nets). We also develop complete crystallographic descriptions for the compounds in our oxidation sequence using trigonal space group $R\overline{3}$.

I.1 Introduction: Background

Much has been written regarding layered atom descriptions for crystalline solids. The subject is critical to many areas of crystallography, e.g., to describe polytypism and polysomatism, phenomena observed in numerous minerals and ceramics (see, for instance, [1,2]). One of the most noteworthy treatises on layer descriptions for oxides was published by Shuichi Iida in 1957 [3]. Iida introduced a graphical technique to subdivide triangular nets of atoms (often referred to as triangular Ising nets [4]) into subnets that mimic classic atomic arrangements such as the *honeycomb lattice* and the now famous *kagome lattice* [5].[1,2] Iida demonstrated the efficacy of these subnets by providing simple descriptions for atomic arrangements in some exceptionally complex crystalline oxides. It is worth noting that while Iida was trying to understand magnetic properties, there are many more uses for his 'layer' model.

The purpose of this report is to expand the layering concepts first proposed by Iida and to formalize the crystallography underlying Iida's models. In this presentation, we will also introduce a new two-dimensional sublattice that Iida discounted in his original treatise. We will demonstrate the methodology underlying our layered atom concepts by considering a hypothetical oxidation sequence in a metal.

---

[1] Kagome means, crudely, "woven basket" in Japanese. Mamoru Mekata published a recent letter in *Physics Today* [5] where he credited Kodi Husimi of Osaka University with introducing the descriptor *kagome lattice* to describe a new antiferromagnetic lattice he observed in a star-to-triangle transformation of a honeycomb lattice. This appellation first made print in 1951 in a paper by Itiro Syôzi, Husimi's colleague [6].

[2] The use of the term "lattice" in this context is a misnomer. There are only five two-dimensional (plane) lattices [7], i.e., Bravais lattices, and these do not include the honeycomb or kagome lattices referred to here. However, we will (somewhat regrettably) hereafter perpetuate the terms "honeycomb lattice" and "kagome lattice," as these are more or less accepted nomenclature in both past and present literature.

Section I.1 References

[1]   A. R. Verma and P. Krishna, *Polymorphism and Polytypism in Crystals* (John Wiley & Sons, Inc., New York, 1966).

[2]   A. Baronnet, "Polytypism and Stacking Disorder," in *Minerals and Reactions at the Atomic Scale: Transmission Electron Microscopy,* P. R. Buseck, Ed. (Mineralogical Society of America, Washington D.C., 1992), Vol. 27, pp. 231–288.

[3]   S. Iida, "Layer Structures of Magnetic Oxides," *J. Phys. Soc. Japan* **12** (3) 222–233 (1957).

[4]   G. H. Wannier, "Antiferromagnetism. The Triangular Ising Net," *Phys. Rev*. **79** (2) 357–364 (1950) .

[5]   M. Mekata, "Kagome: The Story of the Basketweave Lattice," *Phys. Today*, 12–13 February (2003).

[6]   I. Syôzi, "Statistics of Kagomé Lattice," *Prog. Theor. Phys.* **6** (3) 306–308 (1951).

[7]   T. Hahn, Ed. *International Tables for X-ray Crystallography*, Vol. A (D. Riedel, Dordrecht, Netherlands, 1983).

I.2 Introduction: The Basic Concepts for Layer Stacking of Triangular Atom Nets

Figures I.2-1, I.2-2, I.2-3, and I.2-4 illustrate the principal layered atom concepts to be considered in this report. In these figures, we compare and contrast the structures of two model ionic compounds: cesium chloride (CsCl) and sodium chloride (NaCl). Though not oxides, many oxides are isostructural with CsCl and NaCl. The CsCl structure is often referred to as the *B2* structure, especially for intermetallic compounds. The NaCl structure is *B1* but is usually referred to as the *rock salt* structure.

Figure I.2-1 shows the conventional cubic unit cells (*u.c.*) of CsCl and NaCl for comparison. The small atom in the center of the CsCl *u.c.* is a Cs cation surrounded by eight nearest neighbor (*n.n.*) Cl anions in simple cubic (*sc*) geometry. In CsCl (Fig. I.2-1a), each Cs cation is 8-fold coordinated by *n.n.* anions, and equivalently, each Cl anion is 8-fold coordinated by *n.n.* cations. Cesium chloride can be described as two interpenetrating *sc* sublattices: an *sc* Cs cation sublattice and an *sc* Cl anion sublattice. Cesium chloride is described by a single lattice parameter, $a_{cube} = 0.41150(4)$ nm (PDF File 5-607 [1] and Ahtee [2]). The Bravais lattice for CsCl is *sc* and the space group (S.G.) is $Pm\bar{3}m$ (# 221 in the International Tables for Crystallography [3]). The Cl anion is placed at equipoint $1a$ (Wykcoff notation; fractional coordinates $(x, y, z) = (0,0,0)$), while the Cs cation is located at equipoint $1b$ (fractional coordinates $(x, y, z) = \left(\frac{1}{2}, \frac{1}{2}, \frac{1}{2}\right)$).

CsCl   **NaCl**

(a)   **(b)**
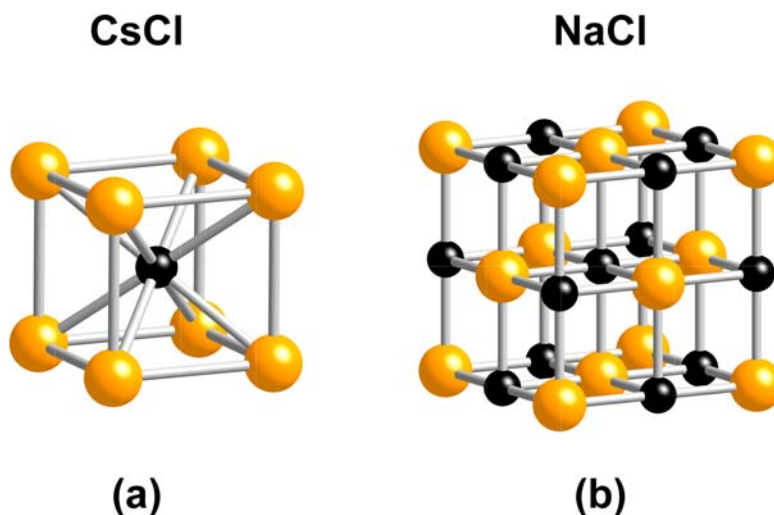
Figure I.2-1. Schematic diagrams (perspective views) showing the conventional unit cells for (a) CsCl and (b) NaCl. Anions are large (yellow); cations are small (black).

By contrast, in NaCl (Fig. I.2-1b) the small atom in the center of the *u.c.* is an Na cation surrounded by 6 *n.n.* Cl anions in regular, octahedral geometry. In NaCl, each Na cation is 6-fold coordinated by *n.n.* anions, and equivalently, each Cl anion is 6-fold coordinated by *n.n.* cations. Sodium chloride can be described as two interpenetrating face-centered cubic (*fcc*) sublattices, an *fcc* Na cation sublattice and an *fcc* Cl anion sublattice. Sodium chloride is described by a single lattice parameter, a_{cube} = 0.562 nm (PDF File 5-628 [1] and Abrahams and Bernstein [4]). The Bravais lattice for NaCl is *fcc* while the S.G. is $Fm\overline{3}m$ (# 225 [3]). The Cl anion is placed at equipoint 4*a* (fractional coordinates (*x*, *y*, *z*) = (0,0,0) + equivalent positions), while the Na cation is located at equipoint 4*b* (fractional coordinates (*x*, *y*, *z*) = $\left(\frac{1}{2},\frac{1}{2},\frac{1}{2}\right)$ + equivalent positions).

In terms of conventional crystallographic descriptions for the CsCl and NaCl structures, the previous paragraphs provide comprehensive descriptions for both compounds. The information provided here constitutes everything one needs to know in order to define the crystallographic structures of CsCl and NaCl in their entireties. But at this point, we wish to introduce our readers to alternative, layered atom descriptions for both CsCl and NaCl. The layered atom descriptions for these structures are equivalent to everything presented above in a crystal structure sense. Nevertheless, with the layered atom approach, we gain some unique insights into these structures that are not immediately apparent in the conventional crystal structure descriptions. **Moreover, we will demonstrate that the layered atom structures of CsCl and NaCl are so similar as to be nearly identical!**

The atomic layers that we are interested in possess atom arrangements that we will refer to as *triangular atom nets*. In this section, we will concern ourselves with triangular atom nets that are atomically pure; that is to say, they contain only one atom type (either cations or anions). To find such atom nets in CsCl and NaCl, we first rotate our views of these structures (shown in perspective in Fig. I.2-1) to views along a <112>-type crystallographic direction (other <*uvw*> views are also possible; <112> is chosen here for illustrative purposes only). Figure I.2-2 shows <112> projected views of the structures for both the CsCl (Fig. I.2-2a) and NaCl (Fig. I.2-2b) *u.c.*s. The <112> views in Figs. I.2-2a and I.2-2b represent projections of 3 × 3 *u.c.* arrays for CsCl and NaCl, respectively. Note in Figs. I.2-2a and I.2-2b that horizontal rows of cations alternate with horizontal rows of anions as one progresses up the projected diagrams for both CsCl and NaCl.

The spacing between pairs of anion rows or pairs of cation rows is denoted by a characteristic length h.
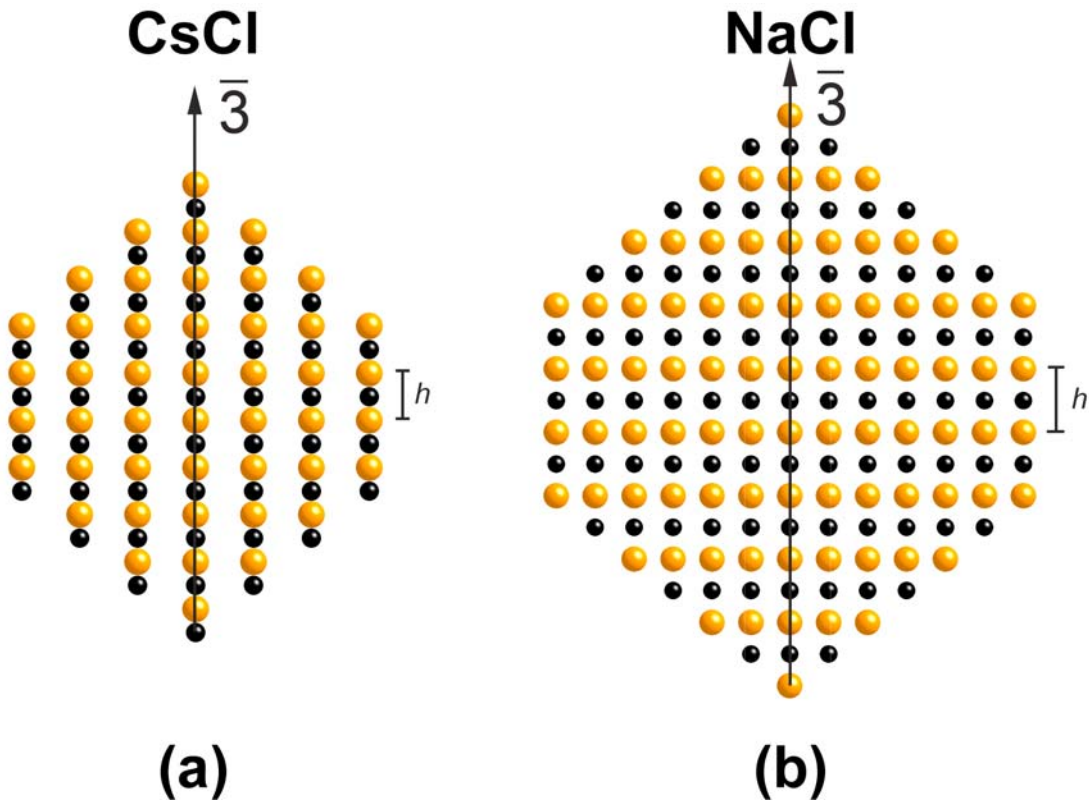
Figure I.2-2. Schematic diagrams showing a volume of 3×3 unit cells viewed along a <112> crystallographic axis for (a) CsCl and (b) NaCl. Anions are large (yellow); cations are small (black).

The *triangular atom nets* of interest in our presentation are perpendicular to the planes of the projections shown in Fig. I.2-2 (that is, perpendicular to the viewing plane or the paper). These triangular atom nets for CsCl and NaCl are illustrated schematically in Fig. I.2-3. The first thing to notice about the triangular atom nets is that they are constructed from equilateral triangles of atoms joined at the triangle edges. The *n.n.* interatomic distance in these layers is denoted by a characteristic length d. The second observation is that the triangular atom nets in CsCl and NaCl are indeed atomically pure: they consist only of cations or anions. The third observation is that the triangular atom nets corresponding to CsCl are less dense (more open) than those

associated with the NaCl structure. We will return to this point shortly. It should also be noted that the triangular atom nets shown in Fig. I.2-3 correspond to {111}-type crystallographic planes, based on a cubic indexing system. In both CsCl and NaCl, the axes along which {111}-type planes are stacked are <111> axes with $\bar{3}$ symmetry. In Figs. I.2-2a and I.2-2b, such stacking axes are labeled $\bar{3}$.
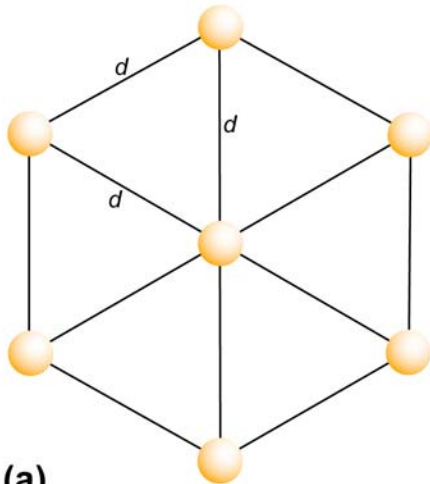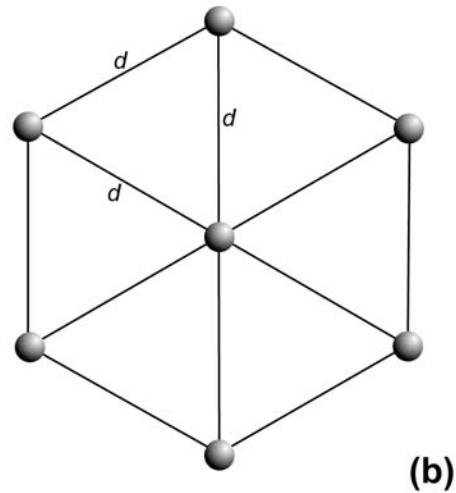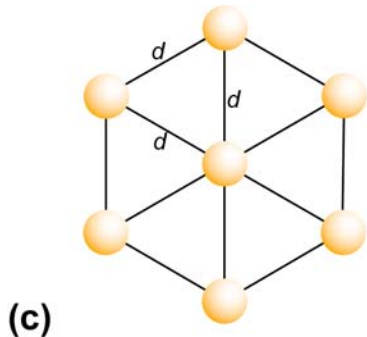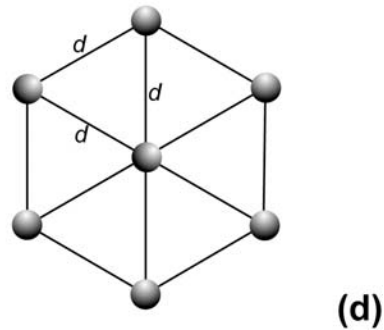
Figure I.2-3. Schematic diagrams showing the triangular atom net arrangements in individual {111} planes (a) CsCl anion plane, (b) CsCl cation plane, (c) NaCl anion plane, and (d) NaCl cation plane. Anions are large (yellow); cations are small (black).

To summarize our observations to this point:

1. For both CsCl and NaCl, all of the atom layers (both cation and anion) perpendicular to any $\bar{3}$ axis (i.e., normal to the <112> projections shown in Figs. I.2-2a and I.2-2b) are perfect *triangular atom nets*.

2. Atom layers in both CsCl and NaCl alternate *cation-anion-cation-anion...*, along any $\bar{3}$ axis (i.e., normal to the <112> projections shown in Figs. I.2-2a and I.2-2b).

3. The spacing, h, between pairs of anion or cation layers along any $\bar{3}$ axis is smaller in CsCl (Fig. I.2-2a) compared with NaCl (Fig. I.2-2b).

4. The spacing, d, between atoms within each *triangular atom net* is larger in CsCl (Figs. I.2-3a and I.2-b) compared with NaCl (Figs. I.2-3c and I.2-3d).

An additional important similarity between the CsCl and NaCl structures (not apparent in Figs. I.2-2 and Fig. I.2-3) is that the *registry shift* between adjacent {111} atom layers is identical in CsCl versus NaCl. *Registry shift* is a concept relating to the projected layered atom arrangements perpendicular to the stacking axis. As perfect triangular atom nets are overlayed along the stacking axis, nature imposes lateral translations between adjacent layers. We will refer to these translations as *registry shifts* between adjacent layers. Interestingly, along a $\bar{3}$ stacking axis, these registry shifts repeat themselves every three anion (or cation) layers in both the CsCl and NaCl structures. These repeating registries are conventionally denoted *A*, *B*, and *C*. Stacking registries are identical in both CsCl and NaCl: the anion sublattice repeats stacking registry in the sequence *ACBACB*…, while the interleaving cation sublattice repeats registry in the sequence *BACBAC*…. Combining anion and cation layers, the stacking sequence along any $\bar{3}$ triangular atom net stacking axis (a <111> crystallographic axis indexed according to a cubic structure) repeats in an *ABCABC*… sequence.

To make sense of all of these observations, we return in Fig. I.2-4 to the <112> projected structures for CsCl and NaCl, but here we consider only a single *u.c.* for each (CsCl in Fig. I.2-4a; NaCl in Fig. I.2-4b). Also, only the central *u.c.* cation is shown for NaCl in Fig. I.2-4b. For NaCl (Fig. I.2-4b), we highlight in shades of orange/red the primitive *u.c.*

which is a 60° rhombohedron. This is the *u.c.* that most appropriately should be compared with the *u.c.* for the CsCl structure shown in Figs. I.2-1a and I.2-4a. The 60° rhombohedral *u.c.* for NaCl contains one formula unit per *u.c.* ($Z = 1$), compared with the conventional, cubic *u.c.* for NaCl, which contains four formula units per *u.c.* ($Z = 4$). For CsCl (Figs. I.2-1a and I.2-4a), the conventional *u.c.* is also the primitive *u.c.* and it is a 90° rhombohedron (i.e., a simple cube) with one formula unit per *u.c.* ($Z = 1$).

An interesting consequence of our recognition of the rhombohedral *u.c.*s for CsCl and NaCl noted above is that we can describe the crystal structures of both compounds in a common, rhombohedral space group: S.G. $R\overline{3}$ (#148 [3]). Table I.2-1 shows details for the lattice parameters and atom positions for CsCl and NaCl using, alternately, cubic and rhombohedral structural descriptions. For rhombohedral S.G. descriptions, both rhombohedral and hexagonal *u.c.* information are provided in Table I.2-1. Note that the hexagonal *u.c.* is three times the volume of the rhombohedral *u.c.* ($Z = 3$ vs. $Z = 1$).

Based on our layered atom descriptions, the relationship between CsCl and NaCl structures can be described like this: Imagine taking the CsCl *u.c.* in its <112> or "edge-on" orientation as shown in Fig. I.2-4a and squeezing on it along the equator of the cell. The CsCl 90° rhombohedral *u.c.* would be forced to shrink laterally and expand longitudinally (vertically in Fig. I.2-4a). If one performs this operation in a uniform manner, at some point one will arrive at a *u.c.* configuration that can be described by a 60° rhombohedron. This is nothing more than the primitive rhombohedral *u.c.* described earlier for the NaCl structure (Fig. I.2-4b). During this deformation process, the *u.c.* of CsCl is narrowed in the waist and elongated in height so that the spacing between adjacent atom layers increases, while the spacing between atoms within each layer is diminished. The triangular atom net patterns within each layer are unchanged by this deformation process and the registry between adjacent atom layers also remains the same.
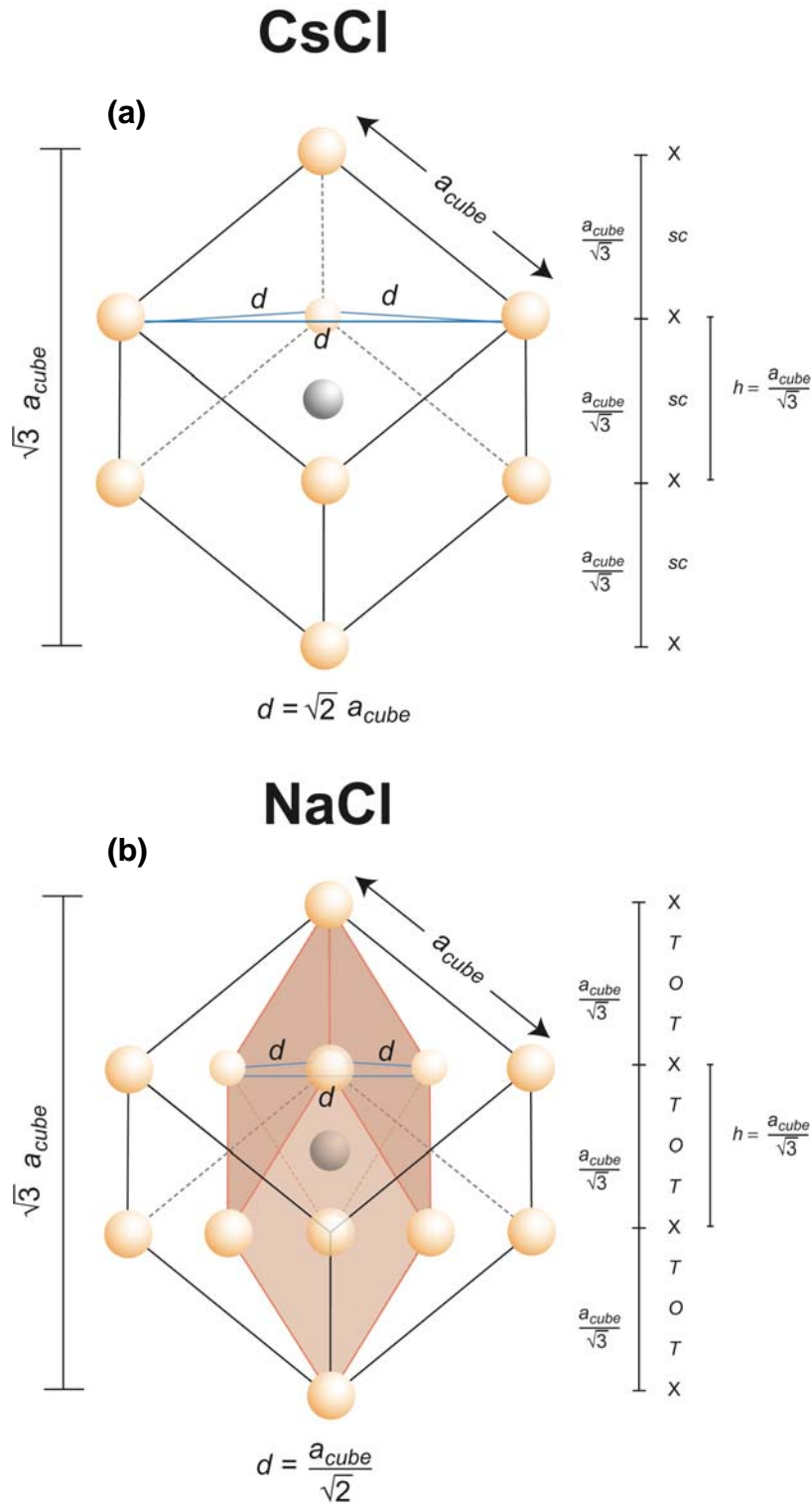
CsCl

NaCl

Figure I.2-4. Schematic diagrams showing <112> axial views of a single unit cell in (a) CsCl and (b) NaCl. In addition to the conventional, cubic unit cells for CsCl and NaCl, the primitive, rhombohedral unit cell for NaCl is highlighted in red in (b). Anions are large (yellow); cations are small (black). Only the unit cell central cation is shown in (b).

The process described here is clearly a "diffusionless" process. Remarkably, this process is also not fictitious; it is known to occur in nature. It occurs in CsCl at T=762 K, such that CsCl is characterized by a 90° rhombohedral *u.c* ($Pm\overline{3}m$) below this temperature [2] and a 60° rhombohedral *u.c* ($Fm\overline{3}m$) above this temperature [5].[1] The structures of these two CsCl polymorphs are summarized in Table I.2-1.

In summary, our layered atom descriptions for CsCl and NaCl reveal that these structures are virtually identical: They consist of *triangular atom nets* stacked along a stacking axis ($\overline{3}$ or <111> in both structures), alternating *cation-anion-cation-anion...* along this axis. Registry shifts progress according to an *ABCABC…* repeat sequence in both structures. The spacing between adjacent layers is larger in NaCl than CsCl, while the spacing between atoms within each layer is smaller in NaCl than CsCl.

---

[1] The low-temperature, *sc* phase of CsCl, is slightly more dense than the high-temperature, *fcc* phase (28.7 vs. 24.1 atoms/nm^3).

Table I.2-1. Lattice parameters and atom positions describing unit cells in the compounds CsCl and NaCl. Both CsCl and NaCl are defined here using cubic, rhombohedral, and hexagonal unit cells. Two polymorphs of CsCl are shown in this table. Cesium chloride is *sc* (S.G. $Pm\bar{3}m$) below T = 742 K [2] and *fcc* (S.G. $Fm\bar{3}m$) above T = 742 K [5]. The rhombohedral and hexagonal descriptions for CsCl shown in this table are based on the low temperature, *sc* phase.

	Cubic Lattice Parameters		Rhombohedral Lattice Parameters		Hexagonal Lattice Parameters	
Compound	$Pm\bar{3}m$	$Fm\bar{3}m$	$R\bar{3}$ (rhombohedral)		$R\bar{3}$ (hexagonal)	
CsCl	$a_{cube}^{sc} =$ 0.41150(4) nm	$a_{cube}^{fcc} =$ 0.6923(10) nm	$a_{rhomb} = a_{cube}^{sc}$ = 0.41150(4) nm	α = 90°	$a_{hex} = \sqrt{2}\, a_{cube}^{sc}$ = 0.58195(5) nm	$c_{hex} = \sqrt{3}\, a_{cube}^{sc}$ = 0.71274(6) nm
NaCl		$a_{cube}^{fcc} = 0.562$ nm	$a_{rhomb} = \dfrac{a_{cube}^{fcc}}{\sqrt{2}}$ = 0.397 nm	α = 60°	$a_{hex} = \dfrac{a_{cube}^{fcc}}{\sqrt{2}}$ = 0.397 nm	$c_{hex} = \sqrt{3}\, a_{cube}^{fcc}$ = 0.973 nm

Wyckoff Equipoint and Fractional Coordinates (*x*, *y*, *z*)				
Compound	$Pm\bar{3}m$	$Fm\bar{3}m$	$R\bar{3}$ (rhombohedral)	$R\bar{3}$ (hexagonal)
CsCl	Cl @ 1*a* (0,0,0)	Cl @ 4*a* (0,0,0) + equivalent positions	Cl @ 1*a* (0,0,0)	Cl @ 3*a* (0,0,0) + equivalent positions
	Cs @ 1*b* $\left(\frac{1}{2},\frac{1}{2},\frac{1}{2}\right)$	Cs @ 4*b* $\left(\frac{1}{2},\frac{1}{2},\frac{1}{2}\right)$ + equivalent positions	Cs @ 1*b* $\left(\frac{1}{2},\frac{1}{2},\frac{1}{2}\right)$	Cs @ 3*b* $\left(0,0,\frac{1}{2}\right)$ + equivalent positions
NaCl**		Cl @ 4*a* (0,0,0) + equivalent positions	Cl @ 1*a* (0,0,0)	Cl @ 3*a* (0,0,0) + equivalent positions
		Na @ 4*b* $\left(\frac{1}{2},\frac{1}{2},\frac{1}{2}\right)$ + equivalent positions	Na @ 1*b* $\left(\frac{1}{2},\frac{1}{2},\frac{1}{2}\right)$	Na @ 3*b* $\left(0,0,\frac{1}{2}\right)$ + equivalent positions

**It should also be noted that the $Fm\bar{3}m$ structure of NaCl can be described in the lower symmetry space group $Pm\bar{3}m$. In this case, Cl atoms are placed at equipoints $1a = (0,0,0)$ and $3c = \left(0,\frac{1}{2},\frac{1}{2}\right)$, $\left(\frac{1}{2},0,\frac{1}{2}\right)$, $\left(\frac{1}{2},\frac{1}{2},0\right)$, while Cs atoms are located at $1b = \left(\frac{1}{2},\frac{1}{2},\frac{1}{2}\right)$ and $3d = \left(\frac{1}{2},0,0\right)\left(0,\frac{1}{2},0\right)$, $\left(0,0,\frac{1}{2}\right)$.

We wish also to call attention to some quantitative geometric relationships between the CsCl and NaCl structures. First, the characteristic interatomic distance, d, within either a CsCl or NaCl triangular atom net is given by (Figs. I.2-4a and I.2-4b):

$$d = \sqrt{2}\, a_{cube} \qquad \text{(CsCl)} \qquad\qquad \text{(I.2-1a)}$$

$$d = \frac{a_{cube}}{\sqrt{2}} \qquad \text{(NaCl)} \qquad\qquad \text{(I.2-1b)}$$

Second, the characteristic spacing, h, between *n.n.* anion (or *n.n.* cation) triangular atom net layers is given by (Figs. I.2-4a and I.2-4b):

$$h = \frac{a_{cube}}{\sqrt{3}} \qquad \text{(both CsCl and NaCl)} \qquad\qquad \text{(I.2-2)}$$

or substituting Eqs. (I.2-1a, I.2-1b) into Eq. (I.2-2), we obtain:

$$h = \frac{d}{\sqrt{6}} \qquad \text{(CsCl)} \qquad\qquad \text{(I.2-3a)}$$

$$h = \frac{2\,d}{\sqrt{6}} = \sqrt{\frac{2}{3}}\, d\,. \qquad \text{(NaCl)} \qquad\qquad \text{(I.2-3b)}$$

Third, the fundamental bond length, $\overline{MX}$, between *n.n.* cations (M) and anions (X) is given by:

$$\overline{MX} = \sqrt{\frac{3}{8}}\, d\,. \qquad \text{(both CsCl and NaCl)} \qquad\qquad \text{(I.2-4)}$$

Finally, we wish to return to the coordination polyhedra concepts that we began with at the outset of this discussion. It is conventional to describe an ionic compound (for which CsCl and NaCl are classic examples) as an anion framework with smaller cations occupying various *interstices* within the anion framework. Let's consider this concept in detail for the CsCl and NaCl structures. As mentioned earlier, the anion frameworks for CsCl and NaCl are *sc* and *fcc* Cl sublattices, respectively. But the situation regarding the Cs and Na cations in these structures and their occupancies of the structural interstices within the anion framework in CsCl versus NaCl is quite fascinating indeed.

We begin our discussion of interstices in CsCl and NaCl by revisiting the rhombohedral *u.c.*s in these compounds. The CsCl 90° and the NaCl 60° rhombohedral *u.c.*s can be thought of as sharing yet one more common feature: Each rhombohedron is made up of a central octahedron of height h, capped on top and bottom by two oppositely oriented tetrahedra, also with heights given by h. The octahedron and tetrahedra making up the CsCl 90° rhombohedron are *irregular*, while the octahedron and tetrahedra that combine to produce the NaCl 60° rhombohedron are *regular*. In Figs. I.2-4a and I.2-4b, the capping tetrahedra appear to be empty, while the central octahedra in both CsCl and NaCl contain cations at their centers. Thus, it seems logical to conclude that in both CsCl and NaCl, all octahedral interstices are *filled* while all tetrahedral interstices are *vacant*. However, this statement is not entirely accurate as we shall see next.

We must consider what is meant by the concept of a polyhedral interstice. In an ionic solid, a polyhedral interstice is generally regarded as the *center of gravity* of the polyhedral unit. This could be a center-of-mass concept, but it could also refer to a center of charge. For a monoatomic anion sublattice (as we have in CsCl and NaCl), each polyhedral unit within this sublattice consists of equivalent anions situated at the vertices of the polyhedron. The center of gravity of such a polyhedron would then be defined as the position in space equidistant from each of the polyhedron vertices. Our intuition is likely to lead us to conclude that the center of gravity, or equivalently, the location of the polyhedral interstice, must lie somewhere within the volume of the polyhedron under consideration. But this is not always true as we will illustrate by comparing interstices in the CsCl and NaCl structures.

Let's consider first the NaCl structure. The central octahedron associated with the NaCl rhombohedral *u.c.* (Fig. I.2-4b) possesses an interstice located precisely at the center of gravity of this regular octahedron. This position coincides with the location of the cation shown in Fig. I.2-4b. There is a layer of cations at the same height as this cation (again, thinking of *height* as a horizontal position along the $\overline{3}$ stacking axis). This height is a distance halfway ($\frac{1}{2}h$) above the adjacent layer of anions (this is illustrated in projection in Fig. I.2-2b). We say that the central anion octahedron in Fig. I.2-4b is *filled* in the sense that the octahedron's interstice is occupied by a cation.

Next, we observe that the capping tetrahedra above and below the central octahedron in Fig. I.2-4b are *empty* in the sense that they are missing atoms at their centers of gravity. It is a simple matter to show from geometry that the center of gravity of each tetrahedron in Fig. I.2-4b is located on an axis perpendicular to the base of the tetrahedron and intercepting the apex of the tetrahedron. Along this axis, the center of gravity resides a distance $\frac{1}{4}h$ from the base of the tetrahedron (where h is the height of the tetrahedron).

To summarize, our discussion to this point reveals that octahedral interstices in NaCl are situated at distances halfway ($\frac{1}{2}h$) between adjacent anion layers, while tetrahedral interstices are located at distances $\frac{1}{4}h$ and $\frac{3}{4}h$ between the same anion layers (these distinct tetrahedral heights arise because the pairs of tetrahedra within each rhombohedral *u.c.* are oppositely oriented). This, in turn, implies that there are layers of tetrahedral (*T*) and octahedral (*O*) interstices between each pair of anion layers. So, as one progresses up the NaCl structure along any $\overline{3}$ axis, the anion layers repeat in sequence *ACBACB...*, with spacing h between each pair of anion layers, while layers of interstices are positioned between these anion layer pairs in sequence *T-O-T*, at heights $\frac{1}{4}h$, $\frac{1}{2}h$, and $\frac{3}{4}h$ (this is shown in Fig. 1.2-4b). In NaCl, only the *O* layers are occupied by cations; the *T* layers are empty.

Now let's consider interstices in the CsCl structure. Figure I.2-4a shows that there is a cation located at the center of gravity of the central octahedron (equidistant from all six anions at the vertices of the octahedron). But now consider the capping tetrahedra that surround this octahedron. At first glance they appear to be empty and we are inclined to identify these as unfilled interstices in the structure. However, it is easy to show geometrically that the center of gravity of each of these irregular tetrahedral lies *outside* of the tetrahedral volume. In fact, the center of gravity of each tetrahedron is located precisely at the center of the 90° rhombohedron shown in Fig. I.2-4a, coincident with the position occupied by the central cation. But upon further consideration, we realize that this result is merely a demonstration that in CsCl, the interstices in the structure are neither tetrahedral nor octahedral; they are simple cubic (*sc*), 8-fold interstices. So, as one progresses up the CsCl structure along any $\overline{3}$ axis, the anion layers repeat in sequence *ACBACB...*, with spacing h between each pair of layers, while layers of *sc* interstices are

interleaved between the anion layers at heights $\frac{1}{2}h$ from each anion layer (this is shown in Fig. 1.2-4a). In CsCl all of the *sc* interstices are occupied by cations.[2]

Section I.2 References

[1]   International Committee for Diffraction Data, *Powder Diffraction File* (Joint Committee on Powder Diffraction Standards, Philadelphia, PA, 1974– present).

[2]   M. Ahtee, "Lattice Constants of Some Binary Alkali Halide Solid Solutions," Annales Academiae Scientiarum Fennicae, Series A6: *Physica* **313** 1–11 (1969).

[3]   T. Hahn, Ed. *International Tables for X-ray Crystallography*, Vol. A (D. Riedel, Dordrecht, Netherlands, 1983).

[4]   S. C. Abrahams and J. L. Bernstein, "Accuracy of an Automatic Diffractometer. Measurements of Sodium Chloride Structure Factors," *Acta Cryst.* **18** 926–932 (1965).

[5]   M. Blackman and I. H. Khan, "The Polymorphism of Thallium and Other Halides at Low Temperatures," *Proc. Phys. Soc., London* **77** 471–475 (1961).

---

[2] We should note that in this comparison of the CsCl and NaCl structures, we can at any time replace cations by anions and vice versa. The anion and cation sublattices in each of these structures are identical and interpenetrating, so that any discussion pertaining to the anion sublattice pertains to the cation sublattice as well.

II.1. Representative Crystal Structures: The Simplest Layering Motifs

Consider a hypothetical metal-oxygen phase diagram with the following solid-state oxidation sequence:

M   : M_2O :   MO   : MO_2 (MO_0: $MO_{0.5}$: MO_1: MO_2),

where M represents the metal species and O is oxygen. The oxygen-to-metal ratio, O/M, varies in this sequence as follows:
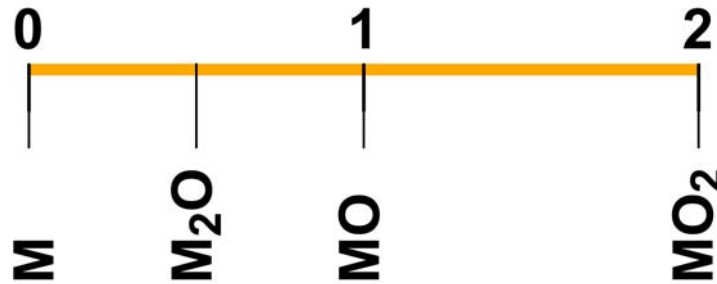
This sequence describes oxidation of the metal species M from monovalent (M^{1+}) to divalent (M^{2+}) to tetravalent (M^{4+}).[1] There are numerous examples of crystalline compounds that can be described by the compositions in this oxidation sequence. Moreover, a variety of crystal structures are associated with each composition (polymorphism). But for the purpose of this discussion, we choose to select structures for each composition that are *representative*. By representative, we mean that materials describable by the stoichiometries listed in this sequence are often (if not predominately) characterized by our selected structures.

We assign the following crystal structures to the compositions in our oxidation sequence:

M   the classic, *face-centered cubic* (*fcc*) structure;

M_2O the *antifluorite* structure;

MO   the *rock salt* structure; and

MO_2 the *fluorite* structure.

---

[1] We do not consider here the trivalent (M^{3r}) cationic species beause the layering motifs in such compounds are more complicated. However, these structures will be considered in detail later in this report.

All of these structures are cubic and all belong to space group (S.G.) $Fm\bar{3}m$ (No. 225 in the International Tables for Crystallography [1]). The cubic unit cells for each structure are illustrated in Fig. II.1-1. In *fcc* M, there are four M atoms per unit cell (*u.c.*), located on special equipoint 4*a* (Wyckoff notation; fractional coordinates (0,0,0) + equivalent positions (EP)). In *rock salt* MO, there are four M atoms per *u.c.* at equipoint 4*a* and four O atoms per *u.c.* at special equipoint 4*b* (fractional coordinates $\left(\frac{1}{2},\frac{1}{2},\frac{1}{2}\right)$ + EP). In this description, we assume a metal atom occupies the origin of the *u.c.*; it is equally permissible to assign O and M to the 4*a* and 4*b* equipoints, respectively, so that oxygen is at the *u.c.* origin. Rock salt is merely two interpenetrating *fcc* sublattices: a cation (M) sublattice and an anion (O) sublattice. In fluorite MO_2, the metal sublattice remains *fcc*, while the interpenetrating oxygen sublattice is *simple cubic* (*sc*). There are four M atoms per *u.c.* located at equipoint 4*a* and eight O atoms per *u.c.* located at special equipoint 8*c* (fractional coordinates $\left(\frac{1}{4},\frac{1}{4},\frac{1}{4}\right)$ + EP). Finally, *antifluorite* M_2O is simply *fluorite* with the cation/anion roles reversed: four O atoms occupy equipoint 4*a* and eight M atoms occupy equipoint 8*c*. Here, the oxygen sublattice is *fcc*; the metal sublattice is *sc*.
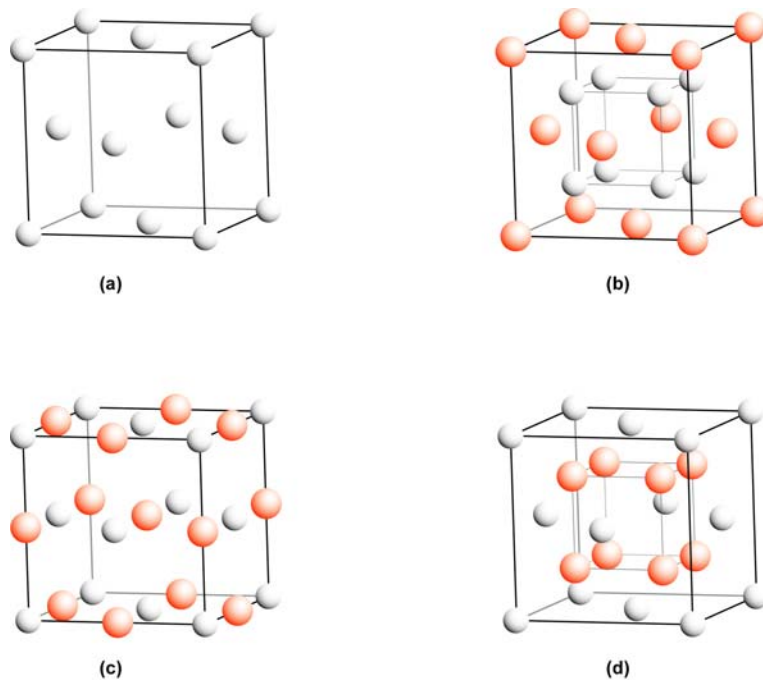
Figure. II.1-1. Perspective diagrams for the cubic unit cells in representative crystal structures: (a) *fcc* metal (M), (b) *antifluorite* (M_2O), (c) *rock salt* (MO), and (d) *fluorite* (MO_2). Metal (M) atoms/cations are represented by black/white spheres. Larger oxygen (O) anions are shown as red/white. Cube unit cell (*u.c.*) edges are of length a_{cube}.

The most convenient way to describe atom layer sequences in these crystal structures is to plot the sequence of atom bearing (and empty) planes in each *u.c.* normal to any one of the cube axes. This is illustrated in Fig. II.1-2 for our hypothetical oxidation sequence.
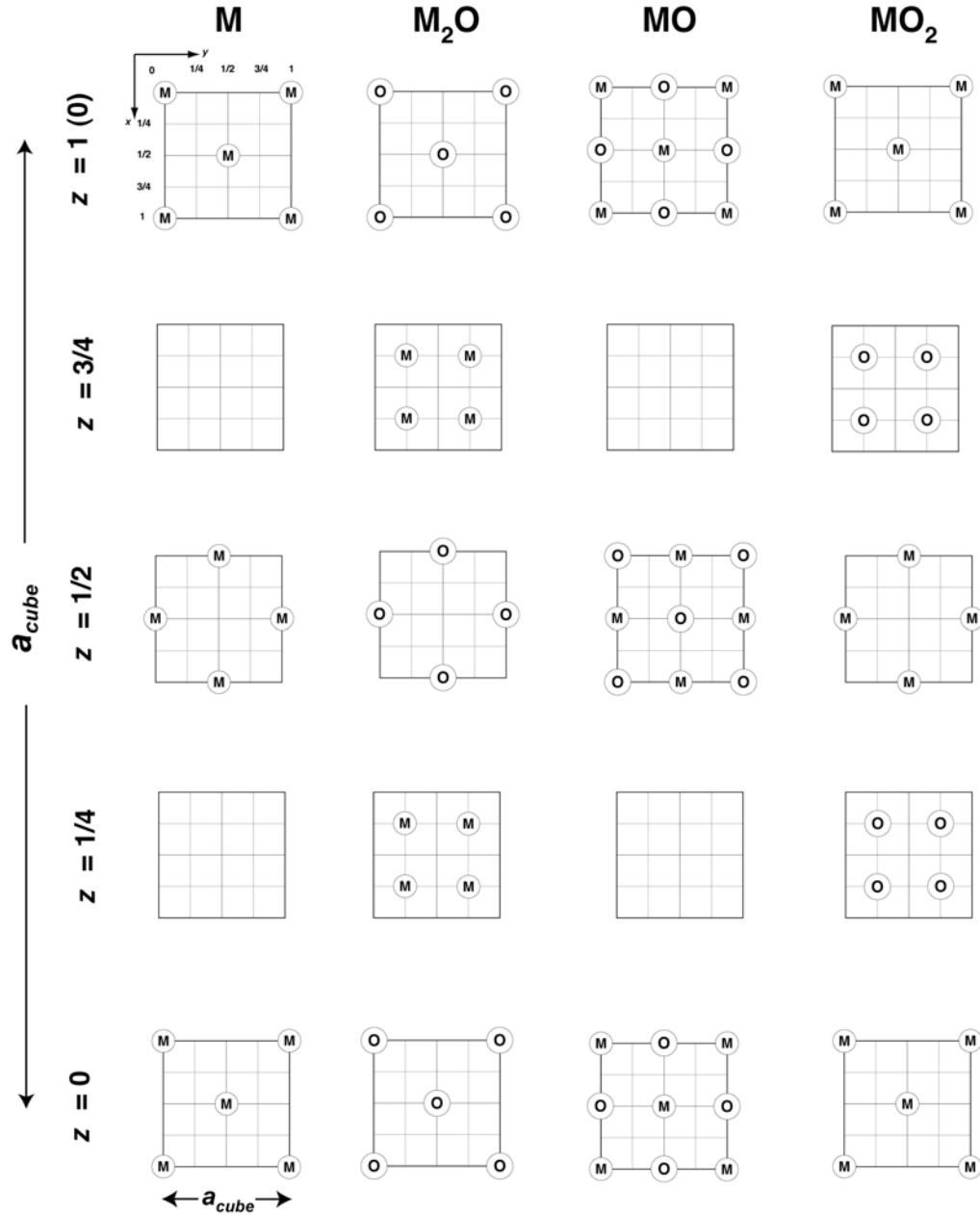
Figure II.1-2. Layer stacking diagrams along the [001] cubic crystallographic axes for representative crystal structures: *fcc* metal (M), *antifluorite* (M_2O), *rock salt* (MO), and *fluorite* (MO_2). Diagrams show planar sections of the unit cells perpendicular to <001> for each structure. Metal cations are labeled "M" and oxygen anions are labeled "O." Diagrams are intended to be read from the bottom up, from unit cell height $z = 0$ to $z = 1$. The edges of the square cells in the stacking diagrams are each of length a_{cube}, where a_{cube} is the cubic *u.c.* length.

Based on Fig. II.1-2, we have the following stacking sequences along any cube axis that describe our representative crystal structures:

fcc M: M M M M . . .

antifluorite M_2O: O M O M . . .

rock salt MO: (MO) (MO) (MO) . . .

fluorite MO_2:   M O M O . . .

where M represents a pure metal layer, O a pure oxygen layer, and (MO) a mixed metal/oxygen layer. The layer sequences described here and illustrated in Fig. II.1-2 represent accurate descriptions of our representative crystal structures. However, they fail to provide physical insight as to how structure can affect properties. Our representative structures all possess *pseudo-close-packed* atomic arrangements.[2] Three-dimensional close-packed atomic arrangements of atoms include *fcc* (also referred to as *cubic close-packed,* or *ccp*) as well as *hexagonal close-packed* (*hcp*) stacking of atoms. In such materials, the most useful layer descriptions involve stacking sequences along axes normal to the so-called *close-packed* planes. Close-packed planes often readily relate to fundamental physical properties. Consider, for instance, deformation mechanisms in pure *fcc* metals (M). Slip in *fcc* materials occurs along close-packed {111} planes, not on cube {100} planes. Similarly, slip in *hcp* materials is often confined to close-packed {0001} planes. In addition, magnetic properties in pseudo-close-packed oxides are often best understood by considering cation spin arrangements in close-packed crystallographic planes.

This said, it is advantageous to transform the layer sequence descriptions for our crystal structures from cube planes to pseudo-close-packed planes. This is accomplished through a cube-to-rhombohedral *u.c.* transformation. The relationship between these cells for an *fcc* metal is shown in Fig. II.1-3. For convenience, we also elect to describe our rhombohedral structures using hexagonal axes. A hexagonal *u.c.* is three times the volume of a rhombohedral, *primitive u.c.* (compare Fig. II.1-3a with Fig. II.1-3b). Figure

---

[2] We use the term *pseudo-close-packed* because the atoms in these layers may not actually touch. For instance, the M atoms in {111} cation planes in MO rock salt and MO_2 fluorite do not contact one another. However, they do form the same atomic arrangement as in {111} planes in a close-packed pure metal. Such atomic arrangements are often referred to as *eutactic* (O'Keefe and Hyde [2]).

II.1-4 shows the hexagonal cell layer atom sequences (following $(100)_{cubic}$-to-$(001)_{hexagonal}$ transformations) for the compositions in our representative crystal series. **Note:** Henceforth, we will refer to any hexagonal areal unit in a layer normal to the *c*-axis of a hexagonal *u.c.* as a *hexcell*.
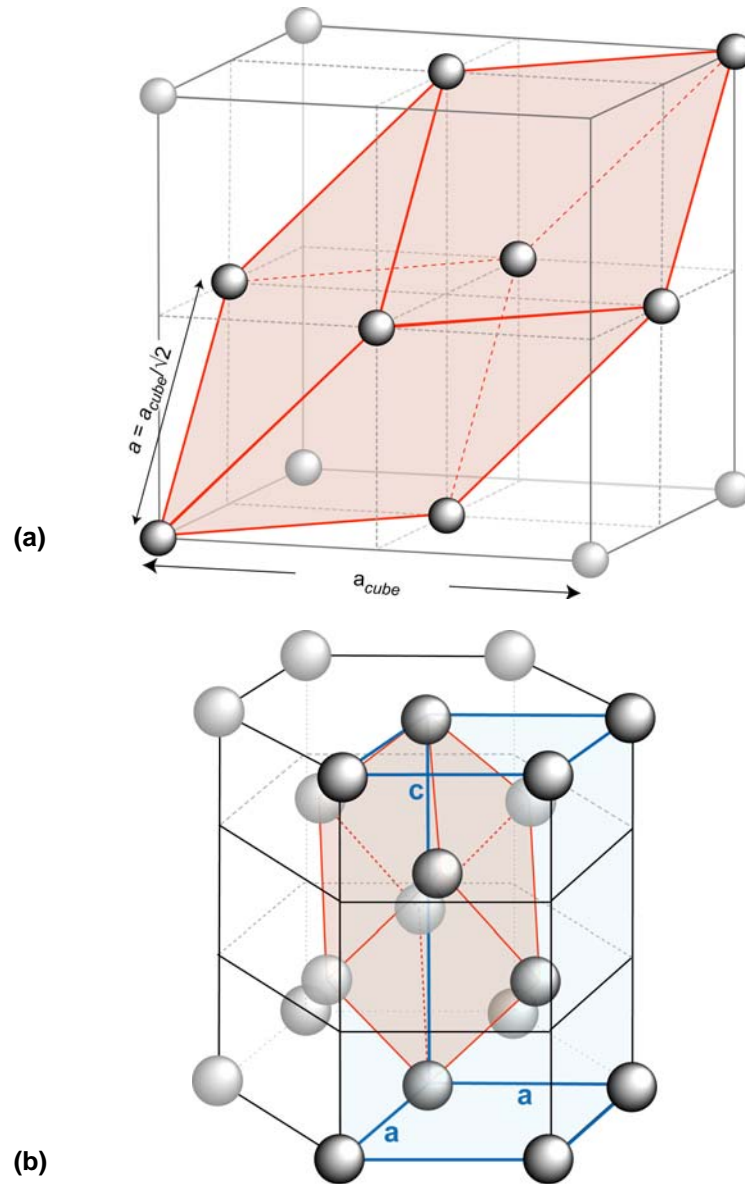
Figure II.1-3. (a) Cubic (gray) and rhombohedral (red) unit cells as they relate to a face-centered cubic (*fcc*) arrangement of atoms (M in this diagram). (b) The same rhombohedral *u.c.* (red) as in (a), shown here in relation to the corresponding hexagonal *u.c.* (shaded blue). Hexagonal *u.c.* axes, *a* and *c*, are also labeled.

Figure II.1-4 illustrates a number of important features of the atomic arrangements in our representative crystal structures. First, all atom bearing layers in these structures are atomically pure: no layers contain mixtures of M and O. Second, each atom bearing layer is simply a fully dense, triangular net, i.e., a *pseudo-close-packed* or *eutactic* arrangement of atoms. A triangular net of atoms is illustrated in Fig. II.1-5. Third, all atom bearing layers are equally dense: each atom bearing layer contains either one M or one O atom per *hexcell*. When the hexcell atomic density is one atom per hexcell, we will refer to this as *subdivision by 1^{sts}* of a triangular atom net. In Section III, we will introduce higher-order subdivisions of triangular atom nets. Finally, it is noteworthy that 12 layers along the *c*-axis of the hexagonal *u.c.* are necessary to fully describe the *fluorite* (and *antifluorite*) structures (versus three layers for *fcc* M and six layers for *rock salt*). We will return to this point later.

Based on Fig. II.1-4, we have the following stacking sequences along the *c*-axis of the hexagonal *u.c.*:

fcc M: M M M M M M M M M...

antifluorite M_2O: M M O M M O M M O...

rock salt MO: M O M O M O M O M O...

fluorite MO_2:   M O O M O O M O O...

As the oxidation state of the compound increases, the number of layers containing O triangular nets increases (O:M increases from 1:2 to 1:1 to 2:1 in these oxides). A summary of the important layer stacking conclusions (so far as the representative crystal structures presented in this introduction are concerned) is as follows: as the oxidation state of the metal cation progresses from M^{1+} to M^{2+} to M^{4+}, the layer stacking *motifs* along *c* that achieve the appropriate compound stoichiometries progress from MMO to MO to MOO. It is within this representative crystal structure framework that we will build the remainder of our layered atom story.
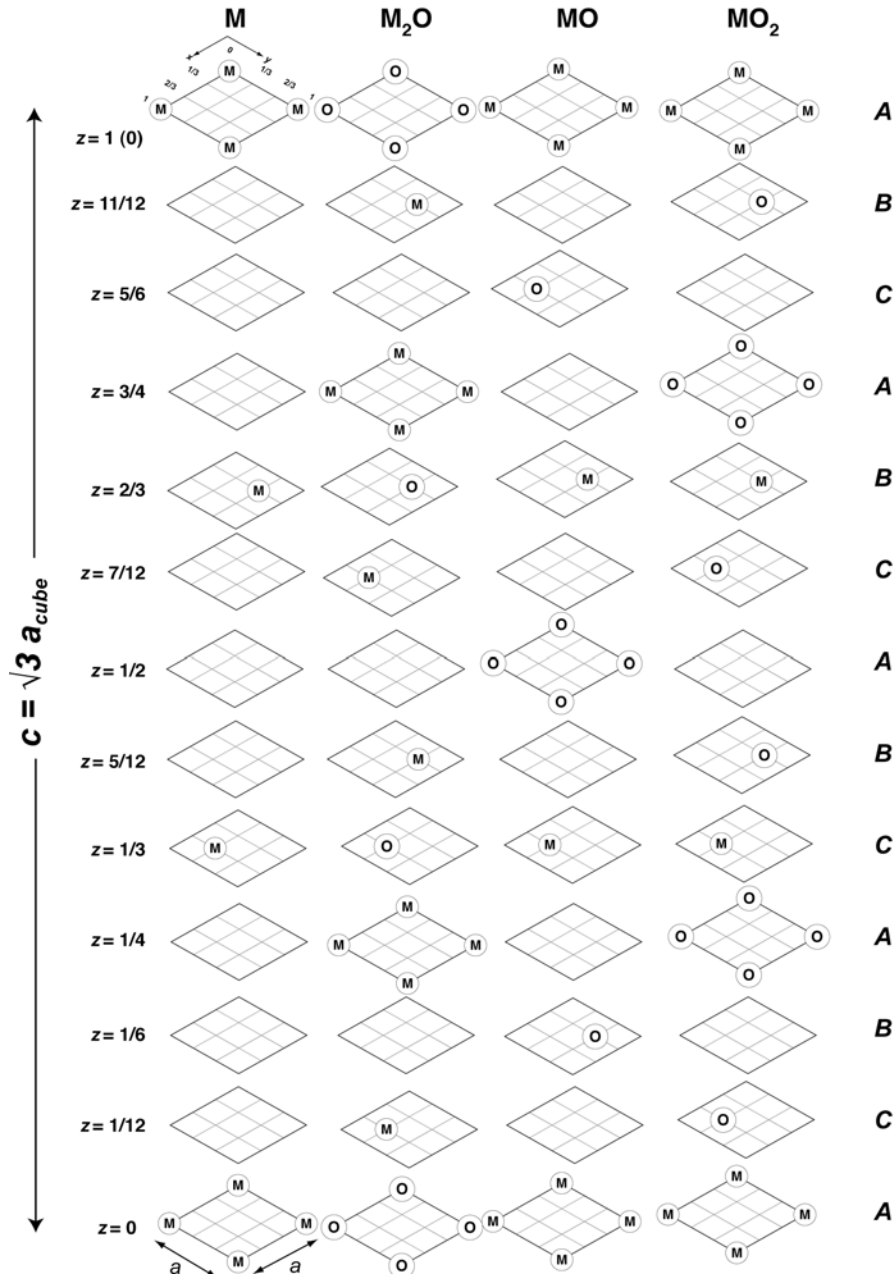
Figure II.1-4. Layer stacking diagrams corresponding to planes normal to the hexagonal c axis ($[001]_{hexagonal}$) for representative crystal structures: *fcc* metal (M), *antifluorite* (M_2O), *rock salt* (MO), and fluorite (MO_2). Diagrams show planar sections of the *u.c.*s perpendicular to c ($[001]_{hexagonal}$) for each structure. Metal cations are labeled "M" and oxygen anions are labeled "O." Diagrams are intended to be read from the bottom up, from *u.c.* height $z = 0$ to $z = 1$. The edges of the hexagonal cells in the stacking diagrams are each of length a, where here a is the hexagonal *u.c.* length ($\frac{1}{\sqrt{2}}$ of the cubic *u.c.* length, a_{cube}). The stacking sequence from $z = 0$ to $z = 1$ is equal to the hexagonal lattice parameter c ($c = \sqrt{3} \ a_{cube}$). The lateral registry of the layers is also denoted by $A, C, B, \ldots$ This is discussed in Section II.3.
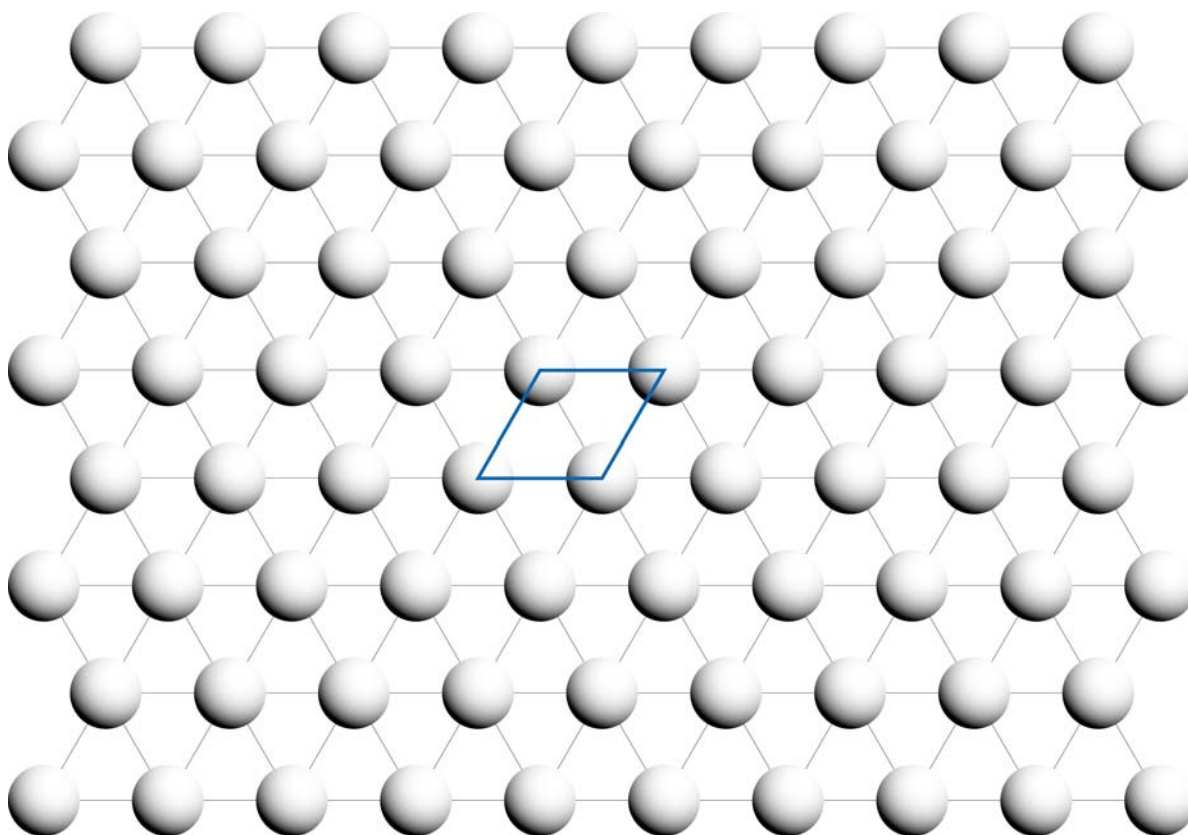
Figure II.1-5. A triangular net of atoms. This is described in the text as a *pseudo-close-packed*, or *eutactic* arrangement of atoms. The *u.c.* for this two-dimensional lattice is the parallelogram shown in blue. Note that there is one atom per *u.c.* located at fractional coordinates $(x, y) = (0,0)$. No subdivision of the *u.c.* is required to describe this lattice. In the text, this is referred to as *subdivision by 1^{sts}* of a triangular atom net.

Section II.1 References

[1]   T. Hahn, Ed. *International Tables for X-ray Crystallography*, Vol. A (D. Riedel, Dordrecht, Netherlands, 1983).

[2]   M. O. O'Keefe and B. G. Hyde, *Crystal Structures. I. Patterns and Symmetry* (Mineralogical Society of America, Washington, D.C., 1996).

II.2. Representative Crystal Structures: Crystallography

It is useful to consider detailed hexagonal *u.c.* crystallographic descriptions for our representative structures. We will base our crystal descriptions on the trigonal S.G. $R\overline{3}$ (No. 148 in the International Tables for Crystallography [1]). This is convenient because nearly all of the structures we will discuss later are accurately described in $R\overline{3}$. Using hexagonal axes, the general equivalent position (GEP) in $R\overline{3}$ has multiplicity 18 and is denoted by the Wyckoff symbol 18*f*. The symmetry operations associated with the GEP in $R\overline{3}$ are shown in Table II.2-1. Special equipoints in $R\overline{3}$ have multiplicities of 9, 6, and 3. If an atom is placed at arbitrary fractional coordinates (x, y, z) in the hexagonal *u.c.*, the action of the $R\overline{3}$ GEP produces 18 atoms in six layers along the c axis (three atoms per layer). Atoms placed on special equipoints produce fewer layers and fewer atoms per layer. **Note:** Hereafter, we will refer to the c-axis of the hexagonal *u.c.* as the $\overline{3}$ axis. In all but one of the structures that we describe in this report, the c-axis is coincident with a line which possesses $\overline{3}$ symmetry through the *u.c.* origin.

Table II.2-1. Symmetry operations for an atom placed at arbitrary *u.c.* fractional coordinates (x, y, z) in space group (S.G.) $R\overline{3}$ (hexagonal setting of the *u.c.*). These are the GEP operations for an atom placed at equipoint 18*f* (Wyckoff notation). The lattice translations for $R\overline{3}$ (hexagonal axes) are $+(0,0,0)$, $+\left(\frac{2}{3},\frac{1}{3},\frac{1}{3}\right)$, and $+\left(\frac{1}{3},\frac{2}{3},\frac{2}{3}\right)$. One obtains all equivalent positions (EP) in the *u.c.* for an atom situated at (x, y, z) by combining any (x, y, z) fractional coordinates with the GEP operations and the lattice translations.

The 6 Symmetry Operations in $R\overline{3}$		
(1) x, y, z	(2) $\overline{y}, x - y, z$	(3) $\overline{x} + y, \overline{x}, z$
(4) $\overline{x}, \overline{y}, \overline{z}$	(5) $y, \overline{x} + y, \overline{z}$	(6) $x - y, x, \overline{z}$

Using hexagonal axes in S.G. $R\overline{3}$, the crystallographic descriptions for our representative crystal structures are shown in Table II.2-2. It should be noted that based on the (x, y, z) fractional coordinates presented in Table II.2-2, the 3*a* and 3*b* equipoints each act to produce three fully dense, triangular atom nets per *u.c.* at fractional *u.c.* heights along z given by $z = 0, \frac{1}{3}, \frac{2}{3}$ and $z = \frac{1}{6}, \frac{1}{2}, \frac{5}{6}$, respectively, while the 6*c* equipoint (with $z = \frac{1}{4}$) acts

to produce six fully dense triangular atom nets per *u.c.*, at fractional *u.c.* heights along $z = \frac{1}{12}, \frac{3}{12}, \frac{5}{12}, \frac{7}{12}, \frac{9}{12}, \frac{11}{12}$. So if composition requires a 1:1 stoichiometry (M:O or O:M), one must place cations and anions on 3*a* and 3*b* equipoints, respectively (or vice versa). If composition dictates that the stoichiometry should be 2:1, one must place the majority element on 6*c* and the minority element on 3*a* (or 3*b*).[1] It should also be noted that the atomic density in all of the layers described here is 1 atom per hexcell (i.e., *subdivision by 1^{sts}* of a triangular atom net).

Table II.2-2. Atom positions in the hexagonal unit cell (*u.c.*) descriptions for representative crystal structures. Fractional coordinates (*x*, *y*, *z*) for the atoms refer to trigonal S.G. $R\bar{3}$ (hexagonal axes). Z is the number of formula units per hexagonal *u.c.* and EP stands for *equivalent positions*. These descriptions produce 12-layer atom stacking sequences along the $\bar{3}$ axes. The atomic density in all of the *u.c.* layers is one atom per hexcell (i.e., *subdivision by 1^{sts}* of a triangular atom net).

Structure	Z	Equipoint (Wyckoff notation)	Fractional coordinates for atoms (*x*, *y*, *z*) in the hexagonal *u.c.*
fcc M	3	M atom at 3*a*	(0,0,0) + EP
antifluorite M$_2$O	3	O atom at 3*a*	(0,0,0) + EP
		M atom at 6*c*	$\left(0,0,z=\frac{1}{4}\right)$ + EP
rock salt MO	3	M atom at 3*a*	(0,0,0) + EP
		O atom at 3*b*	$\left(0,0,\frac{1}{2}\right)$ + EP
fluorite MO$_2$	3	M atom at 3*a*	(0,0,0) + EP
		O atom at 6*c*	$\left(0,0,z=\frac{1}{4}\right)$ + EP

Section II.2 References

[1]   T. Hahn, Ed. *International Tables for X-ray Crystallography,* Vol. A (D. Riedel, Dordrecht, Netherlands, 1983).

---

[1]It is permissible to place the minority element on 3*b* but then there is no atom at the origin of the *u.c.* It is generally preferred to have the origin of the unit cell occupied, so we usually select 3*a* over 3*b* for our crystal structure descriptions. However, in the course of this report, we will present some examples wherein the origin of the *u.c.* is unoccupied. Both 3*a* and 3*b* have point symmetry $\bar{3}$.

II.3. Representative Crystal Structures: Layer Sequences

By examining the triangular atom nets associated with each layer in the structures shown in Fig. II.14, it is apparent that successive triangular nets are repeated but with lateral (x, y) translations from layer to layer. We will denote these (x, y) translations by the term *registry shift*. By examining the lateral positions of the triangular net atom patterns in Fig. II.1-4, it is apparent that registry shifts repeat themselves every three layers. In other words, layer stacking sequences in these structures can be described using the well-established *ABC* stacking notation (used, for example, to describe close-packed layer stacking in *fcc* materials). Table II.3-1 summarizes the layer stacking sequences for the structures presented in Table II.2-2 and Fig. II.1-4, using *ABC* stacking notation to describe the (x, y) registry shifts between adjacent layers.

The action of $R\overline{3}$ symmetry operations can also be understood with reference to Table II.2-2 and Fig. II.1-4. Assuming we denote the layer at height $z = 0$ as registry A, an A layer at any height z maps identically to the layer at corresponding height $–z$. This means that an A layer at height z is identical to the one at height $-z$ (the atom pattern and the pattern registry are the same). On the other hand, a B layer at any height z maps to a C layer at corresponding height $–z$ (and vice versa). Specifically, this means that the atom pattern in the B layer at height z is copied identically to the C layer at height $–z$, but the pattern registry is shifted from B to C. This describes completely $R\overline{3}$ symmetry operations in the hexagonal *u.c.* setting, regardless of the complexity of the crystal structure.

Though the 12-layer description for a structure such as *fcc* M in Table II.3-1 appears to be unnecessary (since most layers are empty), this description proves to be useful in discussions relating to interstitials. In Table II.3-1, each pair of M atom nets in *fcc* M surrounds three empty layers. But the heights of these layers correspond exactly to the layer heights along $\overline{3}$ where tetrahedral and octahedral interstices between nearest neighbor (*n.n.*) M layers are located. Octahedral interstices are located in the centermost portion of the three empty layers, while the two surrounding empty layers contain tetrahedral interstices. We will elaborate on this point in the next section.

Table II.3-1. Summary of the 12-layer atom stacking sequences along $\bar{3}$ in the oxide compounds presented in Table II.2-2. Columns are intended to be read from bottom ($z = 0$) to top ($z = 1$). The registry sequence for the layers in each structure is defined as *ACB* rather than *ABC* as described in the text. These registry definitions are arbitrary. However, the *ACB* description used here is consistent with layered structures discussed later in this report. The registry definitions used here are also shown in Fig. II.1-4.

Layer Height (z) (u.c. fraction)	Registry (*ACB* stacking)	M	M_2O	MO	MO_2
$\frac{12}{12}$ (1)	A	full triangular **M** net	full triangular **O** net	full triangular **M** net	full triangular **M** net
$\frac{11}{12}$	B	empty	full triangular **M** net	empty	full triangular **O** net
$\frac{10}{12}\left(\frac{5}{6}\right)$	C	empty	empty	full triangular **O** net	empty
$\frac{9}{12}\left(\frac{3}{4}\right)$	A	empty	full triangular **M** net	empty	full triangular **O** net
$\frac{8}{12}\left(\frac{2}{3}\right)$	B	full triangular **M** net	full triangular **O** net	full triangular **M** net	full triangular **M** net
$\frac{7}{12}$	C	empty	full triangular **M** net	empty	full triangular **O** net
$\frac{6}{12}\left(\frac{1}{2}\right)$	A	empty	empty	full triangular **O** net	empty
$\frac{5}{12}$	B	empty	full triangular **M** net	empty	full triangular **O** net
$\frac{4}{12}\left(\frac{1}{3}\right)$	C	full triangular **M** net	full triangular **O** net	full triangular **M** net	full triangular **M** net
$\frac{3}{12}\left(\frac{1}{4}\right)$	A	empty	full triangular **M** net	empty	full triangular **O** net
$\frac{2}{12}\left(\frac{1}{6}\right)$	B	empty	empty	full triangular **O** net	empty
$\frac{1}{12}$	C	empty	full triangular **M** net	empty	full triangular **O** net
$\frac{0}{12}$ (0)	A	full triangular **M** net	full triangular **O** net	full triangular **M** net	full triangular **M** net

II.4. Representative Crystal Structures: Coordination Polyhedra

It is also instructive to consider *coordination polyhedra* in relation to the $R\bar{3}$ layer stacking descriptions for our representative oxide compounds.[1] Take MO rock salt for instance. Cations and anions in rock salt are octahedrally coordinated by six *n.n.* ions of opposite sign. These octahedra are apparent in the stacking sequences described in Table II.3-1. Consider a cation M layer at $z = \frac{8}{12}$ with stacking registry *B*. This cation is surrounded by two equidistant anion O layers (heights $z = \frac{6}{12}, \frac{10}{12}$) but with stacking registries *A* and *C*. The result is a *regular* octahedron of O atoms surrounding each M atom in the *B* layer. This is illustrated in Fig.II.4-1. Figures II.4-1a and II.4-1b show an octahedral coordination polyhedron with respect to a cubic cell, while Fig. II.4-1c shows the same octahedron viewed down the $\bar{3}$ axis. In Fig. II.4-1b, the separation between cation M and *n.n.* anion O layers is $\overline{MO} = \frac{1}{\sqrt{6}}\, d$, where d is the *n.n.* atom spacing within each triangular atom net along $\bar{3}$. Finally, we note that a similar analysis to the discussion above reveals that *n.n.* M layers surrounding an O layer act to produce regular, octahedrally coordinated O anions.
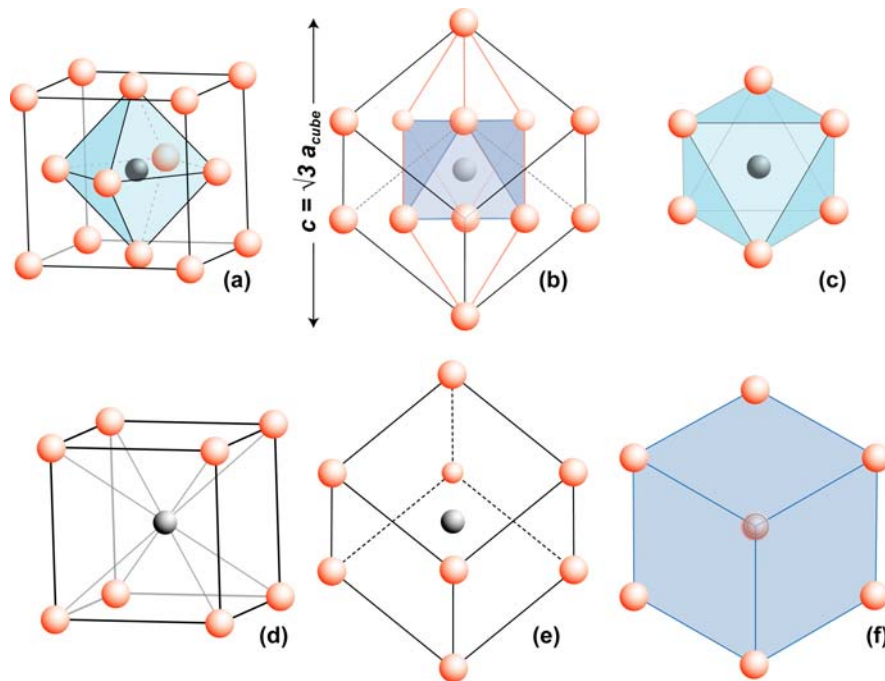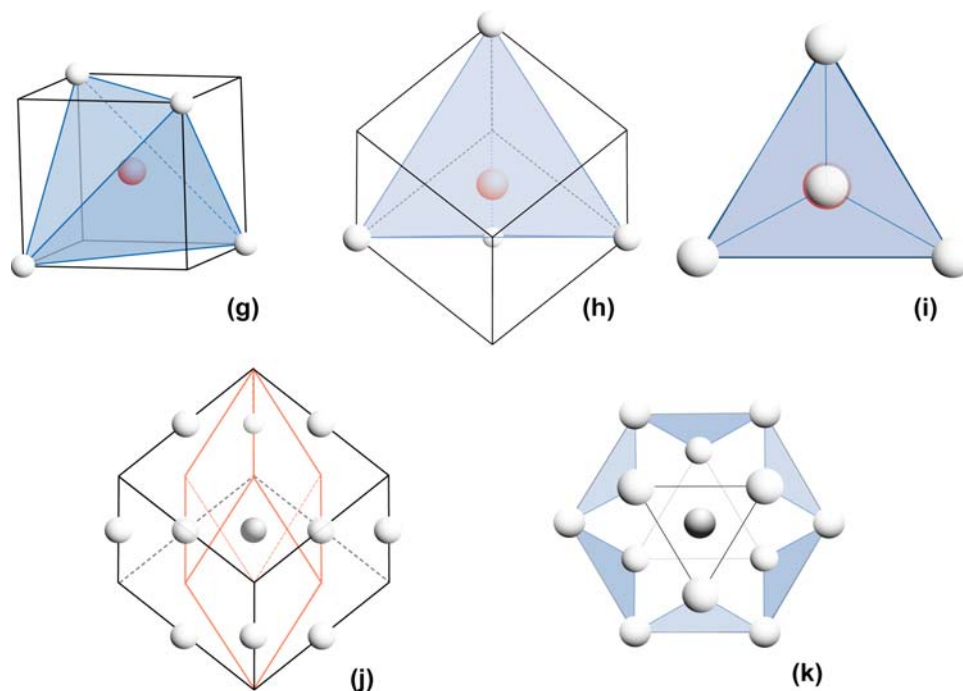
Figure II.4-1. Various views of coordination polyhedra characteristic of the representative crystal structures. M cations are shown as small black/white spheres. O anions are shown as larger red/white spheres. The three views in (a), (b), and (c) show octahedral (6-fold) coordination of an M cation by nearest neighbor (*n.n.*) O anions (octahedra shaded blue): (a) cube perspective; (b) view along a <112>-type cube direction such that $\bar{3}$ is in the plane of the diagram (triangular atom nets are seen edge-on in this projection); (c) view down the $\bar{3}$ axis (triangular atom nets lie in this projection). In (a–c), only the central *u.c.* cation is shown. These diagrams illustrate cation coordination in MO rock salt (anion coordination in rock salt is also octahedral; the same diagrams apply with the atom roles reversed). The three views in (d), (e), and (f) show simple cubic (8-fold) coordination of an M cation by *n.n.* O anions: (d) cube perspective; (e) view down a <112>-type cube direction such that $\bar{3}$ is in the plane of the diagram; (f) view down the $\bar{3}$ axis. Views (d–f) also illustrate cation coordination by *n.n.* anions in MO_2 fluorite. The three views (g), (h), and (i) show tetrahedral (4-fold) coordination of O anions by *n.n.* M cations (tetrahedra shaded blue): (g) cube perspective; (h) view down a <112>-type cube direction such that $\bar{3}$ is in the plane of the diagram; (i) view down the $\bar{3}$ axis. Then (g–i) illustrate anion coordination by *n.n.* cations in MO_2 fluorite (for antifluorite M_2O, the atom roles are reversed). Finally, for the sake of completeness, (j) shows a <112> view of an *fcc* metal *u.c.* (view down a <112>-type cube direction; $\bar{3}$ is in the plane of the diagram) (the *fcc* cell has been translated by a vector $\left[\frac{1}{2},0,0\right]$ so that it appears edge-centered), while (k) shows 12-fold *n.n.* M atom coordination of a central M atom in such an *fcc* structure (view down the $\bar{3}$ axis). The central *u.c.* cation in (j, k) is shaded for clarity. It should also be noted that the black cell edges in (b), (e), and (j), delineating the cube *u.c.* edges, equivalently represent the perimeters of 90° rhombohedral *u.c.*s. The red cell edges in (b) and (j) show the corresponding 60° rhombohedral primitive *u.c.*s for these structures.

Now consider atom coordination in MO_2 fluorite. The M cations in fluorite are 8-fold coordinated by *n.n.* O anions in simple cube (*sc*) geometry, while O anions are each surrounded by four *n.n.* M cations in regular, tetrahedral geometry. The *sc* coordination polyhedron for an M cation is shown in various views in Figs. II.4-1d, II.4-e, and II.4-1f. Note that along the body diagonal of the cube, two O layers are found on either side of the central M cation. These O layer pairs are apparent in the MO_2 layer sequence shown in Table II.3-1. For instance, for the M layer at height $z = \frac{8}{12}$, there are two successive O layers below M (at heights $z = \frac{7}{12}, \frac{5}{12}$) and two O layers above M (at heights $z = \frac{9}{12}, \frac{11}{12}$). These triangular O atom nets stack in such a way as to form perfect simple cubes around each M atom. It is important to note that the two outer O layers must have the same registry as the central M layer (*B* in this example) in order to produce the perfect *sc* coordination. On the other hand, the *n.n.* O layers must be of different registry from each other and from M (*C* and *A* in this example).

It is also important to observe that in viewing these simple cubes along $\bar{3}$, the distance from 1st to 2nd *n.n.* O layers ($\overline{OO}$) is twice that of the central M layer to the 1st *n.n.* O layer ($\overline{MO}$). This is precisely in accordance with layer spacings in a perfect *sc* coordination polyhedron (Fig. II.4-1e). Along a cube body diagonal of length $\sqrt{3}a_{cube}$ (where a_{cube} is the cube edge length), the central M atom divides the body diagonal in half, each half of length $\frac{\sqrt{3}a_{cube}}{2}$. But the triangular O atom nets project onto the body diagonal at fractions 0, $\frac{\sqrt{3}a_{cube}}{3}$, $\frac{2\sqrt{3}a_{cube}}{3}$ and 1 along the diagonal length. So the distance from the central M layer to the 1st *n.n.* O layers is $\frac{\sqrt{3}a_{cube}}{6}$, while the distance from 1st to 2nd *n.n.* O layers is $\frac{\sqrt{3}a_{cube}}{3}$. Thus, $\overline{OO} = 2\ \overline{MO}$. In Fig. II.4-1e, the separation between cation M and *n.n.* anion O layers is $\overline{MO} = \frac{1}{2\sqrt{6}}d$. Figure II.4-1f illustrates an *sc* polyhedron viewed down the $\bar{3}$ axis.

The tetrahedral coordination of each O atom by 4 *n.n.* M atoms can also be realized in the context of our layer stacking sequences. Take for instance an O layer at height $z = \frac{1}{12}$. The *n.n.* M layers occur at heights $z = \frac{0}{12}, \frac{4}{12}$. First, note that the M layers are not equidistant from the O layer. The upper M layer is three times more distant from O than the lower M layer (division by quarters). This is in accordance with tetrahedral stacking when one considers that the center of gravity of a tetrahedron is located $\frac{1}{4}$ of the distance

from the base of the tetrahedron to its apex. So the M layer at $z = \frac{0}{12}$ represents the base layer for tetrahedra surrounding each O atom in the O layer at $z = \frac{1}{12}$. Similarly, the M layer at $z = \frac{4}{12}$ represents the layer containing the apexes of the tetrahedra surrounding the same O atoms. The stacking registry shown in Table II.3-1 is also consistent with this description of tetrahedral coordination. The O layer considered here is registry C, while the M layer below is A and the M layer above is C. Thus, the triangular net A layer will produce triangles of M atoms beneath each O atom, while the M layer above stacks so that each O atom has an M atom directly above it. Figures II.4-1g and II.4-1h show a tetrahedral coordination polyhedron with respect to a cubic cell, while Fig. II.4-1i shows a tetrahedron viewed down the $\overline{3}$ axis. For completeness, Figs.II.4-1j and II.4-1k illustrate 12-fold coordination of an M atom in an *fcc* metal by *n.n.* M atoms.

We have described ion coordination in *fcc* M, MO rock salt, and MO_2 fluorite. The same analysis presented for MO_2 fluorite applies to M_2O antifluorite, only with the cation/anion roles reversed. This concludes our crystallography presentation for our representative crystal structures.

III.1. An Expanded Oxidation Sequence: Layering Motifs

Now, consider a new hypothetical metal-oxygen phase diagram with eight distinct solid-state oxide phases:

M_2O: MO: M_3O_4: M_2O_3: M_7O_{12}: M_4O_7: M_7O_{13}: MO_2

($MO_{0.5}$: $MO_{1.0}$: $MO_{1.33}$: $MO_{1.50}$: $MO_{1.71}$: $MO_{1.75}$: $MO_{1.86}$: $MO_{2.0}$).
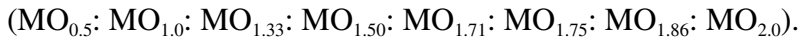
The oxygen-to-metal ratio, O/M, varies in this sequence as follows:
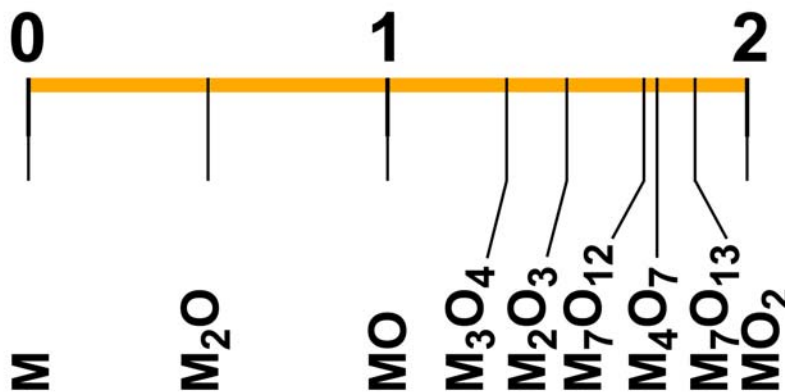
The average cation valence in this oxidation sequence varies as follows:

M^{1+} M^{2+} $M^{2.66+}$ M^{3+} $M^{3.43+}$ $M^{3.5+}$ $M^{3.71+}$ M^{4+}.

We have introduced five new compound stoichiometries in this oxide series. We will demonstrate that layer stacking models can be used to describe the crystal structures of compounds with each of these stoichiometries. Also, we will introduce examples of compounds of each stoichiometry that we can describe crystallographically in S.G. $R\bar{3}$.

The five new compounds occur between the divalent (M^{2+}) and the tetravalent (M^{4+}) oxidation states (MO *rock salt* and MO_2 *fluorite*, respectively). We demonstrated in the previous section that the layer stacking motif (along $\bar{3}$) for the divalent oxide is MO, while for the tetravalent oxide it is MOO, where M and O represent fully dense triangular atom nets. But what are the stacking motifs for the oxides with the intermediate oxidation states (between 2 and 4)? One possibility is as follows. As one progresses from cation valence 2 to valence 4, metal cations (M) are gradually removed from the material.

So beginning at MO *rock salt*, each oxide of higher oxidation state can be described as $M_{\frac{r}{s}}O$, where $\frac{r}{s}$ is the fractional metal deficiency compared with the 1:1 MO stoichiometry. This suggests that we may be able to describe the intermediate oxides as layered materials with layer stacking motifs $M_{\frac{r}{s}}O$, where O represents a fully dense triangular anion net, but $M_{\frac{r}{s}}$ represents a *partially filled* cation net.

It turns out that this supposition is obeyed in natural oxides for the $M^{2.66+}$ (M_3O_4) and M^{3+} (M_2O_3) compounds. However, for the higher oxidation states, $M^{3.43+}$ (M_7O_{12}), $M^{3.5+}$ (M_4O_7), and $M^{3.71+}$ (M_7O_{13}) (and sometimes M^{3+} [M_2O_3]), as we shall see later), nature adopts a layer stacking strategy with a surprising twist: the layer stacking motifs in these compounds are of the form $MO_{\frac{r}{s}}O_{\frac{u}{v}}$ where M represents a fully dense triangular cation net, but $O_{\frac{r}{s}}$ and $O_{\frac{u}{v}}$ represent *partially filled* anion nets (or fully dense if $r=s$ or $u=v$). When both $r=s$ and $u=v$, MO_2 *fluorite* is obtained with an MOO stacking motif, where all layers are fully dense, triangular atom nets. In the next section, we will examine partially filled triangular atom nets in detail.

III.2. An Expanded Oxidation Sequence: Partially Filled Triangular Atom Nets

So what do the partially filled atom layers introduced in the last section look like? This is where Iida's concepts become important. The Iida method [1] proceeds as follows:

(1) Determine the *fractional density*, $\frac{r}{s}$, of the partially filled layer.

(2) Subdivide a triangular atom net into subsets; the number of subdivisions should equal the denominator, *s*, of the fraction in step (1).

(3) Remove subsets from the triangular atom net. The number of subsets to remove is equal to *s–r*, where *r* and *s* are determined in step (1). The remaining lattice represents the structure of the partially filled layer.[1]

---

[1]We are aware of no structure in which *s–r* is other than 1. In other words, all *real* crystal structures are obtained by removing precisely one sublattice from any given Iida subdivision of a triangular atom net.

As an example of this method, consider the M_2O_3 sesquioxide compound in our series. According to the discussion in the previous section, we can employ an $M_{\frac{r}{s}}O$ layer stacking motif for this compound. If we rewrite the M_2O_3 compound stoichiometry as $M_{\frac{2}{3}}O_1$, the fractional density ($\frac{2}{3}$) of the partially filled layer is immediately apparent. So using Iida's method, we divide a triangular metal atom net into three sublattices (*subdivision by 3^{rds}*) and remove $3 - 2 = 1$ of the sublattices. The result is a $\frac{2}{3}$ dense cation layer that is known as the *honeycomb lattice*. This subdivision process is illustrated in Fig. III.2-1. The honeycomb cation lattice is combined with a fully dense triangular anion lattice to produce an $M_{\frac{2}{3}}O$ stacking motif. Upon stacking $M_{\frac{2}{3}}O$ motifs one on top of another, the sesquioxide crystal structure known as *corundum* is generated.[2]

(a)   (b)
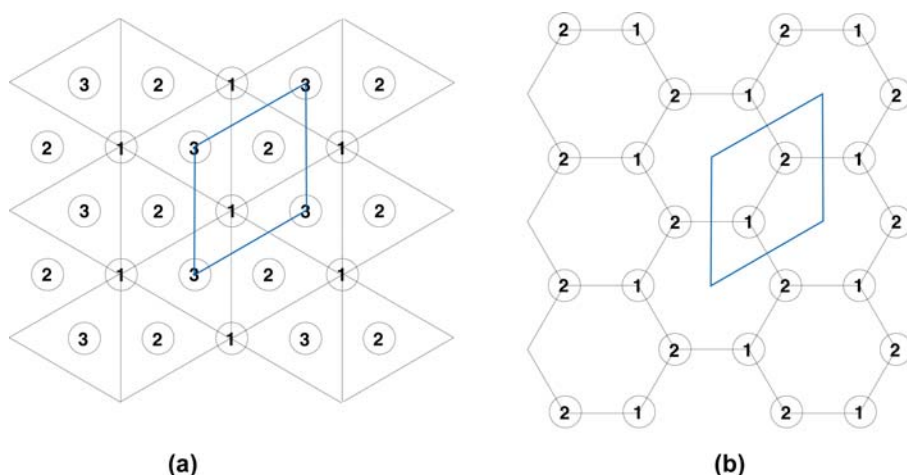
Figure III.2-1. The Iida method for subdivision of a triangular atom net into 3^{rds}. (a) A fully dense triangular atom net partitioned into three subdivisions labeled 1, 2, 3. Iida's partitioning rule dictates that 1st *n.n.* of any one atom in any subdivision must not belong to the same subdivision. Lines emanating from the central atom 1 in the diagram illustrate that the closest 1-type atoms to this central atom are 2nd *n.n.*s, as required by the Iida subdivision rule. The *u.c.* for this lattice is the parallelogram shown in blue. There are three atoms per *u.c.* located at fractional coordinates $(x,y) = (0,0), (\frac{1}{3}, \frac{2}{3}), (\frac{2}{3}, \frac{1}{3})$. (b) This diagram shows the atomic pattern that results upon removal of one sublattice from the triangular atom net in (a) (subdivision 3 in this example). The resulting atomic pattern is the well-known *honeycomb lattice*. It is also described in the text as a 6^3 Archimedean tiling. The honeycomb lattice consists of three atoms per *u.c.* at $(x,y) = (\frac{1}{3}, \frac{2}{3}), (\frac{2}{3}, \frac{1}{3})$ (i.e., $\frac{2}{3}$ dense).

---

[2] This is a somewhat simplified description of the process. As one stacks layers of cations and anions, one must shift the layers laterally so as to minimize Coulombic repulsion between like ions in adjacent layers (or even next-nearest layers). So there is a *registry shift* of the layer motifs that is not accounted for in the discussion presented up to this point. Registry shifts of our layer stacking motifs will be considered later in this report.

Iida indicated in his original paper that there are only two other ways to subdivide a triangular net (other than into 3^{rds}): *subdivision by 4^{ths} and 7^{ths}*. Figure III.2-2 illustrates *subdivision by 4^{ths}*. Upon removal of one of the four sublattices, the famous *kagome lattice* is produced. A $\frac{3}{4}$ dense cation kagome layer combined with a fully dense anion triangular net produces an $M_{\frac{3}{4}}O$ stacking motif. This is the fundamental stacking motif found in the M_3O_4 crystal structure known as *spinel*.[3] So, using *subdivision by 1^{sts}* (Section II), 3^{rds}, and 4^{ths} of triangular atom nets, we have identified characteristic layer stacking motifs for all of the compounds in our oxidation series except the M_7O_{12}, M_4O_7, and M_7O_{13} compounds. These are treated next.

(a)   (b)

Figure III.2-2. Iida's method for subdivision of a triangular atom net into 4^{ths}. (a) A fully dense triangular atom net partitioned into four subdivisions labeled 1–4. Lines emanating from the central atom 1 in the diagram show that the closest 1-type atoms to this central atom are 2nd *n.n.*s, in accordance with Iida's subdivision rule. The *u.c.* for this lattice is the parallelogram shown in blue. There are four atoms per *u.c.* located at fractional coordinates $(x, y) = (0,0), (\frac{1}{2},0), (0,\frac{1}{2}), (\frac{1}{2},\frac{1}{2})$. (b) This diagram illustrates the atomic pattern that results upon removal of one sublattice from the triangular atom net in (a) (subdivision 4 in this example). The resulting atomic pattern is the so-called *kagome lattice*. It is described in the text as a 3.6.3.6 Archimedean tiling. The kagome lattice consists of three atoms per *u.c.* at $(x, y) = (\frac{1}{2},0), (0,\frac{1}{2}), (\frac{1}{2},\frac{1}{2})$ (i.e., $\frac{3}{4}$ dense).

---

[3] Once again, because of registry shift issues, the discussion here is somewhat oversimplified. Other discrepancies with this simplified description are discussed later in this report.

Figure III.2-3 illustrates Iida's *subdivision by 7^{ths}* of a triangular atom net. Iida wrote in his original paper that "[this] subdivision is rather artificial." But to the contrary, we have determined that this subdivision is a ubiquitous feature observed in many complex oxides. In fact, using this subdivision we can model quite elegantly two of the compounds in our series as layered structures: the M_7O_{12} and M_7O_{13} compounds. According to the discussion in the previous section, layering in these higher oxidation state compounds can be described using $MO_{\frac{r}{s}}O_{\frac{u}{v}}$ layer motifs. The atom pattern for the partially filled oxygen layers is obtained using the *subdivision by 7^{ths}* method (Fig. III.2-3). One of seven triangular net sublattices shown in Fig. III.2-3a is removed so as to generate the $\frac{6}{7}$ dense atomic pattern as shown in Fig. III.2-3b. This atomic pattern has a name: it is a *$3^4.6$ Archimedean tiling*.[4] If we combine a fully dense M cation triangular net with two successive $3^4.6$ Archimedean tiling O anion nets, we produce an $MO_{\frac{6}{7}}O_{\frac{6}{7}}$ layer stacking motif. Upon stacking $MO_{\frac{6}{7}}O_{\frac{6}{7}}$ motifs one on top of another, we produce the crystal structure for the M_7O_{12} compound in our oxidation series. Adding slightly more oxygen to the mix, if we combine a fully dense M cation triangular net with one O anion $3^4.6$ Archimedean tiling and one fully dense O anion triangular net, we generate an $MO_{\frac{6}{7}}O$ layer stacking motif. Upon stacking $MO_{\frac{6}{7}}O$ motifs one on top of another, we produce the crystal structure for the M_7O_{13} compound in our oxidation series. To be more precise, to produce the M_7O_{13} crystal structure, nature combines two motifs sequentially; namely, $MO_{\frac{6}{7}}O$ and $MOO_{\frac{6}{7}}$. So the actual layering motif for M_7O_{13} is $MOO_{\frac{6}{7}}MO_{\frac{6}{7}}O$. In this way, each metal layer is always surrounded by two oxygen layers of like density. With this we have described all of the compounds in our oxidation series but one.

The remaining compound is M_4O_7. Here again, nature adopts an $MO_{\frac{r}{s}}O_{\frac{u}{v}}$ layer motif strategy but this time using Iida's *subdivision by 4^{ths}*. In this case, $\frac{3}{4}$ dense O kagome layers are mixed with equal numbers of fully dense O triangular nets and fully dense M triangular nets. The fundamental layering motif is $MO_{\frac{3}{4}}O$. But as with M_7O_{13}, nature

---

[4]An Archimedean tiling is a two-dimensional pattern made from one or more regular, convex polygons (such as triangles, squares, pentagons, hexagons, etc.) but with only one kind of vertex (a vertex is where several polygon edges join at a point) (see, e.g. [2,3]). There exist precisely 11 distinct Archimedean tilings. Three are called *regular* tilings, i.e., made from only one type of N-gon (N=# of sides). The other 8 are called *semiregular* tilings, i.e., made from two or more different N-gons. In our case, the $3^4.6$ Archimedean tiling notation is short for 3.3.3.3.6. This describes the sequence of N-gons that are encountered as one progresses from N-gon to N-gon around a single vertex. Each vertex in our pattern consists of four sequential triangles followed by a hexagon around each vertex. The $3^4.6$ Archimedean tiling actually exists in two enantiomorphic forms (i.e., left- and right-handed forms that cannot be superimposed on their mirror images).

combines two motifs, $MO_{\frac{3}{4}}O$ and $MOO_{\frac{3}{4}}$, to produce $MOO_{\frac{3}{4}}MO_{\frac{3}{4}}O$, the actual layering motif for the compound M_4O_7. Upon stacking this motif one on top of another, one obtains the crystal structure of the M_4O_7 compound. This crystal structure is known as *pyrochlore*. We now have layer stacking motif descriptions for all eight compounds in our expanded oxidation sequence.

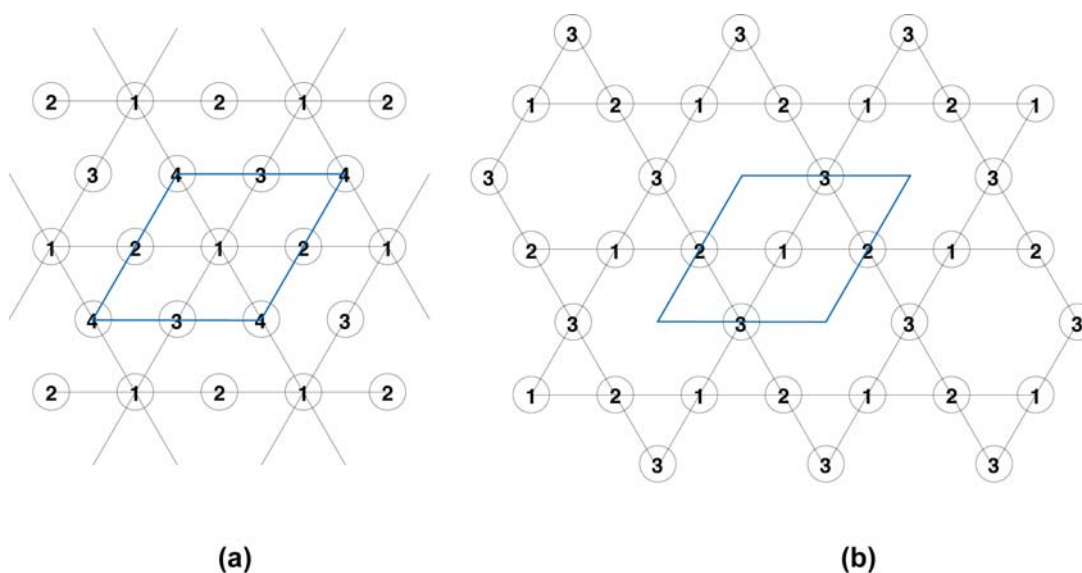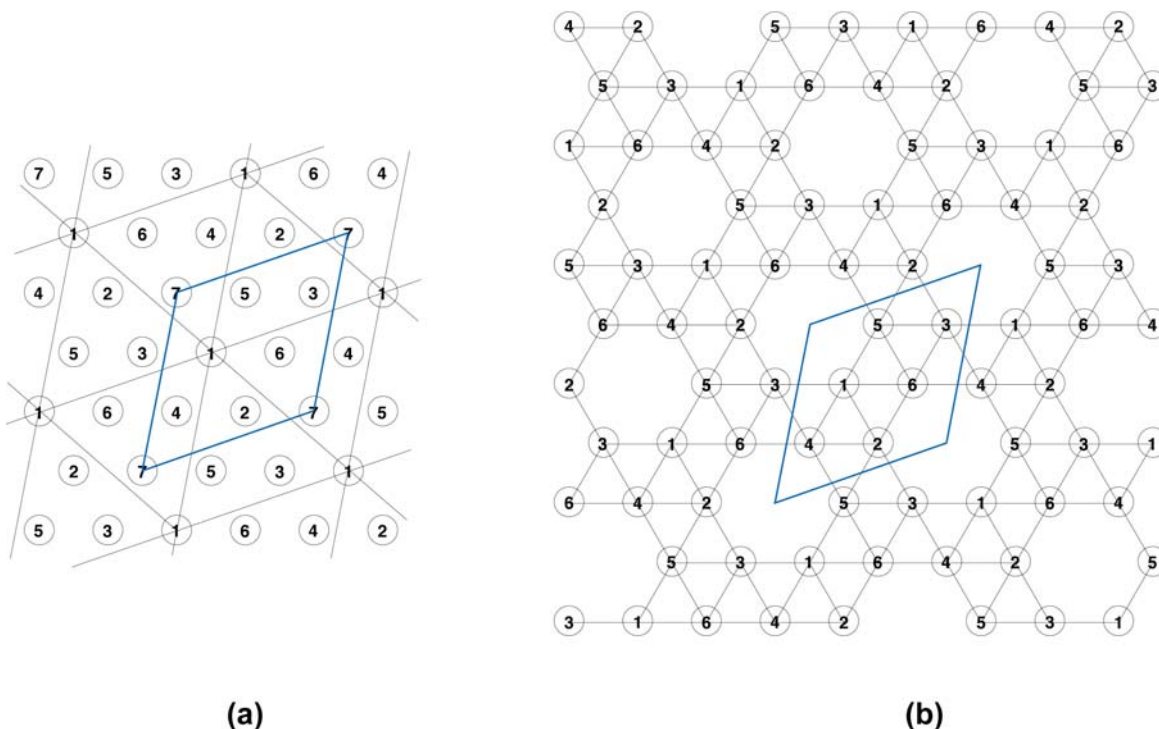**Figure III.2-3.** Iida's method for subdivision of a triangular atom net into 7^{ths}. (a) A fully dense triangular atom net partitioned into seven subdivisions labeled 1–7. Lines emanating from the central atom 1 in the diagram show that the closest 1-type atoms to this central atom are 4th *n.n.*s, which is consistent with Iida's subdivision rule. The *u.c.* for this lattice is the parallelogram shown in blue. There are seven atoms per *u.c.* located at fractional coordinates $(x,y) = (0,0), \left(\frac{3}{21}, \frac{9}{21}\right), \left(\frac{6}{21}, \frac{18}{21}\right), \left(\frac{9}{21}, \frac{6}{21}\right), \left(\frac{12}{21}, \frac{15}{21}\right), \left(\frac{15}{21}, \frac{3}{21}\right), \left(\frac{18}{21}, \frac{12}{21}\right)$. (b) This diagram illustrates the atomic pattern that results upon removal of one sublattice from the triangular atom net in (a) (subdivision 7 in this example). The resulting atomic pattern is equivalent to a $3^4.6$ Archimedean tiling. This tiling lattice consists of six atoms per *u.c.* at $(x,y) = \left(\frac{3}{21}, \frac{9}{21}\right), \left(\frac{6}{21}, \frac{18}{21}\right), \left(\frac{9}{21}, \frac{6}{21}\right), \left(\frac{12}{21}, \frac{15}{21}\right), \left(\frac{15}{21}, \frac{3}{21}\right), \left(\frac{18}{21}, \frac{12}{21}\right)$ (i.e., $\frac{6}{7}$ dense).

To complete the discussion in this section, it is worth noting that *all* of the atom layer patterns presented here qualify as Archimedean tilings. To summarize, these patterns are as follows:

- The *fully dense triangular net (subdivision by 1^{sts})*: a 3^6 (regular) Archimedean tiling (six triangles joining at each vertex)

- The *honeycomb lattice (subdivision by 3^{rds})*: a 6^3 (regular) Archimedean tiling (three hexagons joining at each vertex)

- The *kagome lattice (subdivision by 4^{ths})*: a (3.6.3.6) (semiregular) Archimedean tiling (a sequence triangle-hexagon-triangle-hexagon joining at each vertex)

- The *<unnamed> lattice (subdivision by 7^{ths})*: a $3^4.6$ (semiregular) Archimedean tiling (a sequence triangle-triangle-triangle-triangle-hexagon joining at each vertex)

Section III.2 References

[1]   S. Iida, "Layer Structures of Magnetic Oxides," *J. Phys. Soc. Japan* **12** (3) 222–233 (1957).

[2]   B. Grünbaum and G. C. Shepard, *Tilings and Patterns: An Introductio*n (W. H. Freeman and Company, New York, 1989).

[3]   M. O. O'Keefe and B. G. Hyde, *Crystal Structures. I. Patterns and Symmetry* (Mineralogical Society of America, Washington, D.C., 1996).

III.3. An Expanded Oxidation Sequence: Crystallography

By analogy to the presentation in Section II.2, we can assign complete $R\bar{3}$ crystallographic descriptions to all of the compounds in our expanded oxidation sequence. Using hexagonal axes in S.G. $R\bar{3}$, the crystallographic descriptions for compounds ranging from M_2O_3 to MO_2 in our sequence are shown in Table III.3-1. The order of appearance of compounds in Table III.3-1 is the same as in the oxidation sequence introduced in Section III.1.

Table III.3-1. Atom positions in the hexagonal *u.c.* description for five compounds in our expanded oxidation sequence. Fractional coordinates (x, y, z) for the atoms refer to trigonal space group $R\bar{3}$ (hexagonal axes). As usual, M and O represent metal cations and oxygen anions, respectively, while V represents *vacancies* in the lattice. Z is the number of formula units per hexagonal *u.c.* These descriptions produce 24-layer atom stacking sequences along the $\bar{3}$ axes.

Structure	Z	Equipoint (Wyckoff notation) and Fractional Coordinates (x, y, z) for Atoms in the Hexagonal *u.c.*
M_2O_3	12	M(1) at 3a: $\left(0,0,\mathbf{0}\right)$ + EP M(2) at 9e: $\left(\frac{1}{2},0,\mathbf{0}\right)$ + EP M(3) at 3b: $\left(0,0,\frac{\mathbf{1}}{\mathbf{2}}\right)$ + EP M(4) at 9d: $\left(\frac{1}{2},0,\frac{\mathbf{1}}{\mathbf{2}}\right)$ + EP O(1) at 18f: $\left(\frac{1}{2},0,\frac{\mathbf{3}}{\mathbf{8}}\right)$ + EP O(2) at 18f: $\left(\frac{1}{2},0,\frac{\mathbf{1}}{\mathbf{8}}\right)$ + EP V(1) at 6c: $\left(0,0,\frac{\mathbf{3}}{\mathbf{8}}\right)$ + EP V(2) at 6c: $\left(0,0,\frac{\mathbf{1}}{\mathbf{8}}\right)$ + EP
M_7O_{12}	6	M(1) at 3a: $\left(0,0,\mathbf{0}\right)$ + EP M(2) at 18f: $\left(\frac{1}{7},\frac{3}{7},\mathbf{0}\right)$ + EP M(3) at 3b: $\left(0,0,\frac{\mathbf{1}}{\mathbf{2}}\right)$ + EP

Structure	Z	Equipoint (Wyckoff notation) and Fractional Coordinates (x, y, z) for Atoms in the Hexagonal $u.c.$
		M(4) at 18f: $\left(\frac{1}{7},\frac{3}{7},\mathbf{\frac{1}{2}}\right)$ + EP
		O(1) at 18f: $\left(\frac{1}{7},\frac{3}{7},\mathbf{\frac{3}{8}}\right)$ + EP
		O(2) at 18f: $\left(\frac{1}{7},\frac{3}{7},\mathbf{\frac{5}{8}}\right)$ + EP
		O(3) at 18f: $\left(\frac{1}{7},\frac{3}{7},\mathbf{\frac{1}{8}}\right)$ + EP
		O(4) at 18f: $\left(\frac{1}{7},\frac{3}{7},\mathbf{\frac{7}{8}}\right)$ + EP
		V(1) at 6c: $\left(0,0,\mathbf{\frac{3}{8}}\right)$ + EP
		V(2) at 6c: $\left(0,0,\mathbf{\frac{1}{8}}\right)$ + EP
pyrochlore M$_4$O$_7$	6	M(1) at 3a: $\left(0,0,\mathbf{0}\right)$ + EP
		M(2) at 9e: $\left(\frac{1}{2},0,\mathbf{0}\right)$ + EP
		M(3) at 3b: $\left(0,0,\mathbf{\frac{1}{2}}\right)$ + EP
		M(4) at 9d: $\left(\frac{1}{2},0,\mathbf{\frac{1}{2}}\right)$ + EP
		O(1) at 18f: $\left(\frac{1}{2},0,\mathbf{\frac{3}{8}}\right)$ + EP
		O(2) at 18f: $\left(\frac{1}{2},0,\mathbf{\frac{1}{8}}\right)$ + EP
		O(3) at 6c: $\left(0,0,\mathbf{\frac{3}{8}}\right)$ + EP
		V(1) at 6c: $\left(0,0,\mathbf{\frac{1}{8}}\right)$ + EP
M$_7$O$_{13}$	6	M(1) at 3a: $\left(0,0,\mathbf{0}\right)$ + EP
		M(2) at 18f: $\left(\frac{1}{7},\frac{3}{7},\mathbf{0}\right)$ + EP
		M(3) at 3b: $\left(0,0,\mathbf{\frac{1}{2}}\right)$ + EP
		M(4) at 18f: $\left(\frac{1}{7},\frac{3}{7},\mathbf{\frac{1}{2}}\right)$ + EP
		O(1) at 18f: $\left(\frac{1}{7},\frac{3}{7},\mathbf{\frac{3}{8}}\right)$ + EP

Structure	Z	Equipoint (Wyckoff notation) and Fractional Coordinates (x, y, z) for Atoms in the Hexagonal $u.c.$
		O(2) at 18f: $\left(\frac{1}{7},\frac{3}{7},\frac{5}{8}\right)$ + EP
		O(3) at 18f: $\left(\frac{1}{7},\frac{3}{7},\frac{1}{8}\right)$ + EP
		O(4) at 18f: $\left(\frac{1}{7},\frac{3}{7},\frac{7}{8}\right)$ + EP
		O(5) at 6c: $\left(0,0,\frac{3}{8}\right)$ + EP
		V(1) at 6c: $\left(0,0,\frac{1}{8}\right)$ + EP
fluorite MO$_2$ (4 atoms per hexcell) [Redundant unit cell: 8 times the unit cell volume for the fluorite structure description in Table II.2-2]	24	M(1) at 3a: $\left(0,0,0\right)$ + EP M(2) at 9e: $\left(\frac{1}{2},0,0\right)$ + EP M(3) at 3b: $\left(0,0,\frac{1}{2}\right)$ + EP M(4) at 9d: $\left(\frac{1}{2},0,\frac{1}{2}\right)$ + EP O(1) at 18f: $\left(\frac{1}{2},0,\frac{3}{8}\right)$ + EP O(2) at 18f: $\left(\frac{1}{2},0,\frac{1}{8}\right)$ + EP O(3) at 6c: $\left(0,0,\frac{3}{8}\right)$ + EP O(4) at 6c: $\left(0,0,\frac{1}{8}\right)$ + EP
fluorite MO$_2$ (7 atoms per hexcell) [Redundant unit cell: 14 times the unit cell volume for the fluorite structure description in Table II.2-2]	42	M(1) at 3a: $\left(0,0,0\right)$ + EP M(2) at 18f: $\left(\frac{1}{7},\frac{3}{7},0\right)$ + EP M(3) at 3b: $\left(0,0,\frac{1}{2}\right)$ + EP M(4) at 18f: $\left(\frac{1}{7},\frac{3}{7},\frac{1}{2}\right)$ + EP O(1) at 18f: $\left(\frac{1}{7},\frac{3}{7},\frac{3}{8}\right)$ + EP O(2) at 18f: $\left(\frac{1}{7},\frac{3}{7},\frac{5}{8}\right)$ + EP O(3) at 18f: $\left(\frac{1}{7},\frac{3}{7},\frac{1}{8}\right)$ + EP

Structure	Z	Equipoint (Wyckoff notation) and Fractional Coordinates (x, y, z) for Atoms in the Hexagonal $u.c.$
		O(4) at 18f: $\left(\frac{1}{7}, \frac{3}{7}, \frac{7}{8}\right)$ + EP
		O(5) at 6c: $\left(0, 0, \frac{3}{8}\right)$ + EP
		O(6) at 6c: $\left(0, 0, \frac{1}{8}\right)$ + EP

It is useful to consider separately two groups of compounds in Table III.3-1: Group (1) M_2O_3, M_4O_7, and 8-times redundant MO_2; and Group (2) M_7O_{12}, M_7O_{13}, and 14-times redundant MO_2. Group (1) compounds correspond to triangular atom net *subdivision by 4ths*, while the Group (2) compounds correspond to triangular atom net *subdivision by 7ths*. Atom position descriptions within a given group are nearly identical but for one exception: compared with the MO_2 structure, vacancies (V) replace oxygen (O) in the lower oxidation state compounds. Take for instance 14-times redundant MO_2. Imagine reducing this compound slightly to obtain stoichiometry M_7O_{13}. One can achieve this crystallographically if one replaces O(6) by V(1) at equipoint 6c. Similarly, if we continue to reduce M_7O_{13} down to M_7O_{12}, this is accomplished crystallographically by replacing more oxygen, O(5), with more vacancies, V(2), again at equipoint 6c. This describes the crystallographic relationship between the three compounds in Group (2). An analogous relationship exists between the compounds in Group (1).

III.4. An Expanded Oxidation Sequence: Layer Stacking Sequences

Based on the crystallographic descriptions provided in Table III.3-1, 24-layer atom stacking sequences for 8- and 14-times redundant MO_2 fluorite are shown in Tables III.4-1 and III.4-2, respectively. In Table III.4-1, the atom density for any hexcell in any layer along $\bar{3}$ is 4. In Table III.4-2, the atom density for any hexcell in any layer along $\bar{3}$ is 7.

Table III.4-1. S.G. $R\bar{3}$ 24-layer atom-stacking sequence description for the 8-times redundant *u.c.* of MO_2 fluorite (Table III.3-1). Fractional coordinates for atoms within each layer are shown in parentheses (x, y). In MO_2 fluorite, all layers along $\bar{3}$ are fully dense (four atoms/hexcell).

Layer Height (z) (*u.c.* fraction)	Registry (*ABC* stacking)	1st Equipoint in Each Layer	2nd Equipoint in Each Layer	3rd Equipoint in Each Layer
$\frac{25}{24}$	*B*	**O(1)** **18f** $\left(\frac{10}{21},\frac{2}{21}\right),\left(\frac{13}{21},\frac{11}{21}\right),\left(\frac{19}{21},\frac{8}{21}\right)$	**O(2)** **18f** $\left(\frac{1}{21},\frac{17}{21}\right),\left(\frac{4}{21},\frac{5}{21}\right),\left(\frac{16}{21},\frac{20}{21}\right)$	**O(5)** **6c** $\left(\frac{1}{3},\frac{2}{3}\right)$
$\frac{24}{24}$ (1)	*A*	**M(1)** **3a** $(0,0)$	**M(2)** **18f** $\left(\frac{3}{21},\frac{9}{21}\right),\left(\frac{6}{21},\frac{18}{21}\right),\left(\frac{9}{21},\frac{6}{21}\right),$ $\left(\frac{12}{21},\frac{15}{21}\right),\left(\frac{15}{21},\frac{3}{21}\right),\left(\frac{18}{21},\frac{12}{21}\right)$	
$\frac{23}{24}$	*C*	**O(1)** **18f** $\left(\frac{2}{21},\frac{13}{21}\right),\left(\frac{11}{21},\frac{19}{21}\right),\left(\frac{8}{21},\frac{10}{21}\right)$	**O(2)** **18f** $\left(\frac{5}{21},\frac{1}{21}\right),\left(\frac{17}{21},\frac{16}{21}\right),\left(\frac{20}{21},\frac{4}{21}\right)$	**O(5)** **6c** $\left(\frac{2}{3},\frac{1}{3}\right)$
$\frac{22}{24}\left(\frac{11}{12}\right)$	*(B)*	empty	empty	
$\frac{21}{24}\left(\frac{7}{8}\right)$	*A*	**O(3)** **18f** $\left(\frac{3}{21},\frac{9}{21}\right),\left(\frac{6}{21},\frac{18}{21}\right),\left(\frac{12}{21},\frac{15}{21}\right)$	**O(4)** **18f** $\left(\frac{9}{21},\frac{6}{21}\right),\left(\frac{15}{21},\frac{3}{21}\right),\left(\frac{18}{21},\frac{12}{21}\right)$	**O(6)** **6c** $(0,0)$
$\frac{20}{24}\left(\frac{5}{6}\right)$	*C*	**M(3)** **3a** $\left(\frac{2}{3},\frac{1}{3}\right)$	**M(4)** **18f** $\left(\frac{2}{21},\frac{13}{21}\right),\left(\frac{5}{21},\frac{1}{21}\right),\left(\frac{8}{21},\frac{10}{21}\right),$ $\left(\frac{11}{21},\frac{19}{21}\right),\left(\frac{17}{21},\frac{16}{21}\right),\left(\frac{20}{21},\frac{4}{21}\right)$	
$\frac{19}{24}$	*B*	**O(3)** **18f** $\left(\frac{10}{21},\frac{2}{21}\right),\left(\frac{13}{21},\frac{11}{21}\right),\left(\frac{19}{21},\frac{8}{21}\right)$	**O(4)** **18f** $\left(\frac{1}{21},\frac{17}{21}\right),\left(\frac{4}{21},\frac{5}{21}\right),\left(\frac{16}{21},\frac{20}{21}\right)$	**O(6)** **6c** $\left(\frac{1}{3},\frac{2}{3}\right)$
$\frac{18}{24}\left(\frac{3}{4}\right)$	*(A)*	empty	empty	

Layer Height (z) (u.c. fraction)	Registry (ABC stacking)	1st Equipoint in Each Layer	2nd Equipoint in Each Layer	3rd Equipoint in Each Layer
$\frac{17}{24}$	C	**O(1)** **18f** $\left(\frac{2}{21},\frac{13}{21}\right),\left(\frac{11}{21},\frac{19}{21}\right),\left(\frac{8}{21},\frac{10}{21}\right)$	**O(2)** **18f** $\left(\frac{5}{21},\frac{1}{21}\right),\left(\frac{17}{21},\frac{16}{21}\right),\left(\frac{20}{21},\frac{4}{21}\right)$	**O(5)** **6c** $\left(\frac{2}{3},\frac{1}{3}\right)$
$\frac{16}{24}\left(\frac{2}{3}\right)$	B	**M(1)** **3a** $\left(\frac{1}{3},\frac{2}{3}\right)$	**M(2)** **18f** $\left(\frac{1}{21},\frac{17}{21}\right),\left(\frac{4}{21},\frac{5}{21}\right),\left(\frac{10}{21},\frac{2}{21}\right),$ $\left(\frac{13}{21},\frac{11}{21}\right),\left(\frac{16}{21},\frac{20}{21}\right),\left(\frac{19}{21},\frac{8}{21}\right)$	
$\frac{15}{24}\left(\frac{5}{8}\right)$	A	**O(1)** **18f** $\left(\frac{3}{21},\frac{9}{21}\right),\left(\frac{6}{21},\frac{18}{21}\right),\left(\frac{12}{21},\frac{15}{21}\right)$	**O(2)** **18f** $\left(\frac{9}{21},\frac{6}{21}\right),\left(\frac{15}{21},\frac{3}{21}\right),\left(\frac{18}{21},\frac{12}{21}\right)$	**O(5)** **6c** $(0,0)$
$\frac{14}{24}\left(\frac{7}{12}\right)$	(C)	empty	empty	
$\frac{13}{24}$	B	**O(3)** **18f** $\left(\frac{10}{21},\frac{2}{21}\right),\left(\frac{13}{21},\frac{11}{21}\right),\left(\frac{19}{21},\frac{8}{21}\right)$	**O(4)** **18f** $\left(\frac{1}{21},\frac{17}{21}\right),\left(\frac{4}{21},\frac{5}{21}\right),\left(\frac{16}{21},\frac{20}{21}\right)$	**O(6)** **6c** $\left(\frac{1}{3},\frac{2}{3}\right)$
$\frac{12}{24}\left(\frac{1}{2}\right)$	A	**M(3)** **3a** $(0,0)$	**M(4)** **18f** $\left(\frac{3}{21},\frac{9}{21}\right),\left(\frac{6}{21},\frac{18}{21}\right),\left(\frac{9}{21},\frac{6}{21}\right),$ $\left(\frac{12}{21},\frac{15}{21}\right),\left(\frac{15}{21},\frac{3}{21}\right),\left(\frac{18}{21},\frac{12}{21}\right)$	
$\frac{11}{24}$	C	**O(3)** **18f** $\left(\frac{2}{21},\frac{13}{21}\right),\left(\frac{11}{21},\frac{19}{21}\right),\left(\frac{8}{21},\frac{10}{21}\right)$	**O(4)** **18f** $\left(\frac{5}{21},\frac{1}{21}\right),\left(\frac{17}{21},\frac{16}{21}\right),\left(\frac{20}{21},\frac{4}{21}\right)$	**O(6)** **6c** $\left(\frac{2}{3},\frac{1}{3}\right)$
$\frac{10}{24}\left(\frac{5}{12}\right)$	(B)	empty	empty	
$\frac{9}{24}\left(\frac{3}{8}\right)$	A	**O(1)** **18f** $\left(\frac{3}{21},\frac{9}{21}\right),\left(\frac{6}{21},\frac{18}{21}\right),\left(\frac{12}{21},\frac{15}{21}\right)$	**O(2)** **18f** $\left(\frac{9}{21},\frac{6}{21}\right),\left(\frac{15}{21},\frac{3}{21}\right),\left(\frac{18}{21},\frac{12}{21}\right)$	**O(5)** **6c** $(0,0)$
$\frac{8}{24}\left(\frac{1}{3}\right)$	C	**M(1)** **3a** $\left(\frac{2}{3},\frac{1}{3}\right)$	**M(2)** **18f** $\left(\frac{2}{21},\frac{13}{21}\right),\left(\frac{5}{21},\frac{1}{21}\right),\left(\frac{8}{21},\frac{10}{21}\right),$ $\left(\frac{11}{21},\frac{19}{21}\right),\left(\frac{17}{21},\frac{16}{21}\right),\left(\frac{20}{21},\frac{4}{21}\right)$	
$\frac{7}{24}$	B	**O(1)** **18f** $\left(\frac{10}{21},\frac{2}{21}\right),\left(\frac{13}{21},\frac{11}{21}\right),\left(\frac{19}{21},\frac{8}{21}\right)$	**O(2)** **18f** $\left(\frac{1}{21},\frac{17}{21}\right),\left(\frac{4}{21},\frac{5}{21}\right),\left(\frac{16}{21},\frac{20}{21}\right)$	**O(5)** **6c** $\left(\frac{1}{3},\frac{2}{3}\right)$
$\frac{6}{24}\left(\frac{1}{4}\right)$	(A)	empty	empty	

Layer Height (z) (*u.c.* fraction)	Registry (*ABC* stacking)	1st Equipoint in Each Layer	2nd Equipoint in Each Layer	3rd Equipoint in Each Layer
$\frac{5}{24}$	*C*	**O(3)** **18*f*** $\left(\frac{2}{21},\frac{13}{21}\right),\left(\frac{11}{21},\frac{19}{21}\right),\left(\frac{8}{21},\frac{10}{21}\right)$	**O(4)** **18*f*** $\left(\frac{5}{21},\frac{1}{21}\right),\left(\frac{17}{21},\frac{16}{21}\right),\left(\frac{20}{21},\frac{4}{21}\right)$	**O(6)** **6*c*** $\left(\frac{2}{3},\frac{1}{3}\right)$
$\frac{4}{24}\left(\frac{1}{6}\right)$	*B*	**M(3)** **3*a*** $\left(\frac{1}{3},\frac{2}{3}\right)$	**M(4)** **18*f*** $\left(\frac{1}{21},\frac{17}{21}\right),\left(\frac{4}{21},\frac{5}{21}\right),\left(\frac{10}{21},\frac{2}{21}\right),$ $\left(\frac{13}{21},\frac{11}{21}\right),\left(\frac{16}{21},\frac{20}{21}\right),\left(\frac{19}{21},\frac{8}{21}\right)$	
$\frac{3}{24}\left(\frac{1}{8}\right)$	*A*	**O(3)** **18*f*** $\left(\frac{3}{21},\frac{9}{21}\right),\left(\frac{6}{21},\frac{18}{21}\right),\left(\frac{12}{21},\frac{15}{21}\right)$	**O(4)** **18*f*** $\left(\frac{9}{21},\frac{6}{21}\right),\left(\frac{15}{21},\frac{3}{21}\right),\left(\frac{18}{21},\frac{12}{21}\right)$	**O(6)** **6*c*** $(0,0)$
$\frac{2}{24}\left(\frac{1}{12}\right)$	*(C)*	empty	empty	
$\frac{1}{24}$	*B*	**O(1)** **18*f*** $\left(\frac{10}{21},\frac{2}{21}\right),\left(\frac{13}{21},\frac{11}{21}\right),\left(\frac{19}{21},\frac{8}{21}\right)$	**O(2)** **18*f*** $\left(\frac{1}{21},\frac{17}{21}\right),\left(\frac{4}{21},\frac{5}{21}\right),\left(\frac{16}{21},\frac{20}{21}\right)$	**O(5)** **6*c*** $\left(\frac{1}{3},\frac{2}{3}\right)$
$\frac{0}{24}\left(0\right)$	*A*	**M(1)** **3*a*** $(0,0)$	**M(2)** **18*f*** $\left(\frac{3}{21},\frac{9}{21}\right),\left(\frac{6}{21},\frac{18}{21}\right),\left(\frac{9}{21},\frac{6}{21}\right),$ $\left(\frac{12}{21},\frac{15}{21}\right),\left(\frac{15}{21},\frac{3}{21}\right),\left(\frac{18}{21},\frac{12}{21}\right)$	
$\frac{\bar{1}}{24}$	*C*	**O(1)** **18*f*** $\left(\frac{2}{21},\frac{13}{21}\right),\left(\frac{11}{21},\frac{19}{21}\right),\left(\frac{8}{21},\frac{10}{21}\right)$	**O(2)** **18*f*** $\left(\frac{5}{21},\frac{1}{21}\right),\left(\frac{17}{21},\frac{16}{21}\right),\left(\frac{20}{21},\frac{4}{21}\right)$	**O(5)** **6*c*** $\left(\frac{2}{3},\frac{1}{3}\right)$

Table III.4-2. S.G. $R\bar{3}$ 24-layer atom stacking sequence description for the 14-times redundant unit cell of MO_2 fluorite (Table III.3-1). Fractional coordinates for atoms within each layer are shown in parentheses (x, y). In MO_2 fluorite, all layers along $\bar{3}$ are fully dense (seven atoms/hexcell).

Layer Height (z) $(u.c.$ fraction)	Registry $(ABC$ stacking)	1st Equipoint in Each Layer	2nd Equipoint in Each Layer	3rd Equipoint in Each Layer
$\frac{25}{24}$	B	**O(1)** **18f** $\left(\frac{10}{21},\frac{2}{21}\right),\left(\frac{13}{21},\frac{11}{21}\right),\left(\frac{19}{21},\frac{8}{21}\right)$	**O(2)** **18f** $\left(\frac{1}{21},\frac{17}{21}\right),\left(\frac{4}{21},\frac{5}{21}\right),\left(\frac{16}{21},\frac{20}{21}\right)$	**O(5)** **6c** $\left(\frac{1}{3},\frac{2}{3}\right)$
$\frac{24}{24}$ (1)	A	**M(1)** **3a** $(0,0)$	**M(2)** **18f** $\left(\frac{3}{21},\frac{9}{21}\right),\left(\frac{6}{21},\frac{18}{21}\right),\left(\frac{9}{21},\frac{6}{21}\right),$ $\left(\frac{12}{21},\frac{15}{21}\right),\left(\frac{15}{21},\frac{3}{21}\right),\left(\frac{18}{21},\frac{12}{21}\right)$	
$\frac{23}{24}$	C	**O(1)** **18f** $\left(\frac{2}{21},\frac{13}{21}\right),\left(\frac{11}{21},\frac{19}{21}\right),\left(\frac{8}{21},\frac{10}{21}\right)$	**O(2)** **18f** $\left(\frac{5}{21},\frac{1}{21}\right),\left(\frac{17}{21},\frac{16}{21}\right),\left(\frac{20}{21},\frac{4}{21}\right)$	**O(5)** **6c** $\left(\frac{2}{3},\frac{1}{3}\right)$
$\frac{22}{24}$ $\left(\frac{11}{12}\right)$	(B)	empty	empty	
$\frac{21}{24}$ $\left(\frac{7}{8}\right)$	A	**O(3)** **18f** $\left(\frac{3}{21},\frac{9}{21}\right),\left(\frac{6}{21},\frac{18}{21}\right),\left(\frac{12}{21},\frac{15}{21}\right)$	**O(4)** **18f** $\left(\frac{9}{21},\frac{6}{21}\right),\left(\frac{15}{21},\frac{3}{21}\right),\left(\frac{18}{21},\frac{12}{21}\right)$	**O(6)** **6c** $(0,0)$
$\frac{20}{24}$ $\left(\frac{5}{6}\right)$	C	**M(3)** **3a** $\left(\frac{2}{3},\frac{1}{3}\right)$	**M(4)** **18f** $\left(\frac{2}{21},\frac{13}{21}\right),\left(\frac{5}{21},\frac{1}{21}\right),\left(\frac{8}{21},\frac{10}{21}\right),$ $\left(\frac{11}{21},\frac{19}{21}\right),\left(\frac{17}{21},\frac{16}{21}\right),\left(\frac{20}{21},\frac{4}{21}\right)$	
$\frac{19}{24}$	B	**O(3)** **18f** $\left(\frac{10}{21},\frac{2}{21}\right),\left(\frac{13}{21},\frac{11}{21}\right),\left(\frac{19}{21},\frac{8}{21}\right)$	**O(4)** **18f** $\left(\frac{1}{21},\frac{17}{21}\right),\left(\frac{4}{21},\frac{5}{21}\right),\left(\frac{16}{21},\frac{20}{21}\right)$	**O(6)** **6c** $\left(\frac{1}{3},\frac{2}{3}\right)$
$\frac{18}{24}$ $\left(\frac{3}{4}\right)$	(A)	empty	empty	
$\frac{17}{24}$	C	**O(1)** **18f** $\left(\frac{2}{21},\frac{13}{21}\right),\left(\frac{11}{21},\frac{19}{21}\right),\left(\frac{8}{21},\frac{10}{21}\right)$	**O(2)** **18f** $\left(\frac{5}{21},\frac{1}{21}\right),\left(\frac{17}{21},\frac{16}{21}\right),\left(\frac{20}{21},\frac{4}{21}\right)$	**O(5)** **6c** $\left(\frac{2}{3},\frac{1}{3}\right)$
$\frac{16}{24}$ $\left(\frac{2}{3}\right)$	B	**M(1)** **3a** $\left(\frac{1}{3},\frac{2}{3}\right)$	**M(2)** **18f** $\left(\frac{1}{21},\frac{17}{21}\right),\left(\frac{4}{21},\frac{5}{21}\right),\left(\frac{10}{21},\frac{2}{21}\right),$ $\left(\frac{13}{21},\frac{11}{21}\right),\left(\frac{16}{21},\frac{20}{21}\right),\left(\frac{19}{21},\frac{8}{21}\right)$	

Layer Height (z) (*u.c.* fraction)	Registry (*ABC* stacking)	1st Equipoint in Each Layer	2nd Equipoint in Each Layer	3rd Equipoint in Each Layer
$\frac{15}{24}\left(\frac{5}{8}\right)$	*A*	**O(1)** **18f** $\left(\frac{3}{21},\frac{9}{21}\right),\left(\frac{6}{21},\frac{18}{21}\right),\left(\frac{12}{21},\frac{15}{21}\right)$	**O(2)** **18f** $\left(\frac{9}{21},\frac{6}{21}\right),\left(\frac{15}{21},\frac{3}{21}\right),\left(\frac{18}{21},\frac{12}{21}\right)$	**O(5)** **6c** $(0,0)$
$\frac{14}{24}\left(\frac{7}{12}\right)$	*(C)*	empty	empty	
$\frac{13}{24}$	*B*	**O(3)** **18f** $\left(\frac{10}{21},\frac{2}{21}\right),\left(\frac{13}{21},\frac{11}{21}\right),\left(\frac{19}{21},\frac{8}{21}\right)$	**O(4)** **18f** $\left(\frac{1}{21},\frac{17}{21}\right),\left(\frac{4}{21},\frac{5}{21}\right),\left(\frac{16}{21},\frac{20}{21}\right)$	**O(6) 6c** $\left(\frac{1}{3},\frac{2}{3}\right)$
$\frac{12}{24}\left(\frac{1}{2}\right)$	*A*	**M(3)** **3a** $(0,0)$	**M(4)** **18f** $\left(\frac{3}{21},\frac{9}{21}\right),\left(\frac{6}{21},\frac{18}{21}\right),\left(\frac{9}{21},\frac{6}{21}\right),$ $\left(\frac{12}{21},\frac{15}{21}\right),\left(\frac{15}{21},\frac{3}{21}\right),\left(\frac{18}{21},\frac{12}{21}\right)$	
$\frac{11}{24}$	*C*	**O(3)** **18f** $\left(\frac{2}{21},\frac{13}{21}\right),\left(\frac{11}{21},\frac{19}{21}\right),\left(\frac{8}{21},\frac{10}{21}\right)$	**O(4)** **18f** $\left(\frac{5}{21},\frac{1}{21}\right),\left(\frac{17}{21},\frac{16}{21}\right),\left(\frac{20}{21},\frac{4}{21}\right)$	**O(6)** **6c** $\left(\frac{2}{3},\frac{1}{3}\right)$
$\frac{10}{24}\left(\frac{5}{12}\right)$	*(B)*	empty	empty	
$\frac{9}{24}\left(\frac{3}{8}\right)$	*A*	**O(1)** **18f** $\left(\frac{3}{21},\frac{9}{21}\right),\left(\frac{6}{21},\frac{18}{21}\right),\left(\frac{12}{21},\frac{15}{21}\right)$	**O(2)** **18f** $\left(\frac{9}{21},\frac{6}{21}\right),\left(\frac{15}{21},\frac{3}{21}\right),\left(\frac{18}{21},\frac{12}{21}\right)$	**O(5)** **6c** $(0,0)$
$\frac{8}{24}\left(\frac{1}{3}\right)$	*C*	**M(1)** **3a** $\left(\frac{2}{3},\frac{1}{3}\right)$	**M(2)** **18f** $\left(\frac{2}{21},\frac{13}{21}\right),\left(\frac{5}{21},\frac{1}{21}\right),\left(\frac{8}{21},\frac{10}{21}\right),$ $\left(\frac{11}{21},\frac{19}{21}\right),\left(\frac{17}{21},\frac{16}{21}\right),\left(\frac{20}{21},\frac{4}{21}\right)$	
$\frac{7}{24}$	*B*	**O(1)** **18f** $\left(\frac{10}{21},\frac{2}{21}\right),\left(\frac{13}{21},\frac{11}{21}\right),\left(\frac{19}{21},\frac{8}{21}\right)$	**O(2)** **18f** $\left(\frac{1}{21},\frac{17}{21}\right),\left(\frac{4}{21},\frac{5}{21}\right),\left(\frac{16}{21},\frac{20}{21}\right)$	**O(5)** **6c** $\left(\frac{1}{3},\frac{2}{3}\right)$
$\frac{6}{24}\left(\frac{1}{4}\right)$	*(A)*	empty	empty	
$\frac{5}{24}$	*C*	**O(3)** **18f** $\left(\frac{2}{21},\frac{13}{21}\right),\left(\frac{11}{21},\frac{19}{21}\right),\left(\frac{8}{21},\frac{10}{21}\right)$	**O(4)** **18f** $\left(\frac{5}{21},\frac{1}{21}\right),\left(\frac{17}{21},\frac{16}{21}\right),\left(\frac{20}{21},\frac{4}{21}\right)$	**O(6)** **6c** $\left(\frac{2}{3},\frac{1}{3}\right)$
$\frac{4}{24}\left(\frac{1}{6}\right)$	*B*	**M(3)** **3a** $\left(\frac{1}{3},\frac{2}{3}\right)$	**M(4)** **18f** $\left(\frac{1}{21},\frac{17}{21}\right),\left(\frac{4}{21},\frac{5}{21}\right),\left(\frac{10}{21},\frac{2}{21}\right),$ $\left(\frac{13}{21},\frac{11}{21}\right),\left(\frac{16}{21},\frac{20}{21}\right),\left(\frac{19}{21},\frac{8}{21}\right)$	

III.4. An Expanded Oxidation Sequence: Layer Stacking Sequences

Layer Height (z) (u.c. fraction)	Registry (ABC stacking)	1st Equipoint in Each Layer	2nd Equipoint in Each Layer	3rd Equipoint in Each Layer
$\frac{3}{24}\left(\frac{1}{8}\right)$	A	**O(3)** **18f** $\left(\frac{3}{21},\frac{9}{21}\right),\left(\frac{6}{21},\frac{18}{21}\right),\left(\frac{12}{21},\frac{15}{21}\right)$	**O(4)** **18f** $\left(\frac{9}{21},\frac{6}{21}\right),\left(\frac{15}{21},\frac{3}{21}\right),\left(\frac{18}{21},\frac{12}{21}\right)$	**O(6)** **6c** $(0,0)$
$\frac{2}{24}\left(\frac{1}{12}\right)$	(C)	empty	empty	
$\frac{1}{24}$	B	**O(1)** **18f** $\left(\frac{10}{21},\frac{2}{21}\right),\left(\frac{13}{21},\frac{11}{21}\right),\left(\frac{19}{21},\frac{8}{21}\right)$	**O(2)** **18f** $\left(\frac{1}{21},\frac{17}{21}\right),\left(\frac{4}{21},\frac{5}{21}\right),\left(\frac{16}{21},\frac{20}{21}\right)$	**O(5)** **6c** $\left(\frac{1}{3},\frac{2}{3}\right)$
$\frac{0}{24}\,(0)$	A	**M(1)** **3a** $(0,0)$	**M(2)** **18f** $\left(\frac{3}{21},\frac{9}{21}\right),\left(\frac{6}{21},\frac{18}{21}\right),\left(\frac{9}{21},\frac{6}{21}\right),$ $\left(\frac{12}{21},\frac{15}{21}\right),\left(\frac{15}{21},\frac{3}{21}\right),\left(\frac{18}{21},\frac{12}{21}\right)$	
$\frac{\bar{1}}{24}$	C	**O(1)** **18f** $\left(\frac{2}{21},\frac{13}{21}\right),\left(\frac{11}{21},\frac{19}{21}\right),\left(\frac{8}{21},\frac{10}{21}\right)$	**O(2)** **18f** $\left(\frac{5}{21},\frac{1}{21}\right),\left(\frac{17}{21},\frac{16}{21}\right),\left(\frac{20}{21},\frac{4}{21}\right)$	**O(5)** **6c** $\left(\frac{2}{3},\frac{1}{3}\right)$

It is instructive to consider the layer sequences in these tables in more detail. Take for instance the 24 layers in the *8-times-redundant* fluorite MO_2 (Table III.4-1):

1. M(1) at 3a and M(2) at 9e combine to produce three layers at *u.c.* heights $z = 0, \frac{1}{3}, \frac{2}{3}$ with four cations/hexcell. The equipoint 3a acts to produce three layers with one atom/hexcell while 9e acts to produce three layers at the same heights with three atoms/hexcell. Together 3a and 9e produce three three fully dense, triangular cation nets.

2. M(3) at 3b and M(4) at 9d combine to produce three layers at *u.c.* heights $z = \frac{1}{6}, \frac{1}{2}, \frac{5}{6}$ with four cations/hexcell. The equipoint 3b acts to produce three layers with one atom/hexcell while 9d acts to produce three layers at the same heights with three atoms/hexcell. Together 3b and 9d produce three fully dense, triangular cation nets.

3. O(1) at 18f and O(3) at 6c combine to produce six layers at *u.c.* heights $z = \frac{\bar{1}}{24}, \frac{1}{24},\ \frac{7}{24}, \frac{9}{24},\ \frac{15}{24}, \frac{17}{24}$ with four anions/hexcell. The equipoint 18f acts to produce six layers with three atoms/hexcell while 6c acts to produce six layers at the same heights with one atom/hexcell. Together they produce six fully dense, triangular anion nets.

4. O(2) at 18f and O(4) at 6c combine to produce six layers at $u.c.$ heights $z = \frac{3}{24}, \frac{5}{24}, \quad \frac{11}{24}, \frac{13}{24}, \quad \frac{19}{24}, \frac{21}{24}$ with four anions/hexcell. The equipoint 18f acts to produce six layers with three atoms/hexcell while 6c acts to produce six layers at the same heights with one atom/hexcell. Together they produce six fully dense, triangular anion nets.

Based on this description, the resulting crystal structure is MO$_2$ fluorite. But if instead of oxygen, one were to place *vacancies* at $6c = \left(0, 0, \frac{1}{8}\right)$ (in other words, remove O(4) from the lattice), the M$_4$O$_7$ pyrochlore structure is obtained. In this case, O(2) $= \left(\frac{1}{2}, 0, \frac{1}{8}\right)$ at 18f acts alone to produce anion layers at heights $\frac{3}{24}, \frac{5}{24}, \quad \frac{11}{24}, \frac{13}{24}, \quad \frac{19}{24}, \frac{21}{24}$. The hexcells associated with each of these layers now contain only three atoms/hexcell. Relative to the fully dense cation and O(1)+O(3) anion layers, the O(2) anion layers are $\frac{3}{4}$ dense. Moreover, the atom pattern in each of the layers produced by O(2) is a *kagome lattice*! The resulting pyrochlore stacking motif along $\overline{3}$ is M$_{3^6}$O$_{3^6}$O$_{3.6.3.6}$M$_{3^6}$O$_{3.6.3.6}$O$_{3^6}$, where we have used the Archimedean tiling notation for the atom nets (3^6 represents a fully dense, *triangular net* while 3.6.3.6 represents a $\frac{3}{4}$ dense *kagome lattice*).

Now, let's introduce even more oxygen vacancies into the MO$_2$ structure. Remove both O(3) and O(4) from the *8-times-redundant* fluorite MO$_2$ structure (i.e., oxygen vacancies are placed at $6c = \left(0, 0, \frac{1}{8}\right)$ and $6c = \left(0, 0, \frac{3}{8}\right)$). In this case, we obtain the M$_2$O$_3$ sesquioxide crystal structure. Here, O(1) $= \left(\frac{1}{2}, 0, \frac{3}{8}\right)$ and O(2) $= \left(\frac{1}{2}, 0, \frac{1}{8}\right)$ act by themselves to produce anion layers at heights $\frac{\overline{1}}{24}, \frac{1}{24}, \quad \frac{7}{24}, \frac{9}{24}, \quad \frac{15}{24}, \frac{17}{24}$ and $\frac{3}{24}, \frac{5}{24}, \quad \frac{11}{24}, \frac{13}{24}, \quad \frac{19}{24}, \frac{21}{24}$, respectively. The hexcells associated with each of these layers now contain only three atoms/hexcell. Relative to the fully dense cation layers, the O(1) and O(2) layers are only $\frac{3}{4}$ dense. The atom pattern in each of these layers is a *3.6.3.6 kagome lattice*. The resulting M$_2$O$_3$ sesquioxide stacking motif along $\overline{3}$ is M$_{3^6}$O$_{3.6.3.6}$O$_{3.6.3.6}$.

So far, we have demonstrated the layer sequence relationship between the Group (1) structures discussed in the last section. We obtain a similarly elegant story when we compare and contrast the Group (2) structures: *14-times-redundant* MO$_2$ fluorite, M$_7$O$_{12}$ and M$_7$O$_{13}$. Based on the crystallographic descriptions for these compounds provided in Table III.3-1, the atom density in any fully dense hexcell along $\overline{3}$ is 7. For MO$_2$, the layer densities and stacking sequences shown in Table III.4-2 arise as follows:

1. M(1) at $3a$ and M(2) at $18f$ combine to produce three layers at *u.c.* heights $z = 0, \frac{1}{3}, \frac{2}{3}$ with seven cations/hexcell. The equipoint $3a$ acts to produce three layers with one atom/hexcell. M(2) at $18f = \left(\frac{1}{7}, \frac{3}{7}, 0\right)$ is a somewhat unusual action of the GEP. Instead of producing six layers with three atoms/hexcell, this particular GEP produces only three layers but with six atoms/hexcell. This is caused by the special z coordinate used here, $z = 0$. S.G. symmetry translations in $R\overline{3}$ only produce two additional heights, $z = \frac{1}{3}, \frac{2}{3}$. In any case, $3a$ and $18f$ together produce three fully dense, triangular cation nets.

2. M(3) at $3b$ and M(4) at $18f$ combine to produce three layers at *u.c.* heights $z = \frac{1}{6}, \frac{1}{2}, \frac{5}{6}$ with seven cations/hexcell. Once again, the equipoint $3a$ acts to produce three layers with one atom/hexcell. And again, M(4) at $18f = \left(\frac{1}{7}, \frac{3}{7}, \frac{1}{2}\right)$ acts as an unusual GEP. This GEP produces three layers with six atoms/hexcell due to the special z coordinate used here, $z = \frac{1}{2}$. S.G. symmetry translations in $R\overline{3}$ only produce two additional heights, $z = \frac{1}{6}, \frac{5}{6}$. In any case, $3b$ and $18f$ together produce three fully dense, triangular cation nets.

3. O(1) at $18f$, O(2) at $18f$, and O(5) at $6c$ combine to produce six layers at *u.c.* heights $z = \frac{\overline{1}}{24}, \frac{1}{24}, \frac{7}{24}, \frac{9}{24}, \frac{15}{24}, \frac{17}{24}$ with seven anions/hexcell. For both O(1) and O(2), the equipoint $18f$ acts to produce six layers with three atoms/hexcell while $6c$ acts to produce six layers at the same heights with one atom/hexcell. Together they produce six fully dense, triangular anion nets.

4. O(3) at $18f$, O(4) at $18f$, and O(6) at $6c$ combine to produce six layers at *u.c.* heights $z = \frac{3}{24}, \frac{5}{24}, \frac{11}{24}, \frac{13}{24}, \frac{19}{24}, \frac{21}{24}$ with seven anions/hexcell. For both O(3) and O(4), the equipoint $18f$ acts to produce six layers with three atoms/hexcell while $6c$ acts to produce six layers at the same heights with one atom/hexcell. Together they produce six fully dense, triangular anion nets.

Based on this description, the resulting crystal structure is MO_2 fluorite. But if instead of oxygen, we place *vacancies* at $6c = \left(0, 0, \frac{1}{8}\right)$ (in other words, remove O(6) from the lattice), we generate the M_7O_{13} structure. In this case, O(3) $= \left(\frac{1}{7}, \frac{3}{7}, \frac{1}{8}\right)$ and O(4) $= \left(\frac{1}{7}, \frac{3}{7}, \frac{7}{8}\right)$ at $18f$ act by themselves to produce anion layers at heights $\frac{3}{24}, \frac{5}{24}, \frac{11}{24}, \frac{13}{24}, \frac{19}{24}, \frac{21}{24}$. The hexcells associated with each of these layers now contain only six atoms/hexcell. Relative to the fully dense cation and O(1)+O(2)+O(5) anion

layers, the O(3)+O(4) anion layers are $\frac{6}{7}$ dense. Moreover, the atom pattern in each of the layers produced by O(3)+O(4) is a *$3^4.6$ Archimedean tiling*! Using the Archimedean tiling notation for the atom nets (3^6 represents a *fully dense triangular net* while $3^4.6$ represents a $\frac{6}{7}$ *dense Archimedean tiling*), the resulting M_7O_{13} stacking motif along $\overline{3}$ is $M_{3^6}O_{3^6}O_{3^4.6}M_{3^6}O_{3^4.6}O_{3^6}$.

Now, let's introduce yet more oxygen vacancies. Remove both O(5) and O(6) from the *14-times-redundant* fluorite MO_2 structure (i.e., oxygen vacancies are placed at $6c = \left(0,0,\frac{1}{8}\right)$ and $6c = \left(0,0,\frac{3}{8}\right)$). In this case, we obtain the M_7O_{12} crystal structure. Here, O(1) $= \left(\frac{1}{7},\frac{3}{7},\frac{3}{8}\right)$ and O(2) $= \left(\frac{1}{7},\frac{3}{7},\frac{5}{8}\right)$ act by themselves to produce anion layers at heights $\frac{\overline{1}}{24},\frac{1}{24},\quad\frac{7}{24},\frac{9}{24},\quad\frac{15}{24},\frac{17}{24}$ while O(3) $= \left(\frac{1}{7},\frac{3}{7},\frac{1}{8}\right)$ and O(4) $= \left(\frac{1}{7},\frac{3}{7},\frac{7}{8}\right)$ join to produce anion layers at heights $\frac{3}{24},\frac{5}{24},\quad\frac{11}{24},\frac{13}{24},\quad\frac{19}{24},\frac{21}{24}$. The hexcells associated with each of these layers now contain only six atoms/hexcell. Relative to the fully dense cation layers, the O(1)+O(2) and O(3)+O(4) anion layers are $\frac{6}{7}$ dense. The atom pattern in each of these layers is a *$3^4.6$ Archimedean tiling*. The resulting M_7O_{12} stacking motif along $\overline{3}$ is $M_{3^6}O_{3^4.6}O_{3^4.6}$. Thus, we've demonstrated the layer sequence relationships between the Group (2) structures.

The hexcell layer stacking sequences for all of the structures described in Table III.3-1 are summarized in Table III.4-3 and illustrated schematically in Figs. III.4-1 and III.4-2. Figure III.4-1 shows the hexcell templates used to generate the triangular atom net *subdivisions by 4^{ths}* and by *7^{ths}*. Figure III.4-2 shows the actual layer atom sequences for the structures from Table III.3-1. Twenty-four layers along $\overline{3}$ are used to describe each structure. By examining the layers for each structure, it is apparent that many layer atom patterns repeat but with registry shifts as discussed in Section II.3. By examining the lateral positions of the atom patterns in Fig. III.4-2, it is apparent that registry shifts repeat themselves every three layers. So, layer stacking sequences in these structures can once again be described using ABC stacking notation (as in Table II.3-1).

The layer stacking descriptions in Table III.4-3 and Fig. III.4-2 are doubly redundant along $\overline{3}$ for M_2O_3, M_7O_{12}, and the two MO_2 structures (i.e., the layer sequence in each of these structures repeats after 12 layers). We can remove this redundancy by redefining the atom positions in the respective unit cells. Alternative atom coordinates based on 12-layer descriptions for each of these structures are shown in Table III.4-4 (compare with

Table III.3-1). The MO_2 structures defined using the 12-layer description are alternatively 4-times and 7-times redundant. It is important to note that registry shift definitions are changed upon going from a 24- to a 12-layer description for these structures. In particular, the definitions of B and C are reversed. That is to say, using the layer patterns shown in Fig. III.4-2 (based on 24-layer stacking), the registry sequence in each 12-layer description is ACB rather than ABC. The two descriptions are physically identical. But when comparing the atom positions generated by the fractional coordinates given in Table III.3-1 versus Table III.4-4, one must be aware of this change in registry definitions. The layer stacking sequences corresponding to the crystal structure descriptions in Table III.4-4 are shown in Table III.4-5.

Once again, it is instructive to consider the layer sequences in these tables in more detail. Take for instance the 12 layers in the *7-times-redundant* fluorite MO_2 (Table III.4-4):

1. M(1) at 3*a* and M(2) at 18*f* combine to produce three layers at *u.c.* heights $z = 0, \frac{1}{3}, \frac{2}{3}$ with seven cations/hexcell. Equipoint 3a acts to produce three layers with one atom/hexcell. M(2) at $18f = \left(\frac{1}{7}, \frac{3}{7}, 0\right)$ is a somewhat unusual action of the GEP. Instead of producing six layers with three atoms/hexcell, this particular GEP produces only three layers, but with six atoms/hexcell. This is due to the special z coordinate used here, $z = 0$. S.G. symmetry translations in $R\overline{3}$ only produce two additional heights, $z = \frac{1}{3}, \frac{2}{3}$. In any case, 3*a* and 18*f* together produce three fully dense triangular cation nets.

2. O(1) at 18*f*, O(2) at 18*f*, and O(3) (or V(1)) at 6*c* combine to produce six layers at *u.c.* heights $z = \frac{1}{12}, \frac{3}{12}, \frac{5}{12}, \frac{7}{12}, \frac{9}{12}, \frac{11}{12}$ with seven anions/hexcell. For both O(1) and O(2), the equipoint 18*f* acts to produce six layers with three atoms/hexcell, while 6*c* acts to produce six layers at the same heights with one atom/hexcell. Together they produce six fully dense triangular atom nets.

But if one were to remove O(3) at 6*c*, a set of $\frac{6}{7}$ dense anion layers is produced at heights $z = \frac{1}{12}, \frac{3}{12}, \frac{5}{12}, \frac{7}{12}, \frac{9}{12}, \frac{11}{12}$. These layers are $3^4.6$ Archimedean tilings. The resulting structure is that of the M_7O_{12} oxides.

Similar analyses are left to the reader as an exercise of the actions of the equipoints used in the 12-layer descriptions for the 4-times redundant MO_2 structure and the M_2O_3 structure in Table III.4.4.

Table III.4-3. Summary of 24-layer atom-stacking sequences along $\bar{3}$ in the oxide compounds presented in this section and defined in Table III.3-1. Columns are intended to be read from bottom ($z = 0$) to top ($z = 1$).

Layer Height (z) (u.c. fraction)	Registry (ABC stacking)	M_2O_3	M_7O_{12}	M_4O_7	M_7O_{13}	MO_2 8-Times Redundant	MO_2 14-Times Redundant
$\frac{24}{24}$ (1)	A	$\frac{4}{4}$ full **M**	$\frac{7}{7}$ full **M**	$\frac{4}{4}$ full **M**	$\frac{7}{7}$ full **M**	$\frac{4}{4}$ full **M**	$\frac{7}{7}$ full **M**
$\frac{23}{24}$	C	$\frac{3}{4}$ kagome **O**	$\frac{6}{7}$ Arch. T. **O**	$\frac{4}{4}$ full **O**	$\frac{7}{7}$ full **O**	$\frac{4}{4}$ full **O**	$\frac{7}{7}$ full **O**
$\frac{22}{24}$ $\left(\frac{11}{12}\right)$	(B)	empty	empty	empty	empty	empty	empty
$\frac{21}{24}$ $\left(\frac{7}{8}\right)$	A	$\frac{3}{4}$ kagome **O**	$\frac{6}{7}$ Arch. T. **O**	$\frac{3}{4}$ kagome **O**	$\frac{6}{7}$ Arch. T. **O**	$\frac{4}{4}$ full **O**	$\frac{7}{7}$ full **O**
$\frac{20}{24}$ $\left(\frac{5}{6}\right)$	C	$\frac{4}{4}$ full **M**	$\frac{7}{7}$ full **M**	$\frac{4}{4}$ full **M**	$\frac{7}{7}$ full **M**	$\frac{4}{4}$ full **M**	$\frac{7}{7}$ full **M**
$\frac{19}{24}$	B	$\frac{3}{4}$ kagome **O**	$\frac{6}{7}$ Arch. T. **O**	$\frac{3}{4}$ kagome **O**	$\frac{6}{7}$ Arch. T. **O**	$\frac{4}{4}$ full **O**	$\frac{7}{7}$ full **O**
$\frac{18}{24}$ $\left(\frac{3}{4}\right)$	(A)	empty	empty	empty	empty	empty	empty
$\frac{17}{24}$	C	$\frac{3}{4}$ kagome **O**	$\frac{6}{7}$ Arch. T. **O**	$\frac{4}{4}$ full **O**	$\frac{7}{7}$ full **O**	$\frac{4}{4}$ full **O**	$\frac{7}{7}$ full **O**
$\frac{16}{24}$ $\left(\frac{2}{3}\right)$	B	$\frac{4}{4}$ full **M**	$\frac{7}{7}$ full **M**	$\frac{4}{4}$ full **M**	$\frac{7}{7}$ full **M**	$\frac{4}{4}$ full **M**	$\frac{7}{7}$ full **M**
$\frac{15}{24}$ $\left(\frac{5}{8}\right)$	A	$\frac{3}{4}$ kagome **O**	$\frac{6}{7}$ Arch. T. **O**	$\frac{4}{4}$ full **O**	$\frac{7}{7}$ full **O**	$\frac{4}{4}$ full **O**	$\frac{7}{7}$ full **O**
$\frac{14}{24}$ $\left(\frac{7}{12}\right)$	(C)	empty	empty	empty	empty	empty	empty
$\frac{13}{24}$	B	$\frac{3}{4}$ kagome **O**	$\frac{6}{7}$ Arch. T. **O**	$\frac{3}{4}$ kagome **O**	$\frac{6}{7}$ Arch. T. **O**	$\frac{4}{4}$ full **O**	$\frac{7}{7}$ full **O**
$\frac{12}{24}$ $\left(\frac{1}{2}\right)$	A	$\frac{4}{4}$ full **M**	$\frac{7}{7}$ full **M**	$\frac{4}{4}$ full **M**	$\frac{7}{7}$ full **M**	$\frac{4}{4}$ full **M**	$\frac{7}{7}$ full **M**
$\frac{11}{24}$	C	$\frac{3}{4}$ kagome **O**	$\frac{6}{7}$ Arch. T. **O**	$\frac{3}{4}$ kagome **O**	$\frac{6}{7}$ Arch. T. **O**	$\frac{4}{4}$ full **O**	$\frac{7}{7}$ full **O**
$\frac{10}{24}$ $\left(\frac{5}{12}\right)$	(B)	empty	empty	empty	empty	empty	empty
$\frac{9}{24}$ $\left(\frac{3}{8}\right)$	A	$\frac{3}{4}$ kagome **O**	$\frac{6}{7}$ Arch. T. **O**	$\frac{4}{4}$ full **O**	$\frac{7}{7}$ full **O**	$\frac{4}{4}$ full **O**	$\frac{7}{7}$ full **O**
$\frac{8}{24}$ $\left(\frac{1}{3}\right)$	C	$\frac{4}{4}$ full **M**	$\frac{7}{7}$ full **M**	$\frac{4}{4}$ full **M**	$\frac{7}{7}$ full **M**	$\frac{4}{4}$ full **M**	$\frac{7}{7}$ full **M**
$\frac{7}{24}$	B	$\frac{3}{4}$ kagome **O**	$\frac{6}{7}$ Arch. T. **O**	$\frac{4}{4}$ full **O**	$\frac{7}{7}$ full **O**	$\frac{4}{4}$ full **O**	$\frac{7}{7}$ full **O**
$\frac{6}{24}$ $\left(\frac{1}{4}\right)$	(A)	empty	empty	empty	empty	empty	empty
$\frac{5}{24}$	C	$\frac{3}{4}$ kagome **O**	$\frac{6}{7}$ Arch. T. **O**	$\frac{3}{4}$ kagome **O**	$\frac{6}{7}$ Arch. T. **O**	$\frac{4}{4}$ full **O**	$\frac{7}{7}$ full **O**
$\frac{4}{24}$ $\left(\frac{1}{6}\right)$	B	$\frac{4}{4}$ full **M**	$\frac{7}{7}$ full **M**	$\frac{4}{4}$ full **M**	$\frac{7}{7}$ full **M**	$\frac{4}{4}$ full **M**	$\frac{7}{7}$ full **M**
$\frac{3}{24}$ $\left(\frac{1}{8}\right)$	A	$\frac{3}{4}$ kagome **O**	$\frac{6}{7}$ Arch. T. **O**	$\frac{3}{4}$ kagome **O**	$\frac{6}{7}$ Arch. T. **O**	$\frac{4}{4}$ full **O**	$\frac{7}{7}$ full **O**
$\frac{2}{24}$ $\left(\frac{1}{12}\right)$	(C)	empty	empty	empty	empty	empty	empty
$\frac{1}{24}$	B	$\frac{3}{4}$ kagome **O**	$\frac{6}{7}$ Arch. T. **O**	$\frac{4}{4}$ full **O**	$\frac{7}{7}$ full **O**	$\frac{4}{4}$ full **O**	$\frac{7}{7}$ full **O**
$\frac{0}{24}$ (0)	A	$\frac{4}{4}$ full **M**	$\frac{7}{7}$ full **M**	$\frac{4}{4}$ full **M**	$\frac{7}{7}$ full **M**	$\frac{4}{4}$ full **M**	$\frac{7}{7}$ full **M**

Table III.4-4. Alternative hexagonal *u.c.* descriptions for M_2O_3, M_7O_{12}, and MO_2, compared with the descriptions provided in Table III.3-1. The atom positions provided here remove the double redundancy of the Table III.3-1 descriptions along the $\bar{3}$ axis. The *u.c.* descriptions provided in this table amount to 12-layer atom-stacking sequences along $\bar{3}$ for each structure (instead of 24). Fractional coordinates (x, y, z) for the atoms refer to trigonal S.G. $R\bar{3}$ (hexagonal axes). As usual, M and O represent metal cations and oxygen anions, respectively, while V represents *vacancies* in the lattice. Z is the number of formula units per hexagonal *u.c.*

| Structure	Z	Equipoint (Wyckoff notation) and Fractional Coordinates (x, y, z) for Atoms in the Hexagonal *u.c.*
M_2O_3	6	M(1) at 3*a*: $\left(0,0,\mathbf{0}\right)$ + EP
		M(2) at 9*e*: $\left(\tfrac{1}{2},0,\mathbf{0}\right)$ + EP
		O(1) at 18*f*: $\left(0,\tfrac{1}{2},\tfrac{\mathbf{3}}{\mathbf{4}}\right)$ + EP
		V(1) at 6*c*: $\left(0,0,\tfrac{\mathbf{3}}{\mathbf{4}}\right)$ + EP
M_7O_{12}	3	M(1) at 3*a*: $\left(0,0,\mathbf{0}\right)$ + EP
		M(2) at 18*f*: $\left(\tfrac{1}{7},\tfrac{3}{7},\mathbf{0}\right)$ + EP
		O(1) at 18*f*: $\left(\tfrac{1}{7},\tfrac{3}{7},\tfrac{\mathbf{3}}{\mathbf{4}}\right)$ + EP
		O(2) at 18*f*: $\left(\tfrac{1}{7},\tfrac{3}{7},\tfrac{\mathbf{1}}{\mathbf{4}}\right)$ + EP
		V(1) at 6*c*: $\left(0,0,\tfrac{\mathbf{3}}{\mathbf{4}}\right)$ + EP
fluorite MO_2 (4 atoms per hexcell) [Redundant unit cell: 4 times the unit cell volume for the fluorite structure description in Table II.2-2]	12	M(1) at 3*a*: $\left(0,0,\mathbf{0}\right)$ + EP
		M(2) at 9*e*: $\left(\tfrac{1}{2},0,\mathbf{0}\right)$ + EP
		O(1) at 18*f*: $\left(0,\tfrac{1}{2},\tfrac{\mathbf{3}}{\mathbf{4}}\right)$ + EP
		O(2) at 6*c*: $\left(0,0,\tfrac{\mathbf{3}}{\mathbf{4}}\right)$ + EP
fluorite MO_2 (7 atoms per hexcell) [Redundant unit cell: 7 times the unit cell volume for the fluorite structure description in Table II.2-2]	21	M(1) at 3*a*: $\left(0,0,\mathbf{0}\right)$ + EP
		M(2) at 18*f*: $\left(\tfrac{1}{7},\tfrac{3}{7},\mathbf{0}\right)$ + EP
		O(1) at 18*f*: $\left(\tfrac{1}{7},\tfrac{3}{7},\tfrac{\mathbf{3}}{\mathbf{4}}\right)$ + EP
		O(2) at 18*f*: $\left(\tfrac{1}{7},\tfrac{3}{7},\tfrac{\mathbf{1}}{\mathbf{4}}\right)$ + EP
		O(3) at 6*c*: $\left(0,0,\tfrac{\mathbf{3}}{\mathbf{4}}\right)$ + EP
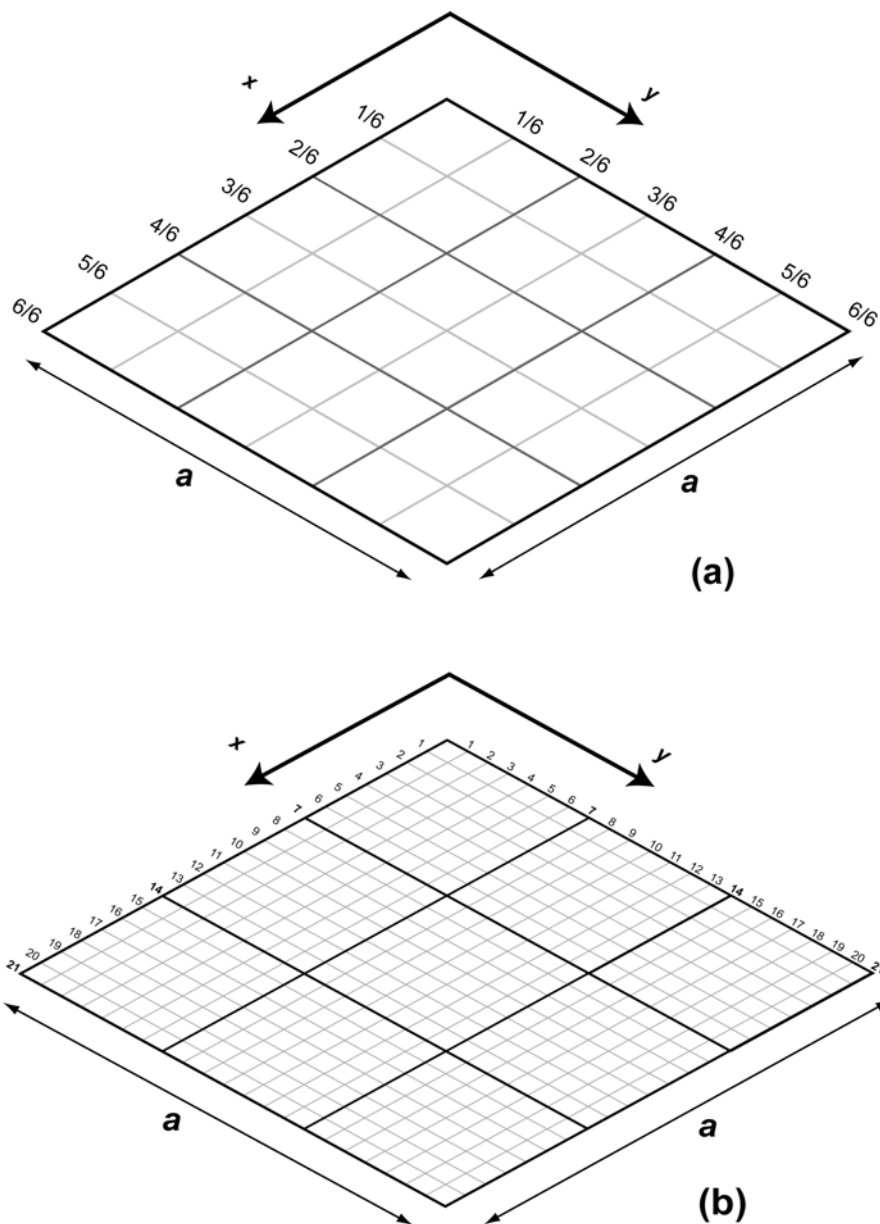
Figure III.4-1. Hexagonal *u.c.* (hexcell) templates for layered atom sequence descriptions along $\bar{3}$ of complex oxide crystal structures. (a) Hexcell template corresponding to triangular atom net *subdivision by 4^{ths}*. Triangular atom net *subdivision by 4^{ths}* results in hexcell (*x, y*) fractional coordinates that are fractions of 6^{ths}. This subdivision is used for layer diagrams describing the Group (1) structures discussed in the text: M_2O_3 sesquioxide, M_4O_7 pyrochlore, and 8-times redundant MO_2 fluorite crystal structures. (b) Hexcell template corresponding to triangular atom net *subdivision by 7^{ths}*. Triangular atom net *subdivision by 7^{ths}* results in hexcell (*x, y*) fractional coordinates that are fractions of 21^{sts}. This subdivision is used for layer diagrams describing the Group (2) structures discussed in the text: M_7O_{12}, M_7O_{13}, and 14-times redundant MO_2 fluorite crystal structures.
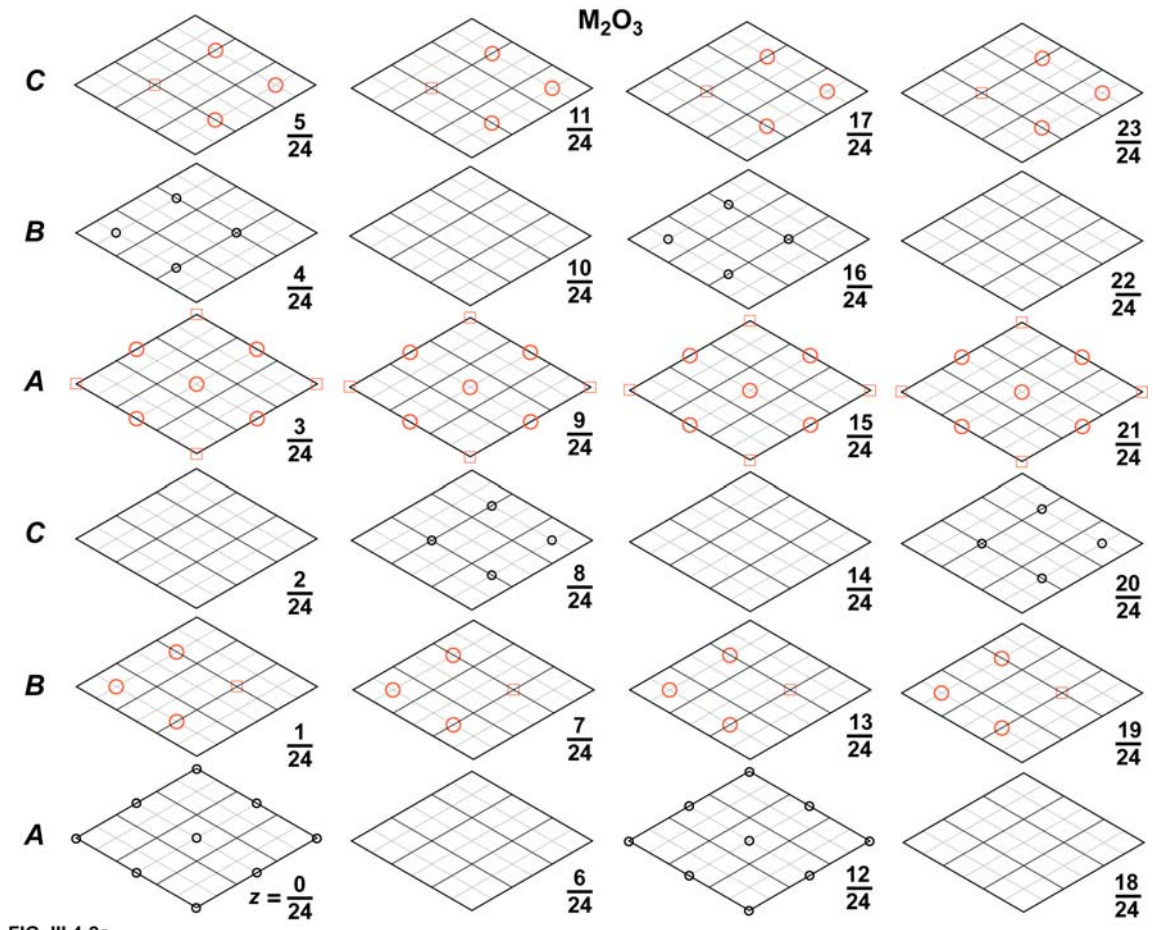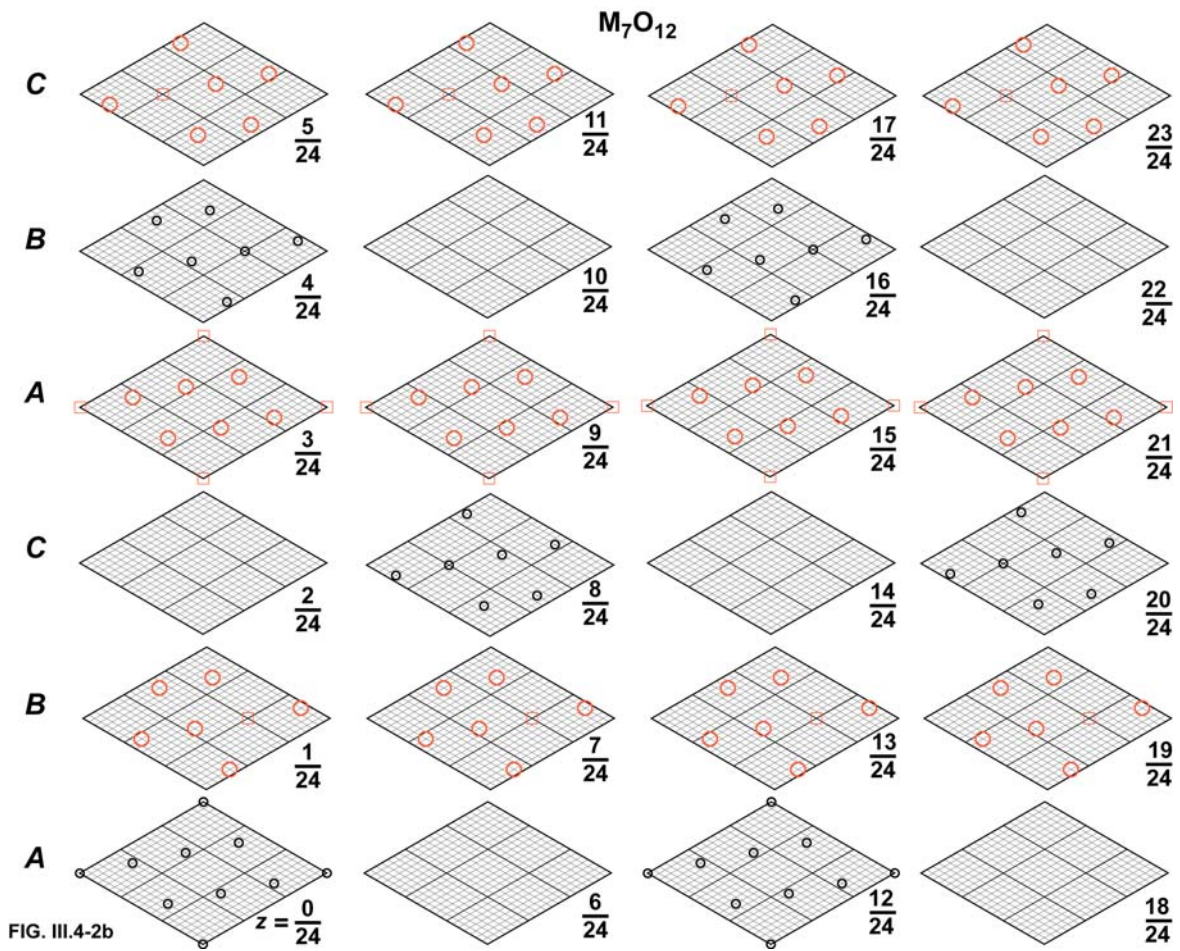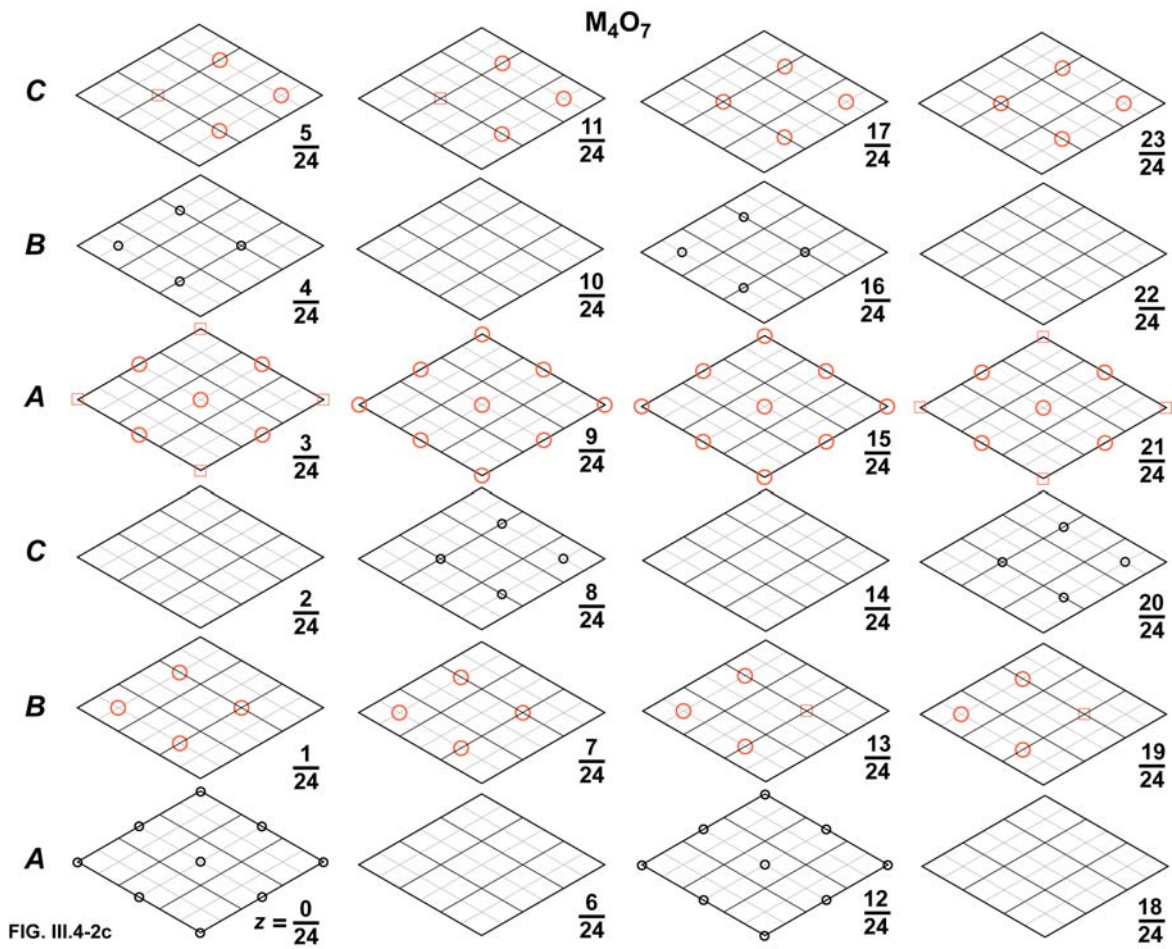
M₂O₃

C $\frac{5}{24}$ $\frac{11}{24}$ $\frac{17}{24}$ $\frac{23}{24}$

B $\frac{4}{24}$ $\frac{10}{24}$ $\frac{16}{24}$ $\frac{22}{24}$

A $\frac{3}{24}$ $\frac{9}{24}$ $\frac{15}{24}$ $\frac{21}{24}$

C $\frac{2}{24}$ $\frac{8}{24}$ $\frac{14}{24}$ $\frac{20}{24}$

B $\frac{1}{24}$ $\frac{7}{24}$ $\frac{13}{24}$ $\frac{19}{24}$

A $z = \frac{0}{24}$ $\frac{6}{24}$ $\frac{12}{24}$ $\frac{18}{24}$

FIG. III.4-2a

III.4. An Expanded Oxidation Sequence: Layer Stacking Sequences   57

FIG. III.4-2b

M_7O_{12}

III.4. An Expanded Oxidation Sequence: Layer Stacking Sequences

M_4O_7

FIG. III.4-2c

M_7O_{13}

FIG. III.4-2.d

III.4. An Expanded Oxidation Sequence: Layer Stacking Sequences
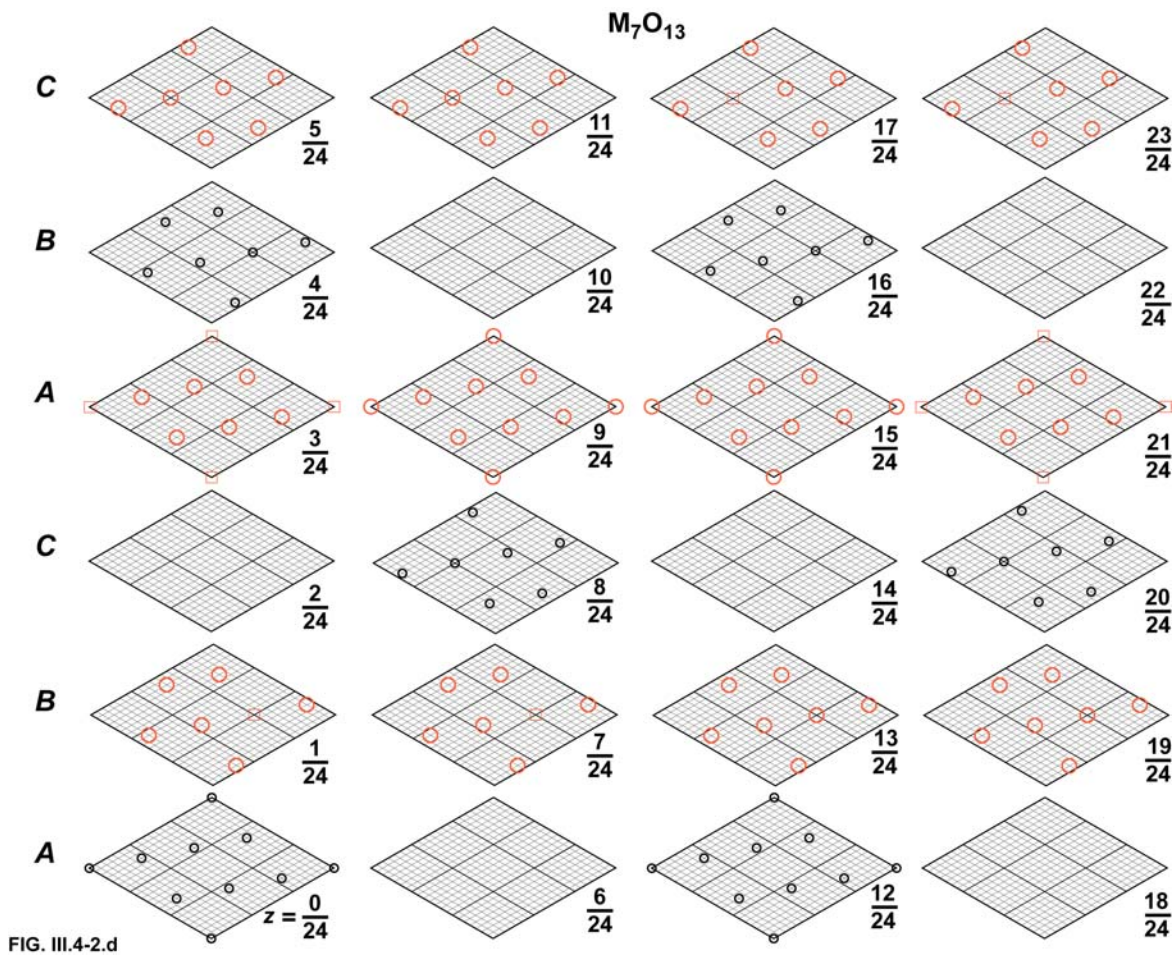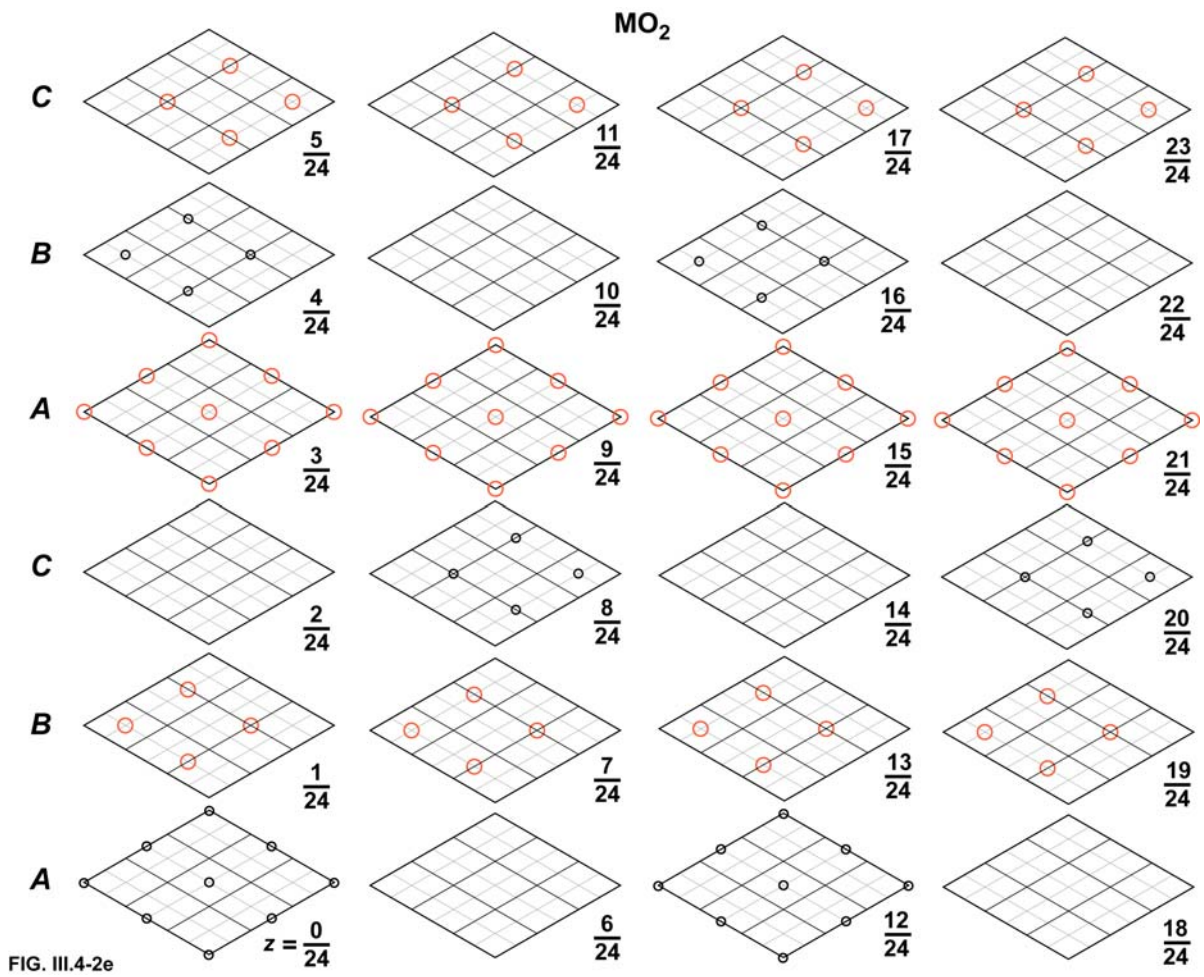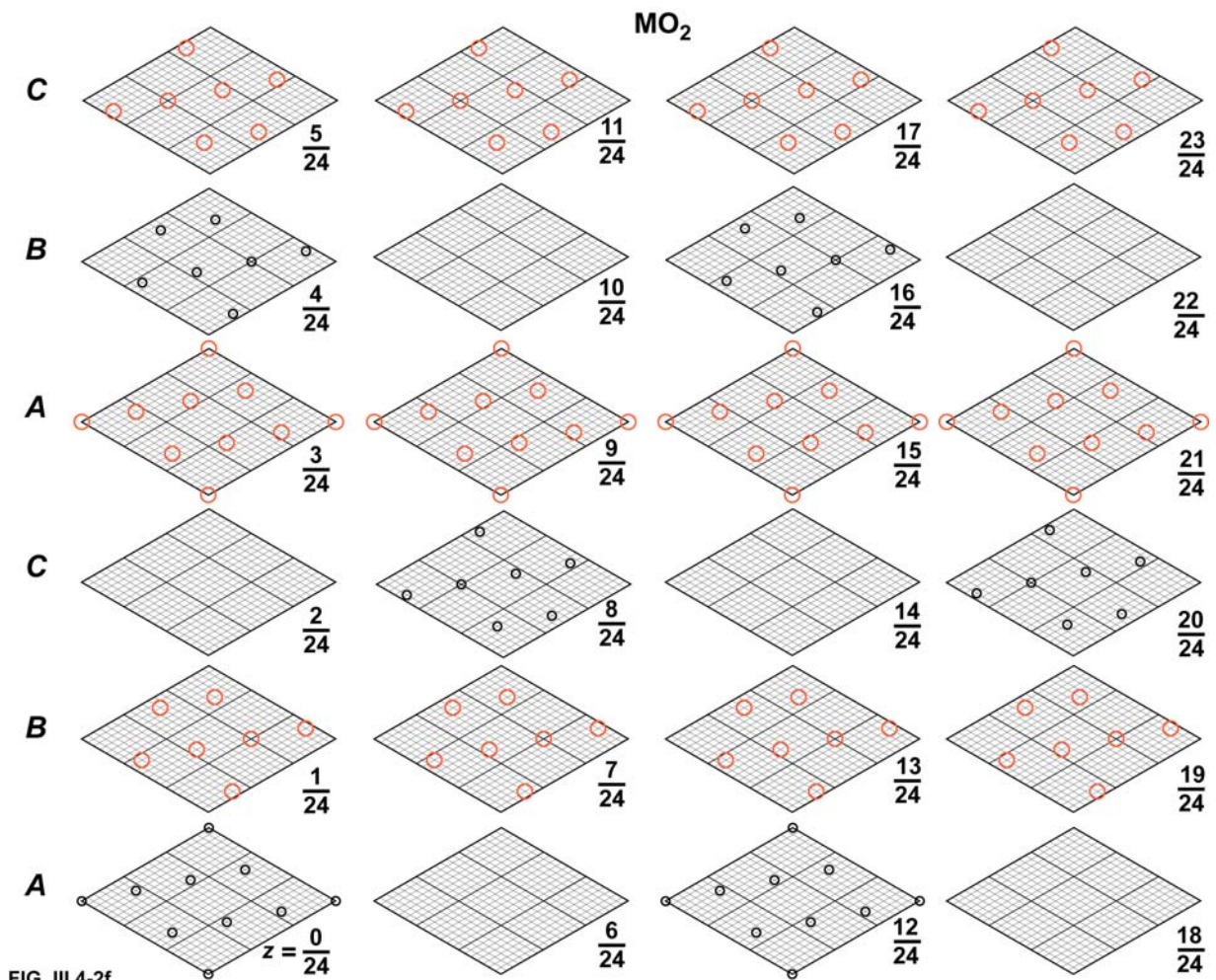
FIG. III.4-2e

Figure III.4-2. Layered atom-stacking sequences along $\bar{3}$ for the following crystal structures: (a) the M_2O_3 sesquioxide, (b) M_7O_{12}, (c) M_4O_7 pyrochlore, (d) M_7O_{13}, (e) 8-times redundant MO_2 fluorite, and (f) 14-times redundant MO_2 fluorite. The stacking sequences are intended to be read from bottom to top along the left-hand column ($z = \frac{0}{24}$ to $z = \frac{5}{24}$) and then bottom to top along each successive column to the right. Each stacking sequence consists of 24 layers, though this description is doubly redundant for the following crystal structures: (a) the M_2O_3 sesquioxide, (b) M_7O_{12}, and (e,f) 8- and 14-times redundant MO_2 fluorite. Metal cations are indicated by small black-outlined circles. Oxygen anions are indicated by large red-outlined circles. Vacancies (which here are assumed to be on the anion sublattice) are indicated by red-outlined squares.

Table III.4-5. Summary of 12-layer atom-stacking sequences along $\bar{3}$ for the oxide compounds presented in Table III.4-4. Columns are intended to be read from bottom ($z = 0$) to top ($z = 1$). Note that the layer stacking sequences shown here are *ACBACB*... rather than *ABCABC*.... This notation is used to indicate that the definitions of registry shifts *B* and *C* are reversed when going from a 24- to 12-layer *u.c.* description of the structure (Table III.4-3 and this table, respectively).

Layer Height (z) (*u.c.* fraction)	Registry (*ABC* stacking)	M_2O_3	M_7O_{12}	MO_2 8-times redundant	MO_2 14-times redundant
$\frac{12}{12}\left(1\right)$	*A*	$\frac{4}{4}$ full **M**	$\frac{7}{7}$ full **M**	$\frac{4}{4}$ full **M**	$\frac{7}{7}$ full **M**
23/24	*(C)*	empty	empty	empty	empty
$\frac{11}{12}$	*B*	$\frac{3}{4}$ kagome **O**	$\frac{6}{7}$ Arch. T. **O**	$\frac{4}{4}$ full **O**	$\frac{7}{7}$ full **O**
21/24	*(A)*	empty	empty	empty	empty
$\frac{10}{12}\left(\frac{5}{6}\right)$	*(C)*	empty	empty	empty	empty
19/24	*(B)*	empty	empty	empty	empty
$\frac{9}{12}\left(\frac{3}{4}\right)$	*A*	$\frac{3}{4}$ kagome **O**	$\frac{6}{7}$ Arch. T. **O**	$\frac{4}{4}$ full **O**	$\frac{7}{7}$ full **O**
17/24	*(C)*	empty	empty	empty	empty
$\frac{8}{12}\left(\frac{2}{3}\right)$	*B*	$\frac{4}{4}$ full **M**	$\frac{7}{7}$ full **M**	$\frac{4}{4}$ full **M**	$\frac{7}{7}$ full **M**
15/24	*(A)*	empty	empty	empty	empty
$\frac{7}{12}$	*C*	$\frac{3}{4}$ kagome **O**	$\frac{6}{7}$ Arch. T. **O**	$\frac{4}{4}$ full **O**	$\frac{7}{7}$ full **O**
13/24	*(B)*	empty	empty	empty	empty
$\frac{6}{12}\left(\frac{1}{2}\right)$	*(A)*	empty	empty	empty	empty
11/24	*(C)*	empty	empty	empty	empty
$\frac{5}{12}$	*B*	$\frac{3}{4}$ kagome **O**	$\frac{6}{7}$ Arch. T. **O**	$\frac{4}{4}$ full **O**	$\frac{7}{7}$ full **O**
9/24	*(A)*	empty	empty	empty	empty
$\frac{4}{12}\left(\frac{1}{3}\right)$	*C*	$\frac{4}{4}$ full **M**	$\frac{7}{7}$ full **M**	$\frac{4}{4}$ full **M**	$\frac{7}{7}$ full **M**
7/24	*(B)*	empty	empty	empty	empty
$\frac{3}{12}\left(\frac{1}{4}\right)$	*A*	$\frac{3}{4}$ kagome **O**	$\frac{6}{7}$ Arch. T. **O**	$\frac{4}{4}$ full **O**	$\frac{7}{7}$ full **O**
5/24	*(C)*	empty	empty	empty	empty
$\frac{2}{12}\left(\frac{1}{6}\right)$	*(B)*	empty	empty	empty	empty
3/24	*(A)*	empty	empty	empty	empty
$\frac{1}{12}$	*C*	$\frac{3}{4}$ kagome **O**	$\frac{6}{7}$ Arch. T. **O**	$\frac{4}{4}$ full **O**	$\frac{7}{7}$ full **O**
1/24	*(B)*	empty	empty	empty	empty
$\frac{0}{12}\left(0\right)$	*A*	$\frac{4}{4}$ full **M**	$\frac{7}{7}$ full **M**	$\frac{4}{4}$ full **M**	$\frac{7}{7}$ full **M**

III.5. An Expanded Oxidation Sequence: Lattice Parameters

Hexagonal *u.c.* lattice parameters, *a* and *c*, for the structures in our expanded oxidation sequence are obtained by the following procedure. Let *d* represent the *n.n.* spacing between atoms in any fully dense, triangular atom net. Nearest neighbor spacing *d* is the fundamental lattice unit that one must know in order to determine the lattice constants.

Hexagon base parameter, *a*, is related to *d* by the following expression:

$$a = \sqrt{\frac{\# \, atoms}{hexcell}} \; d \qquad\qquad\qquad\qquad \text{(III.5-1)}$$

where $\frac{\# \, atoms}{hexcell}$ refers to the number of atoms contained within one fully dense hexcell (for a hexcell corresponding to a specific subdivision of a triangular atom net). For the triangular net subdivisions described in this paper, the following descriptions apply:

Subdivision by 1ˢᵗˢ: $\sqrt{\frac{\# \, atoms}{hexcell}} = \sqrt{1}$;

Subdivision by 3ʳᵈˢ: $\sqrt{\frac{\# \, atoms}{hexcell}} = \sqrt{3}$;

Subdivision by 4ᵗʰˢ: $\sqrt{\frac{\# \, atoms}{hexcell}} = \sqrt{4}$;

Subdivision by 7ᵗʰˢ: $\sqrt{\frac{\# \, atoms}{hexcell}} = \sqrt{7}$.

Hexagon height parameter, *c*, is most easily obtained by first relating *c* to the height, *h*, of a tetrahedron of either M cations or O anions. The height, *h*, of an M (or O) tetrahedron is equivalent to the distance between *n.n.* M (or *n.n.* O) layers along $\bar{3}$. Then the relationship between *c* and *h* is determined by simply counting how many pairs of *n.n.* M (or *n.n.* O) layers occur between *u.c.* height $z = 0$ to $z = 1$ (this is how many M (or O) tetrahedra can be stacked on top of one another from the base to the top of the hexagonal *u.c.*). This gives the following relation between *c* and *h*:

$$c = 3\,h \quad \text{(12-layer } u.c. \text{ description)} \qquad\qquad \text{(III.5-2a)}$$

$$c = 6\,h \quad \text{(24-layer } u.c. \text{ description)} \qquad\qquad \text{(III.5-2b)}$$

But if one assumes that a given structure is characterized by *ideal* layer stacking such that each M (or O) tetrahedron is a *regular* tetrahedron, it is easy to show that:

$$h = \sqrt{\tfrac{2}{3}}\, d .$$ (III.5-3)

Substituting Eq. (III.5-3) alternatively into Eqs. (III.5-2a and III.5-2b), we obtain the following expressions for the *ideal* height of the hexagonal *u.c.*:

$$c = \sqrt{6}\, d \quad \text{(12-layer } u.c. \text{ description)}$$ (III.5-4a)

$$c = 2\sqrt{6}\, d \quad \text{(24-layer } u.c. \text{ description)} .$$ (III.5-4b)

Finally, combining Eqs. (III.5-1) and (III.5-4a) and (III.5-4b), the *ideal* $\frac{c}{a}$ ratios for the crystal structures described in this paper are obtained:

$$\left.\frac{c}{a}\right|_{ideal} = \frac{\sqrt{6}}{\sqrt{\frac{\#\,atoms}{hexcell}}} \quad \text{(12-layer } u.c. \text{ description)}$$ (III.5-5a)

$$\left.\frac{c}{a}\right|_{ideal} = \frac{2\sqrt{6}}{\sqrt{\frac{\#\,atoms}{hexcell}}} \quad \text{(24-layer } u.c. \text{ description).}$$ (III.5-5b)

III.6. An Expanded Oxidation Sequence: Coordination Polyhedra

Finally, as with our presentation in Section II.4, it is interesting to consider how these stacking models relate to coordination polyhedra in some of these compounds.[1] For the structures presented in Sections III.3 and III.4, several distinct coordination polyhedra are generated. Coordination polyhedra for O anions surrounding a central M cation in these structures are shown in Fig. III.6-1.

---

[1] The following discussion assumes *ideal* symmetry (i.e., each structure's $\frac{c}{a}$ ratio obeys one or the other of the *ideal* ratios given in Eqs. (III.5-5a) and (III.5-5b). If $\frac{c}{a}$ deviates from ideality, the coordination polyhedra are distorted from their ideal, *regular* geometries.
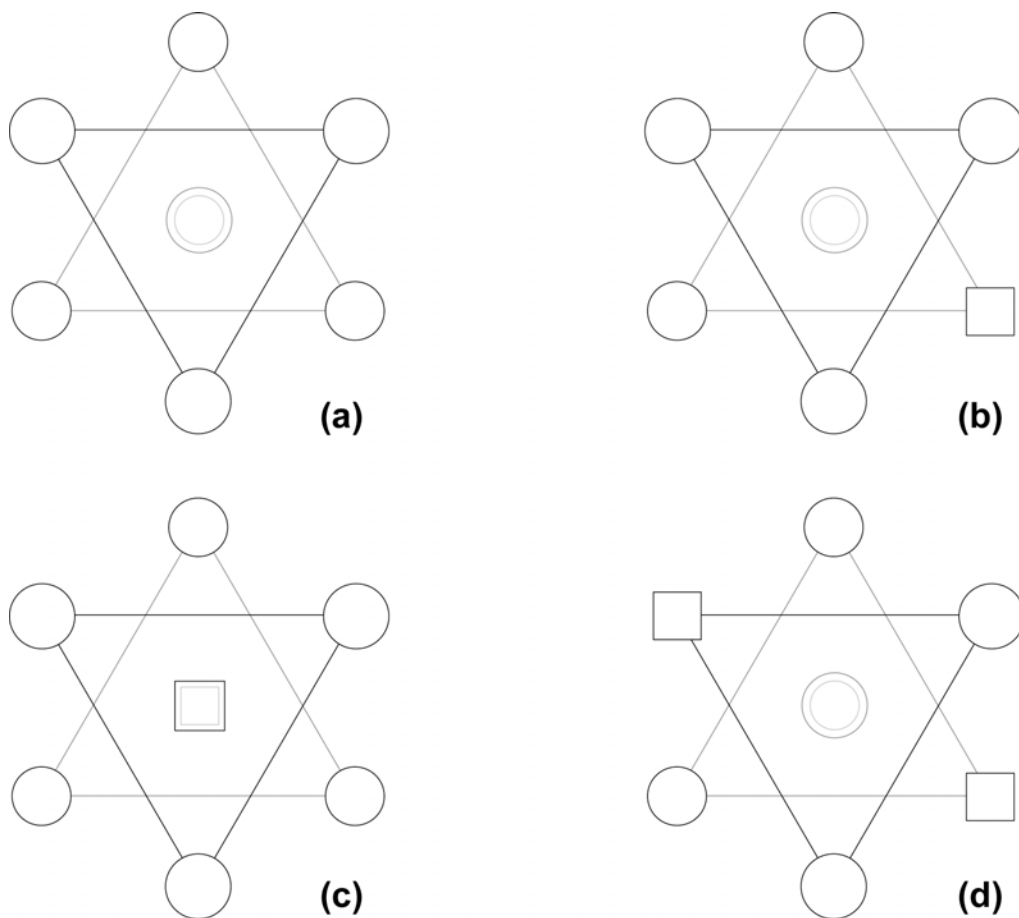
Figure III.6-1. Coordination polyhedra representative of the complex oxide compounds considered in this presentation. These diagrams represent cation (M) coordination polyhedra by *n.n.* anions (O). All diagrams represent projections down the $\bar{3}$ axis. The central M cations are not shown in the diagrams. O anions are represented by hollow circles. O vacancies are denoted by squares. Smaller circles, smaller squares, and lighter-shaded polyhedron edges represent anions, vacancies, and atom layers that are beneath the uppermost features in these projected layer diagrams. (a) 8-fold, ideal *sc* coordination of O anions about a central M cation; (b) 7-fold coordination of a central M cation by *n.n.* O anions (one n.n. anion missing); (c) 6-fold coordination of a central M cation by *n.n.* O anions (two *n.n.* O anions missing—top and bottom layers); (d) 6-fold coordination of a central M cation by *n.n.* O anions (two *n.n.* O anions missing—middle layers). See text for a discussion regarding which crystal structures exhibit these characteristic coordination polyhedra.

Consider M_4O_7 pyrochlore for instance. Cations in pyrochlore are alternately 6-fold (octahedral) and 8-fold (*sc*) coordinated by *n.n.* anions. Consider a cation M layer at $z = \frac{8}{24}$ with stacking registry C. This cation layer is surrounded by two equidistant anion

O layers (heights z = $\frac{7}{24}, \frac{9}{24}$) with stacking registries A and B and two 2nd *n.n.* O layers (heights z = $\frac{5}{24}, \frac{11}{24}$), both with stacking registry C (i.e., equivalent to the M layer). These are conditions for producing *sc* coordination polyhedra as described for MO_2 fluorite in Section II.4. The A and B registry 1st *n.n.* O layers surrounding the M layer are fully dense triangular nets. Thus, every cation in the M layer is at least 6-fold (octahedrally) coordinated by O anions. But the 2nd *n.n.* O layers are only $\frac{3}{4}$ dense. These outer O layers perfectly overlap one another as well as the central M layer (all registry C). Thus, three in four atoms in each of these outer layers combine with the inner O layers to produce 8-fold, regular *sc* coordination polyhedra. On the other hand, one in four triangular net positions in these outer O layers are vacant. Consequently, the cations located between these vacancies are only 6-fold (octahedrally) coordinated. It is important to note that these octahedral coordination polyhedra are not regular octahedra. They are distorted octahedra. The six O atoms in each octahedron are equidistant from the central M atom, but the faces of the octahedron are not regular triangles (in six of the eight triangular faces, one edge is $\sqrt{2}$ times the length of the other two edges). Nevertheless, in summary, the M layer considered here consists of a mixture of 6-fold and 8-fold coordinated cations. These coordination polyhedra are illustrated in Figs. III.6-1a and III.6-1c, respectively.

If, on the other hand, we consider a pyrochlore cation M layer at $z = \frac{4}{24}$ with stacking registry *B*, we find it is surrounded by 1st *n.n.* O layers (heights $z = \frac{3}{24}, \frac{5}{24}$), with stacking registries *A* and *C*. These are $\frac{3}{4}$ dense O layers. However, the 2nd *n.n.* O layers are fully dense triangular nets with the same registry as the central M layer (*B*). Now the apexes of the *sc* coordination units are always occupied (no vacancies), but the distorted octahedral stacking units made from the 1st *n.n.* O layers are alternately full (six O atoms) or deficient (four O atoms). The resulting coordination polyhedra again are distorted octahedral (6-fold) or *sc* (8-fold) units. Three in four coordination polyhedra corresponding to this cation layer are 6-fold; 1 in 4 polyhedra is 8-fold. These polyhedra are illustrated in Figs. III.6-1d and III.6-1a, respectively. The result for pyrochlore is that half of all cation coordination polyhedra are 6-fold and half are 8-fold.

By a similar analysis, it is easy to demonstrate that for the M_2O_3 sesquioxide presented in Sections III.3 and III.4, the structure consists only of 6-fold distorted octahedra. One in four is of the type illustrated in Fig. III.6-1c; three in four are as in Fig. III.6-1d. In

M_7O_{12}, every M layer consists of two distinct coordination polyhedra: 6-fold distorted O octahedra as in Fig. III.6-1c (one in seven) and 7-fold O polyhedra as illustrated in Fig. III.6-1b. (six in seven). In M_7O_{13}, an M-layer at a height such as $z = \frac{4}{24}$ (surrounded by $\frac{6}{7}$ dense 1st *n.n.* O layers) consists of one type of coordination polyhedron: 7-fold (Fig. III.6-1b). On the other hand, an M-layer at a height such as $z = \frac{8}{24}$ (surrounded by fully dense 1st *n.n.* O layers) consists of two types of polyhedra: 6-fold (Fig. III.6-1c) (1 in 7) and 8-fold (Fig. III.6-a) (6 in 7).

In summary, oxygen coordination polyhedra progress as follows around M cations in the structures presented in Sections III.3 and III.4 (distribution shown in parentheses):

M_2O_3 6-fold distorted octahedra (100%);

M_7O_{12} 6-fold distorted octahedra (14%), 7-fold polyhedra (86%);

M_4O_7 6-fold distorted octahedra (50%), 8-fold (*sc*) polyhedra (50%);

M_7O_{13} 6-fold distorted octahedra (7%), 7-fold polyhedra (50%), 8-fold (*sc*) polyhedra (43%); and

MO_2 8-fold (*sc*) polyhedra (100%).

Note that the average coordination number on M cations by *n.n.* O anions increases as average oxidation state of the compound increases. Finally, we note (without proof) that O anion coordination by *n.n.* M cations is 4-fold (*regular* tetrahedral) in all of these compounds.

This concludes our presentation of layer stacking sequences in both representative and complex oxide compounds. Next we will describe how *real* structures compare with these layer stacking model predictions. We will present examples of materials that both conform to and contradict the crystallographic descriptions presented in this report.

IV.1. Real Materials: Introduction

The following presentation is intended to illustrate the validity of our layer stacking model by highlighting a few selected examples of the crystal structures exhibited by real materials. This is by no means intended to be an exhaustive tabulation of all compounds that conform to our model. This is merely an introduction to oxide crystal structures that we hope will pique the readers' interest in the concepts we developed in Sections II and III. We will examine our expanded oxidation sequence of compounds in more or less the reverse order in which it was introduced in Section III.

IV.2.1. Real Materials: MO$_2$ Fluorite and M$_2$O Antifluorite

First, consider the MO$_2$ fluorite structure. The crystallographic descriptions for MO$_2$ fluorite provided in Sections II and III are exact for all compounds in nature that exhibit a cubic fluorite structure and possess a 1:2 M:O stoichiometry. In other words, no atomic distortions or deviations from the atomic position descriptions provided in Sections II and III are ever observed nor are there any lattice parameter deviations from ideality (Eqs. (III.5-1) and (III.5-4a) are valid). The same statements hold for antifluorite-structured compounds. Table II.2-2 should be used for the atom position definitions for the MO$_2$ and M$_2$O fluorite and antifluorite structures. Table II.3-1 shows the layer stacking sequence along $\bar{3}$ for all fluorite and antifluorite compounds. Finally, Table IV.2.1-1 shows a selection of fluorite-structured oxides that are known to conform to the MO$_2$ fluorite structure models presented here. One antifluorite compound is also shown in Table IV.2.1-1.

Table IV.2.1-1. Lattice parameters for both cubic and hexagonal *u.c.* settings for selected oxides that exhibit the MO$_2$ fluorite crystal structure. Hexagonal *u.c.* lattice parameters *a* and *c* are obtained from Eqs. (III.5-1) and (III.5-4a) and using $\frac{\# atoms}{hexcell} = 1$ and $d = \frac{a_{cube}}{\sqrt{2}}$.

Compound	Cube *u.c.* Lattice Parameter a_{cube} (nm)	Hexagonal *u.c.* Lattice Parameter *a*, *c* (nm)	References & Comments
ZrO$_2$	0.527(2)	0.3728 0.9131	[1](@ 2400°C)
HfO$_2$	0.5115(10)	0.3617 0.8860	[2]
CeO$_2$	0.541134(12)	0.3826 0.9373	JCPDF # 34-394 [3]
ThO$_2$	0.55970(3)	0.3958 0.9694	JCPDF # 42-1462 [3]
UO$_2$	0.5467(4)	0.3866 0.9470	JCPDF # 41-1422 [3]
PuO$_2$	0.544	0.385 0.942	JCPDF # 41-1171 [3] (actually, for PuO$_{1.9}$)
Li$_2$O	0.4619	0.3266 0.8000	[4]

Section IV.2.1 References

[1]   D. K. Smith and C. F. Cline, "Verification of Existence of Cubic Zirconia at High Temperature," *J. Am. Ceram. Soc*. **45** (5) 249–250 (1962).

[2]   L. Passerini, "Isoformismo tra Ossidi di Metalli Tetravalenti. I Sistemi: CeO_2-ThO_2; CeO_2-ZrO_2; CeO_2-HfO_2," *Gazzetta Chim. Ital.* **60** 762–766 (1930).

[3]   International Centre for Diffraction Data, Powder Diffraction File (Joint Committee on Powder Diffraction Standards, Philadelphia, PA, 1974 – present).

[4]   E. Zintl, A. Harder, and B. Dauth, "Gitterstruktur der Oxide, Sulfide, Selenide und Telluride des Lithiums, Natriums und Kaliums," *Zeitschrift für Elektrochemie* **40** 588–593 (1934).

IV.2.2. Real Materials: MX$_2$ CdCl$_2$ Structure

We would like to call to the readers' attention to the fascinating relationship between the fluorite structure discussed in the previous section and the so-called CdCl$_2$ structure. CdCl$_2$ is one of the classic trigonal, layered atom compounds. It belongs to S.G. $R\bar{3}m$ (#166) [1], but it can be described exactly using the same $R\bar{3}$ hexagonal *u.c.* description for fluorite given in Table II.2-2. Specifically, in the case of CdCl$_2$, a Cd atom is placed at equipoint 3a ((0,0,0) + EP), while Cl is located at equipoint 6c $\left(\left(0,0,z=\frac{1}{4}\right)\right.$ + EP). This description corresponds to subdivision by 1^{sts} of the CdCl$_2$ triangular atom nets along $\bar{3}$. The atom layer stacking sequence along $\bar{3}$ for CdCl$_2$ is identical to that shown for MO$_2$ fluorite in Fig. II.1-4.

If the exact same $R\bar{3}$ crystal structure descriptions apply to both MO$_2$ fluorite and CdCl$_2$, what are the differences in these structures? The differences begin with the $\frac{c}{a}$ ratio for CdCl$_2$ versus MO$_2$. MO$_2$ possesses the ideal $\frac{c}{a}$ ratio defined in Eq. (III.5-5a) ($\left.\frac{c}{a}\right|_{ideal} = \sqrt{6} = 2.4495$ for MO$_2$ fluorite), while CdCl$_2$ exhibits a greatly exaggerated $\frac{c}{a}$ ratio ($\frac{c}{a} = 4.5351$).

Moreover, compare the actual *a* and *c* lattice parameters for CdCl$_2$ with an MO$_2$ fluorite, say, ZrO$_2$ in Table IV.2-1. For CdCl$_2$, *a* = 0.385 nm and *c* = 1.746 nm, while for ZrO$_2$, *a* = 0.3728 nm and *c* = 0.9131 nm. While the hexagon base parameters, *a,* are similar in the two compounds, the CdCl$_2$ hexagon *u.c.* height, *c*, is nearly twice the ZrO$_2$ *u.c.* height for the same number of atom layers!

What actually happens as one progresses from an MO$_2$ fluorite structure to the CdCl$_2$ structure is that the anion sublattice transforms from *sc* to *fcc*. For this to happen, each X$_4$ tetrahedron (where X represents a general anion) transforms from an irregular tetrahedron in the *sc* structure to a regular tetrahedron in the *fcc* structure. This is illustrated schematically in Fig. IV.2.2-1. In effect, this transformation is achieved by *stretching* all the X$_4$ tetrahedra along $\bar{3}$ until all the tetrahedra sides are of equal length and the included angles are all 60°. If one performs this operation by lengthening the heights of all of the tetrahedra without affecting their base dimensions (base dimensions equal *d*), one obtains the CdCl$_2$ structure. The base parameter for the hexagonal unit cells remains unchanged (*a = d*) during this hypothetical *sc* to *fcc* transformation. On the other hand, the *u.c.* height *c* doubles going from *sc* to *fcc*. The exact $\frac{c}{a}$ ratio for perfect *fcc* stacking

(Fig. IV.2.2-1b) is $2\sqrt{6} = 4.89898$, slightly larger than the $\frac{c}{a}$ ratio for the compound $CdCl_2$. So, $CdCl_2$ has a slightly distorted *fcc* anion sublattice.
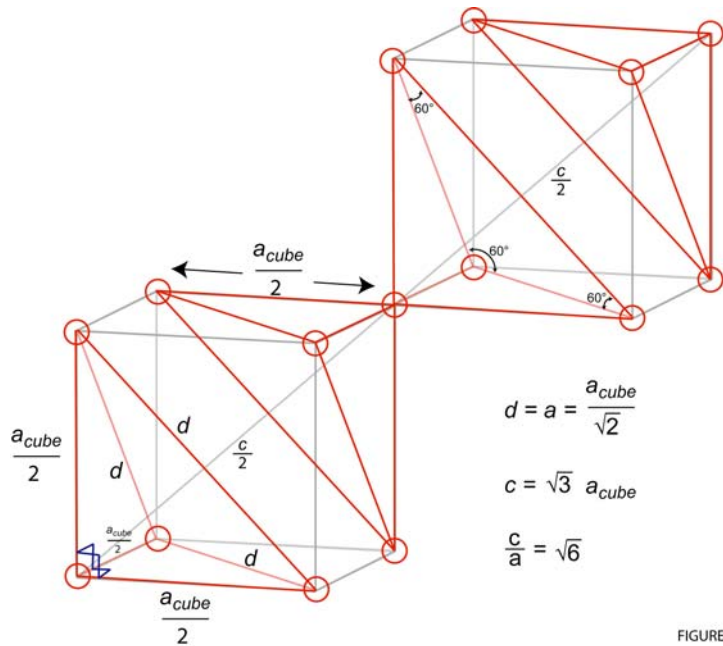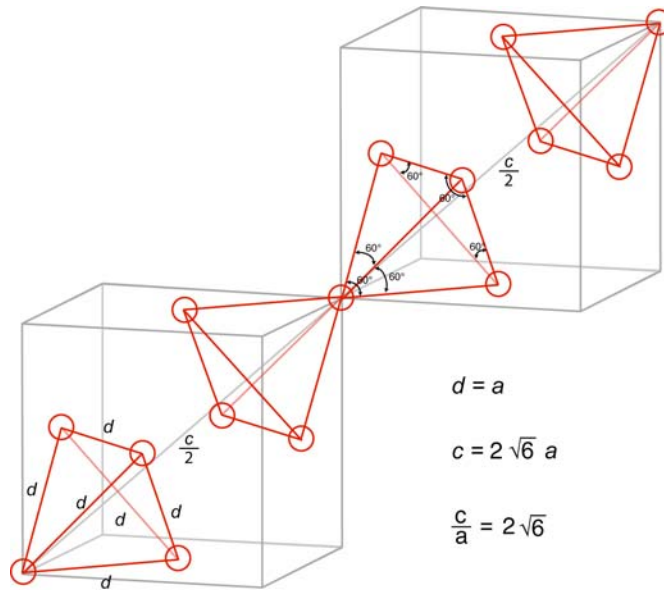

$$d = a = \frac{a_{cube}}{\sqrt{2}}$$

$$c = \sqrt{3}\ a_{cube}$$

$$\frac{c}{a} = \sqrt{6}$$

FIGURE IV.2.2-1a

$$d = a$$

$$c = 2\sqrt{6}\ a$$

$$\frac{c}{a} = 2\sqrt{6}$$

FIGURE IV.2.2-1b

Figure IV.2.2-1. (a) Two *u.c.*s in the *sc* anion sublattice of an MX_2 fluorite-structured compound (X representing an anion). The cells are linked along a $\overline{3}$ axis. The diagram illustrates the *irregular* X_4 tetrahedra that are stacked along $\overline{3}$ in this lattice. (b) Two *u.c.*s in the *fcc* anion sublattice of an MX_2 compound with the $CdCl_2$ structure (not all *u.c.* X atoms are shown in the diagram). This diagram illustrates the *regular* X_4 tetrahedra that are characteristic of the $CdCl_2$ structure.

In Fig. IV.2.2-2, we compare layer stacking along $\bar{3}$ for ZrO_2 fluorite (parameters from Table IV.2.1-1) versus $CdCl_2$. The most striking difference between the two structures is the extraordinary distance between adjacent layers in $CdCl_2$ (Fig. IV.2.2-2b). In fact, the distance is so large that essentially Van der Waals interactions between adjacent Cl layers are responsible for holding the compound together. Cd cations occupy octahedral interstices between adjacent Cl layers, but only every other layer of octahedral interstices is occupied by Cd atoms. Cl atoms are 3-fold coordinated by *n.n.* Cd atoms.

The only oxide reported to possess the $CdCl_2$ structure is Cs_2O. Thus, the $CdCl_2$ structure is more an alternative to the M_2O antifluorite structure than to the MO_2 fluorite structure. Nevertheless, it seemed appropriate to introduce this structure at this juncture in our discussion.
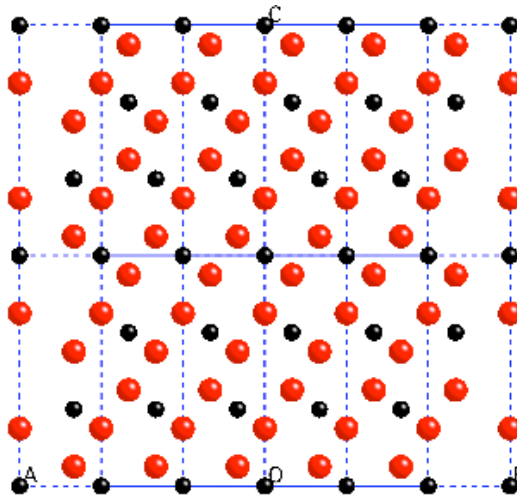
(a)
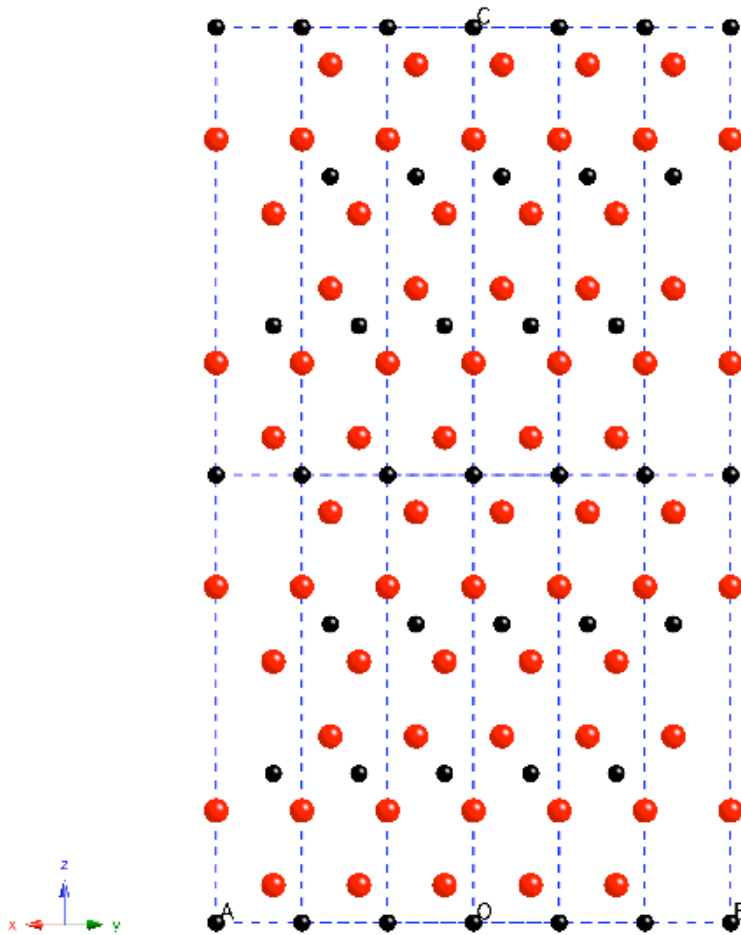
(b)

Figure IV.2.2-2. (a) View of atom layers in ZrO_2 fluorite in a projection parallel to $\overline{3}$ (the $\overline{3}$ axis is the vertical axis in the plane of this drawing). The height of the drawing is 1.8262 nm, which is twice the hexagonal lattice parameter, c, for ZrO_2 (Table IV.2.1-1). Three hexagonal $u.c.$s are shown along the horizontal axis. (b) View of atom layers in $CdCl_2$ in a projection parallel to $\overline{3}$ ($\overline{3}$ is vertical in this drawing). The height of the drawing is 3.492 nm, which is twice the hexagonal lattice parameter, c, for $CdCl_2$ (see text). Three hexagonal $u.c.$s are shown along the horizontal axis.

Section IV.2.2 References

[1]   R. W. G. Wyckoff, *Crystal Structures: Vol. 1* (Interscience Publishers, Inc., New York,   1960).

IV.3. Real Materials: M_7O_{13}

The most notable M_7O_{13} compound in the literature is γ-$Sc_2Zr_5O_{13}$. The γ designation for this compound was introduced by Jean Lefèvre [1]. The hexagonal *u.c.* lattice parameters determined by Lefèvre for γ-$Sc_2Zr_5O_{13}$ are shown in Table IV.3-1. The Lefèvre $\frac{c}{a}$ ratio for the γ-$Sc_2Zr_5O_{13}$ in Table IV.3-1 corresponds very nearly to the ideal $\frac{c}{a}$ ratio proposed in Section III.5 for *subdivision by 7^{ths}* of a triangular atom net and using a 24-layer *u.c.* description for the crystal structure (Eq. (III.5-5b)):

$$\left.\frac{c}{a}\right|_{ideal} = 2\sqrt{\frac{6}{7}} = 1.8516.$$

Thornber, Bevan, and Graham (denoted TBG in the following discussion) succeeded in refining the crystal structure of γ-$Sc_2Zr_5O_{13}$, using x-ray diffraction measurements [2]. TBG hexagonal *u.c.* lattice parameters are also shown in Table IV.3-1, for comparison with Lefèvre's values.

Table IV.3-1. Lattice parameters for the hexagonal setting of the *u.c.* for the compound γ-$Sc_2Zr_5O_{13}$.

Compound	a (nm)	c (nm)	a	Reference
γ-$Sc_2Zr_5O_{13}$	0.9508	1.746	1.836	Lefèvre [1]
γ -$Sc_2Zr_5O_{13}$	0.953(2)	1.744(2)	1.829(8)	Thornber, Bevan, and Graham [2]

TBG atomic coordinates for the *u.c.* atoms in γ-$Sc_2Zr_5O_{13}$ are shown in Table IV.3-2. The fractional coordinates in Table IV.3-2 indicate small distortions from the ideal M_7O_{13} structure presented in Section III. It is also important to note that TBG assumed that the Sc^{3+} and Zr^{4+} ions occupy randomly the cation equipoints (M(1) – M(4)).

Table IV.3-2. Hexagonal *u.c.* description for γ-Sc$_2$Zr$_5$O$_{13}$ according to TBG [2]. Fractional coordinates (x,y,z) for the atoms refer to trigonal space group $R\bar{3}$ (hexagonal axes). As usual, M and O represent metal cations and oxygen anions, respectively. Z is the number of formula units per hexagonal *u.c.* Deviations from ideality are expresed as fractions of *u.c.* lengths $\left(\delta_x, \delta_y, \delta_z\right)$.

| Structure	Z	Equipoint (Wyckoff notation) and Fractional Coordinates (*x, y, z*) for Atoms in the Hexagonal *u.c.*
γ-Sc$_2$Zr$_5$O$_{13}$	6	M(1) at 3*a*: $(0,0,0)$ + EP (0.0000 0.0000 0.0000) ideal (0.0000 0.0000 0.0000) TBG (0.0000 0.0000 0.0000) $\left(\delta_x, \delta_y, \delta_z\right)$ M(2) at 18*f*: $\left(\frac{1}{7}, \frac{3}{7}, 0\right)$ + EP (0.1428 0.4286 0.0000) ideal (0.1450 0.4357 -0.0067) TBG (+0.0022 +0.0071 -0.0067) $\left(\delta_x, \delta_y, \delta_z\right)$ M(3) at 3*b*: $\left(0, 0, \frac{1}{2}\right)$ + EP (0.0000 0.0000 0.5000) ideal (0.0000 0.0000 0.5000) TBG (0.0000 0.0000 0.0000) $\left(\delta_x, \delta_y, \delta_z\right)$ M(4) at 18*f*: $\left(\frac{1}{7}, \frac{3}{7}, \frac{1}{2}\right)$ + EP (0.1428 0.4286 0.5000) ideal (0.1111 0.4049 0.4946) TBG (-0.0317 -0.0237 -0.0054) $\left(\delta_x, \delta_y, \delta_z\right)$ O(1) at 18*f*: $\left(\frac{1}{7}, \frac{3}{7}, \frac{3}{8}\right)$ + EP (0.1428 0.4286 0.3750) ideal (0.1172 0.4095 0.3738) TBG (-0.0256 -0.0191 -0.0012) $\left(\delta_x, \delta_y, \delta_z\right)$ O(2) at 18*f*: $\left(\frac{1}{7}, \frac{3}{7}, \frac{5}{8}\right)$ + EP (0.1428 0.4286 0.6250) ideal (0.1361 0.4691 0.6098) TBG (-0.0067 +0.0405 -0.0152) $\left(\delta_x, \delta_y, \delta_z\right)$ O(3) at 18*f*: $\left(\frac{1}{7}, \frac{3}{7}, \frac{1}{8}\right)$ + EP (0.1428 0.4286 0.1250) ideal (0.1679 0.4223 0.1207) TBG (+0.0251 -0.0063 -0.0043) $\left(\delta_x, \delta_y, \delta_z\right)$ O(4) at 18*f*: $\left(\frac{1}{7}, \frac{3}{7}, \frac{7}{8}\right)$ + EP (0.1428 0.4286 0.8750) ideal (0.1688 0.4601 0.8711) TBG (+0.0260 +0.0315 -0.0039) $\left(\delta_x, \delta_y, \delta_z\right)$ O(5) at 6*c*: $\left(0, 0, \frac{3}{8}\right)$ + EP (0.0000 0.0000 0.3750) ideal (0.0000 0.0000 0.3523) TBG (0.0000 0.0000 -0.0227) $\left(\delta_x, \delta_y, \delta_z\right)$

The main consequence of atomic relaxation away from the ideal M_7O_{13} structure presented in Section III is the formation of "rumpled" cation and anion layers perpendicular to $\bar{3}$. Table IV.3-3 shows how the ideal, 24-layer *u.c.* description for γ-$Sc_2Zr_5O_{13}$ degenerates into a 54-layer description following atom relaxations.

Table IV.3-3. Layer stacking sequence along $\bar{3}$ for the compound γ-$Sc_2Zr_5O_{13}$ as determined in a crystal structure refinement performed by TBG. [2]. M(1), M(2), etc., refer to the equipoint occupancies, as given in Table IV.3-2. The ideal layer stacking sequence, shown in the first column, consists of 24 layers along $\bar{3}$.

Layer Height (z: fraction of u.c. height c)	Registry (ABC stacking)	Layer Constituents	Relaxed Structure Layer Constituents and Layer Heights (z: fraction of u.c. height c) (also deviation parameter δ_z as a fraction of u.c. height c)		
$\frac{25}{24}$ (1.0417)	B	O(1), O(2), O(5)	O(1)	1.0569	$\delta_z^{O(1)} = +0.0152$
			O(2)	1.0405	$\delta_z^{O(2)} = -0.0012$
			O(5)	1.0190	$\delta_z^{O(5)} = -0.0227$
$\frac{24}{24}$ (1.0000)	A	M(1), M(2)	M(2)	1.0067	$\delta_z^{M(2)} = +0.0067$
			M(1)	1.0000	$\delta_z^{M(1)} = 0.0000$
			M(2)	0.9933	$\delta_z^{M(2)} = -0.0067$
$\frac{23}{24}$ (0.9583)	C	O(1), O(2), O(5)	O(5)	0.9810	$\delta_z^{O(5)} = +0.0227$
			O(2)	0.9595	$\delta_z^{O(2)} = +0.0012$
			O(1)	0.9431	$\delta_z^{O(1)} = -0.0152$
$\frac{22}{24}$ (0.9167)	(B)	empty			
$\frac{21}{24}$ (0.8750)	A	O(3), O(4)	O(4)	0.8793	$\delta_z^{O(4)} = +0.0043$
			O(3)	0.8711	$\delta_z^{O(3)} = -0.0039$
$\frac{20}{24}$ (0.8333)	C	M(3), M(4)	M(4)	0.8387	$\delta_z^{M(4)} = +0.0054$
			M(3)	0.8333	$\delta_z^{M(3)} = 0.0000$
			M(4)	0.8279	$\delta_z^{M(4)} = -0.0054$
$\frac{19}{24}$ (0.7917)	B	O(3), O(4)	O(3)	0.7956	$\delta_z^{O(3)} = +0.0039$
			O(4)	0.7874	$\delta_z^{O(4)} = -0.0043$
$\frac{18}{24}$ (0.7500)	(A)	empty			
$\frac{17}{24}$ (0.7083)	C	O(1), O(2), O(5)	O(1)	0.7235	$\delta_z^{O(1)} = +0.0152$
			O(2)	0.7071	$\delta_z^{O(2)} = -0.0012$
			O(5)	0.6856	$\delta_z^{O(5)} = -0.0227$
$\frac{16}{24}$ (0.6667)	B	M(1), M(2)	M(2)	0.6734	$\delta_z^{M(2)} = +0.0067$
			M(1)	0.6667	$\delta_z^{M(1)} = 0.0000$
			M(2)	0.6600	$\delta_z^{M(2)} = -0.0067$
$\frac{15}{24}$ (0.6250)	A	O(1), O(2), O(5)	O(5)	0.6477	$\delta_z^{O(5)} = +0.0227$
			O(2)	0.6262	$\delta_z^{O(2)} = +0.0012$
			O(1)	0.6098	$\delta_z^{O(1)} = -0.0152$
$\frac{14}{24}$ (0.5833)	(C)	empty			

Layer Height (z: fraction of $u.c.$ height c)	Registry (ABC stacking)	Layer Constituents	Relaxed Structure Layer Constituents and Layer Heights (z: fraction of $u.c.$ height c) (also deviation parameter δ_z as a fraction of $u.c.$ height c)		
$\frac{13}{24}$ (0.5417)	B	O(3), O(4)	O(4)	0.5460	$\delta_z^{O(4)} = +0.0043$
			O(3)	0.5378	$\delta_z^{O(3)} = -0.0039$
$\frac{12}{24}$ (0.5000)	A	M(3), M(4)	M(4)	0.5054	$\delta_z^{M(4)} = +0.0054$
			M(3)	0.5000	$\delta_z^{M(3)} = 0.0000$
			M(4)	0.4946	$\delta_z^{M(4)} = -0.0054$
$\frac{11}{24}$ (0.4583)	C	O(3), O(4)	O(3)	0.4622	$\delta_z^{O(3)} = +0.0039$
			O(4)	0.4540	$\delta_z^{O(4)} = -0.0043$
$\frac{10}{24}$ (0.4167)	(B)	empty			
$\frac{9}{24}$ (0.3750)	A	O(1), O(2), O(5)	O(1)	0.3902	$\delta_z^{O(1)} = +0.0152$
			O(2)	0.3738	$\delta_z^{O(2)} = -0.0012$
			O(5)	0.3523	$\delta_z^{O(5)} = -0.0227$
$\frac{8}{24}$ (0.3333)	C	M(1), M(2)	M(2)	0.3400	$\delta_z^{M(2)} = +0.0067$
			M(1)	0.3333	$\delta_z^{M(1)} = 0.0000$
			M(2)	0.3266	$\delta_z^{M(2)} = -0.0067$
$\frac{7}{24}$ (0.2917)	B	O(1), O(2), O(5)	O(5)	0.3144	$\delta_z^{O(5)} = +0.0227$
			O(2)	0.2929	$\delta_z^{O(2)} = +0.0012$
			O(1)	0.2764	$\delta_z^{O(1)} = -0.0152$
$\frac{6}{24}$ (0.2500)	(A)	empty			
$\frac{5}{24}$ (0.2083)	C	O(3), O(4)	O(4)	0.2126	$\delta_z^{O(4)} = +0.0043$
			O(3)	0.2044	$\delta_z^{O(3)} = -0.0039$
$\frac{4}{24}$ (0.1667)	B	M(3), M(4)	M(4)	0.1721	$\delta_z^{M(4)} = +0.0054$
			M(3)	0.1667	$\delta_z^{M(3)} = 0.0000$
			M(4)	0.1613	$\delta_z^{M(4)} = -0.0054$
$\frac{3}{24}$ (0.1250)	A	O(3), O(4)	O(3)	0.1289	$\delta_z^{O(3)} = +0.0039$
			O(4)	0.1207	$\delta_z^{O(4)} = -0.0043$
$\frac{2}{24}$ (0.0833)	(C)	empty			
$\frac{1}{24}$ (0.0417)	B	O(1), O(2), O(5)	O(1)	0.0569	$\delta_z^{O(1)} = +0.0152$
			O(2)	0.0405	$\delta_z^{O(2)} = -0.0012$
			O(5)	0.0190	$\delta_z^{O(5)} = -0.0227$
$\frac{0}{24}$ (0.0000)	A	M(1), M(2)	M(2)	0.0067	$\delta_z^{M(2)} = +0.0067$
			M(1)	0.0000	$\delta_z^{M(1)} = 0.0000$
			M(2)	-0.0067	$\delta_z^{M(2)} = -0.0067$
$\frac{\bar{1}}{24}$ (-0.0417)	C	O(1), O(2), O(5)	O(5)	-0.0190	$\delta_z^{O(5)} = +0.0227$
			O(2)	-0.0405	$\delta_z^{O(2)} = -0.0012$
			O(1)	-0.0569	$\delta_z^{O(1)} = -0.0152$

Figure IV.3-1 shows aspects of the relaxed TBG γ-$Sc_2Zr_5O_{13}$ structure as described in Tables IV.3-1, 2, and 3. The largest (x, y) deviation from ideality within the hexcell planes (4% of the lattice parameter a) occurs in the fully dense, O triangular nets (O(1)+O(2)+O(5)). The projected (x, y) tiling pattern deviations in the $3^4.6$ Archimedean tiling O layers (O(3)+O(4)) are only 3% of a or less. Moreover, these $3^4.6$ Archimedean tiling O layers are rumpled along $\bar{3}$ less than 0.5% of lattice parameter c. Clearly, the *ideal* layer stacking model for M_7O_{13} presented in Section III is a reasonable description for the relaxed γ-$Sc_2Zr_5O_{13}$ crystal structure.

(a)

(b)

(c)
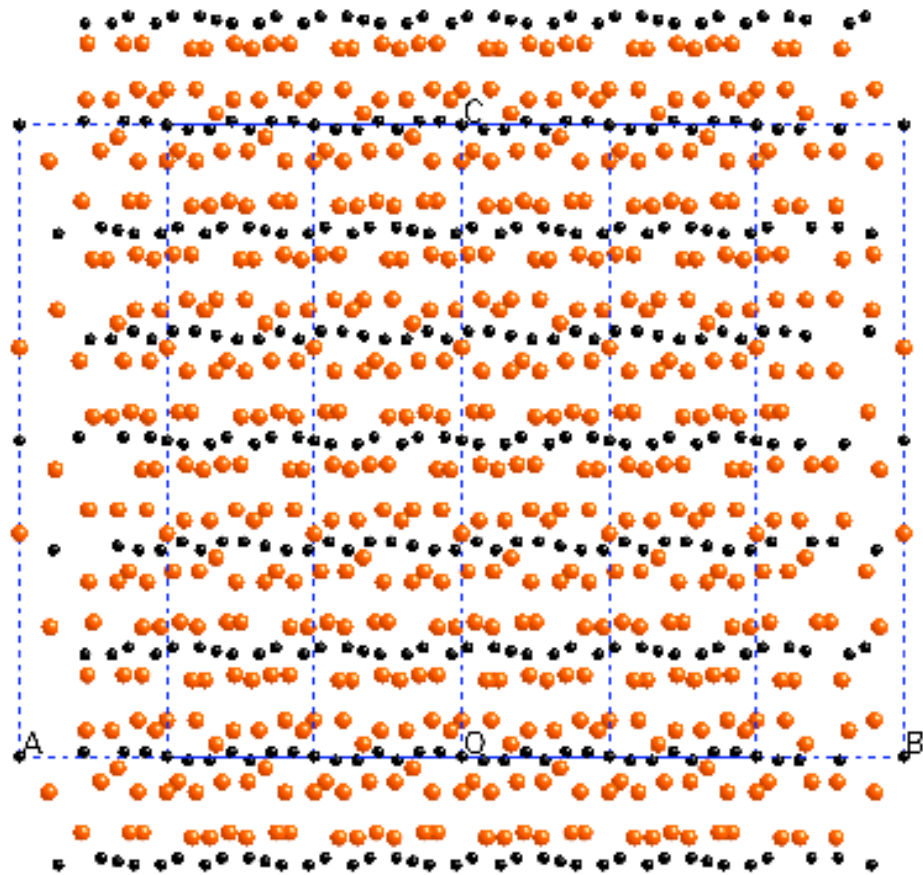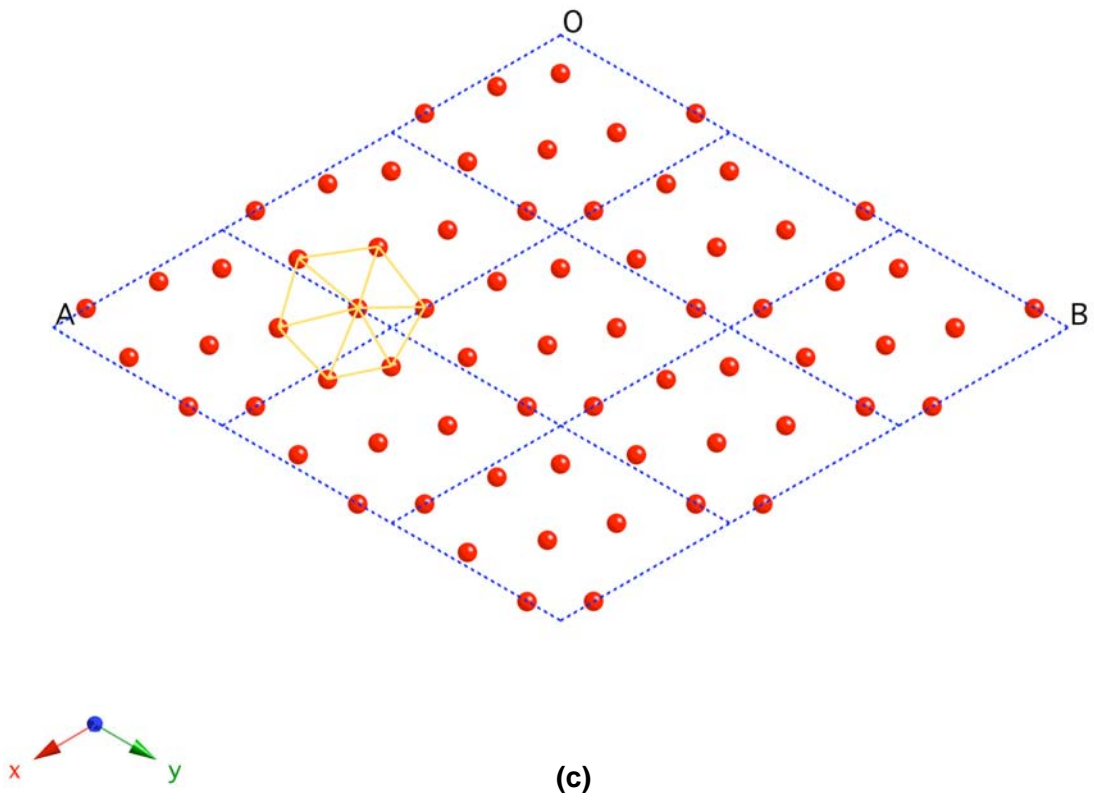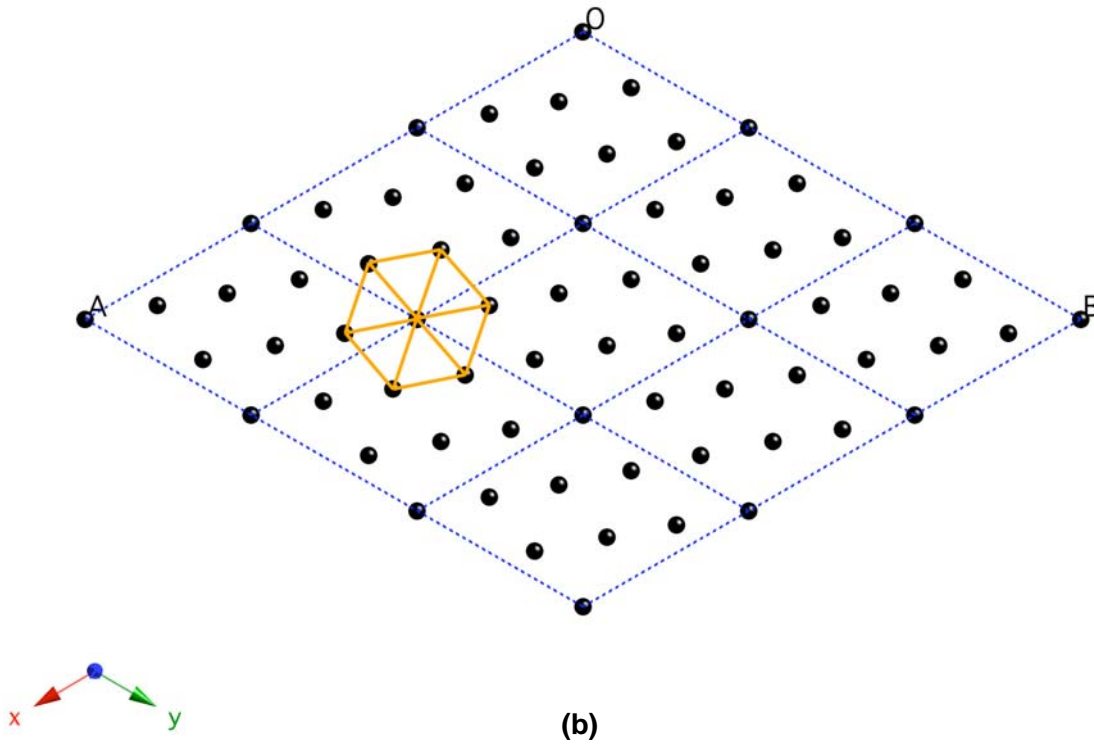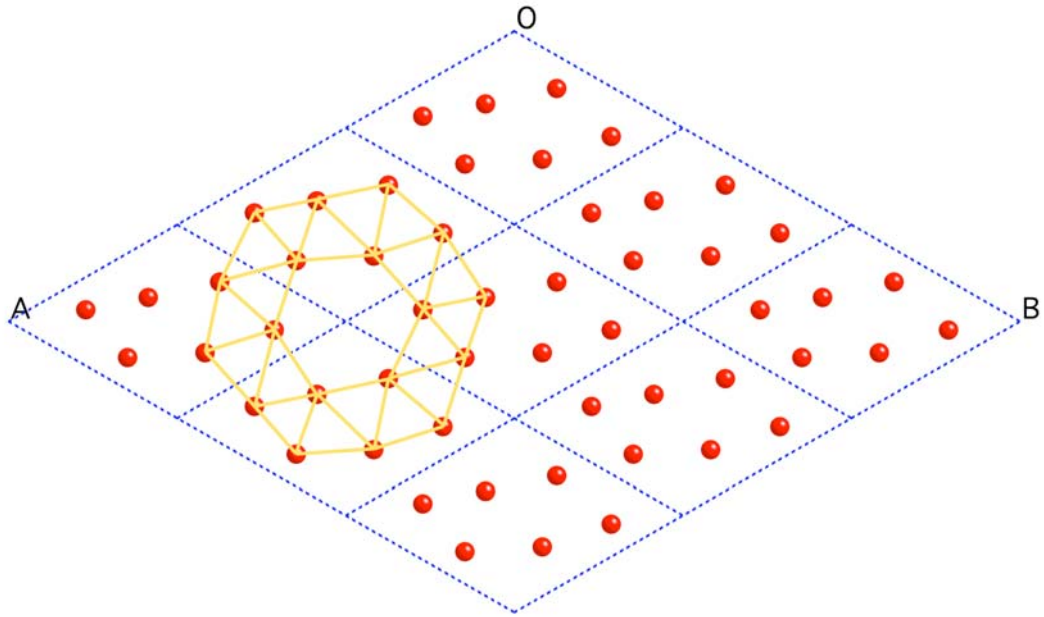
(d)

Figure IV.3-1. Projections of the relaxed crystal structure of γ-$Sc_2Zr_5O_{13}$ structure according to TBG [2]. Cations shown small/black; anions large/red. (a) View parallel to $\bar{3}$ (i.e., $\bar{3}$ lies in the plane of the projection). The dimension of the *u.c.* along the *c*-axis is exaggerated by a factor of 2, in order to better illustrate the rumpled cation and anion layers. One *u.c.* (plus a few extra layers) is shown along the vertical (*z*) axis, while three *u.c.*s are illustrated on the horizontal (*x, y*) axes. (b) View in projection down the $\bar{3}$ axis of the cation triangular net near *u.c.* height $z = 0$ (3×3 *u.c.*s). (c) View in projection down the $\bar{3}$ axis of the $\frac{7}{7}$ fully dense, anion triangular net near *u.c.* height $z = \frac{1}{24}$ (3×3 *u.c.*s). (d) View in projection down the $\bar{3}$ axis of the $\frac{6}{7}$ dense anion $3^4.6$ Archimedean tiling near *u.c.* height $z = \frac{3}{24}$ (3×3 *u.c.*s). Yellow lines in (b, c, d) delineate the characteristic tiling patterns in the respective atom layers.

Section IV.3 References

[1]   J. Lefèvre, "Relations Entre la Structure de Type Fluorine et la Structure de Type Mn_2O_3. Étude du Système Zircone-Oxyde de Scandium," *Ann. Chim. Fr.* t. **8** (1–2) 135–149 (1963).

[2]   M. R. Thornber, D. J. M. Bevan, and J. Graham, "Mixed Oxides of the Type MO_2 (Fluorite)−M_2O_3. III. Crystal Structures of the Intermediate Phases $Zr_5Sc_2O_{13}$ and $Zr_3Sc_4O_{12}$," *Acta Cryst. B* **24** 1183–1190 (1968).

IV.4. Real Materials: M_4O_7 Pyrochlore

M_4O_7 pyrochlore compounds are well described by the layer stacking model presented in Section III. Oxygen layers alternate between fully dense triangular nets and $\frac{3}{4}$ dense pseudo-kagome layers, much like the γ-$Sc_2Zr_5O_{13}$ structure (Section IV.3), in which O layers alternate between fully dense versus $\frac{6}{7}$ dense, $3^4.6$ Archimedean tilings. Moreover, the cations in multication pyrochlores are ordered.

Consider, for instance, $A_2B_2O_7$ pyrochlores. These compounds are mixtures of trivalent A^{3+} and tetravalent B^{4+} cations (or alternatively, divalent A^{2+} and pentavalent B^{5+} cations). $A_2B_2O_7$ pyrochlores mostly belong to the isometric space group $Fd\overline{3}m$ (see a review of oxide pyrochlores by Subramanian, Aravamudan, and Rao (abbreviated SAR in the following discussion) [1]). Using setting II in S.G. $Fd\overline{3}m$ (so that the *u.c.* origin has point symmetry $\overline{3}m$), it is conventional to place B cations at the origin of the cubic unit cell. Upon transformation of atom positions to the corresponding hexagonal *u.c.* in S.G. $R\overline{3}$, Table IV.4-1 shows the resulting atomic position assignments for atoms in $A_2B_2O_7$ oxide pyrochlores.
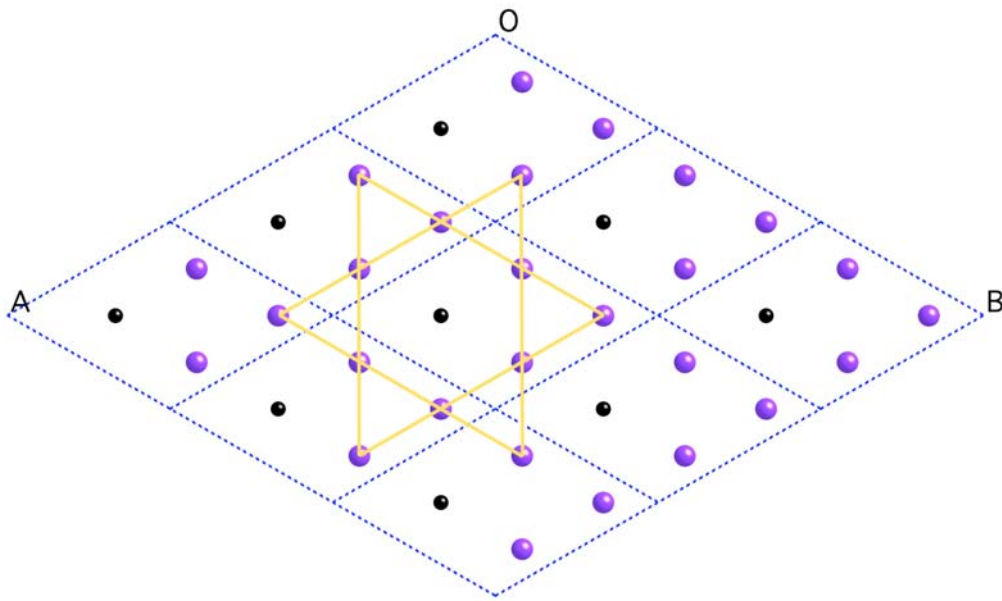
Based on the atom position assignments in Table IV.4-1, cation layers at *u.c.* heights $z = 0, \frac{1}{3}, \frac{2}{3}$ are characterized by kagome lattices of A cations ($\frac{3}{4}$ dense), with B cations located in the interstices within the A kagome lattices ($\frac{1}{4}$ dense). Conversely, at *u.c.* layer heights $z = \frac{1}{6}, \frac{1}{2}, \frac{5}{6}$, B cations produce kagome lattices ($\frac{3}{4}$ dense), while A cations occupy the interstices within the B kagome lattices ($\frac{1}{4}$ dense). These patterns are illustrated in Fig. IV.4-1. We should also note that the anion layers surrounding any (AB) layer are arranged such that the A atoms are 8-fold coordinated and the B atoms are 6-fold coordinated by *n.n.* O atoms. This description for the cation sublattice holds for all *ordered* $A_2B_2O_7$ pyrochlores. However, cation disorder is known to occur in some $A_2B_2O_7$ compounds (see SAR for a discussion [1]). Such disorder can be represented by mixing A and B cations on equipoints $3a$, $3b$, $9d$, and $9e$ in Table IV.4-1.

Table IV.4-1. Atom positions in the hexagonal *u.c.* description for an $A_2B_2O_7$ oxide pyrochlore compound. Fractional coordinates (x, y, z) for the atoms refer to trigonal space group $R\bar{3}$ (hexagonal axes). As usual, A and B represent metal cations while O denotes oxygen anions. Z is the number of formula units per hexagonal *u.c.* The parameter x represents the oxygen parameter for pyrochlore compounds [1]. For the *ideal* pyrochlore structure (Table III.3.1), $x = \frac{3}{8}$. We can also describe deviations from the ideal pyrochlore structure using a deviation parameter, $\delta = \frac{3}{8} - x$. This parameter represents the deviation from ideality of the oxygen sublattice in any given $A_2B_2O_7$ pyrochlore. See text for additional discussion of this oxygen positional parameter. Compare this table with Table III.3-1.

Structure	Z	Equipoint (Wyckoff notation) and Fractional Coordinates (x, y, z) for Atoms in the Hexagonal *u.c.*
pyrochlore $A_2B_2O_7$	6	B(1) at 3*a*: $\left(0,0,0\right) + \mathrm{EP}$
		B(2) at 9*d*: $\left(\frac{1}{2},0,\frac{1}{2}\right) + \mathrm{EP}$
		————————————
		A(1) at 3*b*: $\left(0,0,\frac{1}{2}\right) + \mathrm{EP}$
		A(2) at 9*e*: $\left(\frac{1}{2},0,0\right) + \mathrm{EP}$
		————————————
		O(1) at 18*f*: $\left(\frac{3}{4} - \frac{2}{3}x, \frac{1}{2} - \frac{4}{3}x, \frac{1}{2} - \frac{1}{3}x\right) + \mathrm{EP}$
		or
		O(1) at 18*f*: $\left(\frac{1}{2} + \frac{2}{3}\delta, \frac{4}{3}\delta, \frac{3}{8} + \frac{1}{3}\delta\right) + \mathrm{EP}$
		————————————
		O(2) at 18*f*: $\left(\frac{3}{4} - \frac{2}{3}x, \frac{1}{2} - \frac{4}{3}x, \frac{1}{4} - \frac{1}{3}x\right) + \mathrm{EP}$
		or
		O(2) at 18*f*: $\left(\frac{1}{2} + \frac{2}{3}\delta, \frac{4}{3}\delta, \frac{1}{8} + \frac{1}{3}\delta\right) + \mathrm{EP}$
		————————————
		O(3) at 6*c*: $\left(0,0,z = \frac{3}{8}\right) + \mathrm{EP}$
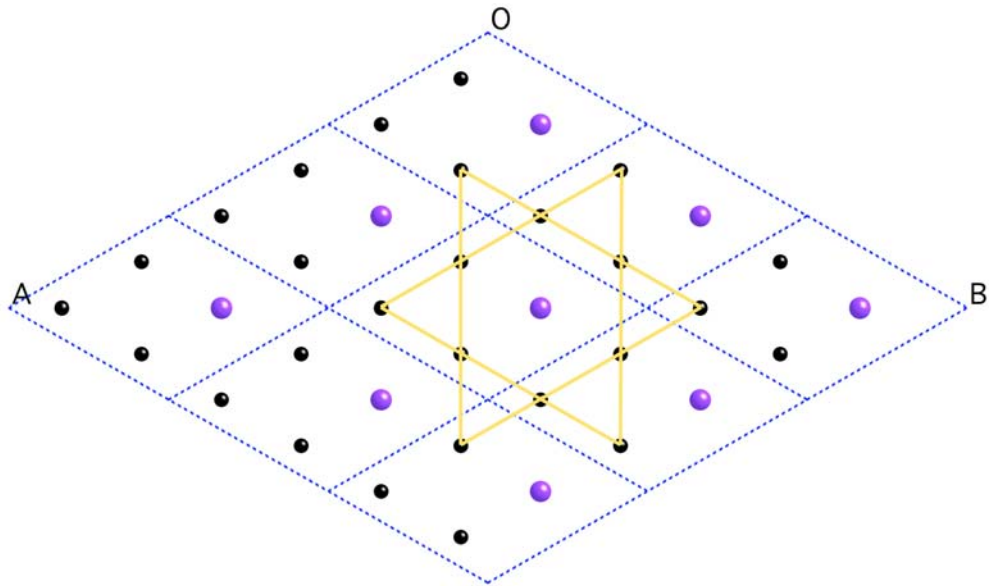
(a)

(b)

Figure IV.4-1. Cation arrangements along $\bar{3}$ in $A_2B_2O_7$, pyrochlores. (a) Cation layer at *u.c.* height $z = \frac{1}{6}$ (stacking registry *B*). (b) Cation layer at *u.c.* height $z = \frac{1}{3}$ (stacking registry *C*). The regions shown represent 3 × 3 hexcell areas (dotted blue lines). A^{3+} (or A^{2+}) cations are shown large/blue. B^{4+} (or B^{5+}) cations are shown small/black. The yellow lines delineate the kagome (Star of David) lattice of B cations in (a) and of A cations in (B).
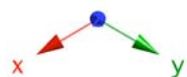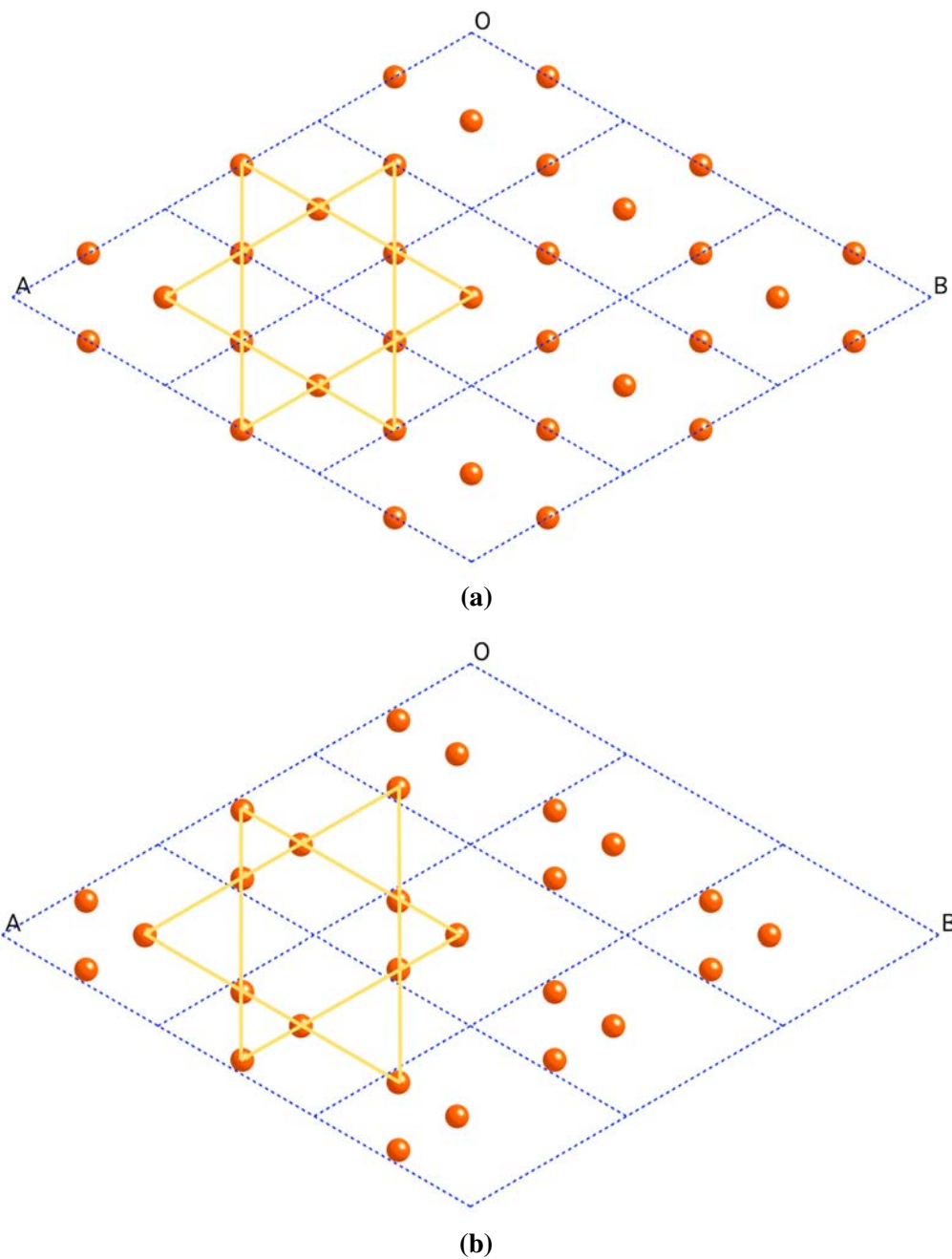
Figure IV.4-2. Effect of oxygen sublattice deviation parameter, δ, on the oxygen atomic patterns in an $A_2B_2O_7$ pyrochlore: (a) $\delta = 0$; (b) $\delta = \frac{1}{16}$. The specific layer shown in these drawings is an O(2) layer at $z = \frac{3}{24}\left(\frac{1}{8}\right)$ in (a) or $z = \frac{7}{48}$ in (b) ($\frac{3}{4}$ dense layers at other heights z appear the same). The kagome tiling pattern and pseudo-kagome pattern produced by the O atoms in (a) and (b), respectively, are superimposed on the diagrams in yellow.

The oxygen sublattice in real $A_2B_2O_7$ pyrochlores is a more complicated story compared with the cation sublattice description provided above. The oxygen sublattice deviates from the *ideal* anion sublattice description for M_4O_7 compounds presented in Table III.3-1. Interestingly, this deviation is described by a single parameter, usually denoted x in the cubic *u.c.* description for pyrochlores (this is a 48f equipoint parameter in S.G. $Fd\overline{3}m$) (SAR [1]). Using this oxygen positional parameter, we can express the anion sublattice deviation from ideality by a parameter which we denote as δ in Table IV.4-1, where $\delta = \frac{3}{8} - x$. For the ideal M_4O_7 structure presented in Table III.3-1, $\delta = 0$. But in the following discussion, we are interested in deviations progressing from ideality ($\delta = 0$) to an interesting layered structure limit in which $\delta = \frac{1}{16}$ (0.0625).

When $\delta = 0$, the corresponding *ideal* cubic *u.c.* oxygen parameter x is given by $x = \frac{3}{8}$ (0.375). Under this condition, the discussion in Section III.6 indicates that 50% of cations (A) are 8-fold coordinated by 1st *n.n.* anions in ideal, *regular sc* geometry, while the remaining cations (B) are 6-fold coordinated by 1st *n.n.* anions in nonregular, highly distorted octahedral coordination units (trigonal antiprisms). But now, imagine that we increase the deviation parameter to $\delta = \frac{1}{16}$ (0.0625) (the cubic *u.c.* oxygen parameter is now given by $x = \frac{5}{16}$ (0.3125)). In this case, while 50% of cations (A) remain 8-fold coordinated by 1st *n.n.* anions, the geometry consists of nonregular, highly distorted *sc* coordination polyhedra. On the other hand, the remaining cations (B) are 6-fold coordinated by 1st *n.n.* anions but now in the form of ideal, *regular* octahedral coordination polyhedra. Most real $A_2B_2O_7$ compounds are closer to $\delta = \frac{1}{16}$ than to $\delta = 0$, which implies that B cations more strongly desire regular, octahedral geometry than A cations prefer regular, *sc* coordination.

Two things happen as the deviation parameter δ progresses from 0 to $\frac{1}{16}$. First, the O layer heights deviate from ideality, some dilating away, others contracting toward their *n.n.* M layers. Second, the (x, y) tiling patterns within the layers along $\overline{3}$ become distorted. Table IV.4-2 shows the layer atom sequence for a hypothetical $A_2B_2O_7$ pyrochlore compound with $\delta = \frac{1}{16}$. For this structure, it is convenient to imagine that the hexagonal *u.c.* along the *c*-axis is divided into 48^{ths}. The O layers at *u.c.* heights $z = \frac{1}{24}, \frac{1}{24}, \quad \frac{7}{24}, \frac{9}{24}, \quad \frac{15}{24}, \frac{17}{24}$ (Table III.4-3), made from equipoints O(1) and O(3), each degenerate into two layers while the O layers at *u.c.* heights $z = \frac{3}{24}, \frac{5}{24}, \quad \frac{11}{24}, \frac{13}{24}, \quad \frac{19}{24}, \frac{21}{24}$, made from equipoint O(2), remain undissociated. Pairs of O(1) anion layers along z dilate away from their intermediate (AB) cation layers, while O(2) cation layer pairs collapse toward their intermediate (AB) cation layers.

Table IV.4-2. Atomic layer sequence comparison in S.G. $R\bar{3}$ between an $A_2B_2O_7$ pyrochlore with oxygen positional parameter $\delta = 0$ versus the same $A_2B_2O_7$ pyrochlore with $\delta = \frac{1}{16}$. This is equivalent to comparing oxygen positional parameters $x = \frac{3}{8}$ with $x = \frac{5}{16}$ in the cubic *u.c.* description for pyrochlores based on a 48*f* equipoint parameter in S.G. $Fd\bar{3}m$. Notice the oxygen layer degeneracy introduced when $\delta = \frac{1}{16}$.

Layer Height (z) (*u.c.* fraction)	$A_2B_2O_7$ Pyrochlore with Oxygen Positional Parameter $\delta = 0$	Layer Height (z) (*u.c.* fraction)	$A_2B_2O_7$ Pyrochlore with Oxygen Positional Parameter $\delta = \frac{1}{16}$
$\frac{25}{24}$	**O(1) 18*f* O(3) 6*c***	$\frac{51}{48}$	**O(1) 18*f***
		$\frac{50}{48}\left(\frac{25}{24}\right)$	**O(3) 6*c***
$\frac{24}{24}$ (1)	**B(1) 3*a* A(1) 9*e***	$\frac{49}{48}$	empty
		$\frac{48}{48}$ (1)	**B(1) 3*a* A(1) 9*e***
$\frac{23}{24}$	**O(1) 18*f* O(3) 6*c***	$\frac{47}{48}$	empty
		$\frac{46}{48}\left(\frac{23}{24}\right)$	**O(3) 6*c***
$\frac{22}{24}\left(\frac{11}{12}\right)$	empty	$\frac{45}{48}\left(\frac{15}{16}\right)$	**O(1) 18*f***
		$\frac{44}{48}\left(\frac{11}{12}\right)$	empty
$\frac{21}{24}\left(\frac{7}{8}\right)$	**O(2) 18*f***	$\frac{43}{48}$	empty
		$\frac{42}{48}\left(\frac{7}{8}\right)$	empty
$\frac{20}{24}\left(\frac{5}{6}\right)$	**A(2) 3*b* B(2) 9*d***	$\frac{41}{48}$	**O(2) 18*f***
		$\frac{40}{48}\left(\frac{5}{6}\right)$	**A(2) 3*b* B(2) 9*d***
$\frac{19}{24}$	**O(2) 18*f***	$\frac{39}{48}\left(\frac{13}{16}\right)$	**O(2) 18*f***
		$\frac{38}{48}\left(\frac{19}{24}\right)$	empty
$\frac{18}{24}\left(\frac{3}{4}\right)$	empty	$\frac{37}{48}$	empty
		$\frac{36}{48}\left(\frac{3}{4}\right)$	empty
$\frac{17}{24}$	**O(1) 18*f* O(3) 6*c***	$\frac{35}{48}$	**O(1) 18*f***
		$\frac{34}{48}\left(\frac{17}{24}\right)$	**O(3) 6*c***
$\frac{16}{24}\left(\frac{2}{3}\right)$	**B(1) 3*a* A(1) 9*e***	$\frac{33}{48}\left(\frac{11}{16}\right)$	empty
		$\frac{32}{48}\left(\frac{2}{3}\right)$	**B(1) 3*a* A(1) 9*e***
$\frac{15}{24}\left(\frac{5}{8}\right)$	**O(1) 18*f* O(3) 6*c***	$\frac{31}{48}$	empty
		$\frac{30}{48}\left(\frac{5}{8}\right)$	**O(3) 6*c***
$\frac{14}{24}\left(\frac{7}{12}\right)$	empty	$\frac{29}{48}$	**O(1) 18*f***
		$\frac{28}{48}\left(\frac{7}{12}\right)$	empty

Layer Height (z) (*u.c.* fraction)	$A_2B_2O_7$ Pyrochlore with Oxygen Positional Parameter $\delta = 0$	Layer Height (z) (*u.c.* fraction)	$A_2B_2O_7$ Pyrochlore with Oxygen Positional Parameter $\delta = \frac{1}{16}$
$\frac{13}{24}$	**O(2) 18f**	$\frac{27}{48}\left(\frac{9}{16}\right)$	empty
		$\frac{26}{48}\left(\frac{13}{24}\right)$	empty
$\frac{12}{24}\left(\frac{1}{2}\right)$	**A(2) 3b B(2) 9d**	$\frac{25}{48}$	**O(2) 18f**
		$\frac{24}{48}\left(\frac{1}{2}\right)$	**A(2) 3b B(2) 9d**
$\frac{11}{24}$	**O(2) 18f**	$\frac{23}{48}$	**O(2) 18f**
		$\frac{22}{48}\left(\frac{11}{24}\right)$	empty
$\frac{10}{24}\left(\frac{5}{12}\right)$	empty	$\frac{21}{48}\left(\frac{7}{16}\right)$	empty
		$\frac{20}{48}\left(\frac{5}{12}\right)$	empty
$\frac{9}{24}\left(\frac{3}{8}\right)$	**O(1) 18f O(3) 6c**	$\frac{19}{48}$	**O(1) 18f**
		$\frac{18}{48}\left(\frac{3}{8}\right)$	**O(3) 6c**
$\frac{8}{24}\left(\frac{1}{3}\right)$	**B(1) 3a A(1) 9e**	$\frac{17}{48}$	empty
		$\frac{16}{48}\left(\frac{1}{3}\right)$	**B(1) 3a A(1) 9e**
$\frac{7}{24}$	**O(1) 18f O(3) 6c**	$\frac{15}{48}\left(\frac{5}{16}\right)$	empty
		$\frac{14}{48}\left(\frac{7}{24}\right)$	**O(3) 6c**
$\frac{6}{24}\left(\frac{1}{4}\right)$	empty	$\frac{13}{48}$	**O(1) 18f**
		$\frac{12}{48}\left(\frac{1}{4}\right)$	empty
$\frac{5}{24}$	**O(2) 18f**	$\frac{11}{48}$	empty
		$\frac{10}{48}\left(\frac{5}{24}\right)$	empty
$\frac{4}{24}\left(\frac{1}{6}\right)$	**A(2) 3b B(2) 9d**	$\frac{9}{48}\left(\frac{3}{16}\right)$	**O(2) 18f**
		$\frac{8}{48}\left(\frac{1}{6}\right)$	**A(2) 3b B(2) 9d**
$\frac{3}{24}\left(\frac{1}{8}\right)$	**O(2) 18f**	$\frac{7}{48}$	**O(2) 18f**
		$\frac{6}{48}\left(\frac{1}{8}\right)$	empty
$\frac{2}{24}\left(\frac{1}{12}\right)$	empty	$\frac{5}{48}$	empty
		$\frac{4}{48}\left(\frac{1}{12}\right)$	empty
$\frac{1}{24}$	**O(1) 18f O(3) 6c**	$\frac{3}{48}\left(\frac{1}{16}\right)$	**O(1) 18f**
		$\frac{2}{48}\left(\frac{1}{24}\right)$	**O(3) 6c**
$\frac{0}{24}\left(0\right)$	**B(1) 3a A(1) 9e**	$\frac{1}{48}$	empty
		$\frac{0}{48}\left(0\right)$	**B(1) 3a A(1) 9e**

Layer Height (z) (*u.c.* fraction)	A$_2$B$_2$O$_7$ Pyrochlore with Oxygen Positional Parameter $\delta = 0$	Layer Height (z) (*u.c.* fraction)	A$_2$B$_2$O$_7$ Pyrochlore with Oxygen Positional Parameter $\delta = \frac{1}{16}$
$\frac{\bar{1}}{24}$	**O(1) 18f O(3) 6c**	$\frac{\bar{1}}{48}$	empty
		$\frac{2}{48}\left(\frac{\bar{1}}{24}\right)$	**O(3) 6c**

As mentioned above, the kagome patterns within the O layers in A$_2$B$_2$O$_7$ pyrochlores also undergo an interesting alteration as one progresses from oxygen deviation parameter $\delta = 0$ to $\delta = \frac{1}{16}$. Figure IV.4-2 shows a comparison between a $\delta = 0$ anion kagome pattern of O(2) atoms in a layer at $z = \frac{3}{24}$, versus the anion pattern obtained in the equivalent layer at $z = \frac{7}{48}$ when $\delta = \frac{1}{16}$. In both patterns, equilateral triangles are corner linked in rings, with prominent central vacancies. But for $\delta = 0$, all triangles are the same size, whereas when $\delta = \frac{1}{16}$, the triangles alternate large/small around each ring. Nearest neighbor bond lengths in a $\delta = \frac{1}{16}$ anion layer are alternately shorter and longer than the *n.n.* bond lengths in a $\delta = 0$ pyrochlore anion layer. Figure IV.4-3 shows the projection of three adjacent layers in a $\delta = \frac{1}{16}$ pyrochlore. Specifically, Fig. IV.4-3 illustrates a B(1) + A(1) cation layer at $z = 0$, surrounded by two adjacent $\delta = \frac{1}{16}$ O(1) layers at $z = \pm\frac{3}{48}\left(\pm\frac{1}{16}\right)$. This diagram illustrates the regular octahedral coordination of B cations by *n.n.* O anions when $\delta = \frac{1}{16}$.

Finally, Table IV.4-3 shows cube and hexagonal *u.c.* lattice parameters for a selection of A$_2$B$_2$O$_7$ pyrochlore compounds as well as oxygen positional and deviation parameters, x and δ, respectively (the latter for use in Table IV.4-1).
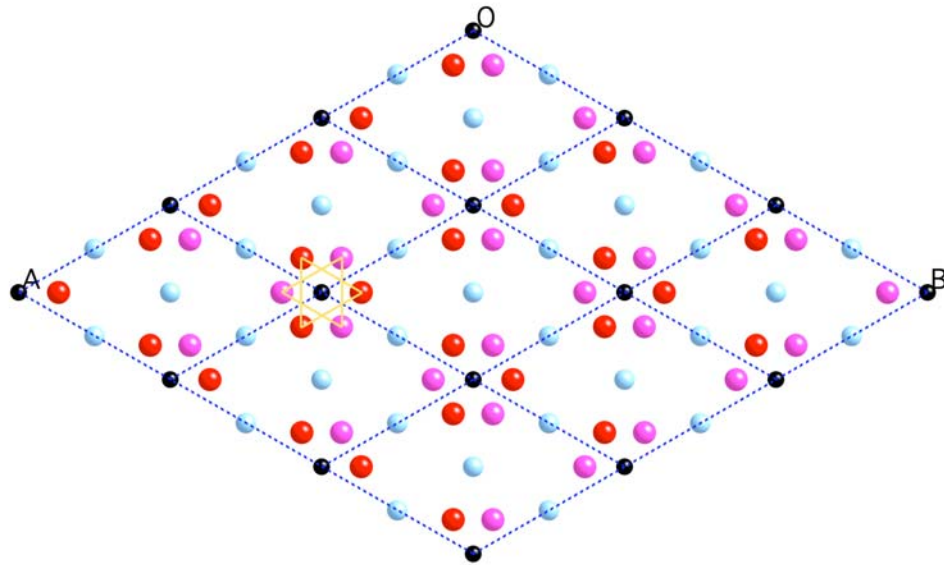
Figure IV.4-3. Superposition of three $A_2B_2O_7$ pyrochlore atomic layers along $\bar{3}$ for a compound with an oxygen positional parameter of $\delta = \frac{1}{16}$. Specifically, the diagram shows an (A(1) + B(1)) cation layer at $z = 0$ (large blue A and small black B atoms, respectively) surrounded by two adjacent O(1) layers at $z = \pm\frac{3}{48}(\pm\frac{1}{16})$ (+atoms in red, –atoms in pink). The diagram illustrates the regular octahedral coordination of B cations by *n.n.* O anions when $\delta = \frac{1}{16}$ (yellow lines). Intermediate O(3) layers at $z = \pm\frac{2}{48}(\pm\frac{1}{24})$ (not shown here) do not participate in 1st *n.n.* coordination of B cations.

Table IV.4-3. Lattice parameters and oxygen positional parameters for a selection of $A_2B_2O_7$ pyrochlore compounds (cube *u.c.* data obtained from SAR [1]). Hexagonal *u.c.* lattice parameters a and c are obtained from the cube *u.c.* length, a_{cube}, using the M_4O_7 relationships $a = 2\,d$ (Eq. (III.5-1) and $\frac{\#\ atoms}{hexcell} = 4$) and $c = 2\,\sqrt{6}\,d$ (24-layer stacking, Eq. (III.5-4b)), where *n.n.* spacing d is given by $d = \frac{a_{cube}}{2\sqrt{2}}$. Also, the relationship used here between oxygen positional and deviation parameters, x and δ, is $\delta = \frac{3}{8} - x$. Note that the first seven compounds are 3+4+ pyrochlores, while the last two are 2+5+ pyrochlores.

Compound	a_{cube} (nm) (cubic *u.c.* lattice parameter)	a, c (nm) (hexagonal *u.c.* lattice parameters)	x (oxygen sublattice positional parameter)	δ (oxygen sublattice deviation parameter)
$La_2Sn_2O_7$	1.0701	0.7567 1.8535	0.325	0.050
$Sm_2Ti_2O_7$	1.0233	0.7236 1.7724	0.327	0.048
$Gd_2Ti_2O_7$	1.0185	0.7202 1.7641	0.322	0.053
$Er_2Ti_2O_7$	1.0087	0.7133 1.7471	0.331	0.044
$Lu_2Ti_2O_7$	1.0018	0.7084 1.7352	0.330	0.045
$Y_2Ti_2O_7$	1.0095	0.7138 1.7485	0.328	0.047
$Y_2Sn_2O_7$	1.0373	0.7335 1.7967	0.338	0.037
$Hg_2Nb_2O_7$	1.0453	0.7391 1.8105	0.323	0.052
$Hg_2Ta_2O_7$	1.0452	0.7391 1.8103	0.322	0.053

Section IV.4 References

[1]   M. A. Subramanian, G. Aravamudan, and G. V. Subba Rao, "Oxide Pyrochlores - A Review," *Prog. Solid St. Chem.* **15** 55 (1983) .

IV.5. Real Materials: M_7O_{12}

M_7O_{12} compounds are ubiquitous in the literature. Examples include the iota (ι) phase found in mono-cationic oxides (also often called binary oxides) such as Ce_7O_{12}, Pr_7O_{12}, and Tb_7O_{12} [1] while many others consist of two cation species, especially $A_4B_3O_{12}$ compounds, which are mixtures of A^{3+} and B^{4+} cations (see, for example, Ref. [2]). In addition, there exists an $A_6B_1O_{12}$ compound produced by combining A^{3+} and B^{6+} cations, epitomized by the oxide $U_1Y_6O_{12}$ [3].

The most commonly cited crystal structure refinement found in the literature for an M_7O_{12} compound is a refinement for δ-$Sc_4Zr_3O_{12}$ by Thornber, Bevan, and Graham (TBG) [4]. However, we have determined that TBG made an error defining the registry of successive layers along $\bar{3}$. Specifically, they placed M(1) at equipoint $3a$, which produces cation stacking registry C at height $z = \frac{1}{3}$. But then they assigned M(2) to equipoint $18f$ in such a way as to produce cation stacking registry B at a height z very near to $z = \frac{1}{3}$. The M(1) and M(2) equipoint definitions provided by TBG are incompatible. We have not found a means to unambiguously recover the actual structure intended by the TBG refinement. Thus, we suggest here that the TBG structure refinement must be discarded from crystal structure discussions for M_7O_{12} compounds. Two alternative refinements for δ-$Sc_4Zr_3O_{12}$ that have the correct stacking registries are by Rossell [5] (also PDF-30-1126 [6]) and Red'ko and Lopato [7]. The Rossell refinement is shown in Table IV.5-1.

Two other crystal structure refinements for M_7O_{12} compounds are noteworthy and they are reproduced in Tables IV.5-2 and IV.5-3. Table IV.5-2 shows the refined structure for Tb_7O_{12} by Zhang, Von Dreele, and Eyring (ZVE) [8], while Table IV.5-3 reproduces the refinement of $U_1Y_6O_{12}$ due to Bartram [3].

Table IV.5-1. Hexagonal *u.c.* description for δ-$Sc_4Zr_3O_{12}$, according to Rossell [5]. Fractional coordinates (*x*, *y*, *z*) for the atoms refer to trigonal space group $R\bar{3}$ (hexagonal axes). Sc and Zr represent metal cations and O represents oxygen anions. *Z* is the number of formula units per hexagonal *u.c.* Deviations from ideality are expressed as fractions of *u.c.* lengths, $(\delta_x, \delta_y, \delta_z)$. This data should be compared with Table III.4-4, in particular to the ideal, 12-layer hexagonal *u.c.* description for M_7O_{12}. The Rossell hexagonal *u.c.* lattice parameters are *a* = 0.9396(1) nm and *c* = 0.8720(2) nm.

Structure	*Z*	Equipoint (Wyckoff notation) and Fractional Coordinates (*x*, *y*, *z*) for Atoms in the Hexagonal *u.c.*
δ-$Sc_4Zr_3O_{12}$	3	ScZr(1) at 3*a*: $(0,0,0)$ + EP
		(0.0000 0.0000 0.0000) ideal
		(0.0000 0.0000 0.0000) Rossell
		(0.0000 0.0000 0.0000) $(\delta_x, \delta_y, \delta_z)$
		(site occupancy is $\frac{4}{7}$ Sc and $\frac{3}{7}$ Zr)
		_____
		ScZr(2) at 18*f*: $\left(\frac{1}{7}, \frac{3}{7}, 0\right)$ + EP
		(0.1429 0.4286 0.0000) ideal
		(0.2906(12) 0.410(1) 0.0162(9)) Rossell
		(+0.1477 -0.0185 +0.0163) $(\delta_x, \delta_y, \delta_z)$
		(site occupancy is $\frac{4}{7}$ Sc and $\frac{3}{7}$ Zr)
		_____
		O(1) at 18*f*: $\left(\frac{1}{7}, \frac{3}{7}, \frac{3}{4}\right)$ + EP
		(0.1429 0.4286 0.7500) ideal
		(0.293(6) 0.453(5) 0.774(4)) Rossell
		(+0.1507 +0.0249 +0.0244) $(\delta_x, \delta_y, \delta_z)$
		_____
		O(2) at 18*f*: $\left(\frac{1}{7}, \frac{3}{7}, \frac{1}{4}\right)$ + EP
		(0.1429 0.4286 0.2500) ideal
		(0.304(5) 0.453(5) 0.281(6)) Rossell
		(+0.1616 +0.0249 +0.0316) $(\delta_x, \delta_y, \delta_z)$

Table IV.5-2. Hexagonal *u.c.* description for ι-Tb$_7$O$_{12}$, based on a crystal structure refinement by ZVE [8]. Fractional coordinates (*x*, *y*, *z*) for the atoms refer to trigonal space group $R\bar{3}$ (hexagonal axes). Tb represents metal cations and O represents oxygen anions. *Z* is the number of formula units per hexagonal *u.c.* Deviations from ideality are expressed as fractions of *u.c.* lengths, $(\delta_x, \delta_y, \delta_z)$. This data should be compared with Table III.4-4, in particular to the ideal, 12-layer hexagonal *u.c.* description for M$_7$O$_{12}$. The ZVE hexagonal *u.c.* lattice parameters are *a* = 0.99229(8) nm and *c* = 0.92637(4) nm.

Structure	Z	
ι-Tb$_7$O$_{12}$	3	Tb(1) at 3*a*: $(0,0,0)$ + EP
		(0.00000 0.00000 0.00000) ideal
		(0.00000 0.00000 0.00000) ZVE
		(0.00000 0.00000 0.00000) $(\delta_x, \delta_y, \delta_z)$
		————————————————
		Tb(2) at 18*f*: $\left(\frac{1}{7}, \frac{3}{7}, 0\right)$ + EP
		(0.14286 0.42857 0.00000) ideal
		(0. 12214(7) 0. 41043(4) -0.01638(2)) ZVE
		(-0.02071 -0.01814 -0.01638) $(\delta_x, \delta_y, \delta_z)$
		————————————————
		O(1) at 18*f*: $\left(\frac{1}{7}, \frac{3}{7}, \frac{3}{4}\right)$ + EP
		(0.1429 0.4286 0.7500) ideal
		(0.1473(1) 0.4470(0) 0.7309(9)) ZVE
		(+0.0044 +0.0184 -0.0190) $(\delta_x, \delta_y, \delta_z)$
		————————————————
		O(2) at 18*f*: $\left(\frac{1}{7}, \frac{3}{7}, \frac{1}{4}\right)$ + EP
		(0.1429 0.4286 0.2500) ideal
		(0.1624(3) 0.4594(6) 0.2229(5)) ZVE
		(+0.0196 +0.0309 -0.0270) $(\delta_x, \delta_y, \delta_z)$

Table IV.5-3. Hexagonal *u.c.* description for $U_1Y_6O_{12}$, according to Bartram [3]. Fractional coordinates (*x*, *y*, *z*) for the atoms refer to trigonal space group $R\bar{3}$ (hexagonal axes). U and Y represent metal cations and O represents oxygen anions. *Z* is the number of formula units per hexagonal *u.c.* Deviations from ideality are expressed as fractions of *u.c.* lengths, $(\delta_x, \delta_y, \delta_z)$. This data should be compared with Table III.4-4, in particular to the ideal, 12-layer hexagonal *u.c.* description for M_7O_{12}. The Bartram hexagonal *u.c.* lattice parameters are *a* = 0.9934 nm and *c* = 0.9364 nm.

Structure	Z	Equipoint (Wyckoff notation) and Fractional Coordinates (*x*, *y*, *z*) for Atoms in the Hexagonal *u.c.*
$U_1Y_6O_{12}$	3	U(1) at 3*a*: $(0,0,0)$ + EP
		(0.0000 0.0000 0.0000) ideal
		(0.0000 0.0000 0.0000) Bartram
		(0.0000 0.0000 0.0000) $(\delta_x, \delta_y, \delta_z)$
		_____
		Y(1) at 18*f*: $\left(\frac{1}{7}, \frac{3}{7}, 0\right)$ + EP
		(0.1429 0.4286 0.0000) ideal
		(0.1224 0.4170 0.0235) Bartram
		(-0.0205 -0.0116 +0.0235) $(\delta_x, \delta_y, \delta_z)$
		_____
		O(1) at 18*f*: $\left(\frac{1}{7}, \frac{3}{7}, \frac{3}{4}\right)$ + EP
		(0.1429 0.4286 0.7500) ideal
		(0.174 0.476 0.784) Bartram
		(+0.031 +0.047 +0.034) $(\delta_x, \delta_y, \delta_z)$
		_____
		O(2) at 18*f*: $\left(\frac{1}{7}, \frac{3}{7}, \frac{1}{4}\right)$ + EP
		(0.1429 0.4286 0.2500) ideal
		(0.140 0.447 0.268) Bartram
		(-0.003 +0.018 -0.018) $(\delta_x, \delta_y, \delta_z)$

Deviations from ideality in Tb_7O_{12} and $U_1Y_6O_{12}$ are very similar to the deviations described for M_7O_{13} compounds described in Section IV.3. Cation layers become rumpled along $\bar{3}$ such that each ideal cation layer degenerates into three layers with distinct z coordinates. However, the in-plane distortions are small (4% or less), so that when viewed in projection along $\bar{3}$, the cation sublattice consists of fully dense, triangular atom nets. An example of such a cation net in $U_1Y_6O_{12}$ is illustrated in Fig. IV.5-1. It is interesting to note that the cations in $U_1Y_6O_{12}$ are found to be ordered whereas the cations in most M_7O_{12} compounds are believed to randomly occupy the M(1) and M(2) cation sites (Table III.4-4). In $U_1Y_6O_{12}$, U occupies the $3a$ equipoint (M(1) in Table III.4-4) while Y occupies the $18f$ GEP (M(2) in Table III.4-4). Figure IV.5-1a illustrates this ordering of U^{6+} and Y^{3+} cations in $U_1Y_6O_{12}$. In each cation layer along $\bar{3}$, the Y^{3+} cations are themselves arranged in a $3^4.6$ Archimedean tiling, while the U^{6+} cations fill the interstices within this tiling pattern.

Figure IV.5-1b shows the layered O anion arrangement projected down $\bar{3}$ in $U_1Y_6O_{12}$. In the ideal structure, these anions would reside at height $z = \frac{1}{12}$. But in the real, relaxed structure, each anion layer degenerates into two layers at heights surrounding the ideal z. Nevertheless, in-plane distortions are small as in the case of the cations, so that when viewed in projection along $\bar{3}$, the anion sublattice appears as a slightly distorted, $3^4.6$ Archimedean tiling. Layered structures in Tb_7O_{12} (not shown here) are very similar to the $U_1Y_6O_{12}$ layer arrangements shown in Fig. IV.5-1. So the $3^4.6$ Archimedean tiling can be used to describe both anion and cation arrangements in M_7O_{12} compounds!

Figure IV.5-2 shows projections perpendicular to $\bar{3}$ of the relaxed crystal structures for Tb_7O_{12} and $U_1Y_6O_{12}$. As mentioned above, cation and anion layers appear rumpled in this projection. But these distortions away from ideality are small. For instance, in the $U_1Y_6O_{12}$ compound, the deviations from ideal along the c-axis are only 1.8% (O(2)), 2.3% (Y(1)), and 3.4% (O(1)) of lattice parameter c (the U cations are in ideal positions). Similar deviations are associated with the Tb_7O_{12} compound.
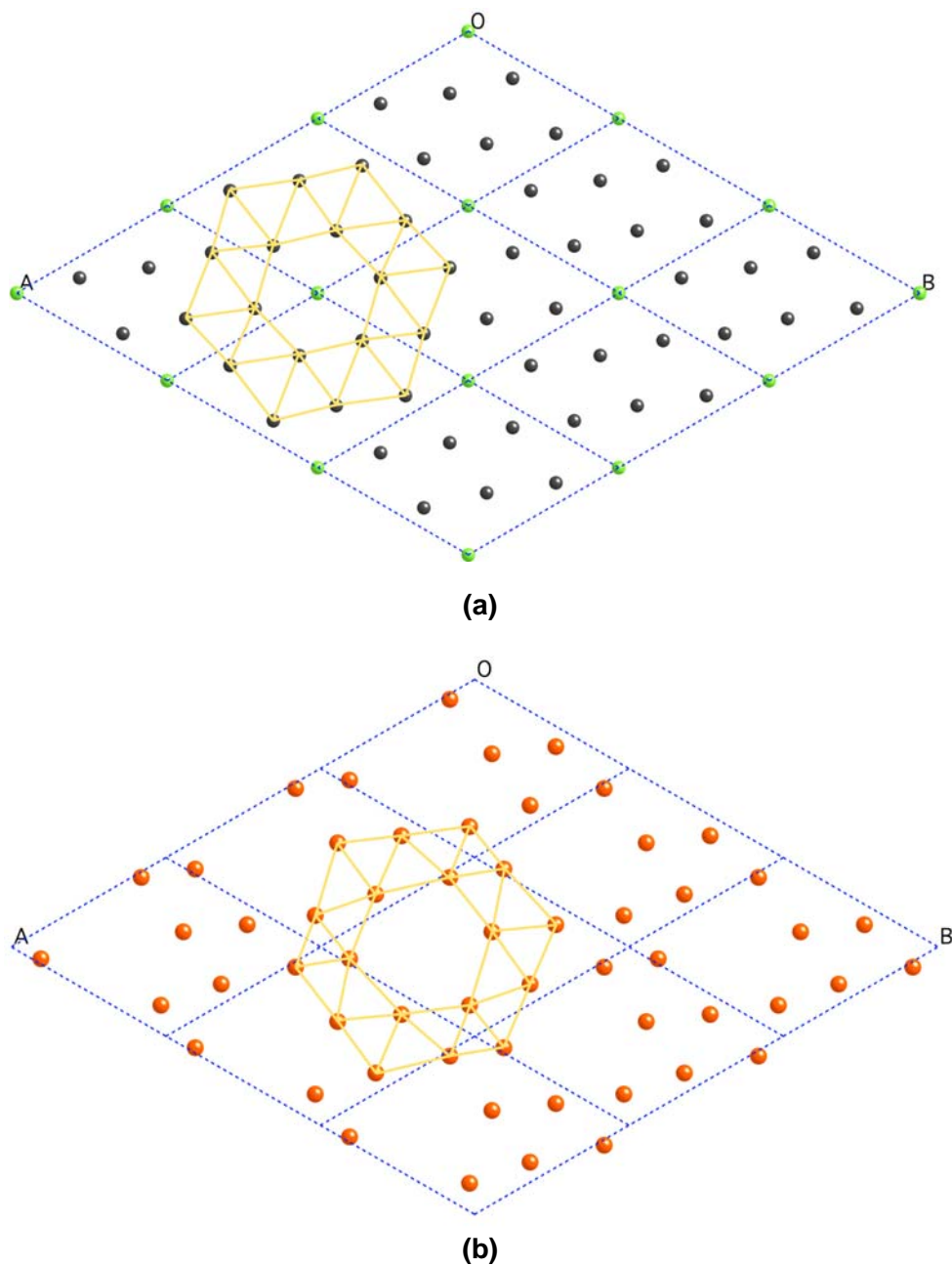
(a)

(b)

Figure IV.5-1. (a) Projection of the cation arrangement in $U_1Y_6O_{12}$, for cation layers normal to $\bar{3}$ at *u.c.* heights $z = 0$, ±0.0235 (Bartram's refined structure [3]). The region shown represents 4×4 hexcell area. U^{6+} cations are shown in small/green; Y^{3+} cations are in larger/blue-black. Y^{3+} ions by themselves form a $\frac{6}{7}$ dense, slightly distorted $3^4.6$ Archimedean tiling. U^{6+} cations are $\frac{1}{7}$ dense in this rumpled planar array. Together the Y^{3+} and U^{6+} cations form a fully dense, slightly distorted triangular atom net. (b) Projection of the anion arrangement in $U_1Y_6O_{12}$, for anion layers normal to $\bar{3}$ at *u.c.* heights $z = 0.0653$, 0.1173 (Bartram's refined structure [3]). O^{2-} anions are shown in red. These anions form a $\frac{6}{7}$ dense, slightly distorted $3^4.6$ Archimedean tiling. Yellow lines in (a, b) delineate the characteristic tiling patterns in the respective atom layers.
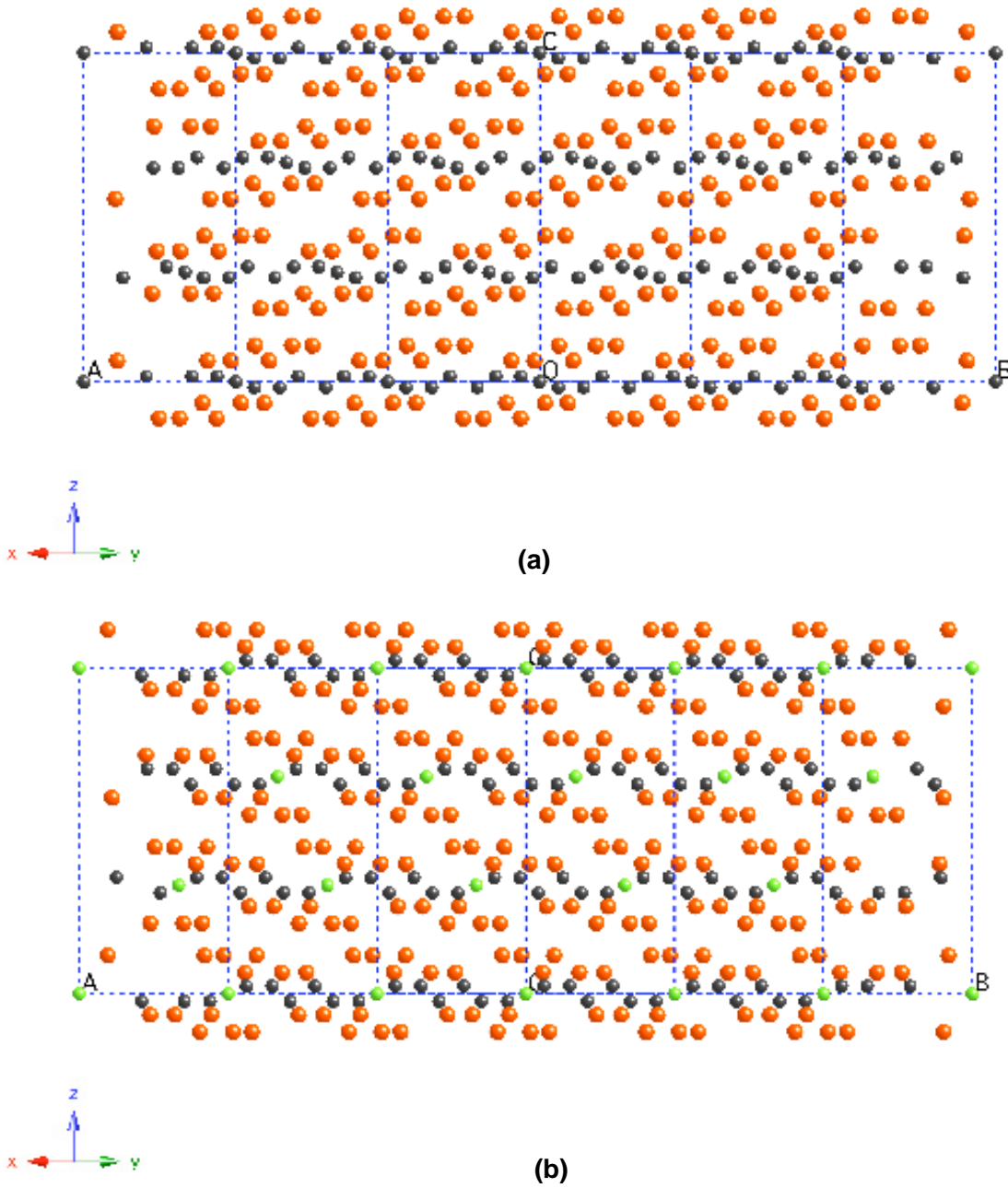
Figure IV.5-2. Projections parallel to $\bar{3}$ of the relaxed crystal structures for (a) Tb_7O_{12} according to ZVE [5]; and (b) $U_1Y_6O_{12}$ according to Bartram [3]. Cations are shown small/black or green; anions are shown large/red. The dimensions of the *u.c.* along the *c*-axis are exaggerated by a factor of 2, in order to better illustrate the rumpled cation and anion layers. In each diagram, one *u.c.* is shown along the vertical (*z*) axis (plus a few extra layers), while three *u.c.*s are illustrated on the horizontal (*x*, *y*) axes.

A selection of some additional oxides known to exhibit the M_7O_{12} crystal structure are shown in Table IV.5-4. Lattice parameter $\frac{c}{a}$ ratios are also shown. Recall from Section III.5 that the ideal, 12-layer $\frac{c}{a}$ ratio for *subdivision by 7^{ths}* of a triangular atom net is given by $\frac{c}{a} = \sqrt{\frac{6}{7}} = 0.9258$ (Eq. (III.5-5a)). Table IV.5-4 also shows $\frac{c}{a}$ deviations from ideality for these real compounds. The $\frac{c}{a}$ ratios for the M_7O_{12} compounds in Table IV.5-4 correspond very nearly to the ideal $\frac{c}{a}$ ratio described above. The largest $\frac{c}{a}$ deviations from ideality are approximately 1%. For $A_4B_3O_{12}$ compounds, the largest $\frac{c}{a}$ deviations occur when the disparities between A^{3+} and B^{4+} cation radii are largest.

Table IV.5-4. Unit cell parameters for a selection of M_7O_{12} compounds. $\delta\left(\frac{c}{a}\right)$ represents the deviation of the real structure *u.c.* parameters from the ideal layer stacking structures.

Compound	a (nm)	c (nm)	$\frac{c}{a}$	$\delta\left(\frac{c}{a}\right)$	Reference
Tb_7O_{12}	0.99229(8)	0.92637(4)	0.93356(4)	+0.00774	[5]
Ce_7O_{12}	1.037	0.9671	0.9326	+0.0068	[1]
Pr_7O_{12}	0.99220(1)	0.92631(3)	0.93359(4)	+0.00777	[1]
$U_1Y_6O_{12}$	0.9934	0.9364	0.9426	+0.0168	[3]
$Sc_4Zr_3O_{12}$	0.9396(2)	0.8706(3)	0.9266(3)	+0.00081	[2]
$Sc_4Hf_3O_{12}$	0.9369(2)	0.8692(3)	0.9277(5)	+0.00193	[2]
$Lu_4Zr_3O_{12}$	0.9636(1)	0.8990(2)	0.9330(3)	+0.00721	[2]
$Lu_4Hf_3O_{12}$	0.9608(2)	0.8981(3)	0.9347(5)	+0.00893	[2]
$Yb_4Zr_3O_{12}$	0.9654(1)	0.9021(2)	0.9344(4)	+0.00862	[2]
$Yb_4Hf_3O_{12}$	0.9639(2)	0.9007(3)	0.9344(4)	+0.00862	[2]
$Tm_4Zr_3O_{12}$	0.9677(2)	0.9042(3)	0.9344(2)	+0.00862	[2]
$Tm_4Hf_3O_{12}$	0.9649(2)	0.9025(3)	0.9353(4)	+0.00860	[2]
$Er_4Zr_3O_{12}$	0.9698(1)	0.9054(2)	.9336(1)	+0.00779	[2]
$Er_4Hf_3O_{12}$	0.9681(1)	0.9063(2)	.9362(3)	+0.01041	[2]
$Ho_4Zr_3O_{12}$	0.9732(1)	0.9109(2)	.9360(1)	+0.01019	[2]
$Y_4Zr_3O_{12}$	0.9738(2)	0.9119(3)	.9364(5)	+0.01063	[2]

Section IV.5 References

[1]   J. Zhang, Z. C. Kang, and L. Eyring, "The Binary Higher Oxides of the Rare Earths," *J. Alloys Comp.* **192** 57–63 (1993).

[2]   L. M. Lopato, V. P. Red'ko, G. I. Gerasimyuk, and A. V. Shevchenko, "Synthesis and Properties of $M_4Zr_3O_{12}$ and $M_4Hf_3O_{12}$ Compounds (M - Rare Earth Element)," *Neorg. Mater.* **27** (8) 1718–1722 (1991).

[3]   S. F. Bartram, "Crystal Structures of the Rhombohedral $MO_3 \cdot 3R_2O_3$ Compounds (M = U, W, or Mo) and Their Relation to Ordered R_7O_{12} Phases," *Inorg. Chem.* **5** (5) 749–754 (1966).

[4]   M. R. Thornber, D. J. M. Bevan, and J. Graham, "Mixed Oxides of the Type MO_2 (Fluorite) - M_2O_3. III. Crystal Structures of the Intermediate Phases $Zr_5Sc_2O_{13}$ and $Zr_3Sc_4O_{12}$," *Acta Cryst. B* **24** 1183–1190 (1968).

[5]   H. J. Rossell, "Crystal Structures of Some Florite-Related M_7O_{12} Compounds," *J. Sol. State Chem.* **19** 103–111 (1976).

[6]   International Committee for Diffraction Data, Powder Diffraction File (Joint Committee on Powder Diffraction Standards, Philadelphia, PA, 1974– present).

[7]   V. P. Red'ko and L. M. Lopato, "Crystal Structure of $M_4Zr_3O_{12}$ and $M_4Hf_3O_{12}$ Compounds (M-Rare Earth)," *Izvestiya Akademii Nauk SSSR, Neorganicheskie Materialy* **27** 1905–1910 (1991).

[8]   J. Zhang, R. B. Von Dreele, and L. Eyring, "The Structures of Tb_7O_{12} and $Tb_{11}O_{20}$," *J. Sol. State Chem.* **104** 21–32 (1993).

IV.6.1. Real Materials: M₂O₃ Sesquioxides

IV.6.1. Real Materials: M$_2$O$_3$ Sesquioxides

Sesquioxides are arguably the most interesting of all compounds discussed in this paper. The sesquioxide stoichiometry seems to be the oxidation state where the transition from the MO to the MOO layer stacking motif occurs. Both MO and MOO sesquioxides occur in nature, along with compounds that possess other motifs such as a fascinating (MO)M motif, which we will discuss shortly. We will now examine individually the most common sesquioxide crystal structures..

IV.6.2. Real Materials: A_2O_3 Corundum

We introduced the corundum structure in Section III of this paper. Table IV.6.2-1 shows the crystallographic description for corundum compounds using hexagonal axes in S.G. $R\overline{3}$. Corundum actually belongs to S.G. $R\overline{3}c$, which is to say that it possesses higher symmetry than is described by S.G. $R\overline{3}$. Nevertheless, we define the corundum structure in Table IV.6.2-1 with respect to S.G. $R\overline{3}$ so it can be easily compared with the $R\overline{3}$ structures presented earlier in this paper.

Table IV.6.2-1. Atom positions in the hexagonal *u.c.* description for corundum (A_2O_3) compounds. Fractional coordinates (*x*, *y*, *z*) for the atoms refer to trigonal space group $R\overline{3}$ (hexagonal axes). As usual, A represents metal cations and O represents oxygen anions. V represents a cation sublattice vacancy. Z is the number of formula units per hexagonal *u.c.* Corundum is normally assigned to S.G. $R\overline{3}c$ with hexagonal *u.c.* lattice parameters given by *a* and *c*. Parameters Δx and Δz represent anion and cation positional deviation parameters, respectively.

Structure	Z	Equipoint (Wyckoff notation) and Fractional Coordinates (*x*, *y*, *z*) for Atoms in the Hexagonal *u.c.*
Corundum A_2O_3	6	V(1) at 3*a*: $\left(0,0,0\right)$ + EP V(2) at 3*b*: $\left(0,0,\frac{1}{2}\right)$ + EP ——————————— A(1) at 6*c*: $\left(0,0,\frac{1}{6}-\Delta z\right)$ + EP A(2) at 6*c*: $\left(0,0,\frac{1}{3}+\Delta z\right)$ + EP ——————————— O(1) at 18*f*: $\left(\frac{1}{3}+\Delta x,\frac{1}{3},\frac{1}{12}\right)$ + EP

Table IV.6.2-2 shows the layer stacking sequence along $\overline{3}$ produced by the corundum crystal structure description in Table IV.6.2-1. Figure IV.6.2-1 illustrates this stacking sequence for a compound with the ideal corundum structure. The hexagonal *u.c.* of corundum is described by a 12-layer stacking sequence with an MO stacking motif. Atom arrangements in the *u.c.* hexcells utilize Iida's *subdivision by 3^{rds}* of a triangular atom net [1]. Anion layers alternate registry BCBC…, such that the anion sublattice forms a hexagonal close-packed (*hcp*) lattice. All cation layers are of registry A and $\frac{2}{3}$ dense compared with the fully dense anion layers. The ideal (*x, y*) position of the missing atom

in successive cation layer hexcells varies according to the sequence $(0,0)$, $(\frac{1}{3},\frac{2}{3})$,$(\frac{2}{3},\frac{1}{3})$. Each cation layer forms a honeycomb lattice, as discussed in Section III.2 and illustrated in Fig. III.2-1. All anion layers are fully dense, triangular nets.

All corundum-structured oxides exhibit deviations from the ideal corundum structure as described by deviation parameters Δx and Δz in Tables IV.6.2-1 and IV.6.2-2 (Δx and Δz represent anion and cation positional deviation parameters, respectively). The cation deviation parameter Δz results in rumpling of the honeycomb cation layers along $\overline{3}$. The anion deviation parameter Δx results in in-plane distortions of the anion triangular nets. Ideal versus real corundum crystal structures are shown in Fig. IV.6-2.

Corundum compounds exist in nature and are also produced synthetically. Two examples are shown in Table IV.6.2-3: corundum (Al_2O_3) and hematite (Fe_2O_3). Single crystal Al_2O_3 is known as sapphire, while Fe_2O_3 is commonly referred to as rust.

The sesquioxide polymorph corundum forms in compounds with small radii cations, such as Al^{3+} and Fe^{3+}. Small cations are needed to fit into the relatively small interstices within the corundum hcp anion sublattice. Some oxides containing two different small cationic species also conform to the corundum structure described in Tables IV.6.2-1 and Table IV.62. In these compounds, cation species A occupies the A(1) equipoint while cation species B occupies the A(2) equipoint (Table IV.6.2-1). These ABO_3 compounds are known as ilmenites, named after the mineral ilmenite, $FeTiO_3$. The ilmenite $FeTiO_3$ is also described in Table IV.6.2-3.

Table IV.6.2-2. S.G. $R\bar{3}$ 12-layer stacking sequence description for A_2O_3 corundum compounds (Table IV.6.2-1). Fractional coordinates for atoms within each layer in the hexagonal *u.c.* are shown in parentheses (x, y, z).

| Layer Height (z) (*u.c.* fraction)	Registry $(A, B, or C)$	Ideal Atom Arrangements	Equipoint and Fractional Coordinates (x, y, z) for Atoms in the Hexagonal *u.c.*
$\frac{12}{12}(1)$	A	$\frac{2}{3}$ dense honeycomb net	A(2) @ **6c** $(\frac{1}{3},\frac{2}{3},+\Delta z)$ $(\frac{2}{3},\frac{1}{3},-\Delta z)$
$\frac{11}{12}$	C	fully dense triangular net	O(1) @ **18f** $\left(+\Delta x,\frac{1}{3}+\Delta x,\frac{11}{12}\right)$ $\left(\frac{1}{3},-\Delta x,\frac{11}{12}\right)$ $\left(\frac{2}{3}-\Delta x,\frac{2}{3},\frac{11}{12}\right)$
$\frac{10}{12}\left(\frac{5}{6}\right)$	A	$\frac{2}{3}$ dense honeycomb net	A(1) @ **6c** $(0,0,\frac{5}{6}+\Delta z)$ $(\frac{1}{3},\frac{2}{3},\frac{5}{6}-\Delta z)$
$\frac{9}{12}\left(\frac{3}{4}\right)$	B	fully dense triangular net	O(1) @ **18f** $\left(0,\frac{2}{3}+\Delta x,\frac{3}{4}\right)$ $\left(\frac{1}{3}-\Delta x,\frac{1}{3}-\Delta x,\frac{3}{4}\right)$ $\left(\frac{2}{3}+\Delta x,0,\frac{3}{4}\right)$
$\frac{8}{12}\left(\frac{2}{3}\right)$	A	$\frac{2}{3}$ dense honeycomb net	A(2) @ **6c** $(0,0,\frac{2}{3}-\Delta z)$ $(\frac{2}{3},\frac{1}{3},\frac{2}{3}+\Delta z)$
$\frac{7}{12}$	C	fully dense triangular net	O(1) @ **18f** $\left(-\Delta x,\frac{1}{3},\frac{7}{12}\right)$ $\left(\frac{1}{3}+\Delta x,+\Delta x,\frac{7}{12}\right)$ $\left(\frac{2}{3},\frac{2}{3}-\Delta x,\frac{7}{12}\right)$
$\frac{6}{12}\left(\frac{1}{2}\right)$	A	$\frac{2}{3}$ dense honeycomb net	A(1) @ **6c** $(\frac{1}{3},\frac{2}{3},\frac{1}{2}+\Delta z)$ $(\frac{2}{3},\frac{1}{3},\frac{1}{2}-\Delta z)$
$\frac{5}{12}$	B	fully dense triangular net	O(1) @ **18f** $\left(+\Delta x,\frac{2}{3},\frac{5}{12}\right)$ $\left(\frac{1}{3},\frac{1}{3}+\Delta x,\frac{5}{12}\right)$ $\left(\frac{2}{3}-\Delta x,-\Delta x,\frac{5}{12}\right)$
$\frac{4}{12}\left(\frac{1}{3}\right)$	A	$\frac{2}{3}$ dense honeycomb net	A(2) @ **6c** $(0,0,\frac{1}{3}+\Delta z)$ $(\frac{1}{3},\frac{2}{3},\frac{1}{3}-\Delta z)$
$\frac{3}{12}\left(\frac{1}{4}\right)$	C	fully dense triangular net	O(1) @ **18f** $\left(0,\frac{1}{3}-\Delta x,\frac{1}{4}\right)$ $\left(\frac{1}{3}-\Delta x,0,\frac{1}{4}\right)$ $\left(\frac{2}{3}+\Delta x,\frac{2}{3}+\Delta x,\frac{1}{4}\right)$

Layer Height (z) (u.c. fraction)	Registry (A,B, or C)	Ideal Atom Arrangements	Equipoint and Fractional Coordinates (x, y, z) for Atoms in the Hexagonal u.c.
$\frac{2}{12}\left(\frac{1}{6}\right)$	A	$\frac{2}{3}$ dense honeycomb net	A(1) @ **6c** $(0,0,\frac{1}{6}-\Delta z)$ $(\frac{2}{3},\frac{1}{3},\frac{1}{6}+\Delta z)$
$\frac{1}{12}$	B	fully-dense triangular net	O(1) @ **18f** $\left(-\Delta x,\frac{2}{3}-\Delta x,\frac{1}{12}\right)$ $\left(\frac{1}{3}+\Delta x,\frac{1}{3},\frac{1}{12}\right)$ $\left(\frac{2}{3},+\Delta x,\frac{1}{12}\right)$
$\frac{0}{12}\left(0\right)$	A	$\frac{2}{3}$ dense honeycomb net	A(2) @ **6c** $(\frac{1}{3},\frac{2}{3},+\Delta z)$ $(\frac{2}{3},\frac{1}{3},-\Delta z)$

A₂O₃ Corundum
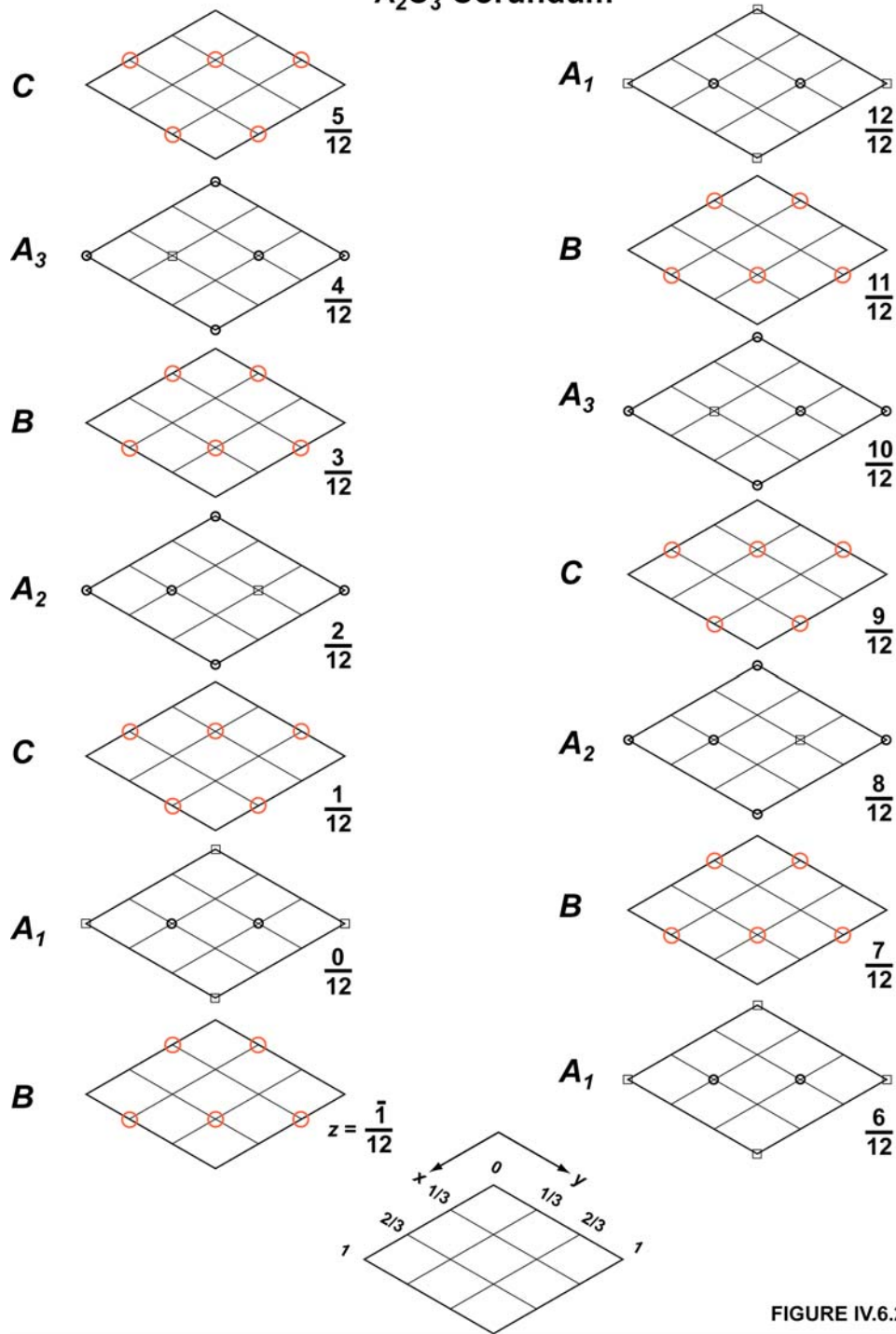
Figure IV.6.2-1. Layer stacking sequence along $\bar{3}$ for the ideal corundum crystal structure. Diagrams are intended to be read from bottom to top, left to right, from minimum to maximum height, z. Corundum *u.c.* hexcells utilize *subdivision by 3^{rds}* of a triangular atom net. Metal cations are small black-outlined circles; oxygen anions are large red-outlined circles. Vacancies on the cation sublattice are indicated by black-outlined squares.

(a)

(b)

(c)

(d)
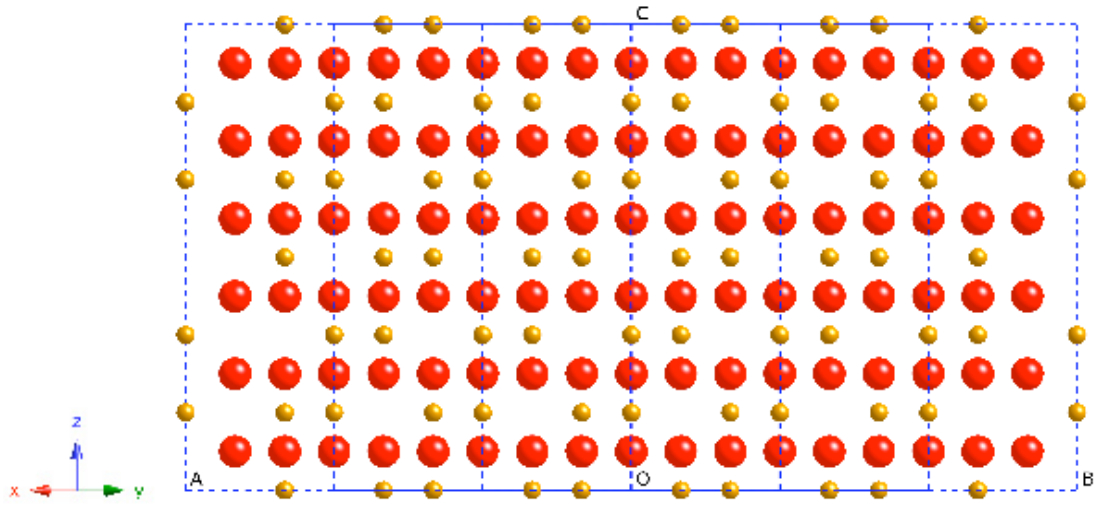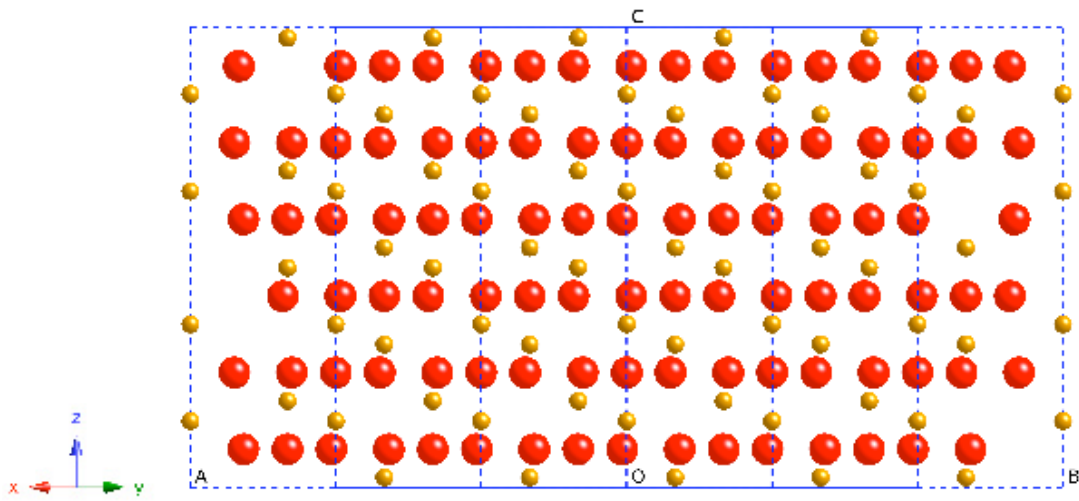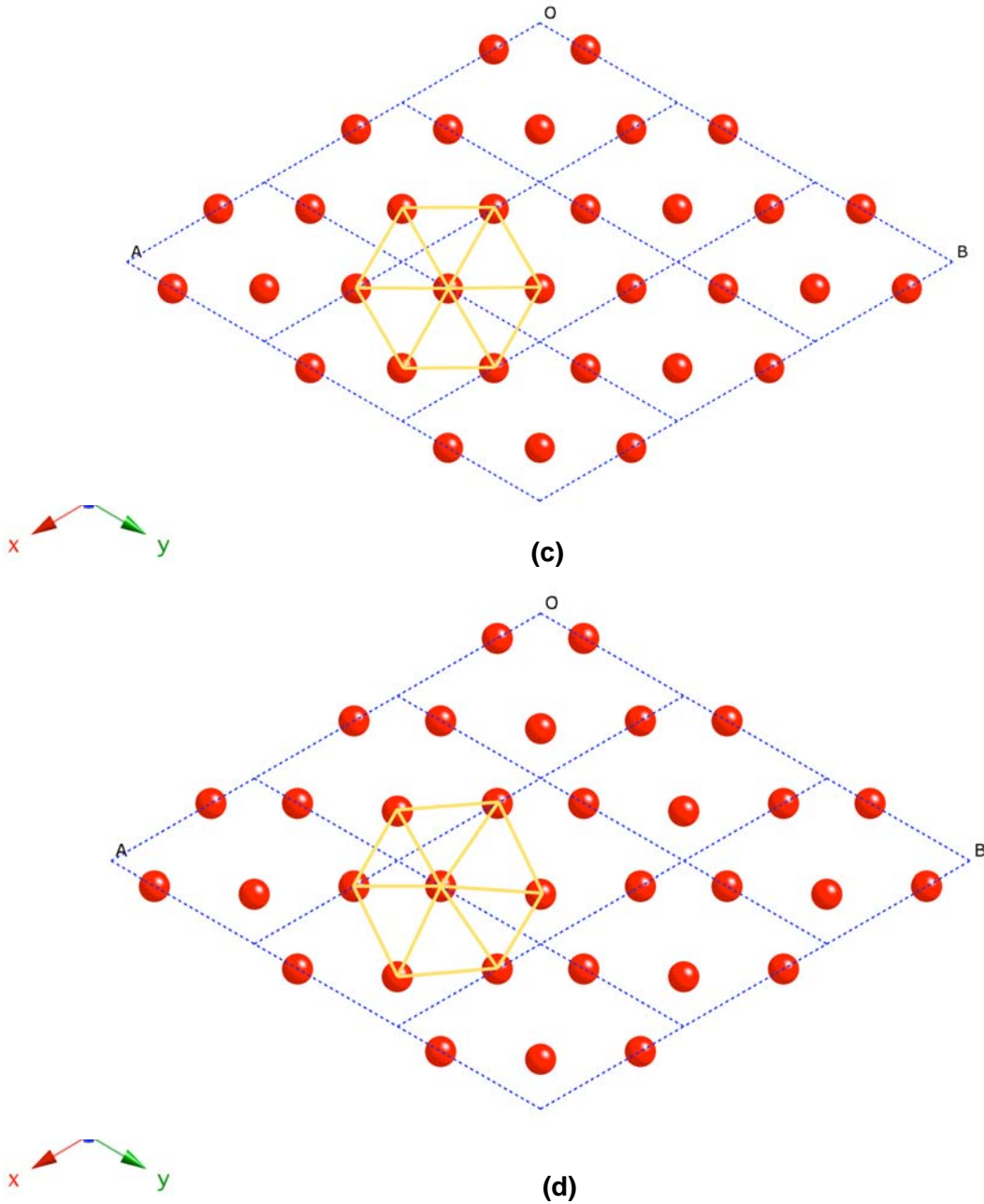
Figure IV.6.2-2. Comparison of the ideal versus real Fe_2O_3 corundum structure. For the real structure, anion and cation positional deviation parameters are given by $\Delta x = 0.031$ and $\Delta z = 0.022$ [3] (of course, ideal parameters are $\Delta x = 0.0$ and $\Delta z = 0.0$). (a) View of atom layers in ideal Fe_2O_3 in a projection parallel to $\bar{3}$ (the $\bar{3}$ axis is the vertical axis in the plane of this drawing). The height of the drawing is 1.375 nm, equal to the hexagonal lattice parameter, c. Three *u.c.*s are shown along the horizontal axis. (b) Same as (a) except using deviation parameters for the real Fe_2O_3 structure. Note the *rumpling* of the cation layers in (b) compared with (a). (c) Anion layer at $z = \frac{3}{12}$ in ideal Fe_2O_3. This is a perfect triangular net of atoms. (d) Anion layer at $z = \frac{3}{12}$ in real Fe_2O_3. This is a *distorted* triangular net of atoms. Yellow lines in (c, d) delineate the characteristic tiling patterns in the respective atom layers.

Table IV.6.2-3. Lattice parameters a and c for the hexagonal setting of the *u.c.* for selected corundum-structured compounds. Also shown are anion and cation positional deviation parameters Δx and Δz, respectively (for use in Tables IV.6.2-1 and Table IV.6-2). Note that the compound ilmenite has an additional anion deviation parameter, Δy.

Compound	a (nm)	c (nm)	$\dfrac{c}{a}$	Anion Deviation Parameter Δx (fraction of lattice parameter a)	Cation Deviation Parameter Δz (fraction of lattice parameter c)	Reference
α -Al_2O_3 *corundum*	0.47145(10)	1.2851(22)	2.7258(87)	+0.02733	+0.01867	[2]
α-Fe_2O_3 *hematite*	0.504	1.375	2.728	+0.0313	+0.0217	[3]
$FeTiO_3$ *ilmenite*	0.509	1.409	2.768	+0.0203 ($\Delta y =$ -0.0170)	+0.0227	[4]

Section IV.6.2 References

[1]   S. Iida, "Layer Structures of Magnetic Oxides," *J. Phys. Soc. Japan* **12** (3) 222–223 (1957).

[2]   H. d'Amour, D. Schiferl, H. Schulz, W. Denner, and W. B. Holzapfel, "High-Pressure Single-Crystal Structure Determinations for Ruby up to 90 kbar Using an Aautomatic Diffractometer," *J. Appl. Phys.* **49** 4411–4416 (1978).

[3]   D. E. Cox, W. J. Takei, C. Miller, and G. Shirane, "A Magnetic and Neutron Diffraction Study of the Fe_2O_3 - V_2O_3 system," *J. Phys. Chem. Solids* **23** 863–874 (1962).

[4]   G. Shirane, D. E. Cox, W. J. Takei, and S. L. Ruby, "A Study of the Magnetic Properties of the $FeTiO_3$ - Fe_2O_3 System by Neutron Diffraction and Mossbauer Effect," *J. Phys. Soc. Japan* **17** 1598–1611 (1962).

IV.6.3. Real Materials: A₂O₃ C-Type Bixbyite

When cations are too large to fit into the interstices in the corundum pseudo-close-packed anion sublattice, sesquioxide compounds form in different crystal structures, some adopting the MOO rather than the MO layer stacking motif. The most well known of these structures is the so-called C-type rare earth (RE) sesquioxide structure, also known as bixbyite after the mineral bixbyite, β-Mn_2O_3.

In Table III.3-1, we introduced an M_2O_3 sesquioxide crystal structure formed using the MOO layer stacking motif along $\overline{3}$. We showed the 12-layer atom stacking sequence for this structure in Table III.4-5. The cation layers are fully dense triangular atom nets, while each anion layer is a $\frac{3}{4}$ dense kagome lattice. We introduced this structure because it seemed to us to be a natural structural member of the MOO structural sequence presented in Section III. In fact, we initially anticipated that this structure description would equate to the $R\overline{3}$ S.G. description for bixbyite.

However, the C-type bixbyite structure proves to be different from our hypothetical M_2O_3 structure presented in Section III in a surprising way. Bixbyite is a cubic sesquioxide belonging to S.G. $Ia\overline{3}$ (see, e.g., Wyckoff [1]). When we transform bixbyite to a hexagonal *u.c.* description in S.G. $R\overline{3}$, the structure that results is shown in Table IV.6.3-1. The layer stacking sequence along $\overline{3}$ obtained from this description of bixbyite is identical to the 12-layer sequence given for M_2O_3 in Table III.4-5 (and Fig. III.4-2a from layer height $z = 0$ to $z = \frac{1}{2}$) but for one exception: the O anion layers, while being $\frac{3}{4}$ dense compared with fully dense triangular atom nets, are not in the form of kagome lattices (as indicated in Table III.4-5 and Fig. III.4-2a). An example of the actual, $\frac{3}{4}$ dense bixbyite O anion layer is shown in Fig. IV.6.3-1. The voids (or vacancy complexes) in the O lattice in Fig. IV.6.3-1 have the appearance of a wishbone. Thus, we are inclined to call this a wishbone kagome lattice, as opposed to the conventional Star of David kagome lattice. Without atomistic simulation, it is not obvious why in bixbyites the wishbone kagome anion lattice is preferred over the conventional kagome pattern.

Table IV.6.3-1. Atom positions in the hexagonal *u.c.* description for C-type bixbyite (A_2O_3) sesquioxides. Fractional coordinates (x, y, z) for the atoms refer to trigonal space group $R\bar{3}$ (hexagonal axes). As usual, A represents metal cations and O represents oxygen anions. V represents anion sublattice vacancies. Z is the number of formula units per hexagonal *u.c.* Bixbyite is normally assigned to isometric S.G. $Ia\bar{3}$. Also shown are the cation and anion positional deviation parameters for bixbyite (δu and $(\Delta x, \Delta y, \Delta z)$, respectively). These parameters are fractions of the cube *u.c.* lattice parameter, a_{cube}. Δu refers to the deviation of cation fractional coordinate x at cube equipoint 24*d* in S.G. $Ia\bar{3}$ from its ideal value, $u = 0$. $(\Delta x, \Delta y, \Delta z)$ represent the deviations of anion fractional coordinates (x, y, z) at cube equipoint 48*e* in S.G. $Ia\bar{3}$ from their ideal values, $(x, y, z) = \left(\frac{3}{8}, \frac{1}{8}, \frac{3}{8}\right)$.

| Structure	Z	Equipoint (Wyckoff notation) and Fractional Coordinates (x, y, z) for Atoms in the Hexagonal *u.c.*
A_2O_3 *bixbyite*	24	A(1) at 3*b*: $\left(0, 0, \frac{1}{2}\right)$ + EP A(2) at 9*d*: $\left(\frac{1}{2}, 0, \frac{1}{2}\right)$ + EP A(3) at 18*f*: $\left(\frac{1}{12} - \frac{2}{3}\delta u, \frac{1}{6} - \frac{1}{3}\delta u, \frac{1}{6} + \frac{2}{3}\delta u\right)$ + EP A(4) at 18*f*: $\left(\frac{1}{4} + \frac{2}{3}\delta u, \frac{1}{3}\delta u, \frac{1}{2} - \frac{2}{3}\delta u\right)$ + EP ——————————————— O(1) at 18*f*: $\left(\frac{1}{6} - \frac{2}{3}\Delta x + \frac{1}{3}\Delta y - \frac{1}{3}\Delta z, \frac{1}{12} - \frac{1}{3}\Delta x - \frac{1}{3}\Delta y - \frac{2}{3}\Delta z, \frac{1}{12} + \frac{2}{3}\Delta x + \frac{2}{3}\Delta y - \frac{2}{3}\Delta z\right)$ + EP O(2) at 18*f*: $\left(\frac{1}{6} - \frac{2}{3}\Delta x - \frac{1}{3}\Delta y + \frac{1}{3}\Delta z, \frac{1}{3} - \frac{1}{3}\Delta x + \frac{1}{3}\Delta y + \frac{2}{3}\Delta z, \frac{1}{12} + \frac{2}{3}\Delta x - \frac{2}{3}\Delta y + \frac{2}{3}\Delta z\right)$ + EP O(3) at 18*f*: $\left(\frac{5}{12} - \frac{1}{3}\Delta x - \frac{2}{3}\Delta y + \frac{1}{3}\Delta z, \frac{1}{12} - \frac{2}{3}\Delta x - \frac{1}{3}\Delta y - \frac{1}{3}\Delta z, \frac{1}{12} - \frac{2}{3}\Delta x + \frac{2}{3}\Delta y + \frac{2}{3}\Delta z\right)$ + EP O(4) at 18*f*: $\left(\frac{1}{6} - \frac{1}{3}\Delta x + \frac{2}{3}\Delta y - \frac{1}{3}\Delta z, \frac{7}{12} - \frac{2}{3}\Delta x + \frac{1}{3}\Delta y + \frac{1}{3}\Delta z, \frac{1}{12} - \frac{2}{3}\Delta x - \frac{2}{3}\Delta y - \frac{2}{3}\Delta z\right)$ + EP ——————————————— V(1) at 18*f*: $\left(\frac{5}{12}, \frac{1}{3}, \frac{1}{12}\right)$ + EP V(2) at 6*c*: $\left(0, 0, \frac{1}{4}\right)$ + EP
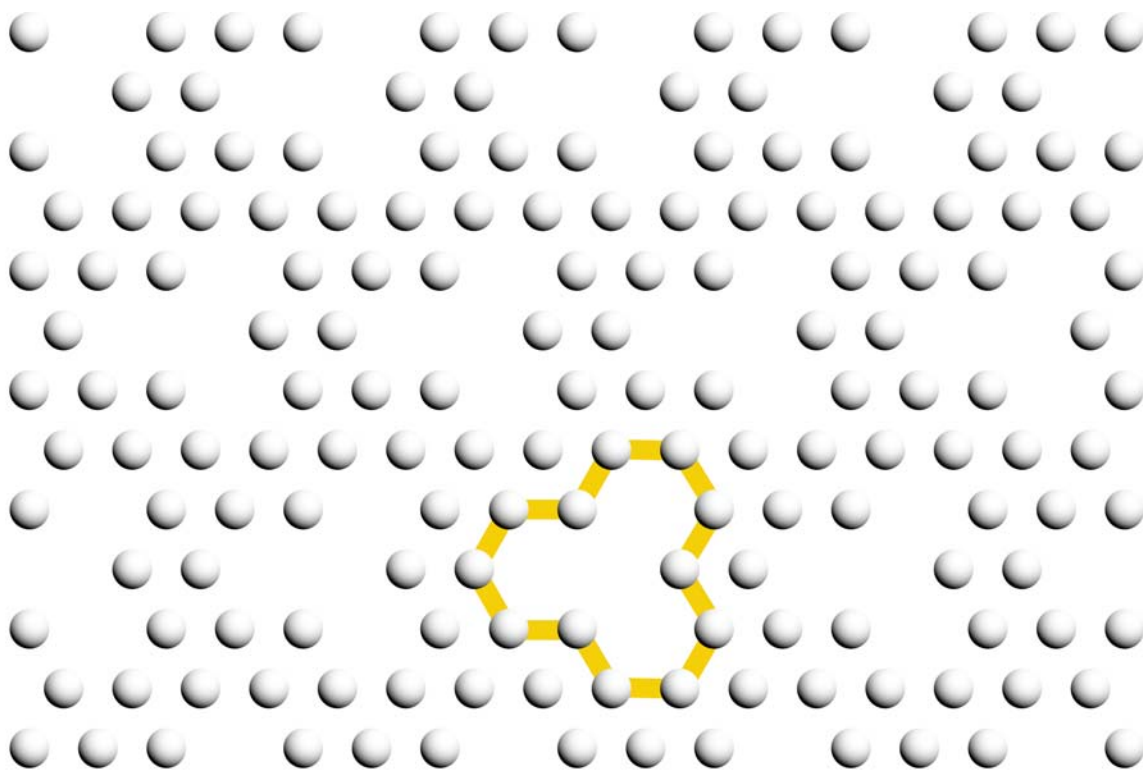
Figure IV.6.3-1. Schematic diagram showing the atom pattern in an ideal $\frac{3}{4}$ dense O anion layer (along $\overline{3}$) in a C-type bixbyite sesquioxide. In the text, we denote this pattern the *wishbone kagome lattice*. The wishbone shape characteristic of the anion vacancy complexes in bixbyite is shown as a yellow outline.

The hexagonal *u.c.* description of C-type bixbyite that emerges upon consideration of the wishbone kagome lattices of O anions along $\overline{3}$, involves a 12-layer structure that utilizes *subdivision by 16^{ths}* of a triangular atom net. Figure IV.6.3-2 illustrates how this comes about. In Fig. IV.6.3-2, we show a triangular atom net along with Iida's *subdivision by 4^{ths}* superimposed on the atoms (equivalent to Fig. III.2-2a). To produce a wishbone kagome lattice, we use a different sublattice elimination procedure to produce partially filled triangular atom nets compared with the Iida subdivision rules presented in Section III.2. Instead of removing just one sublattice from a triangular net (such as sublattice 4 in Fig. IV.6.3-2 which produces a kagome lattice), we remove one atom from each of the sublattices, all *n.n.* to one another. This is illustrated in the case of *subdivision by 4^{ths}* of a triangular atom net by the red highlighted atoms in Fig. IV.6.3-2. But to achieve an overall, $\frac{3}{4}$ dense, kagome-like layer, we perform this operation at only $\frac{1}{4}$ of the sites on

the reference sublattice (sublattice 1 in Fig. IV.6.3-2). This is why the resulting hexcell defining the wishbone kagome lattice contains 16 atom sites rather than a smaller number. Using this procedure to produce a partially filled triangular atom net, we obtain a hexcell description that involves *subdivision by 16ths* of a fully dense, triangular atom net.
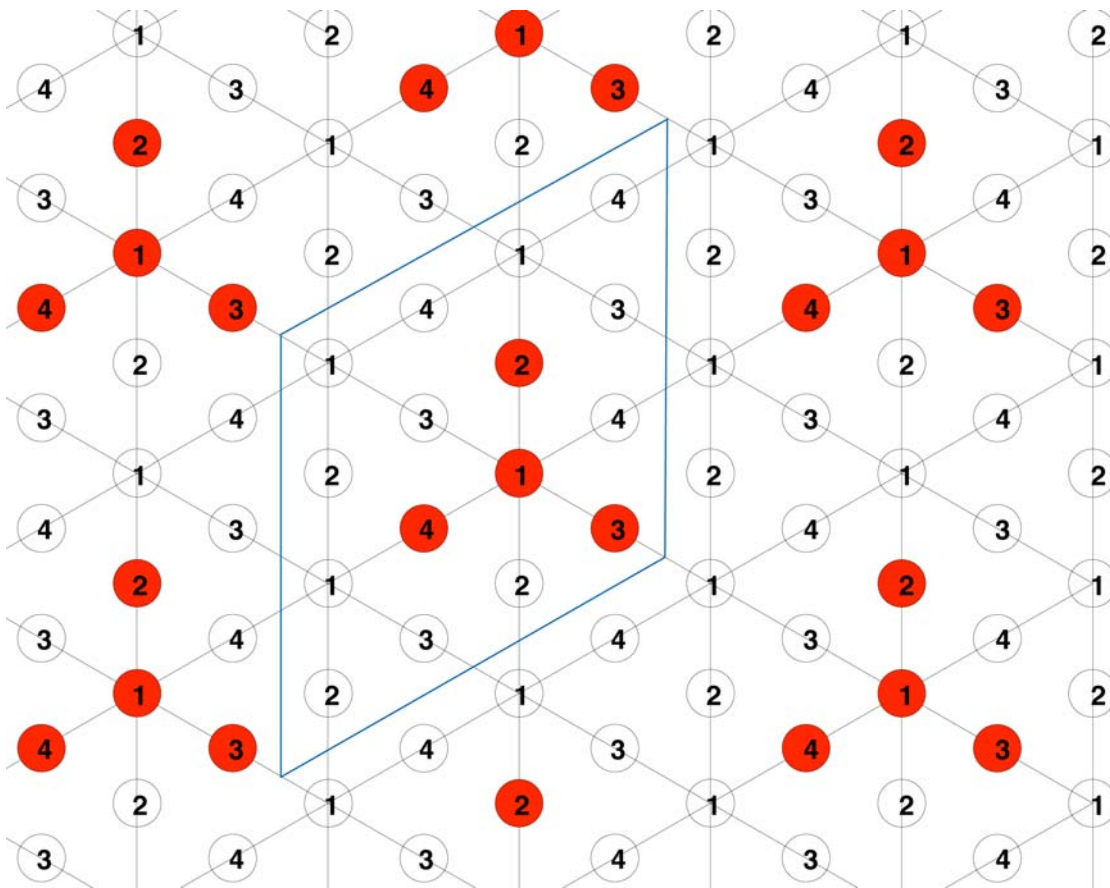
Figure IV.6.3-2. Schematic diagram showing Iida's *subdivision by 4ths* of a triangular atom net. Also highlighted in red are the atoms in the triangular net which must be removed to produce the wishbone kagome lattice, a characteristic of the anion layers along $\bar{3}$ in C-type bixbyite sesquioxides. Finally, the hexcell associated with the bixbyite hexagonal *u.c.* is inscribed on the diagram in blue. This hexcell contains 16 atoms.

Table IV.6.3-2 and Fig. IV.6.3-3 show the layer atom sequence along $\bar{3}$ that defines the ideal C-type bixbyite structure. Bixbyite is defined by a 12-layer atom stacking sequence with an MOO layer stacking motif along $\bar{3}$. Small deviations from ideality are observed in real bixbyite compounds. These are considered in Tables IV.6.3-1 and IV.6.3-3 but are ignored in Table IV.6.3-2 or Fig. IV.6.3-3.

Table IV.6.3-2. S.G. $R\bar{3}$ 12-layer stacking sequence description for A_2O_3 C-type bixbyite sesquioxides (Table IV.6.3-1). This table shows the ideal layer stacking description for bixbyite. Some bixbyite compounds exhibit small deviations from the ideal bixbyite structure. These deviations are described in Tables IV.6.3-1 and Table IV.6.3-3, but they are not taken into account in this table.

Layer Height (z) (u.c. fraction)	Registry (A,B, or C) Subscripts indicate changes in registry for the wishbone vacancy complexes in the O layers.	Ideal Atom Arrangements	Equipoints for atoms residing in each layer. Subscripts represent the number of atoms (or vacancies) contributed to each hexcell by a given equipoint.
$\frac{12}{12}$ (1)	A	*empty*	
$\frac{11}{12}$	B_2	$\frac{3}{4}$ wishbone kagome lattice	$O(1)_3$ $O(2)_3$ $O(3)_3$ $O(4)_3$ $V(1)_3$ $V(2)_1$
$\frac{10}{12}$ $\left(\frac{5}{6}\right)$	C	fully dense triangular net	$A(1)_1$ $A(2)_3$ $A(3)_6$ $A(4)_6$
$\frac{9}{12}$ $\left(\frac{3}{4}\right)$	A_2	$\frac{3}{4}$ wishbone kagome lattice	$O(1)_3$ $O(2)_3$ $O(3)_3$ $O(4)_3$ $V(1)_3$ $V(2)_1$
$\frac{8}{12}$ $\left(\frac{2}{3}\right)$	B	*empty*	
$\frac{7}{12}$	C_2	$\frac{3}{4}$ wishbone kagome lattice	$O(1)_3$ $O(2)_3$ $O(3)_3$ $O(4)_3$ $V(1)_3$ $V(2)_1$
$\frac{6}{12}$ $\left(\frac{1}{2}\right)$	A	fully dense triangular net	$A(1)_1$ $A(2)_3$ $A(3)_6$ $A(4)_6$
$\frac{5}{12}$	B_1	$\frac{3}{4}$ wishbone kagome lattice	$O(1)_3$ $O(2)_3$ $O(3)_3$ $O(4)_3$ $V(1)_3$ $V(2)_1$
$\frac{4}{12}$ $\left(\frac{1}{3}\right)$	C	*empty*	
$\frac{3}{12}$ $\left(\frac{1}{4}\right)$	A_1	$\frac{3}{4}$ wishbone kagome lattice	$O(1)_3$ $O(2)_3$ $O(3)_3$ $O(4)_3$ $V(1)_3$ $V(2)_1$
$\frac{2}{12}$ $\left(\frac{1}{6}\right)$	B	fully dense triangular net	$A(1)_1$ $A(2)_3$ $A(3)_6$ $A(4)_6$
$\frac{1}{12}$	C_1	$\frac{3}{4}$ wishbone kagome lattice	$O(1)_3$ $O(2)_3$ $O(3)_3$ $O(4)_3$ $V(1)_3$ $V(2)_1$
$\frac{0}{12}$ (0)	A	*empty*	

Table IV.6.3-3. Cube and hexagonal *u.c.* lattice parameters for a selection of A_2O_3 C-type bixbyite sesquioxides. Hexagonal *u.c.* lattice parameters *a* and *c* are obtained from the cube *u.c.* length, a_{cube}, using $a = 4\,d$ (Eq. (III.5-1)), where $\frac{\#atoms}{hexcell} = 16$, and the 12-layer relationship $c = \sqrt{6}d$ (Eq. (III.5-4a)), where *n.n.* spacing *d* is given by $d = \frac{a_{cube}}{2\sqrt{2}}$. Cation and anion positional deviation parameters (δu and (Δx, Δy, Δz)) are for use in Table IV.6.3-1.

Compound	a_{cube} (nm) (cubic *u.c.* lattice parameter)	d (nm) $d = \frac{a_{cube}}{2\sqrt{2}}$	*a, c* (nm) (hexagonal *u.c.* lattice parameters)	δu (fraction of hexagonal *u.c.* lattice parameter, *a*)	Δx, Δy, Δz (fractions of cubic *u.c.* lattice parameter, a_{cube})	Reference
β-Mn_2O_3	0.942	0.333	1.332 0.816	-0.0347(8)	+0.003(1) +0.042(1) +0.004(1)	Fert [2]
Y_2O_3	1.05981(7)	0.37470(2)	1.4988(1) 0.91782(9)	-0.03236(3)	+0.0157(2) +0.0268(2) +0.0051(2)	Maslen et al. [3]
Dy_2O_3	1.06706(7)	0.37726(5)	1.5090(6) 0.92410(7)	-0.03163(2)	+0.0155(2) +0.0266(2) +0.0052(2)	Maslen et al. [3]
Er_2O_3	1.0548(1)	0.3729(3)	1.4917(3) 0.9134(9)	-0.0330(6)	+0.019(1) +0.024(1) +0.005(1)	Fert [2]

A₂O₃ Bixbyite
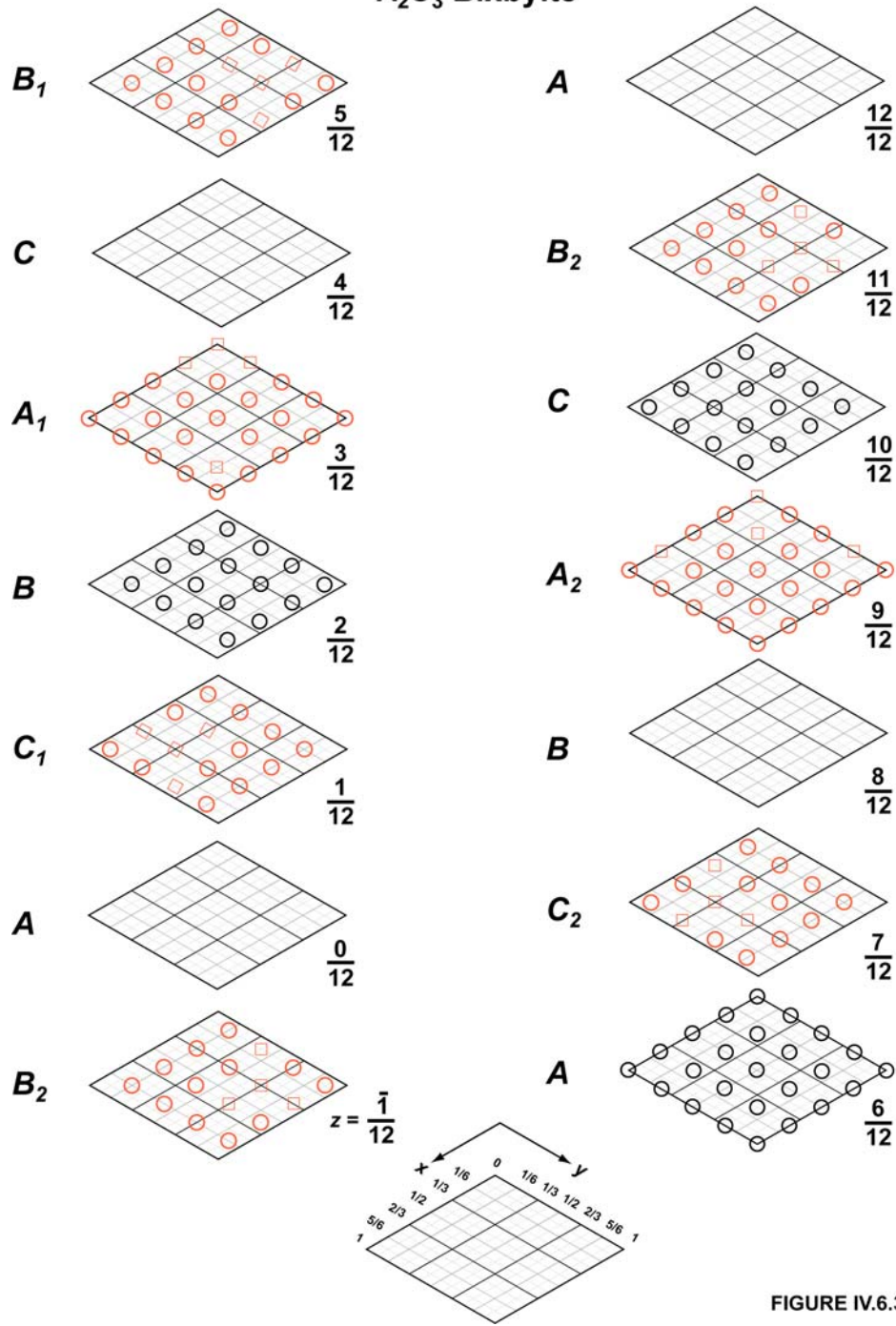
Figure IV.6.3-3. Layer stacking sequence along $\bar{3}$ for the ideal C-type bixbyite sesquioxide crystal structure. Diagrams are intended to be read from bottom to top, left to right, from minimum to maximum height, z. The height of the layer sequence from $z = 0$ to 1 is equivalent to the hexagonal lattice parameter c. The hexcell edges are equivalent to the hexagonal lattice parameter a. Bixbyite *u.c.* hexcells utilize *subdivision by 16^{ths}* of a triangular atom net. Metal cations are black-outlined circles; oxygen anions are larger red-outlined circles. Vacancies on the anion sublattice are indicated by red-outlined squares.

In addition to the mineral Mn_2O_3, a number of rare earth sesquioxides crystallize in the C-type bixbyite structure. Specifically, high atomic number RE ions (the latter part of the so-called rare earth contraction) form bixbyite structures. Hexagonal *u.c.* parameters for some of these compounds are shown in Table IV.6.3-3.

Deviations from the ideal C-type bixbyite structure described in Table IV.6.3-2 and illustrated in Fig. IV.6.3-3 produce rumpled cation and anion layers along $\bar{3}$, as well as distortions of the tiling patterns within the layers along $\bar{3}$. These distortions are illustrated for the compound Dy_2O_3 in Fig. IV.6.3-4.

(a)

(b)

(c)

(d)
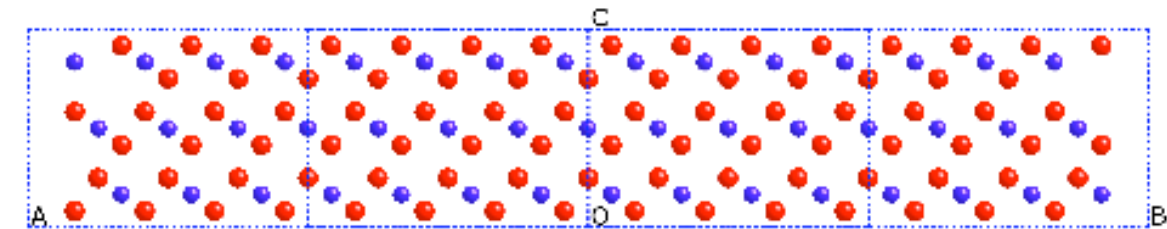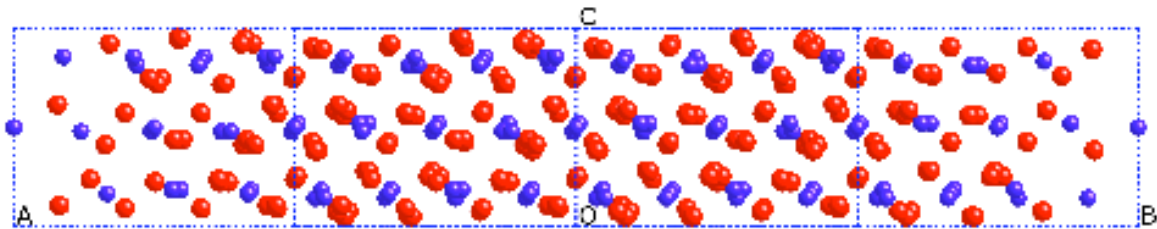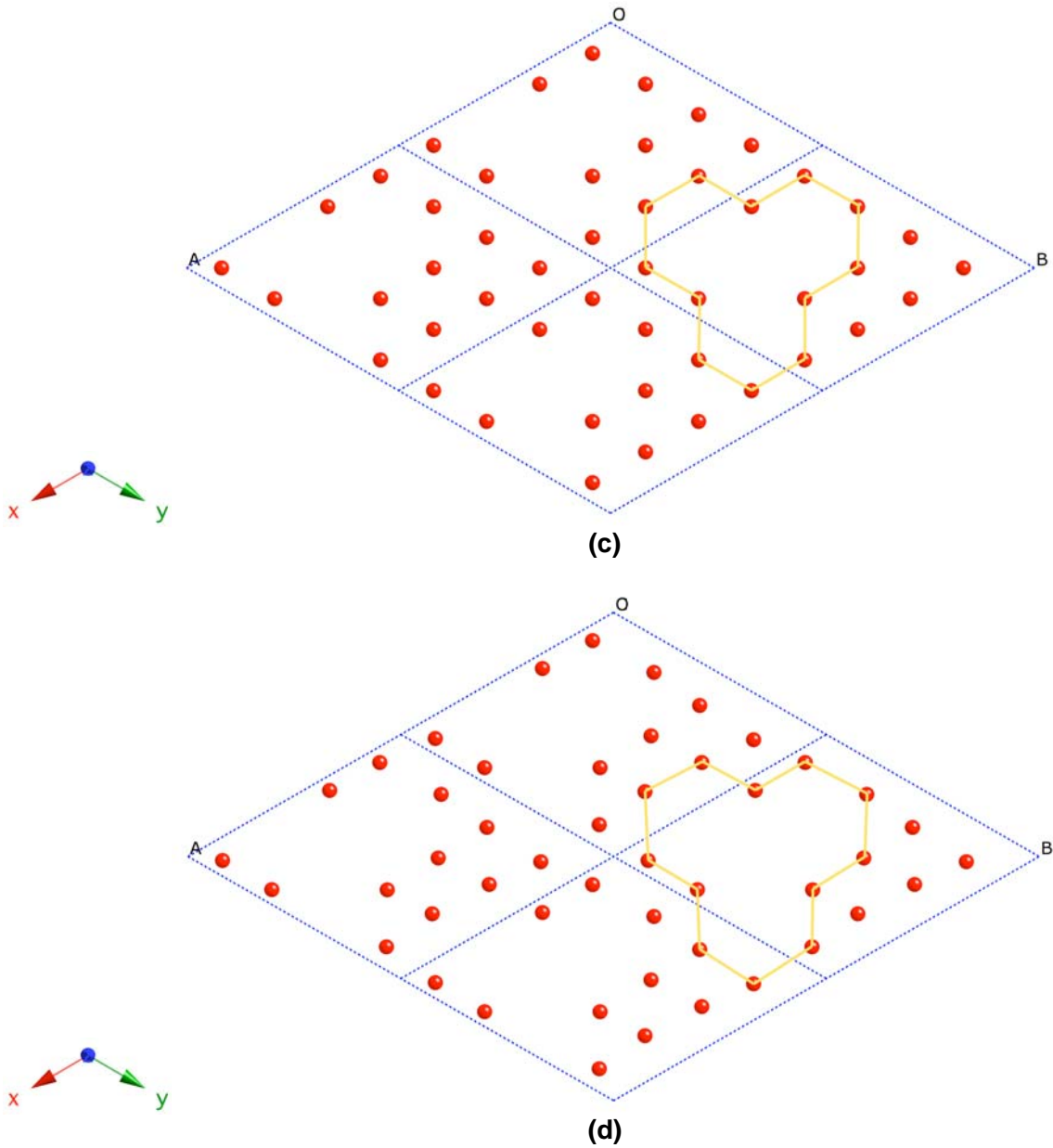
Figure IV.6.3-4. Atom layers along $\bar{3}$ in the C-type bixbyite sesquioxide Dy_2O_3. Deviation parameters for these diagrams were obtained from Table IV.6.3-3 [3]. (a, b) Views of atom layers in ideal and real Dy_2O_3, respectively, in a projection parallel to $\bar{3}$ (the $\bar{3}$ axis is the vertical axis in the plane of this drawing). The height of the drawing is 0.92410 nm, equal to the hexagonal lattice parameter, c. Two $u.c.$s are shown along the horizontal axis. (c, d) Views down the $\bar{3}$ axis of O anion layers in ideal and real Dy_2O_3, respectively. Four hexcells are shown in each diagram. These diagrams illustrate the effects of deviation from ideality of the wishbone kagome anion lattices in bixbyites. The ideal layer height for the anion layers illustrated in (c, d) is $z = \frac{1}{12}$. The wishbone O anion vacancy complex is outlined in yellow in both diagrams.

Section IV.6.3 References

[1]   R. W. G. Wyckoff, *Crystal Structures Vol. 2: Inorganic Compounds RX_n, R_nMX_2, R_nMX_3* (John Wiley & Sons, New York, 1964).

[2]   A. Fert, "Structure de Quelques Oxydes de Terres Rares," *Bull. Soc. Francaise de Mineral. et de Cristall.* **85** 267–270 (1962).

[3]   E. N. Maslen, V. A. Streltsov, and N. Ishizawa, "A Synchrotron X-ray Study of the Electron Density in *C*-type Rare Earth Oxides," *Acta Cryst. B* **52** 414–422 (1996).

IV.6.4. Real Materials: A_2O_3 A-Type Rare Earth

The largest RE ions (low atomic number REs at the beginning of the RE contraction) are not compatible with the bixbyite structure. Nevertheless, oxides of these elements still crystallize in a structure with trigonal symmetry. This structure is called the A-type RE structure. The A-rare earth structure utilizes a unique MOOMO layer stacking motif along the $\bar{3}$ symmetry axis. Moreover, the A-type RE structure cannot be described in S.G. $R\bar{3}$. It possesses lower symmetry and belongs to S.G. $P\bar{3}m1$ [1]. The crystal structure parameters for the A-type RE structure are shown in Table IV.6.4-1, using a $P\bar{3}$ S.G. description rather than $P\bar{3}m1$, for easy comparison to the $R\bar{3}$ S.G. descriptions of the structures presented earlier.[1]

Table IV.6.4-1. Atom positions in the hexagonal *u.c.* description for A-type RE (A_2O_3) sesquioxides. Fractional coordinates (*x*, *y*, *z*) for the atoms refer to trigonal space group $P\bar{3}$ (hexagonal axes with *u.c.* lattice parameters given by *a* and *c*). As usual, A represents metal cations and O represents oxygen anions. *Z* is the number of formula units per hexagonal *u.c.* A-type REs are normally assigned to S.G. $P\bar{3}m1$.

Structure	Z	Equipoint (Wyckoff notation) and Fractional Coordinates (*x*, *y*, *z*) for Atoms in the Hexagonal *u.c.*
A-type RE A_2O_3	1	A(1) at 2*d*: $\left(\frac{1}{3}, \frac{2}{3}, z = \frac{1}{4} - \Delta z_A\right) + $ EP ——————————————— O(1) at 1*a*: $\left(0,0,0\right) + $ EP O(2) at 2*d*: $\left(\frac{1}{3}, \frac{2}{3}, z = \frac{2}{3} - \Delta z_O\right) + $ EP

Table IV.6.4-2 and Fig. IV.6.4-1 illustrate the atom stacking sequence along $\bar{3}$ that defines the A-type RE structure (based on the crystal structure description in Table IV.6.4-1). These are 12-layer stacking descriptions for this structure, though only six layers contain atoms. The 12-layer description is useful for visualizing the unusual spacing of atom layers along $\bar{3}$ in these compounds.

---

[1] The same six GEP $R\bar{3}$ symmetry operations defined in Table II.2-1 are used to define the GEP symmetry operations for S.G. $P\bar{3}$, the difference being that $P\bar{3}$ lacks the lattice translation symmetry operations, $+\left(\frac{2}{3}, \frac{1}{3}, \frac{1}{3}\right)$ and $+\left(\frac{1}{3}, \frac{2}{3}, \frac{2}{3}\right)$.

Table IV.6.4-2. S.G. $P\bar{3}$ layer stacking sequence description for A_2O_3 A-type RE sesquioxides (Table IV.6.4-1). This table shows a 12-layer stacking description for A-type RE compounds, though there are actually only six atom-bearing layers along $\bar{3}$. The 12-layer description shown here illustrates the unusual spacing of the atom layers compared to other compounds discussed in the paper. Some A-type REs exhibit deviations along z from the ideal structure such that layer heights along $\bar{3}$ are slightly displaced from ideality. These deviations are described by deviation parameters Δz_A and Δz_O for cations and anions, respectively.

Layer Height (z) (u.c. fraction)	Registry (A, B, or C) of Individual Layers	Layer Atom Arrangements	Equipoints and Fractional Coordinates (x, y, z) for Atoms Residing in Each Layer
$\frac{12}{12}\left(1\right)$	A	fully dense triangular net	O(1) at $\left(0,0,0\right)$
$\frac{11}{12}$		empty	
$\frac{10}{12}\left(\frac{5}{6}\right)$		empty	
$\frac{9}{12}\left(\frac{3}{4}\right)$	C	fully dense triangular net	A(1) at $\left(\frac{2}{3},\frac{1}{3},\frac{3}{4}+\Delta z_A\right)$
$\frac{8}{12}\left(\frac{2}{3}\right)$	B	fully dense triangular net	O(2) at $\left(\frac{1}{3},\frac{2}{3},\frac{2}{3}-\Delta z_O\right)$
$\frac{7}{12}$		empty	
$\frac{6}{12}\left(\frac{1}{2}\right)$	(A)	empty	
$\frac{5}{12}$		empty	
$\frac{4}{12}\left(\frac{1}{3}\right)$	C	fully dense triangular net	O(2) at $\left(\frac{2}{3},\frac{1}{3},\frac{1}{3}+\Delta z_O\right)$
$\frac{3}{12}\left(\frac{1}{4}\right)$	B	fully dense triangular net	A(1) at $\left(\frac{1}{3},\frac{2}{3},\frac{1}{4}-\Delta z_A\right)$
$\frac{2}{12}\left(\frac{1}{6}\right)$		empty	
$\frac{1}{12}$		empty	
$\frac{0}{12}\left(0\right)$	A	fully dense triangular net	O(1) at $\left(0,0,0\right)$
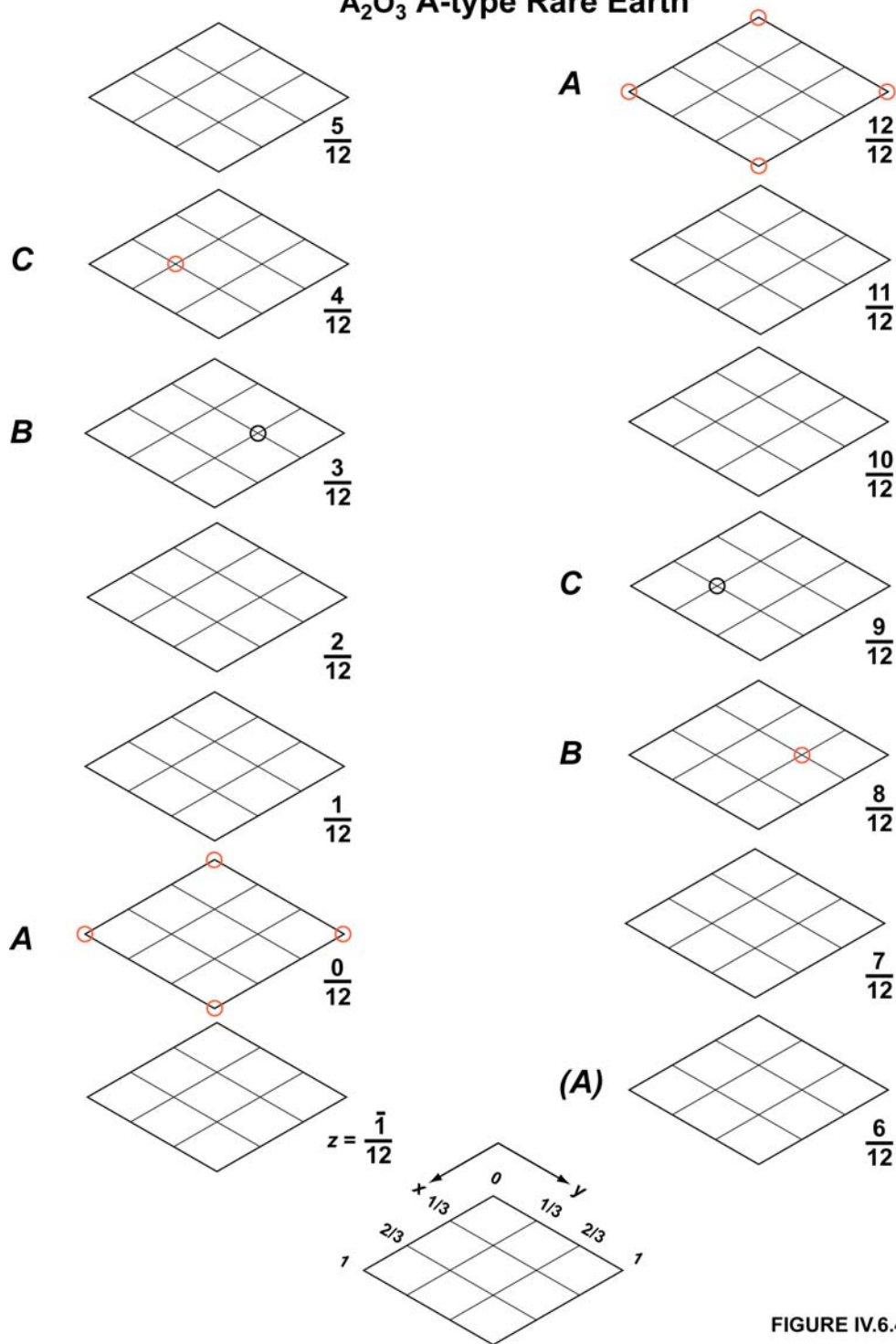
Figure IV.6.4-1. Layer stacking sequence along $\overline{3}$ for the ideal A-type RE A_2O_3 crystal structure. Diagrams are intended to be read from bottom to top, left to right, from minimum to maximum height, z. Unit cell hexcells utilize *subdivision by 1^{sts}* of a triangular atom net. Metal cations are black-outlined circles; oxygen anions are red-outlined circles.

The hexcells associated with each layer contain only one atom per layer (*subdivision by 1^{sts} of a triangular atom net*). Therefore, all of the layers in the structure, whether M or O, are fully dense triangular nets of atoms. The registry of the layers along $\bar{3}$ varies in an *A*, *B*, *C* fashion, as in most structures discussed previously. The anion sublattice is *fcc* (*ACBACB…*), while the cation sublattice is *hcp* (*BCBC…*). There are slight deviations of the cation and anion layer heights from their ideal heights, so these *fcc* and *hcp* sublattice descriptions are only approximate. An example of an A-rare earth oxide is La_2O_3. Unit cell parameters for La_2O_3 are shown in Table IV.6.4-3.

Table IV.6.4-3. Unit cell parameters for the sesquioxide La_2O_3, a typical example of an A-type RE compound. Deviation parameters Δz_A and Δz_O for cation and anion sublattices, respectively, are for use in Tables IV.6.4-1 and Table IV.6.4-2.

Compound	a (nm)	c (nm)	$\dfrac{c}{a}$	Δz_A	Δz_O	Reference
La_2O_3	0.39373	0.61299	1.55688	+0.005	+0.022	Wyckoff [1]

Section IV.6.4 References

[1]   R. W. G. Wyckoff, *Crystal Structures Vol. 2: Inorganic Compounds RX$_n$, R$_n$MX$_2$, R$_n$MX$_3$* (John Wiley & Sons, New York, 1964).

IV.6.5. Real Materials: ABO_3 Perovskite

We've shown that sesquioxides with small cations crystallize in a structure with an MO layer motif; larger cations form an MOO layer motif structure while the largest cations adopt a structure that utilizes an MOOMO motif. But an interesting anomaly occurs when a compound consists of both small and large cations. Consider a complex oxide with two cationic species, A and B, in which the A and B species are characterized by large and small ionic radii, respectively. It may be the case that the B cations are small enough to fit naturally into interstices in a close-packed anion lattice, but sometimes the large A cations are too big to fit into these interstices. In these instances, nature introduces an interesting structural twist. The oversized A cations join with the O anions to form a cation/anion pseudo-close-packed framework, while the small B cations are fitted into interstices within this close-packed lattice. This is the fundamental principle for constructing ABO_3 sesquioxide compounds known as perovskites.

There are numerous examples of ABO_3 perovskites, but perovskite structures belong to several different space groups, due to small lattice distortions which vary as a function of cation chemistry. For the sake of clarity, we will consider only one perovskite structure, one with ideal, cubic symmetry. Such a compound is $BaTiO_3$. At elevated temperature (T > 200°C), the perovskite $BaTiO_3$ possesses cubic symmetry and belongs to S.G. $Pm\overline{3}m$ [1]. Upon transformation to hexagonal *u.c.* coordinates, we find that this structure can be described in S.G. $R\overline{3}$, with the crystal structure description shown in Table IV.6.5-1.

The $R\overline{3}$ *u.c.* description for perovskite involves six atom-bearing layers along the $\overline{3}$ symmetry axis, though it is convenient to describe the structure using 12 layers to allow comparison to other crystal structures presented in this paper. This is shown in Table IV.6.5-2 and illustrated in Fig. IV.6.5-1. This structure description also utilizes the Iida *subdivision by 4^{ths}* concept for triangular atom nets. Three of the six atom-bearing layers in the hexagonal *u.c.* consist only of B cations in a $\frac{1}{4}$ dense layer, while the other three interleaved layers contain one A cation and three O anions per hexcell per layer. These atoms are arranged so as to produce $\frac{1}{4} + \frac{3}{4} = \frac{4}{4}$ dense (AO) triangular atom nets.

Table IV.6.5-1. $R\overline{3}$ hexagonal *u.c.* description for a cubic ABO_3 perovskite compound. Cubic perovskite compounds are normally assigned to S.G. $Pm\overline{3}m$ with cubic lattice parameter given by a_{cube}. An example is the compound $BaTiO_3$ at temperatures greater than 200°C.

Structure	Z	Equipoint and Fractional Coordinates (x, y, z) for Atoms in the Hexagonal *u.c.*
Perovskite ABO_3	3	A at 3a: $\quad$ $(0,0,0)$ + EP
		B at 3b: $\quad$ $\left(0,0,\frac{1}{2}\right)$ + EP
		O at 9e: $\quad$ $\left(\frac{1}{2},0,0\right)$ + EP

Table IV.6.5-2. $R\bar{3}$ space group layer sequence description for cubic ABO_3 perovskite compounds (Table IV.6.5-1). Fractional coordinates for atoms within each layer are shown in parentheses, (x, y). This table utilizes a 12-layer stacking description along $\bar{3}$ for the structure, though atoms reside in only 6 of the 12 layers. Both (AO) and B sublattices are arranged with *fcc* stacking geometries (*ACBACB*...).

Layer Height (z) (*u.c.* fraction)	Registry (*A, B, or C*)	Layer Atom Arrangements	Equipoint and Fractional Coordinates (x, y) for Atoms in the Hexagonal *u.c.*
$\frac{12}{12}$ (1)	*A*	$\frac{3}{4}$ dense O kagome net *plus* $\frac{1}{4}$ dense A net	A @ **3a** $(0,0)$ O @ **9e** $\left(\frac{1}{2},0\right),\left(0,\frac{1}{2}\right),\left(\frac{1}{2},\frac{1}{2}\right)$
$\frac{11}{12}$	*(B)*	empty	
$\frac{10}{12}$ $\left(\frac{5}{6}\right)$	*C*	$\frac{1}{4}$ dense B net	B @ **3b** $\left(\frac{2}{3},\frac{1}{3}\right)$
$\frac{9}{12}$ $\left(\frac{3}{4}\right)$	*(A)*	empty	
$\frac{8}{12}$ $\left(\frac{2}{3}\right)$	*B*	$\frac{3}{4}$ dense O kagome net *plus* $\frac{1}{4}$ dense A net	A @ **3a** $\left(\frac{1}{3},\frac{2}{3}\right)$ O @ **9e** $\left(\frac{2}{6},\frac{1}{6}\right),\left(\frac{5}{6},\frac{1}{6}\right),\left(\frac{5}{6},\frac{4}{6}\right)$
$\frac{7}{12}$	*(C)*	empty	
$\frac{6}{12}$ $\left(\frac{1}{2}\right)$	*A*	$\frac{1}{4}$ dense B net	B @ **3b** $(0,0)$
$\frac{5}{12}$	*(B)*	empty	
$\frac{4}{12}$ $\left(\frac{1}{3}\right)$	*C*	$\frac{3}{4}$ dense O kagome net *plus* $\frac{1}{4}$ dense A net	A @ **3a** $\left(\frac{2}{3},\frac{1}{3}\right)$ O @ **9e** $\left(\frac{1}{6},\frac{2}{6}\right),\left(\frac{1}{6},\frac{5}{6}\right),\left(\frac{4}{6},\frac{5}{6}\right)$
$\frac{3}{12}$ $\left(\frac{1}{4}\right)$	*(A)*	empty	
$\frac{2}{12}$ $\left(\frac{1}{6}\right)$	*B*	$\frac{1}{4}$ dense B net	B @ **3b** $\left(\frac{1}{3},\frac{2}{3}\right)$
$\frac{1}{12}$	*(C)*	empty	
$\frac{0}{12}$ (0)	*A*	$\frac{3}{4}$ dense O kagome net *plus* $\frac{1}{4}$ dense A net	A @ **3a** $(0,0)$ O @ **9e** $\left(\frac{1}{2},0\right),\left(0,\frac{1}{2}\right),\left(\frac{1}{2},\frac{1}{2}\right)$
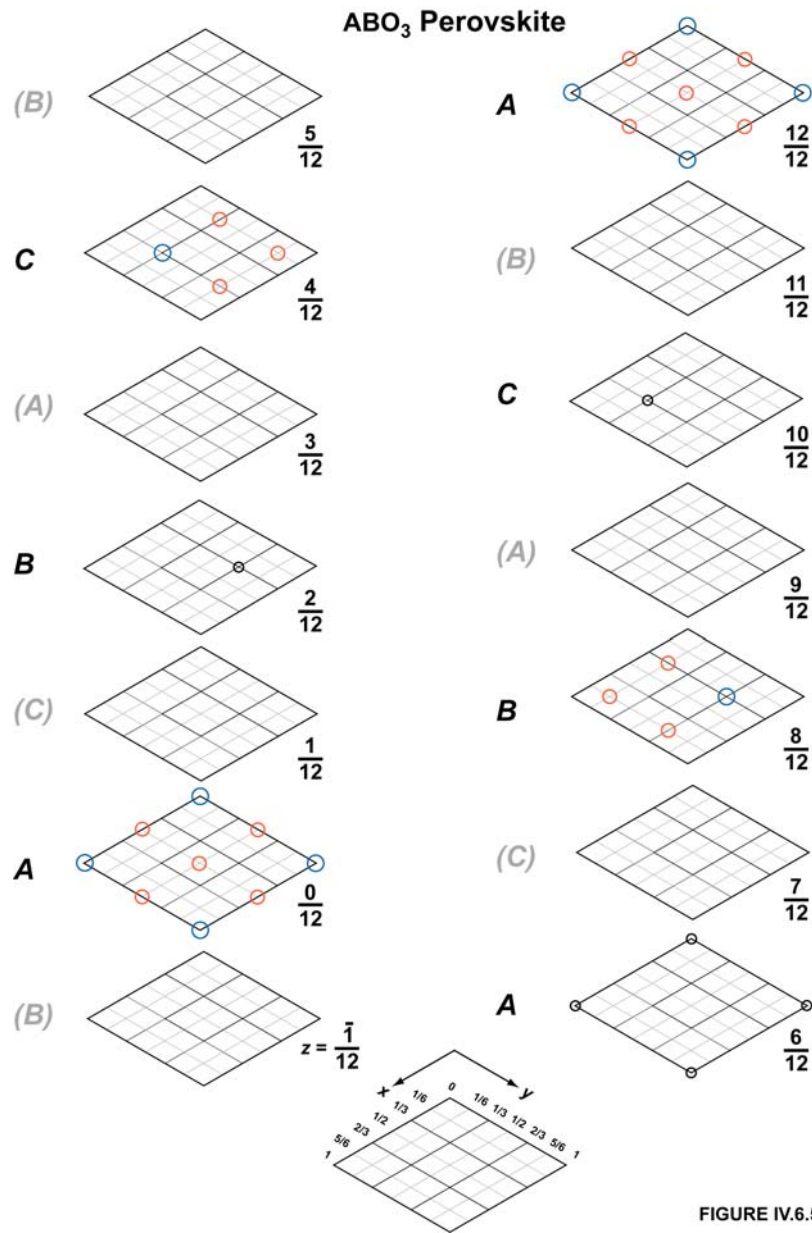
Figure IV.6.5-1. Layer stacking sequence along $\overline{3}$ for the ideal ABO_3 perovskite crystal structure. The diagram shows a 12-layer stacking sequence, though atoms only occupy 6 of the 12 layers. Diagrams are intended to be read from bottom to top, left to right, from minimum to maximum height, z. The height of the layer sequence from $z = 0$ to 1 is equivalent to the hexagonal lattice parameter c. The hexcell edges are equivalent to the hexagonal lattice parameter a. Perovskite *u.c.* hexcells utilize Iida's *subdivision by 4^{ths}* of triangular atom nets. Layers in the (AO) sublattice are $(\frac{1}{4} + \frac{3}{4})$ dense, while M sublattice layers are $\frac{1}{4}$ dense (note that a $\frac{1}{4}$ dense layer still retains the appearance of a triangular atom net). The larger A cations are large blue-outlined circles, while the smaller B cations are small, black-outlined circles. Oxygen anions are large red-outlined circles. A cations are somewhat exaggerated in size to emphasize their role in forming a close-packed framework for the perovskite structure.

Alternating perovskite (AO) and B layers are shown edge-on in Fig. IV.6.5-2a. A single perovskite (AO) cation/anion layer along $\bar{3}$ is shown in Fig. IV.6.5-2b. Notice that the fully dense (AO) layer is formed by combining a $\frac{3}{4}$ dense kagome O atom pattern with a $\frac{1}{4}$ dense A atom pattern. This is analogous to the (AB) layers in pyrochlore compounds, as discussed in Section IV.4 (Fig. IV.4-1). The registry of the layers along $\bar{3}$ varies in an A, B, C, fashion, as in structures discussed previously. If one examines the layer patterns carefully, it is easy to demonstrate that the small B cations lie in octahedral interstices between (AO) layers and are surrounded by 6 *n.n.* O anions while A cations are coordinated by 12 *n.n.* O anions in three successive (AO) layers. Lattice parameters a and c for the hexagonal *u.c.* description of the cubic perovskite $BaTiO_3$ are shown in Table IV.6.5-3.

Table IV.6.5-3. Lattice parameters for both the cubic and hexagonal *u.c.* settings for the perovskite compound, $BaTiO_3$. Hexagonal *u.c.* lattice parameters a and c are obtained from the cube *u.c.* length, a_{cube}, using the relationships $a = \sqrt{\frac{\# \, atoms}{hexcell}} \, d$ (Eq. (III.5-1); $\frac{\# \, atoms}{hexcell} = 4$) and $c = \sqrt{6} \, d$ (12-layer *u.c.* description, Eq. (III.5-4a)), where d is the *n.n.* spacing in the (BaO) triangular atom nets ($d = \frac{a_{cube}}{\sqrt{2}}$). $BaTiO_3$ is cubic and belongs to S.G. $Pm\bar{3}m$ over the temperature range 474–1645 K (201–1372°C) (Edwards et al. [1]). The cubic lattice parameter, a_{cube}, given here is for the lower limit of this range.

Compound	Cube *u.c.* Lattice Parameter a_{cube} (nm)	Hexagonal *u.c.* Lattice Parameters a, c (nm)	References & Comments
$BaTiO_3$	0.39953(3)	0.56502(5) 0.69201(1)	Edwards et al. [1] T = 474 K (201°C)

(a)

(b)
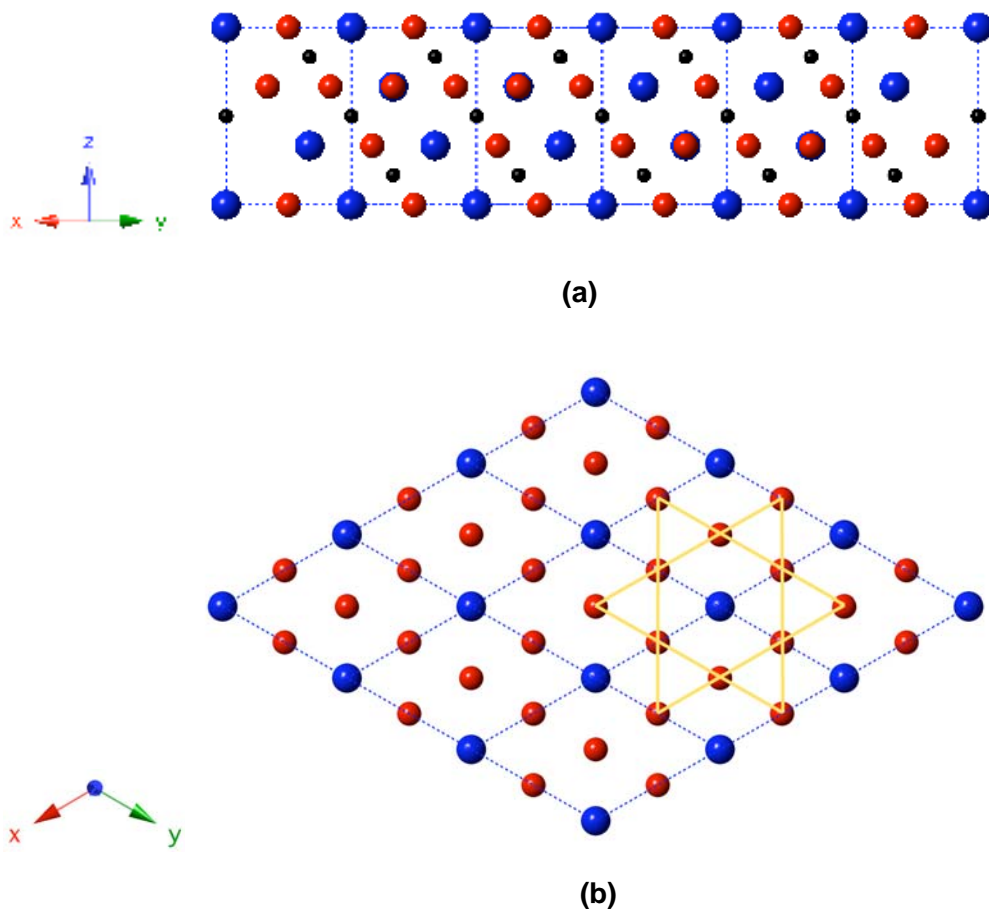
Figure IV.6.5-2. Atom layers along $\overline{3}$ in the cubic ABO_3 sesquioxide, $BaTiO_3$ perovskite. (a) View of atom layers in $BaTiO_3$ in a projection parallel to $\overline{3}$ (the $\overline{3}$ axis is the vertical axis in the plane of this drawing). The height of the drawing is 0.69209(8) nm, equal to the hexagonal lattice parameter, c (Table IV.6.5-3). Three *u.c.*s are shown along the horizontal axis. (b) View down the $\overline{3}$ axis of a (BaO) cation/anion layer at *u.c.* height $z = 0$. Nine (3 × 3) hexcells are shown in this diagram. The kagome O anion lattice in the (BaO) layer is outlined in yellow

In summary, using a hexagonal u.c. description for the structure, ABO_3 perovskites are constructed using an (MO)M layer stacking motif along the $\overline{3}$ hexagonal symmetry axis. When large size disparities exist between cations in certain complex oxides, one can anticipate that mixed cation/anion pseudo-close packed layers may form in these compounds.

Section IV.6.5 References

[1]   J. W. Edwards, S. R. and H. L. Johnston, "Structure of Barium Titanate at Elevated Temperatures," *J. Am. Chem. Soc.* **73** 2934–2935 (1951).

IV.7.1 Real Materials: M_3O_4 Compounds

Though there are many oxides in nature that possess the M_3O_4 stoichiometry, we will limit our discussion in this section to two crystal structures. One is the ubiquitous *spinel* crystal structure, which is not only an important structure in its own right but is often utilized as a fundamental structural component in much more complex crystal structures. The second structure discussed here is a hypothetical M_3O_4 crystal structure that to us seems to be a natural member of the Iida subdivision models presented in this report. Though we are not aware of the existence of this structure in nature, we include it in our presentation, in case it proves useful after all.

IV.7.2 Real Materials: AB_2O_4 Spinel

The *spinel* crystal structure was introduced in Section III of this report. The typical chemical formula for a spinel compound is AB_2O_4. There are so many compounds that exhibit the spinel structure that we will cite only one composition in this discussion, that being the mineral spinel, $MgAl_2O_4$. The spinel structure belongs to S.G. $Fd\overline{3}m$ (for a review of spinel compounds, see Sickafus et al. [1]). Upon transformation to hexagonal *u.c.* coordinates, we find that this structure can be described in S.G. $R\overline{3}$, with the crystal structure description shown in Table IV.7.2-1. This hexagonal structure can be represented using a 24-layer description for the u.c. along the $\overline{3}$ hexagonal symmetry axis, as shown in Table IV.7.2-2 and illustrated in Fig. IV.7.2-1.

An analysis of Table IV.7.2-2 reveals that spinel conforms to an MO layer stacking motif along $\overline{3}$. The Iida *subdivision by 4ths* concept for triangular atom nets can be used to describe the structure of the individual layers; O layers are fully dense ($\frac{4}{4}$) triangular atom nets, while half of the cation layers (the pure B layers) are characterized by $\frac{3}{4}$ dense kagome lattices (Fig. III.2-2b). But the other cation "layers" (consisting of two A atoms and one B atom per hexcell) are actually 3-fold degenerate, rather than being individual layers along $\overline{3}$. So it is only when these layers are projected onto one intermediate height between adjacent anion layers that spinel can be viewed as being a true MO layer stacking compound. In actuality, the structure is more complicated than the idealized structure presented in Section III.

Table IV.7.2-1. Atom positions in the hexagonal *u.c.* description for spinel (AB_2O_4) compounds. Fractional coordinates (x, y, z) for the atoms refer to trigonal space group $R\bar{3}$ (hexagonal axes). As usual, A and B represent metal cations and O represents oxygen anions. Z is the number of formula units per hexagonal *u.c.* Spinel is normally assigned to S.G. $Fd\bar{3}m$ [1]. The following description was produced starting with a cubic *u.c.* in setting 2 for S.G. $Fd\bar{3}m$, i.e., with the origin of the *u.c.* at an inversion center (point symmetry $\bar{3}m$). Moreover, it was assumed that the origin of the *u.c.* is on an octahedral vacancy (that is, a vacancy on the cation sublattice). The Wyckoff position of this origin is 16c. With these assumptions, the hexagonal *u.c.* produced upon transformation also contains an octahedral vacancy at the origin of the *u.c.* The Wyckoff notation for this site in S.G. $R\bar{3}$ is 3a. The parameter u is called the oxygen positional parameter, while δu represents the oxygen deviation parameter, a dilation away from the ideal positional parameter, $u = \frac{1}{4}$ (the latter also corresponds to ideal, *ccp* anion stacking). The ideal oxygen positional parameter $u = \frac{1}{4}$ refers specifically to setting 2 in S.G. $Fd\bar{3}m$.

Structure	Z	Equipoint (Wyckoff notation) and Fractional Coordinates (x, y, z) for Atoms in the Hexagonal *u.c.*
Spinel AB_2O_4	6	A(1) at 6c: $\left(0,0,\frac{1}{8}\right)$ + EP
		B(1) at 3b: $\left(0,0,\frac{1}{2}\right)$ + EP
		B(2) at 9e: $\left(\frac{1}{2},0,0\right)$ + EP
		O(1) at 6c: $\left(0, 0, \frac{1}{4} + \delta u\right)$ + EP
		or
		O(1) at 6c: $\left(0, 0, u\right)$ + EP
		O(2) at 18f: $\left(\frac{1}{6} + \frac{4}{3}\,\delta u, \frac{1}{3} + \frac{8}{3}\,\delta u, \frac{1}{12} - \frac{1}{3}\,\delta u\right)$ + EP
		or
		O(2) at 18f: $\left(-\frac{1}{6} + \frac{4}{3}\,u, -\frac{1}{3} + \frac{8}{3}\,u, \frac{1}{6} - \frac{1}{3}\,u\right)$ + EP
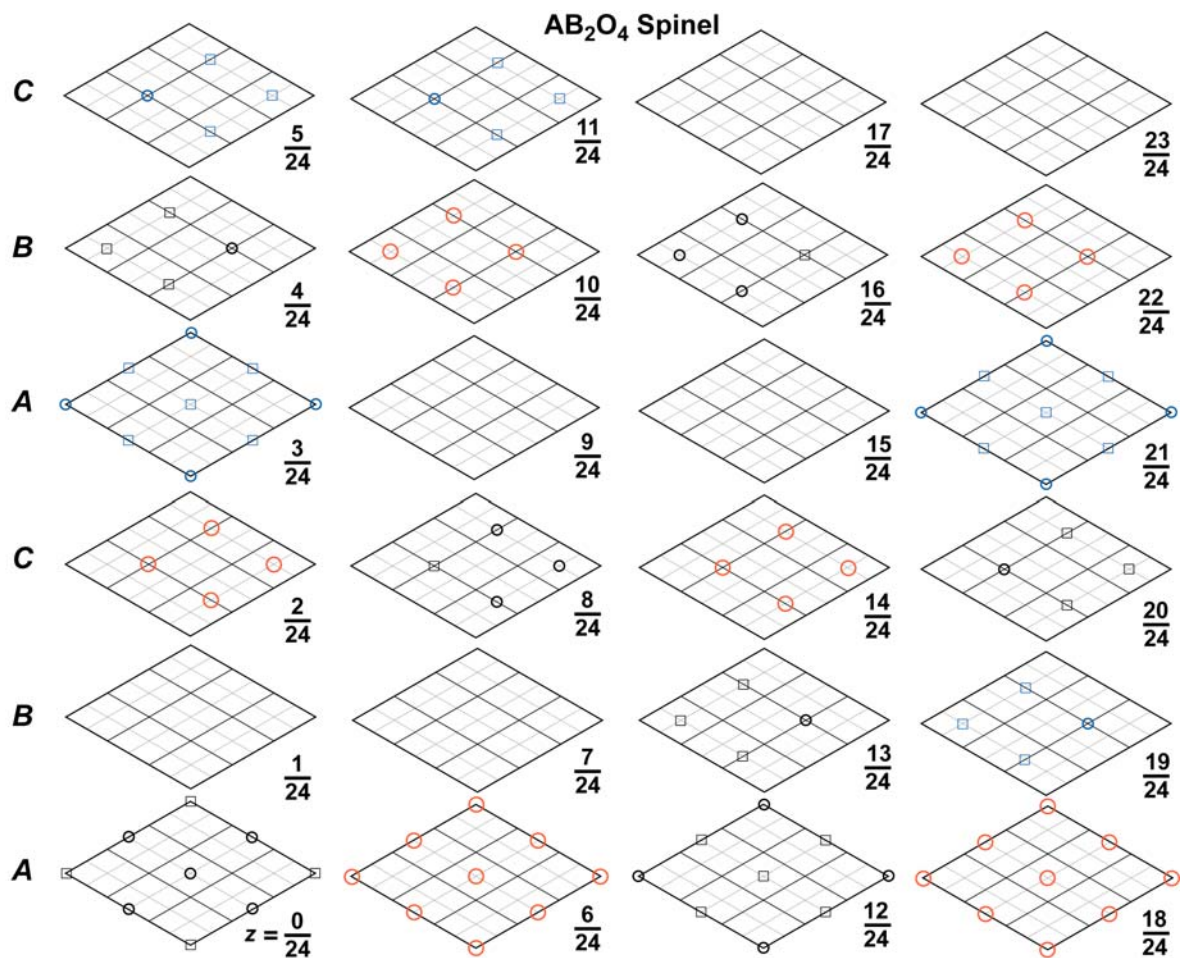
Figure IV.7.2-1. Layer stacking sequence along $\bar{3}$ for the ideal spinel crystal structure. Spinel is described by a 24-layer stacking sequence along $\bar{3}$. Diagrams are intended to be read from bottom to top, left to right, from minimum to maximum height, z. The height of the diagram from $z = 0$ to $z = 1$ is equivalent to the hexagonal lattice parameter c. The edges of the hexcells in the diagram are equal to hexagonal $u.c.$ length a. Spinel $u.c.$ hexcells utilize Iida's *subdivision by 4^{ths}* of a triangular atom net. Metal cations are small blue- and black-outlined circles (representing A and B cations, respectively); oxygen anions are large red-outlined circles. Vacancies on the cation sublattice are indicated by blue- and black-outlined squares. The setting for the $u.c.$ in this description for spinel places a B cation vacancy at the $u.c.$ origin (this is an inversion center with point symmetry $\bar{3}m$). The layer of B cations in the z = 0 layer forms a kagome lattice.

Table IV.7.2-2. S.G. $R\overline{3}$ 24-layer atom stacking sequence description for AB_2O_4 spinel compounds (based on Table IV.7.2-1). Fractional coordinates for atoms within each layer are shown in parentheses (x, y) for atoms at ideal layer heights z, or (x,y,z) for atoms at heights z that deviate from ideality. The parameter δu represents the oxygen deviation parameter, a dilation away from the ideal positional parameter, $u = \frac{1}{4}$ (for setting 2 in cubic S.G. $Fd\overline{3}m$).

| Layer Height (z) (u.c. fraction)	Registry (ABC stacking)	1st Equipoint in Each Layer	2nd Equipoint in Each Layer
$\frac{25}{24}$	(B)	empty	empty
$\frac{24}{24}$ (1)	A	**B(2) 9e** $\left(\frac{1}{2},0\right),\left(0,\frac{1}{2}\right),\left(\frac{1}{2},\frac{1}{2}\right)$	
$\frac{23}{24}$	(C)	empty	empty
$\frac{22}{24}\left(\frac{11}{12}\right)$	B	**O(1) 6c** $\left(\frac{1}{3},\frac{2}{3},\frac{11}{12}+\delta u\right)$	**O(2) 18f** $\left(\frac{5}{6}-\frac{4}{3}\delta u,\frac{4}{6}-\frac{8}{3}\delta u,\frac{11}{12}+\frac{1}{3}\delta u\right),$ $\left(\frac{5}{6}-\frac{4}{3}\delta u,\frac{1}{6}+\frac{4}{3}\delta u,\frac{11}{12}+\frac{1}{3}\delta u\right),$ $\left(\frac{2}{6}+\frac{8}{3}\delta u,\frac{1}{6}+\frac{4}{3}\delta u,\frac{11}{12}+\frac{1}{3}\delta u\right)$
$\frac{21}{24}\left(\frac{7}{8}\right)$	A	**A(1) 6c** $\left(0,0\right)$	
$\frac{20}{24}\left(\frac{5}{6}\right)$	C	**B(1) 3b** $\left(\frac{2}{3},\frac{1}{3}\right)$	
$\frac{19}{24}$	B	**A(1) 6c** $\left(\frac{1}{3},\frac{2}{3}\right)$	
$\frac{18}{24}\left(\frac{3}{4}\right)$	A	**O(1) 6c** $\left(0,0,\frac{3}{4}-\delta u\right)$	**O(2) 18f** $\left(\frac{1}{2}+\frac{4}{3}\delta u,+\frac{8}{3}\delta u,\frac{3}{4}-\frac{1}{3}\delta u\right),$ $\left(-\frac{8}{3}\delta u,\frac{1}{2}-\frac{4}{3}\delta u,\frac{3}{4}-\frac{1}{3}\delta u\right),$ $\left(\frac{1}{2}+\frac{4}{3}\delta u,\frac{1}{2}-\frac{4}{3}\delta u,\frac{3}{4}-\frac{1}{3}\delta u\right)$
$\frac{17}{24}$	(C)	empty	empty
$\frac{16}{24}\left(\frac{2}{3}\right)$	B	**B(2) 9e** $\left(\frac{2}{6},\frac{1}{6}\right),\left(\frac{5}{6},\frac{1}{6}\right),\left(\frac{5}{6},\frac{4}{6}\right)$	
$\frac{15}{24}\left(\frac{5}{8}\right)$	(A)	empty	empty
$\frac{14}{24}\left(\frac{7}{12}\right)$	C	**O(1) 6c** $\left(\frac{2}{3},\frac{1}{3},\frac{7}{12}+\delta u\right)$	**O(2) 18f** $\left(\frac{1}{6}-\frac{4}{3}\delta u,\frac{2}{6}-\frac{8}{3}\delta u,\frac{7}{12}+\frac{1}{3}\delta u\right),$ $\left(\frac{1}{6}-\frac{4}{3}\delta u,\frac{5}{6}+\frac{4}{3}\delta u,\frac{7}{12}+\frac{1}{3}\delta u\right),$ $\left(\frac{4}{6}+\frac{8}{3}\delta u,\frac{5}{6}+\frac{4}{3}\delta u,\frac{7}{12}+\frac{1}{3}\delta u\right)$
$\frac{13}{24}$	B	**A(1) 6c** $\left(\frac{1}{3},\frac{2}{3}\right)$	
$\frac{12}{24}\left(\frac{1}{2}\right)$	A	**B(1) 3b** $\left(0,0\right)$	
$\frac{11}{24}$	C	**A(1) 6c** $\left(\frac{2}{3},\frac{1}{3}\right)$	

$\frac{10}{24}\left(\frac{5}{12}\right)$	B	O(1) 6c $\left(\frac{1}{3},\frac{2}{3},\frac{5}{12}-\delta u\right)$	O(2) 18f $\left(\frac{5}{6}+\frac{4}{3}\delta u,\frac{4}{6}+\frac{8}{3}\delta u,\frac{5}{12}-\frac{1}{3}\delta u\right),$ $\left(\frac{5}{6}+\frac{4}{3}\delta u,\frac{1}{6}-\frac{4}{3}\delta u,\frac{5}{12}-\frac{1}{3}\delta u\right),$ $\left(\frac{2}{6}-\frac{8}{3}\delta u,\frac{1}{6}-\frac{4}{3}\delta u,\frac{5}{12}-\frac{1}{3}\delta u\right)$
$\frac{9}{24}\left(\frac{3}{8}\right)$	(A)	empty	empty
$\frac{8}{24}\left(\frac{1}{3}\right)$	C	B(2) 9e $\left(\frac{1}{6},\frac{2}{6}\right),\left(\frac{1}{6},\frac{5}{6}\right),\left(\frac{4}{6},\frac{5}{6}\right)$	
$\frac{7}{24}$	(B)	empty	empty
$\frac{6}{24}\left(\frac{1}{4}\right)$	A	O(1) 6c $\left(0,0,\frac{1}{4}+\delta u\right)$	O(2) 18f $\left(\frac{1}{2}-\frac{4}{3}\delta u,-\frac{8}{3}\delta u,\frac{1}{4}+\frac{1}{3}\delta u\right),$ $\left(+\frac{8}{3}\delta u,\frac{1}{2}+\frac{4}{3}\delta u,\frac{1}{4}+\frac{1}{3}\delta u\right),$ $\left(\frac{1}{2}-\frac{4}{3}\delta u,\frac{1}{2}+\frac{4}{3}\delta u,\frac{1}{4}+\frac{1}{3}\delta u\right)$
$\frac{5}{24}$	C	A(1) 6c $\left(\frac{2}{3},\frac{1}{3}\right)$	
$\frac{4}{24}\left(\frac{1}{6}\right)$	B	B(1) 3b $\left(\frac{1}{3},\frac{2}{3}\right)$	
$\frac{3}{24}\left(\frac{1}{8}\right)$	A	A(1) 6c $(0,0)$	
$\frac{2}{24}\left(\frac{1}{12}\right)$	C	O(1) 6c $\left(\frac{2}{3},\frac{1}{3},\frac{1}{12}-\delta u\right)$	O(2) 18f $\left(\frac{1}{6}+\frac{4}{3}\delta u,\frac{2}{6}+\frac{8}{3}\delta u,\frac{1}{12}-\frac{1}{3}\delta u\right),$ $\left(\frac{1}{6}+\frac{4}{3}\delta u,\frac{5}{6}-\frac{4}{3}\delta u,\frac{1}{12}-\frac{1}{3}\delta u\right),$ $\left(\frac{4}{6}-\frac{8}{3}\delta u,\frac{5}{6}-\frac{4}{3}\delta u,\frac{1}{12}-\frac{1}{3}\delta u\right)$
$\frac{1}{24}$	(B)	empty	empty
$\frac{0}{24}\,(0)$	A	B(2) 9e $\left(\frac{1}{2},0\right),\left(0,\frac{1}{2}\right),\left(\frac{1}{2},\frac{1}{2}\right)$	
$\frac{\bar{1}}{24}$	(C)	empty	empty

Upon careful analysis, the layer stacking descriptions for spinel presented in Table IV.7.2-2 and Fig. IV.7.2-1 reveal both the tetrahedral coordination of A cations and the octahedral coordination of B cations by *n.n.* O anions. There is also a positional parameter for oxygen anions in spinel, usually denoted by the variable u. The spinel crystal structure presented in Tables IV.7.2-1 and IV.7.2-2 was obtained assuming that the original cubic unit cell was placed in setting 2 of S.G. $Fd\bar{3}m$ such that an octahedral vacancy occurs at the origin of the *u.c.* This *u.c.* origin has point symmetry $\bar{3}$ (i.e., it is an inversion center). With these definitions, the ideal oxygen positional parameter is given by $u=\frac{1}{4}$. In this case the anion sublattice is a perfect *fcc* arrangement of atoms. In general, the anion sublattice undergoes a dilation, δu, away from the ideal fractional

coordinate, $u = \frac{1}{4}$. In the case of natural $MgAl_2O_4$, this deviation from ideality is given approximately by $\delta u = 0.0133(3)$ [2] (u and δu are both fractions of the cube lattice parameter, a_{cube}). This results in a small rumpling of the O anion layers along $\overline{3}$ in the hexagonal description of the spinel structure. In addition, the fully dense O anion triangular nets are slightly distorted within the plane of each net. These effects are illustrated in Fig. IV.7.2-2. Lattice parameters a and c for the hexagonal $u.c.$ description of the $MgAl_2O_4$ spinel are shown in Table IV.7.2-3.

Table IV.7.2-3. Lattice parameters for both the cubic and hexagonal $u.c.$ settings for the spinel compound $MgAl_2O_4$. Hexagonal $u.c.$ lattice parameters a and c are obtained from the cube $u.c.$ length, a_{cube}, using the relationships $a = \sqrt{\frac{\#\,atoms}{hexcell}}\, d$ (Eq. (III.5-1); $\frac{\#\,atoms}{hexcell} = 4$) and $c = 2\sqrt{6}\, d$ (24-layer $u.c.$ description, Eq. (III.5-4b)), where d is the $n.n.$ spacing in the Al kagome atom nets ($d = \frac{a_{cube}}{2\sqrt{2}}$).

Compound	Cube $u.c.$ Lattice Parameter a_{cube} (nm)	Hexagonal $u.c.$ Lattice Parameters a, c (nm)	Oxygen Positional Parameter, u Oxygen Deviation Parameter, δu (deviation from ideal $u = \frac{1}{4}$)	References & Comments
$MgAl_2O_4$	0.80898(9)	0.57204(2) 1.40121(0)	$u = 0.2633(3)$ $\delta u = 0.0133(3)$	Finger et al. [2] JCPDF 21-1152 natural spinel

(a)

(b)
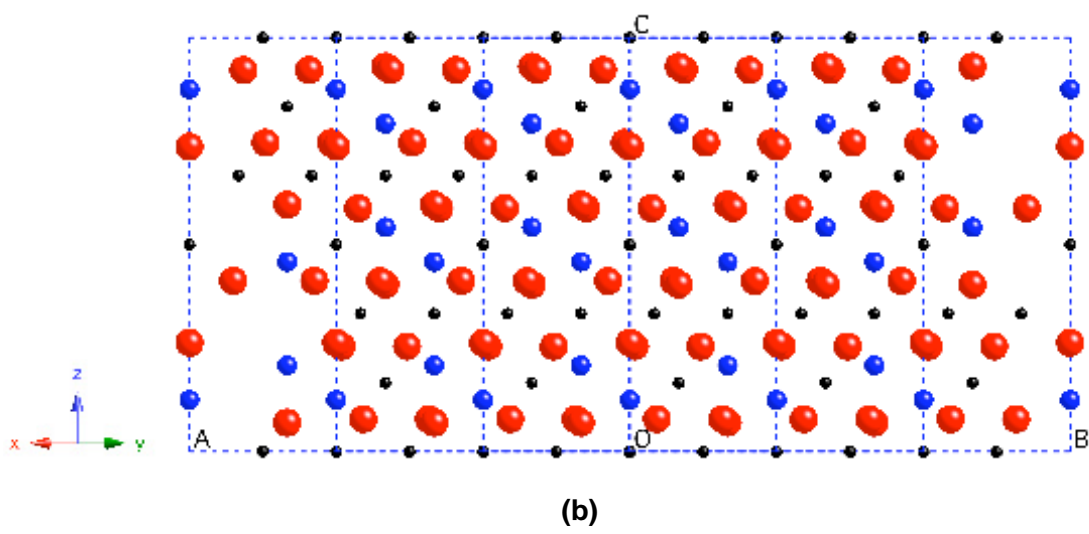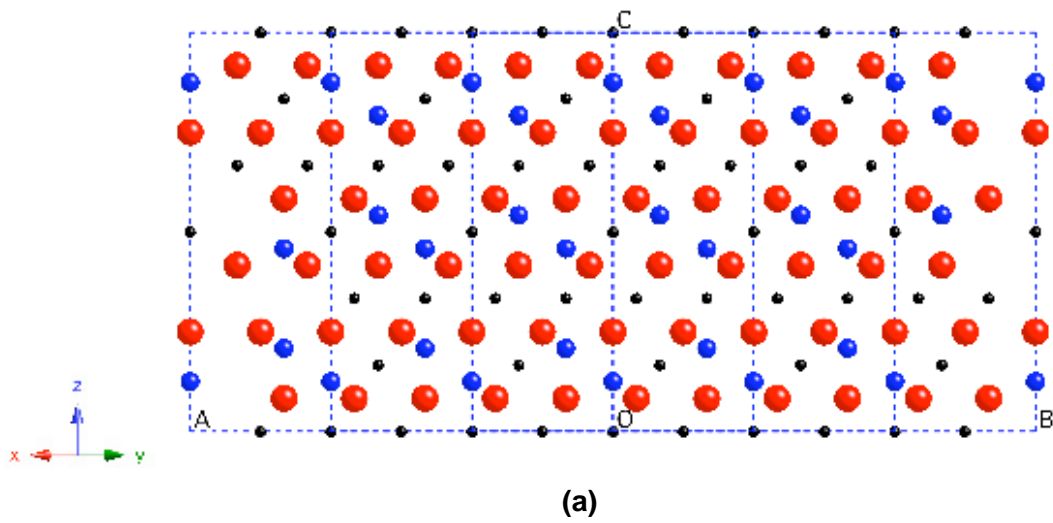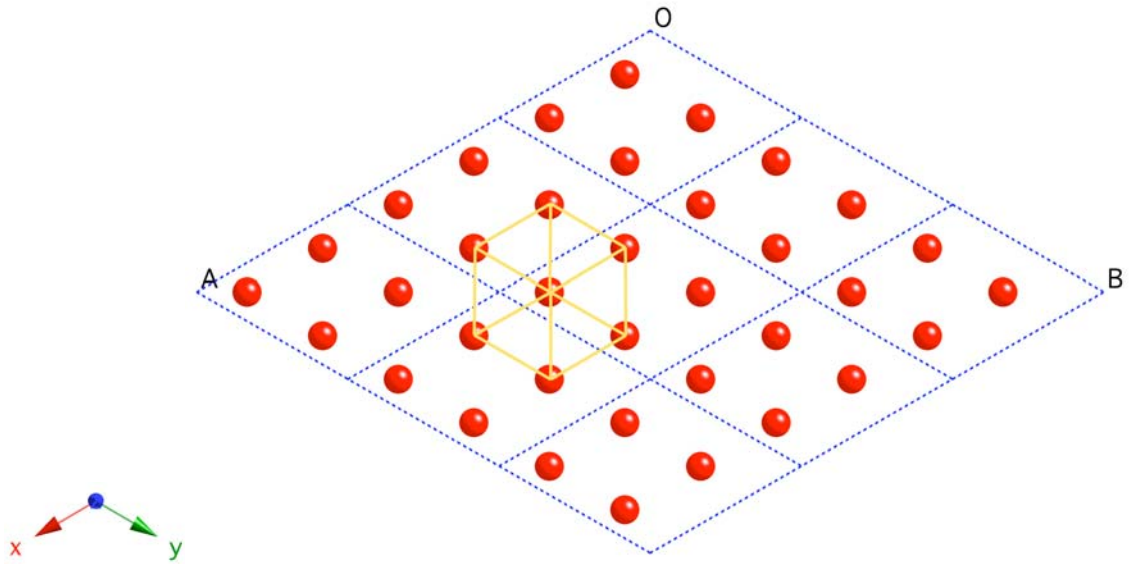
(c)
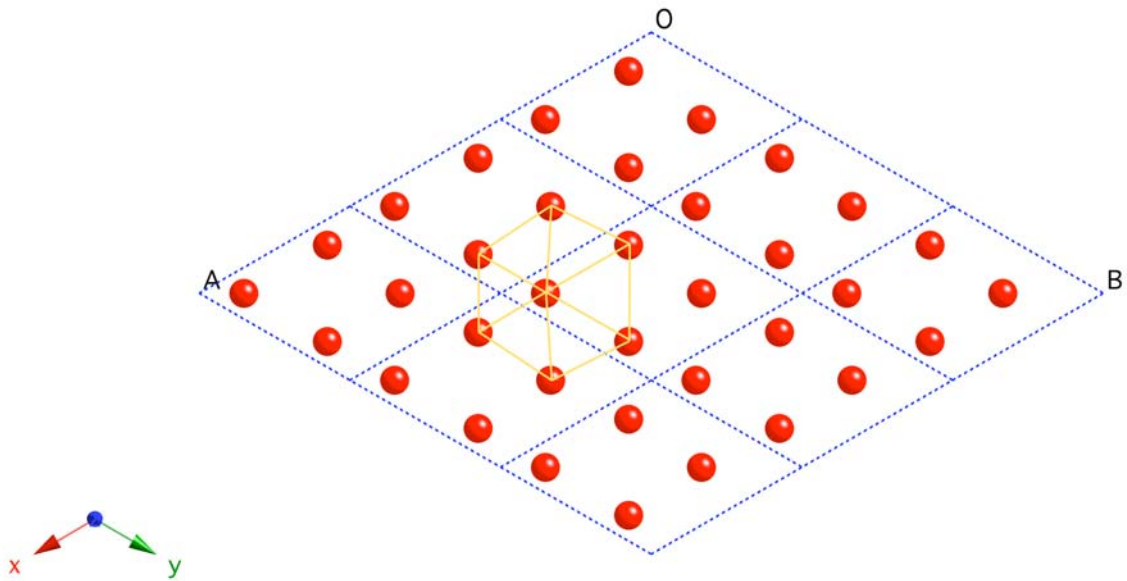
(d)
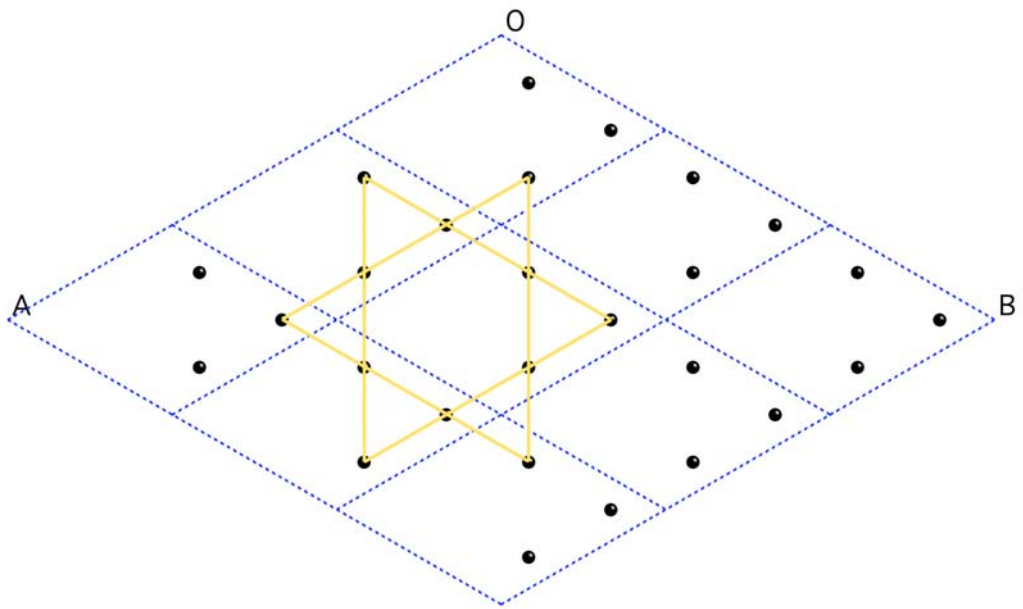
(e)
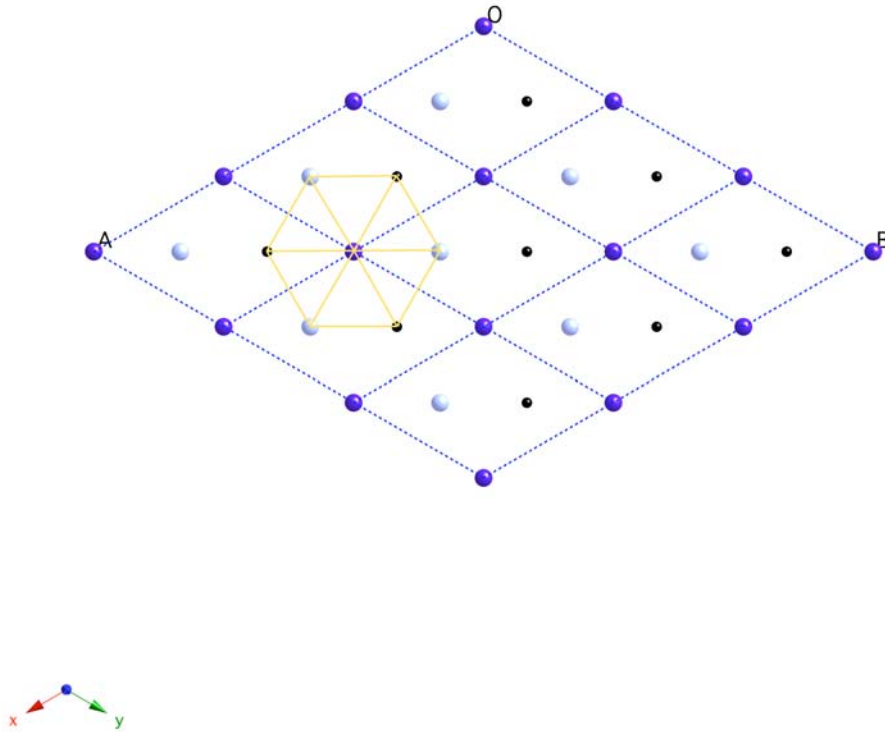
(f)

Figure IV.7.2-2. Atom layers along $\bar{3}$ in the spinel compound, $MgAl_2O_4$. Lattice parameters and oxygen positional parameters for these diagrams were obtained from Table IV.7.2-3 [2]. (a, b) Views of atom layers in ideal and real $MgAl_2O_4$, respectively, in a projection parallel to $\bar{3}$ (the $\bar{3}$ axis is the vertical axis in the plane of this drawing). The height of the drawing is 1.40121(0) nm, equal to the hexagonal lattice parameter, c. Three *u.c.*s are shown along the horizontal axis. Slight rumpling of the oxygen layers along $\bar{3}$ is evident in (b). (c, d) Views down the $\bar{3}$ axis of O anion layers in ideal and real $MgAl_2O_4$, respectively (ideal height $z = \frac{5}{12}$). Nine (3 × 3) hexcells are shown in each diagram. These diagrams illustrate the effects of deviation from ideality of the fully dense triangular anion nets in spinel. (e) Kagome lattice of Al cations at height $z = \frac{1}{3}$ viewed down the $\bar{3}$ axis. The characteristic kagome star is shown in yellow. (f) A projected view (down $\bar{3}$) of Mg, Al, and Mg layers at heights $z = \frac{3}{24}, \frac{4}{24}, \frac{5}{24}$. Taken together, these three cation layers form a $\frac{3}{4}$ dense net of atoms, compared with the areal density of atoms in the *n.n.* anion layers. It is interesting to observe that the tiling pattern produced by the cations in this diagram is a fully dense triangular net of atoms, just as it is in the *n.n.* anion layers. But the cation net consists of three atoms per hexcell, whereas the surrounding anion nets consist of four atoms per hexcell. In other words, the cation layer uses Iida's *subdivision by 3^rds* of a triangular atom net, while the anion layers utilize *subdivision by 4^ths*. Using Eq. (II.5-1), we conclude that the *n.n.* projected cation-cation spacing in this cation "layer" is greater than the *n.n.* anion-anion spacing in adjacent anion layers by the factor $\frac{2}{\sqrt{3}}$.

Section IV.7.2 References

[1]   K. E. Sickafus, J. M. Wills, and N. W. Grimes, "Structure of Spinel," *J. Am. Ceram. Soc.* **82** (12) 3279–3292 (1999).

[2]   L. W. Finger, R. M. Hazen, and A. M. Hofmeister, "High-Pressure Crystal Chemistry of Spinel ($MgAl_2O_4$) and Magnetite (Fe_3O_4): Comparison with Silicate Spinels," *Phys. Chem. Minerals* **13** 215–220 (1986).

IV.7.3 Real Materials: A Hypothetical M_3O_4 Compound

To complete the discussion of M_3O_4 compositions, we present here an additional hypothetical crystal structure. We propose that the MOO layer stacking motif concept can be extended down to the oxidation state associated with the M_3O_4 stoichiometry ($M^{2.66+}$). It turns out we can simulate an M_3O_4 compound stoichiometry using the MOO layer stacking motif if we use Iida's *subdivision by 3^{rds}* concept for the subdivision of triangular atom nets. We produce this structure by interleaving two $\frac{2}{3}$ dense *honeycomb* O anion nets between successive pairs of fully dense M cation nets (each $\frac{3}{3}$ dense). We use the same A, B, C, layer registry concepts as developed for previous structures discussed in this presentation. This crystal structure does not belong to S.G. $R\overline{3}$: it belongs to the orthorhombic S.G. *Immm* (#71). Nevertheless, this structure can still be described based on a hexagonal *u.c.* with a 12-layer atom stacking sequence along the *c*-axis. This stacking sequence is shown in Table IV.7.3-1 and Fig. IV.7.3-1.

We are not aware of the existence of this crystal structure in nature. However, it seemed to be a natural member of the set of structures that we presented in this paper, especially in that it utilizes the MOO layer stacking motif and Iida's *subdivision by 3^{rds}* concept, which had not been used together in any structure presented until now. Even if this structure is found not to exist, it may prove to be an integral component of a more complex oxide structure. This is by analogy to certain complex oxides that utilize the spinel crystal structure as a building block within their own crystal frameworks (e.g., the compound magnetoplumbite, $BaFe_{12}O_{19}$ [1]). Thus, we present this hypothetical structure in the event that it does find application in an as yet unidentified material. One might anticipate finding this structure in oxides consisting of both large divalent and trivalent cations (M^{2+} and M^{3+}). Were these cations to order in the M layers along the *c*-axis, the symmetry would be reduced from *Immm*.

Table IV.7.3-1. 12-layer atom stacking sequence description for a hypothetical M_3O_4 compound. Fractional coordinates for atoms within each layer are shown in parentheses (x, y) for atoms at layer heights z as shown in the left-hand column. This structure utilizes Iida's *subdivision by 3^{rds}* of a triangular atom net. The stacking motif along the z-axis is MOO, wherein the M layers are $\frac{3}{3}$ fully dense triangular cation nets, while each O layer is a $\frac{2}{3}$ dense anion honeycomb lattice. The hexagonal *u.c.* lattice parameter a is obtained using the relationship $a = \sqrt{\frac{\#\ atoms}{hexcell}}\, d$ (Eq. (III.5-1); $\frac{\#\ atoms}{hexcell} = 3$) where d is the *n.n.* spacing in the M layer triangular atom nets. Hexagonal parameter c is undefined, though $c = \sqrt{6}\, d$ (12-layer *u.c.* description, Eq. (III.5-4a)) would yield an apparent cubic symmetry.

Layer Height (z) (*u.c.* fraction)	Registry (*ABC* stacking)	Layer Atom Pattern	Hexcell Fractional Coordinates (x, y) (*u.c.* fraction)
$\frac{12}{12}$ (1)	A	$\frac{3}{3}$ fully dense **M**	$(0,0)$, $\left(\frac{1}{3},\frac{2}{3}\right)$, $\left(\frac{2}{3},\frac{1}{3}\right)$
$\frac{11}{12}$	C	$\frac{2}{3}$ *honeycomb* **O**	$\left(\frac{1}{3},0\right)$, $\left(0,\frac{1}{3}\right)$
$\frac{10}{12}$ $\left(\frac{5}{6}\right)$	(B)	empty	empty
$\frac{9}{12}$ $\left(\frac{3}{4}\right)$	A	$\frac{2}{3}$ *honeycomb* **O**	$\left(\frac{1}{3},\frac{2}{3}\right)$, $\left(\frac{2}{3},\frac{1}{3}\right)$
$\frac{8}{12}$ $\left(\frac{2}{3}\right)$	C	$\frac{3}{3}$ fully dense **M**	$\left(\frac{1}{3},0\right)$, $\left(0,\frac{1}{3}\right)$, $\left(\frac{2}{3},\frac{2}{3}\right)$
$\frac{7}{12}$	B	$\frac{2}{3}$ *honeycomb* **O**	$\left(\frac{2}{3},0\right)$, $\left(0,\frac{2}{3}\right)$
$\frac{6}{12}$ $\left(\frac{1}{2}\right)$	(A)	empty	empty
$\frac{5}{12}$	C	$\frac{2}{3}$ *honeycomb* **O**	$\left(\frac{1}{3},0\right)$, $\left(0,\frac{1}{3}\right)$
$\frac{4}{12}$ $\left(\frac{1}{3}\right)$	B	$\frac{3}{3}$ fully dense **M**	$\left(\frac{2}{3},0\right)$, $\left(0,\frac{2}{3}\right)$, $\left(\frac{1}{3},\frac{1}{3}\right)$
$\frac{3}{12}$ $\left(\frac{1}{4}\right)$	A	$\frac{2}{3}$ *honeycomb* **O**	$\left(\frac{1}{3},\frac{2}{3}\right)$, $\left(\frac{2}{3},\frac{1}{3}\right)$
$\frac{2}{12}$ $\left(\frac{1}{6}\right)$	(C)	empty	empty
$\frac{1}{12}$	B	$\frac{2}{3}$ *honeycomb* **O**	$\left(\frac{2}{3},0\right)$, $\left(0,\frac{2}{3}\right)$
$\frac{0}{12}$ (0)	A	$\frac{3}{3}$ fully dense **M**	$(0,0)$, $\left(\frac{1}{3},\frac{2}{3}\right)$, $\left(\frac{2}{3},\frac{1}{3}\right)$
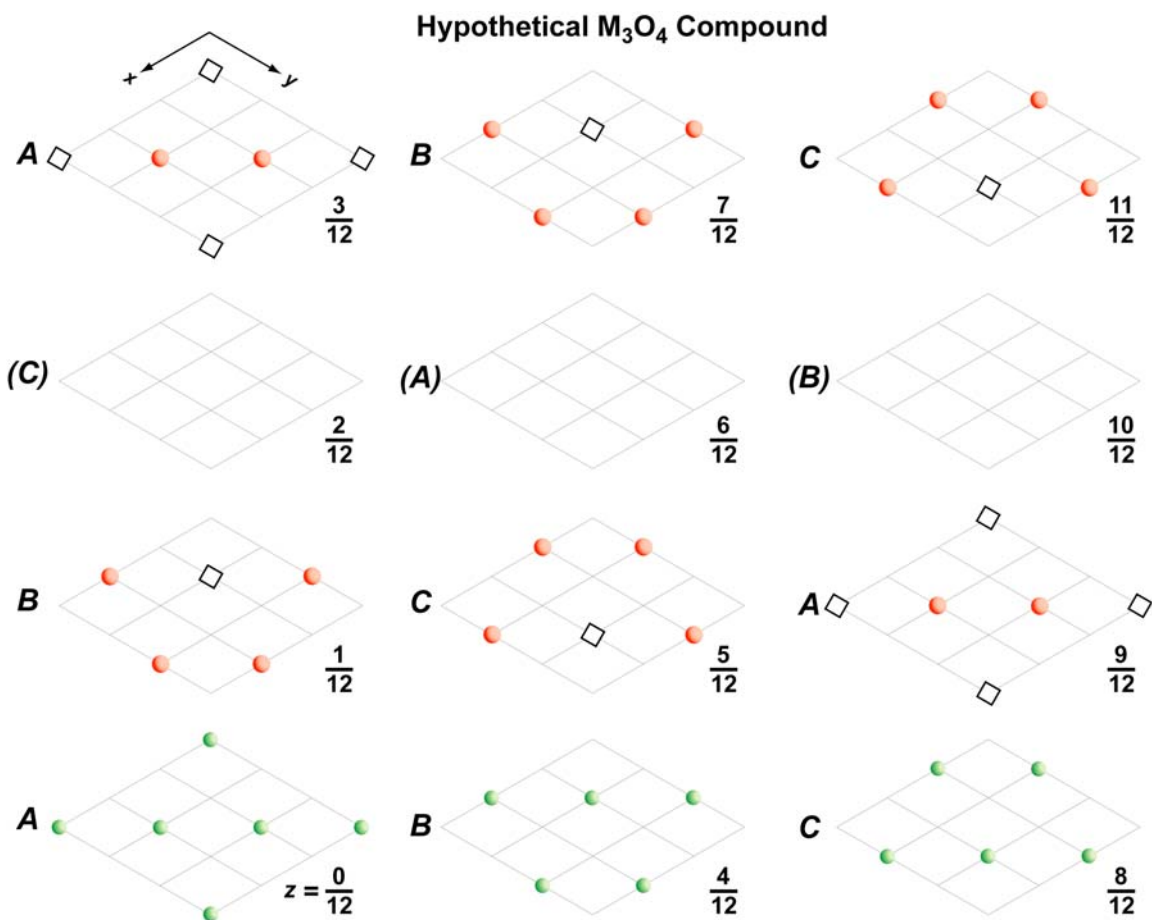
Figure IV.7.3-1. Layer stacking sequence along the z-axis for a hypothetical M_3O_4 crystal structure discussed in the text. This structure is described by a 12-layer stacking sequence along z. The diagram is intended to be read from bottom to top, left to right, from minimum to maximum height, z. The height of the diagram from $z = 0$ to $z = 1$ is equivalent to the hexagonal lattice parameter c. The edges of the hexcells in the diagram are equal to hexagonal *u.c.* length a. This structure utilizes Iida's *subdivision by 3^{rds}* of a triangular atom net. Metal M cations are small green spheres; oxygen O anions are large red spheres. Vacancies on the anion sublattice are indicated by black-outlined squares. M layers are fully dense triangular atom nets. O layers form honeycomb lattices of anions.

Section IV.7.3 References

[1]   S. Iida, "Layer Structures of Magnetic Oxides," *J. Phys. Soc. Japan* **12** (3) 222–233 (1957).

V.1 A Generalized Geometrical Model

In this section, we attempt to generalize some of the concepts of layer stacking of triangular atom nets that we have introduced in this report. We also offer some potential applications for these concepts.

Figure V.1-1a shows schematically a triangular atom net and a portion of a series of hexcells that form the bases for hexagonal unit cells made from layers of triangular atom nets (or derivatives of such nets). In this series, the number of atoms per hexcell increases in the sequence 1, 3, 7, 13, 21, 31, 43, 57, 73, 91, … The first member of this series (the one atom hexcell) has cell sides equal in length to the characteristic spacing d within the triangular atom net. Recall that the length of a hexcell side is equivalent to lattice parameter a in a hexagonal unit cell. For the remaining members of the series described above, the lattice parameter a is given by $a = \sqrt{\frac{\#\,atoms}{hexcell}}\; d$ (Eq. (III.5-1)).

Figure V.1-1b shows the one atom hexcell from Fig. V.1-1a along with two additional hexcells that are multiples of the one atom hexcell: namely, hexcells with edges twice and three times as long as that of the one atom hexcell. These represent the first hexcells in another series of cells with edges of lengths 1, 2, 3, … times the characteristic spacing d within a triangular atom net.

The two series above can be combined to produce a series of hexcell sequences. For instance, Fig. V.1-1c shows a few members of a series of hexcells wherein the cell edges are *twice* the lengths of the corresponding cell edges in the sequence shown in Fig. V.1-1a. In this series, the number of atoms per hexcell increases in the sequence 4, 12, 28, 52, 84, 124, … The base lattice parameters of these cells are again given by $a = \sqrt{\frac{\#\,atoms}{hexcell}}\; d$ (Eq. (III.5-1)).

The next series in this sequence involves hexcells wherein the cell edges are *three times* the lengths of the corresponding cell edges in the sequence shown in Fig. V.1-1a. The first members of this series are shown in Fig. V.1-1d. In this series, the number of atoms per hexcell increases in the sequence 9, 27, 62, 117, … The base lattice parameters of these cells are again given by $a = \sqrt{\frac{\#\,atoms}{hexcell}}\; d$ (Eq. (III.5-1)).

(a)

V.1 A Generalized Geometrical Model
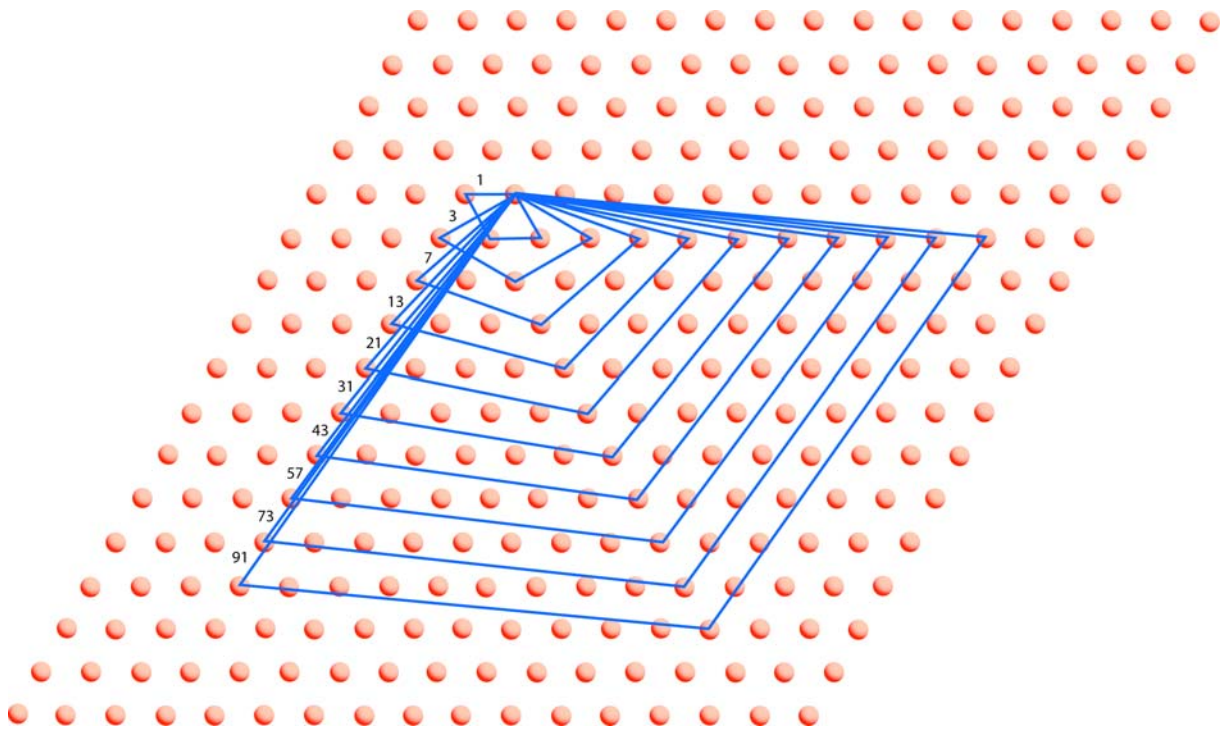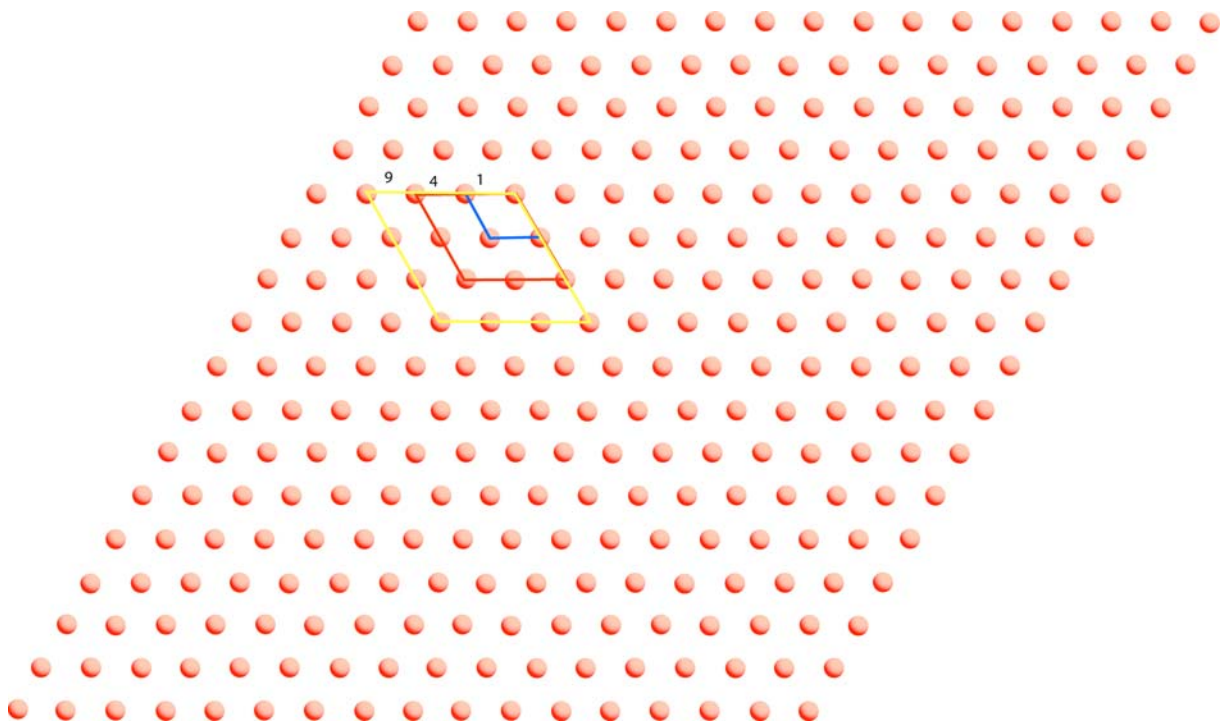
(b)
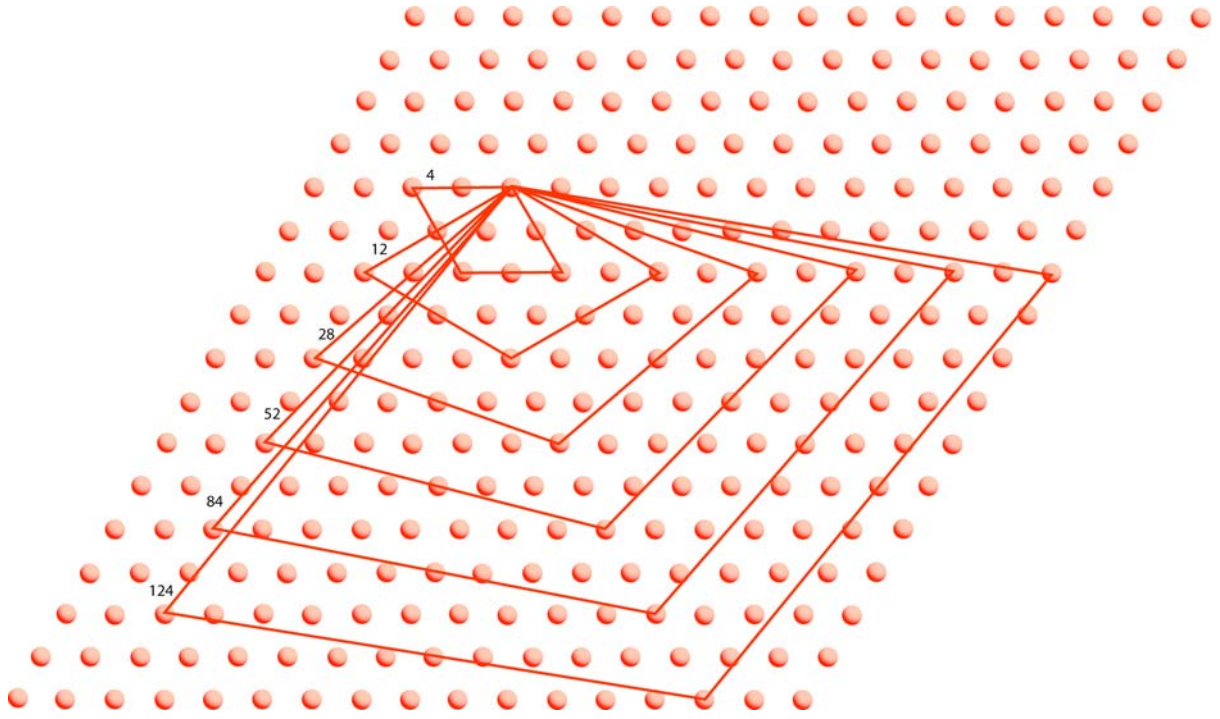
(c)
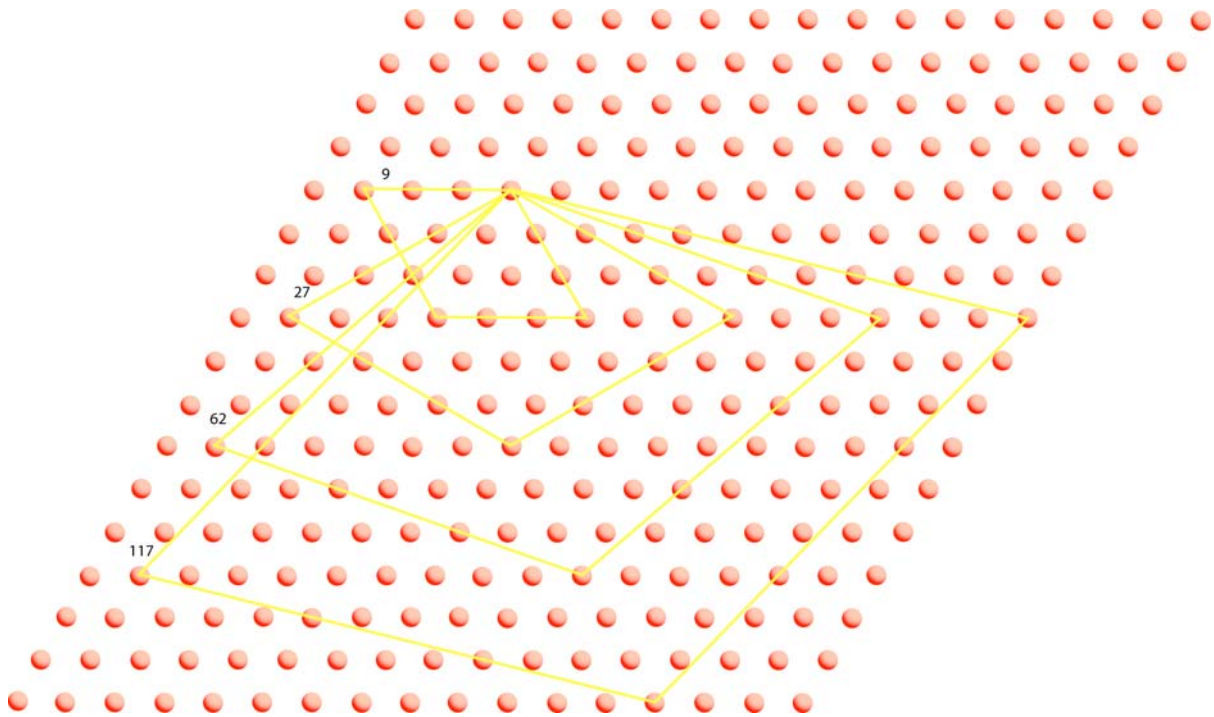
(d)

Figure V.1-1. Each drawing (a–d) shows schematically a triangular atom net along with various hexcells that might form the bases for hexagonal unit cells made from layers of triangular atom nets (or derivatives of such nets). (a) Shows a first-order hexcell series ($m = 1$ in Eq. (V.1-1)), such that as n is incremented, the number of atoms per hexcell increases in the sequence 1, 3, 7, 13, 21, 31, 43, 57, 73, 91, … The first member of this series (the one atom hexcell) has cell sides equal in length to the characteristic spacing d within the triangular atom net. (b) Shows first-order ($m = 1$), second-order ($m = 2$), and third-order ($m = 3$) hexcells, where $n = 0$ in all cases. The number of atoms per hexcell in this series increases in the sequence 1, 4, 9, … (c) Shows a second-order hexcell series ($m = 2$ in Eq. (V.1-1)), such that as n is incremented, the number of atoms per hexcell increases in the sequence 4, 12, 28, 52, 84, 124, …(d) Shows a third-order hexcell series ($m = 3$ in Eq. (V.1-1)), such that as n is incremented, the number of atoms per hexcell increases in the sequence 9, 27, 62, 117, …

We can make a generalized statement regarding the number of atoms in a hexcell corresponding to the series/sequences described above as follows: given two integers, n and m, in two infinite series of integers, the corresponding number of atoms/hexcell is given by

$$\frac{\text{\# atoms}}{\text{hexcell}} = m^2 \left(\left(n \left(n+1 \right) \right) + 1 \right); \quad \left(m, 1, \infty \right), \left(n, 0, \infty \right) \text{ fully dense triangular atom net.} \quad \text{(V.1-1)}$$

The hexcells defined by Eq. (V.1-1) correspond with fully dense triangular nets. Stacking such layers in 12- and 24-layer sequences as described in this report will produce structures such as MO rock salt and MO_2 fluorite. But to obtain more complex stoichiometries, one must utilize deficient triangular atom nets in the stacking. For a given hexcell, the simplest deficient triangular atom net is obtained by removing the atom at the origin of the hexcell. Then the number of atoms in the hexcell is given by:

$$\frac{\text{\# atoms}}{\text{hexcell}} = m^2 \left(\left(n \left(n+1 \right) \right) + 1 \right) - 1; \quad \left(m, 1, \infty \right), \left(n, 0, \infty \right) \quad \text{deficient triangular atom net} \quad \text{(V.1-2)}$$

Using this methodology, the Iida *honeycomb* lattice (*subdivision by 3^{rds}*; 3^6 regular Archimedean tiling (Section III.2) is obtained from Eq. (V.1-2) with $m = 1$, $n = 1$ (Fig. V.1-1a). The Iida *kagome* lattice (*subdivision by 4^{ths}*; 3.6.3.6 semiregular Archimedean tiling; Section III.2) is obtained from Eq. (V.1-2) with $m = 2$, $n = 1$ (Figs. V.1-1b and V.1-1c). The Iida *subdivision by 7^{ths}* lattice (3^4.6 semiregular Archimedean tiling; Section III.2) is obtained from Eq. (V.1-2) with $m = 1$, $n = 2$ (Fig. V.1-1a). We anticipate that nature employs additional, higher-order hexcells in the series/sequences described above in more complex compounds. Also, more complex deficient triangular atom nets can be envisioned (compared with the removal of the atom at the hexcell origin described here).

Using the hexcells defined above, one can create a real or hypothetical crystal structure by stacking hexcells, either fully dense (Eq. (V.1-1)) or deficient (Eq.(V.1-2)), along a stacking axis. Ultimately, the stacking periodicity defines the hexagonal lattice parameter c of the structure. One could stack atom nets in 12- or 24-layer sequences as described in this report, using MX or MXX motifs (M = cation; X = anion) or perhaps other motifs, where M or X might be deficient layers compared with a fully dense, triangular atom net. This methodology can be used to predict crystal structures and complex compound stoichiometries.

It should be noted that real crystal structures are sometimes nothing more than slight distortions away from these idealized, predicted crystal structures. Also, atomic relaxations often cause symmetry reductions so that real structures are orthorhombic or monoclinic distortions compared with the idealized, hexagonal structures created using our layer stacking concepts. Because of the distortions away from ideality, the layer stacking concepts discussed here usually go unrecognized. Nevertheless, our layer stacking methodology offers a simple means to understand the general principles underlying the construction of highly complex crystal structures.

To illustrate how to apply the concepts developed in this report, let's consider a complex scandium zirconate compound called the beta phase. This phase is denoted β in the phase diagram shown in Fig. V.2-2 [1]. We have already considered δ-$Sc_4Zr_3O_{12}$ and γ-$Sc_2Zr_5O_{13}$ compounds (Fig. V.2-2) in previous sections (Sections IV.5 and IV.3, respectively). Many compositions have been reported for the β phase and there is considerable debate regarding the crystal structure of this phase. One β composition discussed recently in the literature by Wurst et al. is β-$Sc_{12}Zr_{50}O_{118}$ [2]. It is instructive to interrogate this structure using our layering ideas.
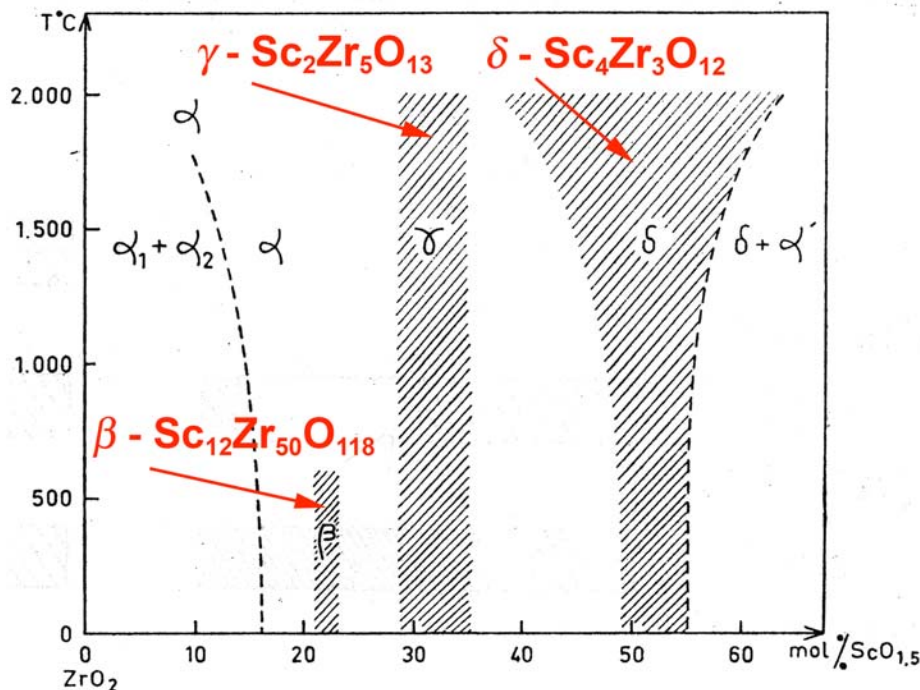
Figure V.1-2. Phase diagram for the ZrO_2 – Sc_2O_3 (or ZrO_2 - $ScO_{1.5}$) binary oxide system, according to Lefèvre [1]. The δ, γ, and β phases discussed in this report are labeled in red.

The lattice parameters for the β-$Sc_{12}Zr_{50}O_{118}$ structure published by Wurst et al. [2] are $a = 1.98170(5)$ nm and $c = 1.80059(6)$ nm. The characteristic spacing d between atoms in the pseudo-triangular atom nets in this structure varies from $d = 0.3479$ to 0.3744 nm. Using an average $d = 0.355$ nm and considering Eq. (III.5-1), $a = \sqrt{\frac{\# atoms}{hexcell}} d$, and the hexcell sequence from Eq. (V.1-1) where $m = 1$ (such that the number of atoms per hexcell increases in the sequence 1, 3, 7, 13, 21, 31, 43, 57, 73, 91, …), we find that the hexcell in the aforementioned sequence that has a corresponding base lattice parameter a close to the published value, $a = 1.98170(5)$ nm, is the 31 atom hexcell ($m = 1$, $n = 5$ in Eq. (V.1-1)). For $d = 0.355$ nm and using 31 atoms per hexcell, we find (from Eq. (III.5-1)) $a = 0.19765$ nm, in good agreement with the Wurst et al. value [2].

Next, we speculate that the Wurst et al. value for lattice parameter c should be compared with the predicted parameter c, based on either 12- or 24-layer stacking. Equations (III.5-4a) and (III.5-4b) indicate that c depends on the characteristic *n.n.* spacing d as follows: $c = \sqrt{6}\, d$ or $c = 2\sqrt{6}\, d$, for 12- and 24-layer stacking, respectively. For 12-layer stacking and using $d = 0.355$ nm, we find $c = 0.86957$ nm for 12-layer stacking versus c value, $c = 1.80059(6)$ nm [2], corresponds to a 24-layer stacking sequence.

Based on this information, we can make several predictions regarding specifics of the layer stacking sequence for β-$Sc_{12}Zr_{50}O_{118}$. First, consider that the oxygen (O) to metal (M) ratio in this compound is 1.9. This is much closer to MO_2 compared with MO stoichiometry. Thus, we should anticipate an MOO layer stacking motif similar to fluorite, rather than an MO motif as in rock salt. But the 24-layer stacking sequence indicates that the stacking must be complex, in the sense that adjacent layers may have different numbers of atoms in their hexcell arrangements. We infer this from the example of pyrochlore (M_4O_7) compounds that we presented in Section IV.4. Let's take a moment to review the pyrochlore structure.

Pyrochlores are made from stacking triangular atom nets made from hexcells with four atoms per cell. This corresponds to $m = 2$, $n = 1$ for the hexcell sequences defined in Eq. (V.1-1). In pyrochlores, fully dense oxygen triangular atom nets alternate with oxygen deficient layers to produce a layer stacking sequence that we can describe using the following motif shorthand: OMOoMo. Here, M and O represent fully dense cation and anion triangular nets, respectively, while o represents an oxygen deficient atom layer (specifically, the o layers are $\frac{3}{4}$ dense with respect to the M and O layers; actually, they are kagome layers). The complexity of the pyrochlore stacking motif dictates that the

number of layers necessary to repeat the stacking sequence is large (24 layers in this case). But our interest in pyrochlore is this: Because we have determined that β-$Sc_{12}Zr_{50}O_{118}$ utilizes a 24-layer atom stacking sequence, we can anticipate a complex layer stacking motif for β-$Sc_{12}Zr_{50}O_{118}$ such as that of pyrochlore, i.e., OMOoMo.

To understand details of the layer stacking for β-$Sc_{12}Zr_{50}O_{118}$, we must also consider the stoichiometry of the β phase in more detail. A perfect MO_2 fluorite consisting of 31 atom hexcells must necessarily utilize a 12-layer atom stacking sequence with an MOO layer stacking motif. This in turn implies that all of the layers consist of fully dense, 31 atom hexcells. The contents of the hexagonal *u.c.* for this structure is $M_{93}O_{186}$ ($Z = 93$). In order for this compound to be charge neutral, all of the metal cations must be 4+ valence, so that the formula for this compound must be $Zr_{93}O_{186}$ (no Sc doping is possible here). This description of the *u.c.* for fluorite is 31 times redundant compared with the basic fluorite hexagonal *u.c.* defined in Table II.2-2.

Though we have determined that the β phase will utilize 24-layer stacking, let's first consider the case where this compound stacks in a similar fashion to the M_7O_{12} compounds presented in Section IV.5. In this case, we use a 12-layer atom stacking model, but every oxygen layer is missing one O atom per hexcell (stacking motif Moo; M represents a 31 atom hexcell, while o represents a 30 atom hexcell). It is easy to show that for 31 atom, fully dense hexcells, the contents of the hexagonal *u.c.* for this structure is $M_{93}O_{180}$ and the composition of the *u.c.* must be $Sc_{12}Zr_{81}O_{180}$. The corresponding compound stoichiometry is $Sc_4Zr_{27}O_{60}$. But this is not the β-phase stoichiometry, $Sc_{12}Zr_{50}O_{118}$ ($Sc_6Zr_{25}O_{59}$), according to Wurst et al. We must consider alternative models.

Next, we consider a pyrochlore-like *u.c.* made with 24-layer stacking and an OMOoMo stacking motif. This is analogous to the stacking found in γ-$Sc_2Zr_5O_{13}$ (Section IV.3). Again utilizing 31 atom, fully dense hexcells, and assuming that the oxygen deficient layers contain 30 atoms per hexcell (O and M represent 31 atom hexcells, while o represents a 30 atom hexcell (one missing atom per hexcell)), we find that the contents of the hexagonal *u.c.* for this structure is $M_{186}O_{366}$ and the composition of the *u.c.* must be $Sc_{12}Zr_{174}O_{366}$. The corresponding compound stoichiometry is $Sc_4Zr_{58}O_{122}$. But again, this is not the β-phase stoichiometry, $Sc_{12}Zr_{50}O_{118}$ ($Sc_6Zr_{25}O_{59}$), according to Wurst et al. Again, we must consider alternative models.

We find the solution as follows: Consider once again a perfect MO_2 fluorite consisting of 31 atom hexcells but with a 24-layer atom stacking sequence with an MOO layer stacking

motif. Assuming that all of the layers consist of fully dense, 31 atom hexcells, we find that contents of the hexagonal *u.c.* for this structure is $M_{186}O_{372}$ ($Z = 186$). This description of the *u.c.* for fluorite is 62 times redundant compared with the basic fluorite hexagonal *u.c.* defined in Table II.2-2. Now, let's assume that the Wurst et al. β- phase is equivalent to this description for fluorite except that some of the oxygen layers are deficient. This implies that the total cation content of the *u.c.* must be M_{186}. This is three times the cation count according to the Wurst et al. formula for the β-phase, $Sc_{12}Zr_{50}O_{118}$ ($M_{62}O_{118}$). So the contents of the corresponding Wurst et al. β-phase *u.c.* should be $Sc_{36}Zr_{150}O_{354}$ ($M_{186}O_{354}$). Compared with the composition of fluorite ($M_{186}O_{372}$), this suggests that the Wurst et al. β-phase is missing 18 oxygen atoms per *u.c.* These vacant anion sites are spread over 12 oxygen layers in the 24-layer atom stacking model. In principle, there are of course numerable ways to arrange 12 vacancies over $12 \times 31 = 372$ lattice sites. But what if we utilize the pyrochore layer stacking motif, OMOoMo? If we let M and O represent fully dense triangular cation and anion nets, respectively (31 atoms per hexcell), then o must represent an anion layer consisting of 28 oxygen atoms (or equivalently, three oxygen vacancies). This model yields the appropriate *u.c.* contents, $M_{186}O_{354}$, in order to obtain the Wurst et al. stoichiometry for the β-phase, $Sc_{36}Zr_{150}O_{354}$ (equivalent to $Sc_{12}Zr_{50}O_{118}$ or $Sc_{6}Zr_{25}O_{59}$).

The arrangement of the three oxygen vacancies per anion deficient layer in β-$Sc_{12}Zr_{50}O_{118}$ represents a whole new topic, beyond the scope of the discussion presented in our report. It turns out that oxygen vacancies in anion-deficient fluorites bind together in so-called *coordination defects* (CDs) (e.g., see Martin [3] and a series of papers by Eyring and colleagues [4–6]), rather than spacing themselves to maximize separation distances (as one would predict based on Coulombic interaction considerations). Nevertheless, our layer stacking concepts have made it possible to obtain a nearly complete description for the structure of this highly complex oxide structure. In fact, if we place three vacancies within each anion deficient layer at the maximal separation possible within each hexcell and utilize ABCABC… 24-layer stacking with an OMOoMo atom stacking motif, we obtain an ideal starting structure for atomistic simulations to describe the relaxed, atomic structure of β-$Sc_{12}Zr_{50}O_{118}$. This suggests one utility for our layered atom stacking concepts in complex crystalline materials. In the following section, we will propose a few additional applications for our layered atom stacking concepts.

Section V.1 References

[1]   J. Lefèvre, "Relations Entre la Structure de Type Fluorine et la Structure de Type Mn_2O_3. Étude du Système Zircone-Oxyde de Scandium," *Ann. Chim. Fr.* **t. 8** (**1–2**) 135–149 (1963).

[2]   K. Wurst, E. Schweda, and D. J. M. Bevan, J. Mohyla, K. S. Wallwork, and M. Hofmann, "Single-Crystal Structure Determination of $Zr_{50}Sc_{12}O_{118}$," *Solid State Sciences* **5** 1491–1497 (2003).

[3]   R. L. Martin, "Structural Theory for Non-Stoichiometry. Part I. Defect Fluorite-Typ*e Structures: Lanthanoid Oxides MO$_x$ with 1.7 < x < 2.0," J. Chem. Soc., Dalton Trans.* 1335–1350 (1974).

[4]   Z. C. Kang, J. Zhang, and L. Eyring, "The Structural Principles that Underlie the Higher Oxides of the Rare Earths," *Z.Anorg. Allg. Chem.* **622** 465–472 (1996).

[5]   Z. C. Kang and L. Eyring, "The Structural Basis of the Fluorite-Related Rare Earth Higher Oxides," *Aust. J. Chem.* **49** 981–996 (1997).

[6]   Z. C. Kang and L. Eyring, "A Compositional and Structural Rationalization of the Higher Oxides of Ce, Pr, and Tb," *J. Alloys Comp.* **249** 206–212 (1997).

V.2 Potential Applications for Layered Atom Stacking Concepts

In the final section of our report, we introduce briefly a few potential applications for the layered atom stacking concepts that we developed in this report. We already have shown that our concepts can be applied to modeling nonstoichiometry in complex oxides with structures related to the MO_2 fluorite structure (Section V.1). Three additional applications will be mentioned below: (1) diffusion mechanisms, (2) epitaxy, and (3) deformation mechanisms.

Figure V.2-1 illustrates a simple diffusion mechanism for atoms arranged in a $3^4.6$ Archimedean tiling. This mechanism makes use of the obvious "holes" in the tiling pattern. We anticipate that this mechanism will play a role in atomic mobility in materials that utilize the $3^4.6$ Archimedean tiling arrangement in their structures. Examples include $Sc_2Zr_5O_{13}$ (Section IV.3) and $Sc_4Zr_3O_{12}$ (and similar M_7O_{12} compounds; Section IV.5). We can also anticipate that this diffusion mechanism will play a role in fast ion conduction in these oxides at high temperatures. The analogous concept applies to any compound consisting of atomic layers made from triangular atom nets but with missing atoms in these nets (honeycomb and kagome lattices are two examples).

(a)

(b)
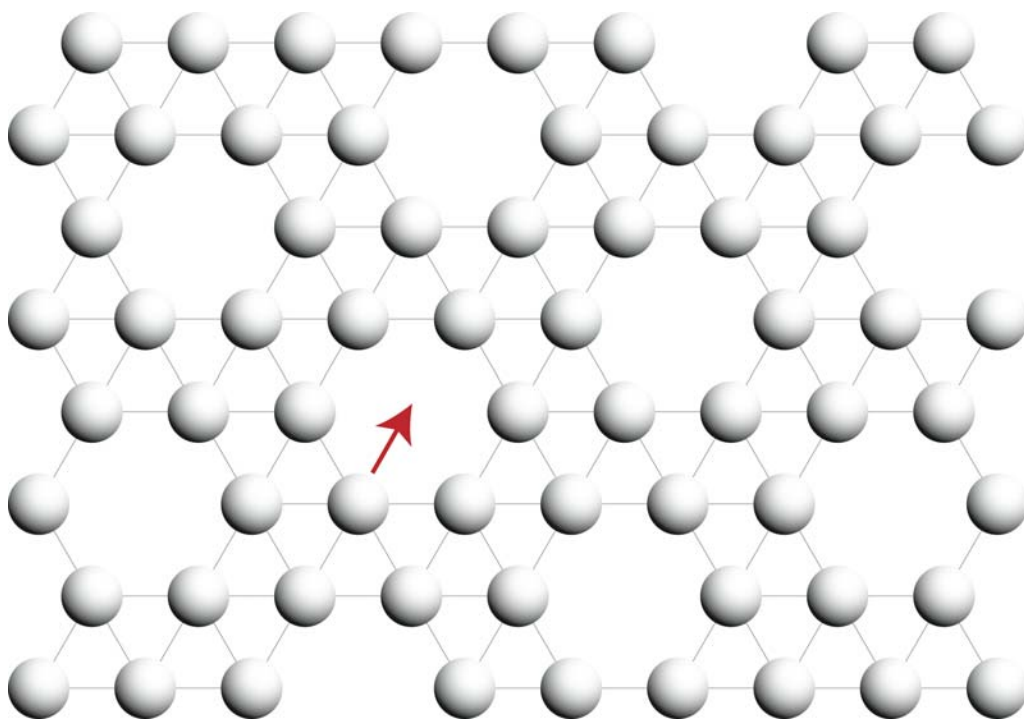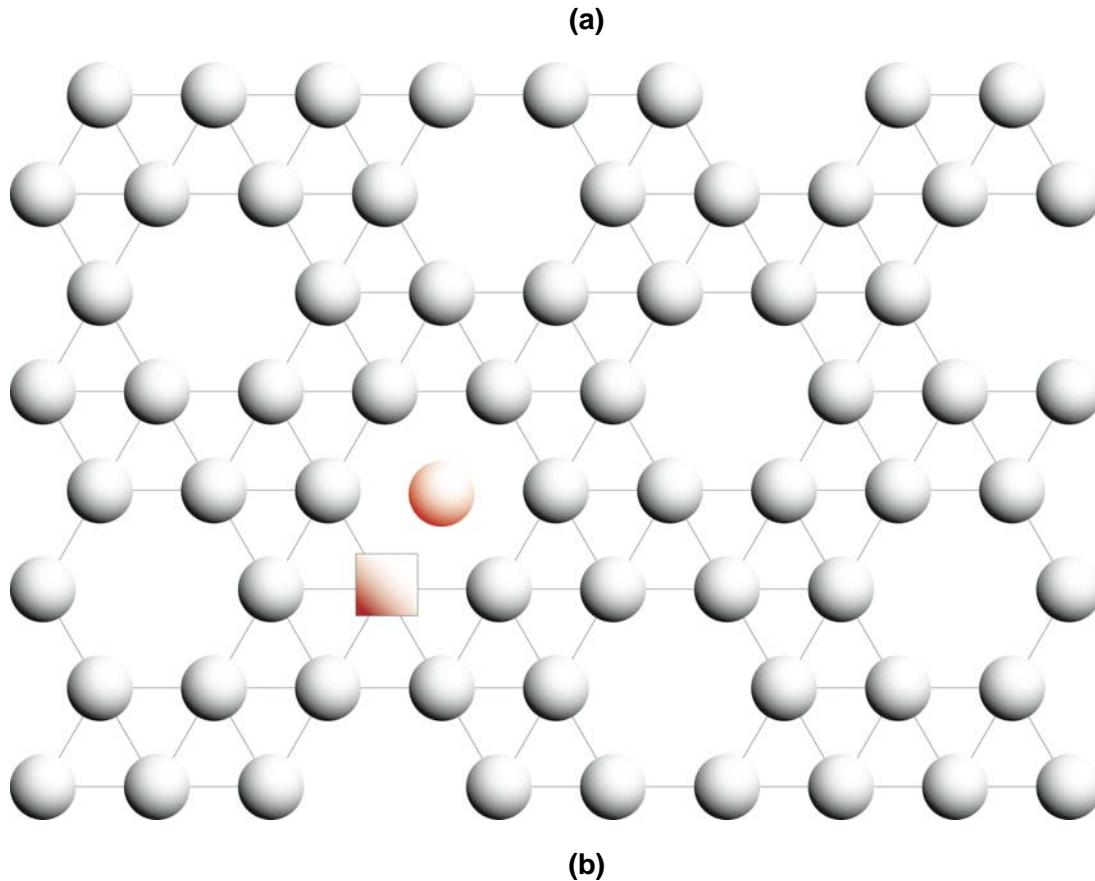
Figure V.2-1. A proposed interstitial diffusion mechanism for compounds consisting of layers based on triangular atom nets with individual atom layers arranged in $3^4.6$ Archimedean tilings. (a) A pristine $3^4.6$ Archimedean tiling atom layer, with the jump direction for an atom in the tiling highlighted in red. (b) The atom arrangement following the jump of the atom in (a) into an interstice in the tiling pattern. The interstitial atom created by this motion is highlighted in red. The vacancy left behind in the lattice is shown as a red-shaded square. Together, these two defects constitute a Frenkel pair. This Frenkel diffusion mechanism may play a role in ion conduction, particularly oxygen ion conduction, in M_7O_{12} and M_7O_{13} compounds (discussed in Sections IV.5 and IV.3, respectively).

Sometimes, layer concepts also provide a simple means to understand diffusion in nonoxides. Take for instance the intermetallic compound molybdenum disilicide ($MoSi_2$) (Laves phase $C11_b$ (see, e.g., [1])). Figure V.2-2 illustrates the atomic arrangement in a $\{1\bar{1}0\}$ plane in this tetragonal compound (I4/mmm; S.G. # 139 [2]). The Si atoms in this plane are arranged in a *honeycomb* lattice, while the Mo atoms fill the interstices to produce a fully dense triangular atom net. Atomic jump vectors between nearest neighbor Si sites are also indicated by arrows in Fig. V.2-2. The concept of diffusion in $MoSi_2$ at high temperature is as follows: The Mo sublattice is essentially frozen, even at relatively high temperature [1]. But at high temperature, the Si sublattice contains numerous Si

vacancies, as a result of thermally induced disorder [1]. Thus, Si diffusion can proceed via the Si-Si jump vectors illustrated in the $MoSi_2$ layer shown in Fig. V.2-2. With respect to our triangular atom net description for $MoSi_2$, Si atoms are offered three possible jumps within an $MoSi_2$ triangular atom net layer (Fig. V.2-2), while two more equivalent, *out-of-plane* jumps are also possible, either directly above or below the plane shown in Fig. V.2-2.[1] The layers above and below the layer shown in Fig. V.2-2 are identical in structure and composition ($MoSi_2$). They are simply shifted in registry such that the stacking sequence along the axis normal to these planes is *ABAB…* The diffusion process can be thought of as follows: Si atoms may be viewed as meandering through a "forest" of immovable Mo "trees," themselves arranged in a sort of three-dimensional, rigid lattice. Thus, the triangular atom net offers an extraordinarily simple means to visualize diffusion in this seemingly complex structure.

We also wish to propose that the layered atom concepts developed in this report are applicable to situations where epitaxial atomic arrangements are concerned. We illustrate the importance of epitaxial phase relationships with one example, in an effort to promote the broader applicability of this concept. Figure V.2-3 shows a transmission electron microscopy (TEM) image of an epitaxial layer of monoclinic (B-type) Dy_2O_3, atop a substrate layer of cubic (C-type) Dy_2O_3. This phase boundary was produced by an ion-irradiation-induced phase transition of C-type Dy_2O_3 [4]. Layers perpendicular to the image plane in Fig. V.2-3 are based on triangular atom nets, both in the C-type and B-type phases of Dy_2O_3. Stacking in C-type Dy_2O_3 is based on an Moo layer stacking motif along a $\bar{3}$ crystallographic axis, with fully dense Dy layers interleaved with pairs of O-deficient layers (3/4 dense wishbone kagome layers, according to the description provided in Section IV.6.3). The cation and anion layers for C-type Dy_2O_3 are illustrated schematically in Fig.V.2-4.

---

[1] We should note that the discussion here is for an idealized $MoSi_2$ structure. In the actual $MoSi_2$ structure, the lattice is distorted slightly from the triangular atom net description provided here (see JCPDF #41-612 [3]). Thus, for real $MoSi_2$ the Si-Si interatomic distance shown in Fig. V.2-2 (0.2618 nm) degenerates into two distances, 0.2614 and 0.2621 nm. But this represents a mere 0.27% distortion away from the ideal triangular atom net description for this structure.
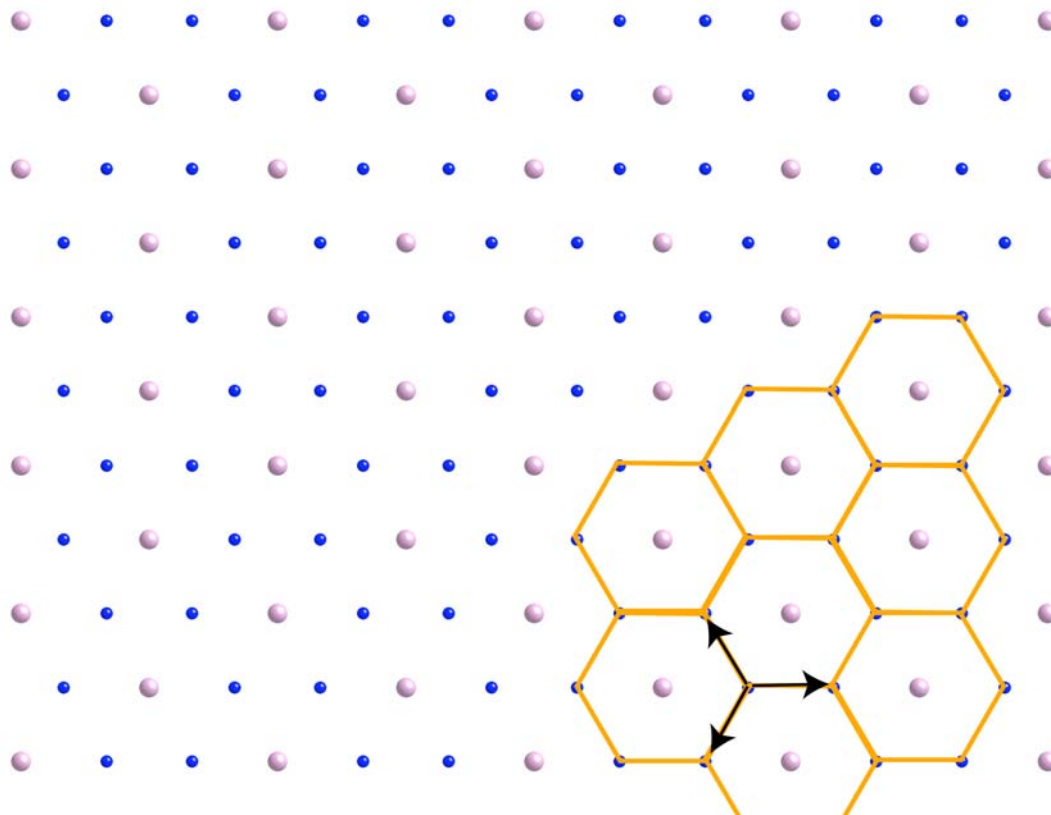
Figure V.2-2. A proposed diffusion mechanism for silicon atoms in the intermetallic compound molybdenum disilicide, $MoSi_2$. The diagram shows a $\{1\overline{1}0\}$ layer in this compound. The layer is based on a triangular atom net. The silicon atoms (small blue) are arranged in a honeycomb lattice (as illustrated in the lower-right portion of the diagram), while the Mo atoms (large gray) fill the interstices in the honeycomb Si lattice. Jointly, the Mo and Si atoms form a fully dense, triangular atom net. Arrows in the lower-right portion of the diagram indicate possible jump vectors for an Si atom to three neighboring Si sublattice sites within this $MoSi_2$ triangular atom net layer. Two more (identical) *out-of-plane* Si-Si jumps are possible to the $MoSi_2$ layers immediately above and below the layer shown here (the jump distance is 0.2618 nm; this assumes ideal tetragonal lattice parameters given by $a = 0.3206$ nm and $c = \sqrt{6}\, a = 0.785306$ nm). Such Si-Si jumps require that the adjacent Si atom sites be empty (i.e., be occupied by vacancies). This is the situation at high temperatures when the Si sublattice undergoes Frenkel disorder.
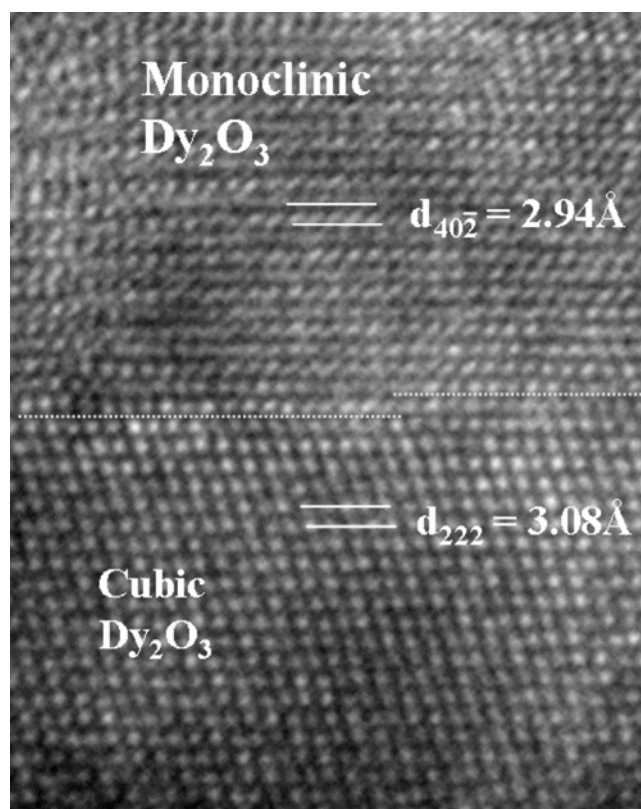
Figure V.2-3. TEM micrograph of a B-type Dy_2O_3/C-type Dy_2O_3 interface. The image reveals a sharp transition from C-type to B-type Dy_2O_3. This phase boundary was created by ion irradiation of pristine C-type Dy_2O_3 [3].
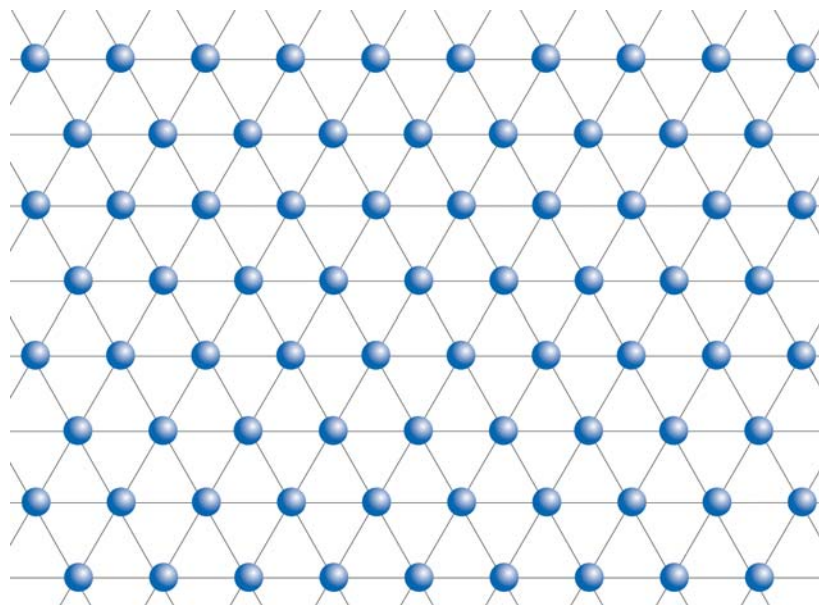
(a)
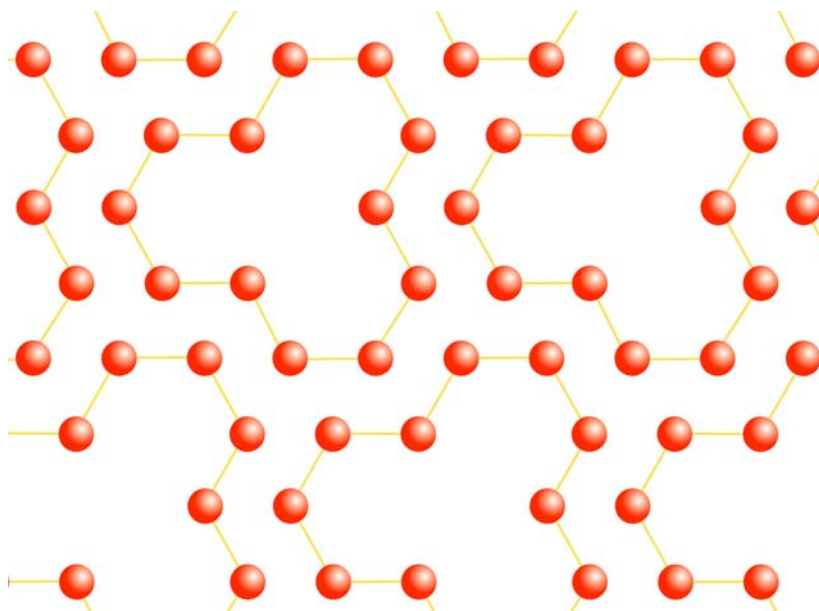
(b)

Figure V.2-4. $\{111\}_c$ planes in the cubic, C-type polymorph of Dy_2O_3 (commonly referred to as the *bixbyite* phase). (a) A pure metal (M) cation layer consisting of a fully dense, triangular net of cations. (b) A pure oxygen (O) anion layer consisting of a $\frac{3}{4}$ dense net of anions with vacancy complexes in the shapes of wishbones (outlined in yellow). We referred to this structure as the wishbone kagome lattice in Section IV.6.3. The diagrams of the $\{111\}_c$ planes shown here refer to an *ideal* bixbyite (cation and anion positional deviation parameters (Table IV.6.3-1) are all zero).

The corresponding cation and anion layers in B-type Dy_2O_3 are illustrated schematically in Fig. V.2-5. In these idealized drawings of the B-type sesquioxide structure, cation and anion layers are nothing more than fully dense, triangular atom nets. Moreover, these triangular atom nets stack in a sequence that utilizes the stacking motif OMOMO. Figure V.2-6 shows a model for the epitaxial relationship between the C-type and B-type Dy_2O_3 phases observed in Fig. V.2-3. The layer stacking motifs for the C and B phases are indicated in this diagram. Though our layer stacking concepts do not provide an explanation for why C-type Dy_2O_3 is transformed to the B-type polymorph under ion irradiation, the layer stacking concepts we have developed in this report clearly aid our visualization of the epitaxial relationship between the parent and daughter phases during this transformation.

Another illustration of possible applications for our layer atom stacking concepts involves deformation mechanisms in complex compounds. Consider, for instance, atomic slip mechanisms in the oxide spinel ($MgAl_2O_4$). Mitchell [5] has recently reviewed slip in spinel and a diagram showing possible slip systems for {111} <110> slip are shown in Fig. V.2-7. Though various dislocation dissociation mechanisms are proposed in the Mitchell review, the most important result to call to the readers' attention is that the perfect slip vector for {111} <110> slip in spinel involves a 1/2 <110> Burgers vector. This vector also happens to coincide with the repeat unit for the kagome lattice of cations in spinel (Fig. V.2-7).
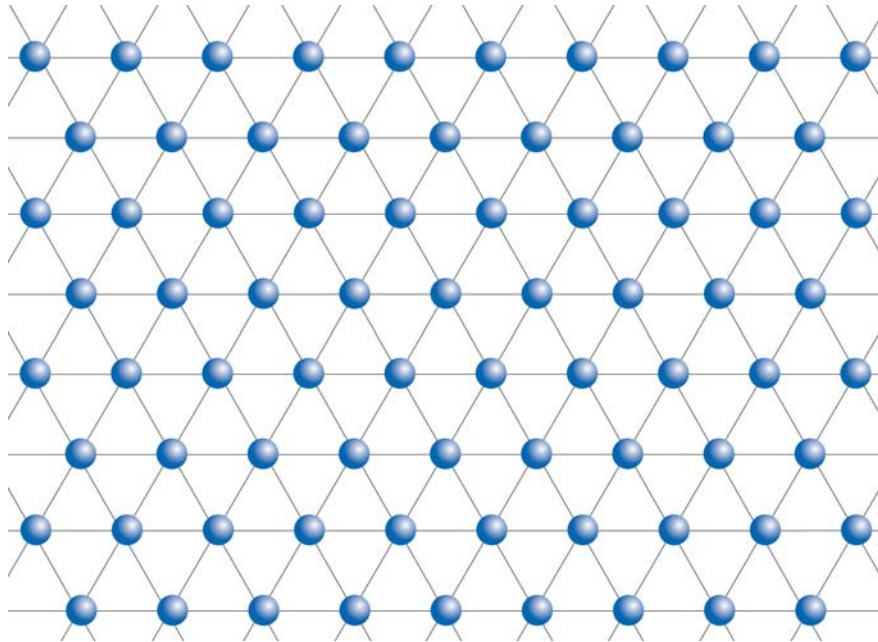
(a)
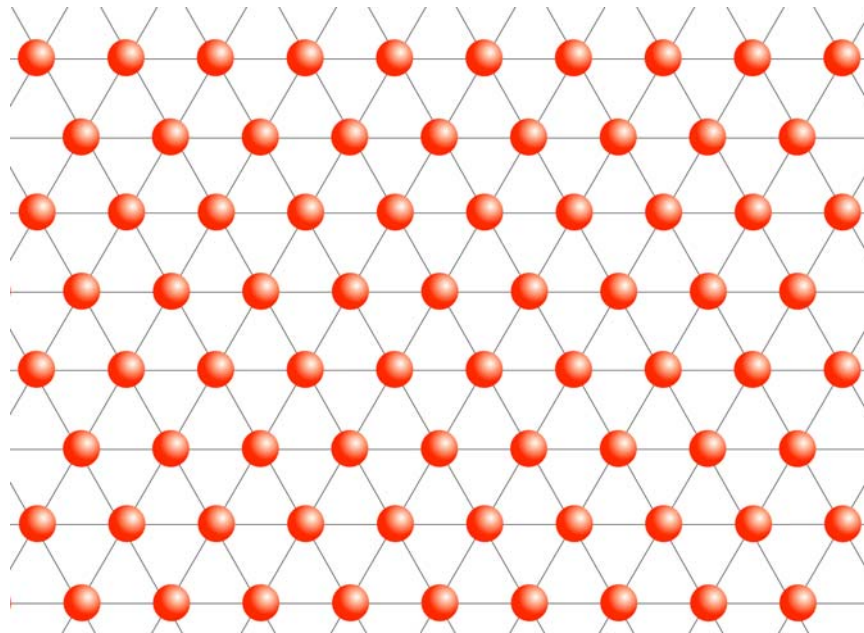
(b)

Figure V.2-5. $\left(20\overline{1}\right)_m$ planes in the monoclinic, B-type polymorph of Dy_2O_3. (a) A pure metal (M) cation layer consisting of a fully dense, triangular net of cations. (b) A pure oxygen (O) anion layer consisting of a fully dense, triangular net of anions. The diagrams here correspond to an ideal monoclinic unit cell in which one of the lattice parameters is constrained.
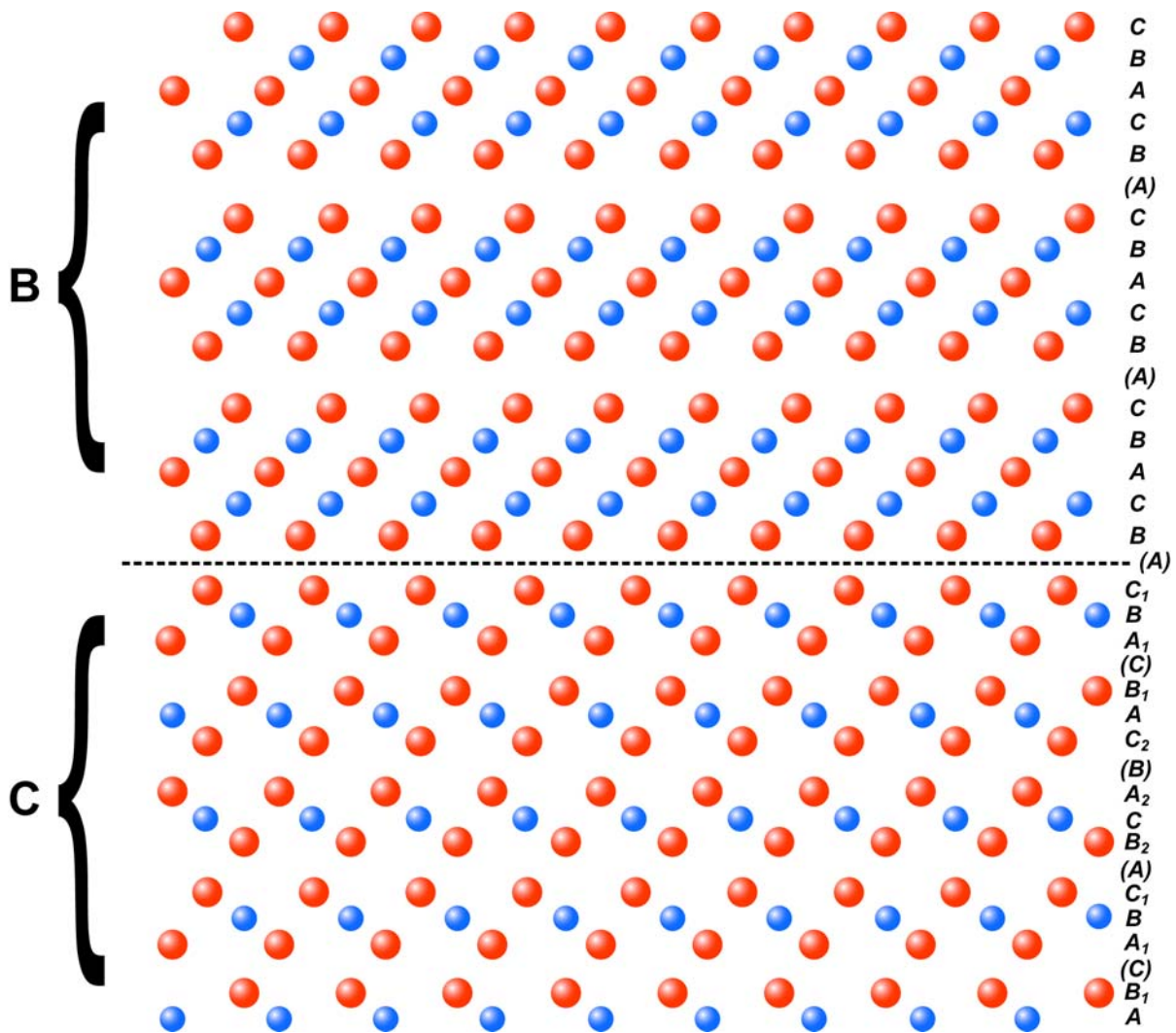
Figure V.2-6. Schematic diagram showing a proposed model for the interface between grains of C- and B-type Dy_2O_3 shown in Fig. V.2-3. $\{111\}_c$-type cubic planes and $\left(20\bar{1}\right)_m$-type monoclinic planes are viewed edge-on in this diagram. This model assumes that the B/C interface occurs between successive oxygen layers. Layer registries are also shown in the diagram (for an explanation of the nomenclature, refer to Ref. [3]). The cubic (C) phase is viewed down a $\left\langle 1\bar{1}0\right\rangle_c$-type direction while the monoclinic phase is viewed along a $\left[1\bar{3}2\right]_m$ direction in this drawing. Thus, this diagram illustrates the entire epitaxial relationship observed in Fig. V.2-3 (i.e., $\left(20\bar{1}\right)_m \parallel \{111\}_c$ and $\left[1\bar{3}2\right]_m \parallel \left\langle 1\bar{1}0\right\rangle_c$).
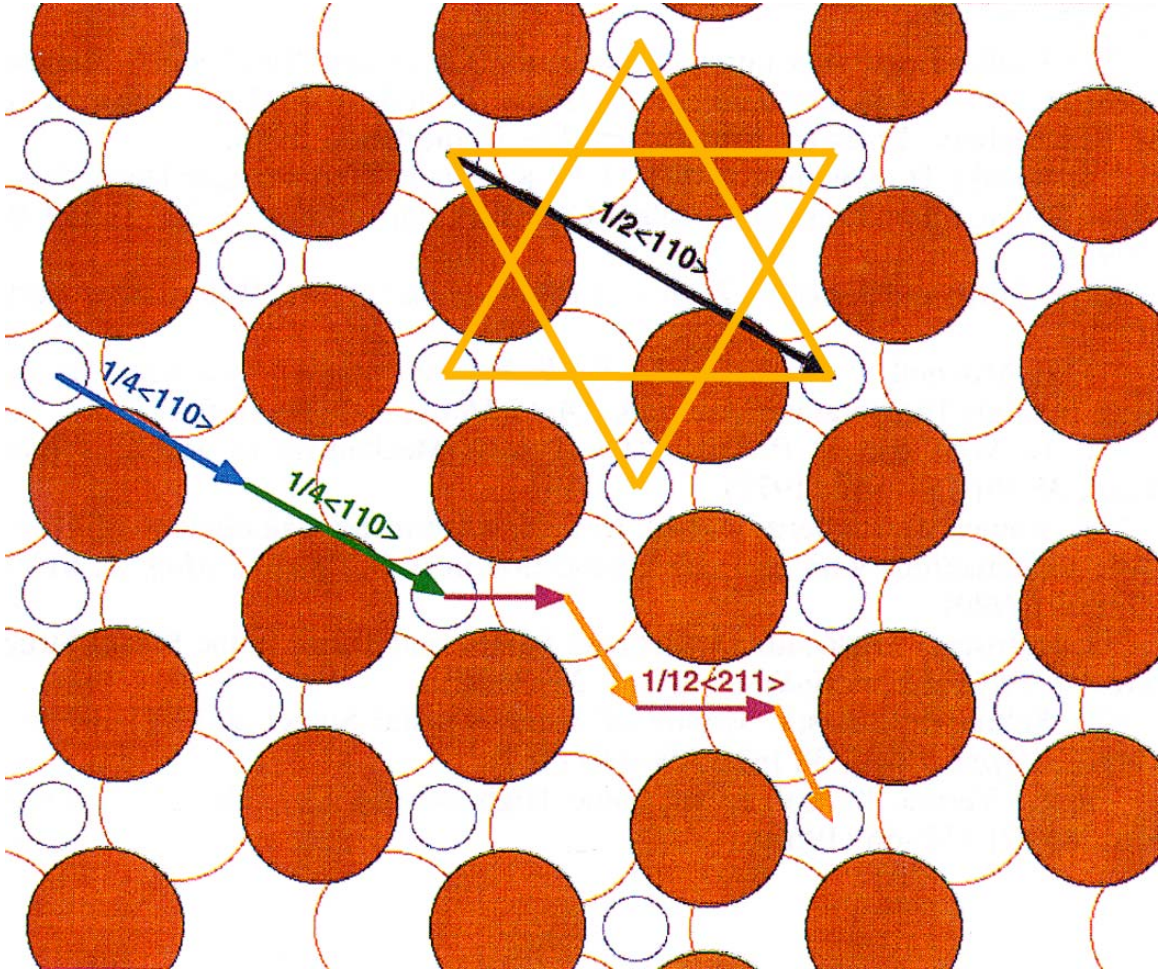
Figure V.2-7. Schematic diagram of {111} <110> slip in spinel (MgAl$_2$O$_4$). This drawing from Mitchell [4] has been modified to highlight the kagome lattice of cations (gold Star of David). Two adjacent {111} anion layers are shown in the diagram: red-shaded circles represent the top layer of anions; large hollow circles represent the bottom anion layer. An intermediate layer of cations is shown as smaller hollow circles. The cations in this layer form a kagome lattice, as indicated by the Star of David. The perfect 1/2 <110> Burgers vector for {111} slip is shown in black. Also shown beneath this vector are variously colored vectors representing possible dislocation dissociation schemes.

We offer the following nuggets of speculation regarding deformation mechanisms:

(1) Slip systems in complex materials are likely to be found in materials with layers involving triangular atom nets or derivatives thereof. This is because triangular atom nets, being quite atomically dense, tend to be accompanied by large layer

spacings between these nets (hence, making sliding of one layer over another less arduous).

(2)   If triangular atom nets in a particular compound are atom deficient (in other words, they include vacant sites so as to form special tiling patterns such as honeycomb or kagome), then the perfect Burgers vector for slip in these planes should connect nearest neighbor "holes" in the *deficient* triangular atom nets. Now for certain compounds this vector length may be quite large. For instance, in δ-$Sc_4Zr_3O_{12}$ (Section IV.5), this length is given by $a = \sqrt{\frac{\#\,atoms}{hexcell}}\,d = \sqrt{7}\,d$ (Eq. (III.5-1)). For δ-$Sc_4Zr_3O_{12}$, $a = 0.9396$ nm (Table IV.5-3), which would be the predicted length of the Burgers vector for basal slip in this compound. Compare this with the 1/2 <110> perfect Burgers vector for {111} slip in spinel, ~0.5685 nm. The large Burgers vector associated with basal slip in δ-$Sc_4Zr_3O_{12}$ may suggest that this compound is creep-resistant at high temperature. By similar arguments, this may be a means to search for new, creep-resistant materials.

Another potential use for our layering concepts is to fabricate layered membranes from complex oxides using an engineered, systematic gradation of oxidation state from one side of the membrane to the other, with layers based on triangular atom nets parallel to the membrane thickness. This may be beneficial in fuel cell design. In addition, our layered atom concepts can be used to predict radiation damage effects in complex oxides (such as the threshold energies for displacement of constitutive elements). These two ideas will not be developed further in this report. We only mention them here for the interested reader.

This concludes our discussion of possible applications for the layered atom stacking concepts developed in this report.

Section V.2 References

[1]   S. Divinski, M. Salamon, and H. Mehrer, "Silicon Diffusion in Molybdenum Disilicide: Correlation Effects," *Phil. Mag.* **84** (8) 757–772 (2004).

[2]   T. Hahn, Ed. *International Tables for X-ray Crystallography*, Vol. A (D. Riedel, Dordrecht, Netherlands, 1983).

[3]   International Committee for Diffraction Data, *Powder Diffraction File* (Joint Committee on Powder Diffraction Standards, Philadelphia, PA, 1974–present).

[4]   M. Tang, P. Lu, J. A. Valdez, and K. E. Sickafus, "Heavy Ion Irradiation-Induced Phase Transformation in Polycrystalline Dy_2O_3," *Philos. Mag.* **86 (11)** (2006) 1597-1613.

[5]   T. E. Mitchell, "Dislocations and Mechanical Properties of MgO-Al_2O_3 Spinel Single Crystals," *J. Am. Ceram. Soc.* **82** (12) 3305–3316 (1999).

VI. Conclusions

We have presented a systematic layer stacking model to describe crystal structures of complex materials. Our principal illustration of the concepts underlying our model involves oxides with metal cations of increasing oxidation state (M cations with valences ranging from M^{1+} to M^{4+}). We have used concepts relating to geometric subdivisions of a triangular atom net to describe the layered atom patterns in these compounds (concepts originally proposed by Shuichi Iida). We demonstrated that as a function of increasing oxidation state (from M^{1+} to M^{4+}), the layer stacking motif used to generate each successive structure (specifically, motifs along a $\overline{3}$ symmetry axis) progresses through the following sequence: MMO, MO, $M_{\frac{r}{s}}O$, $MO_{\frac{r}{s}}O_{\frac{u}{v}}$, MOO (where M and O represent fully dense triangular atom nets and $\frac{r}{s}$ and $\frac{u}{v}$ are fractions used to describe partially filled triangular atom nets). We selected eight oxide stoichiometries to demonstrate this progression of motifs. We also developed complete crystallographic descriptions for most of the compounds representing our selected stoichiometries using space group $R\overline{3}$.

This model has important potential applications. One example is to provide simplified crystallographic descriptions for oxygen migration in complex oxides that exhibit the property of fast ion conduction at high temperatures (Section V.2). Another example application is to predict high-temperature deformation mechanisms in complex, refractory oxides (Section V.2). Several additional applications are discussed in Sections V.1 and V.2 of this report.